THE UNIVERSITY OF MICHIGAN

INDUSTRY PROGRAM OF THE COLLEGE OF ENGINEERING

THE RESPONSE OF LAMINAR INCOMPRESSIBLE FLUID FLOW AND HEAT TRANSFER TO TRANSVERSE WALL VIBRATION

Robert J. Schoenhals

A dissertation submitted in partial fulfillment
of the requirements for the degree of
Doctor of Philosophy in the
University of Michigan
1960

January, 1961

IP-489

ACKNOWLEDGMENTS

The author wishes to express appreciation to Professor John A. Clark, chairman of the doctoral committee, under whose direction this work was performed. Gratitude is also extended to Professors Gordon J. Van Wylen, Arthur G. Hansen, Julian R. Frederick, and Kenneth F. Gordon for their interest and co-operation.

The writer is grateful to Professor Chia-Shun Yih who made valuable suggestions during the early stages of the analytical work and to Professor Vedat S. Arpaci who gave freely of his time during the continuing stages of the program and also offered many valuable suggestions.

Special credit is due Mr. Frank Randak and Mr. Cahit Akfirat for their fine work in connection with the experimental program.

The research support of the National Science Foundation and the fellowship support of the General Electric Company are gratefully acknowledged.

Many thanks go to Norlene Martin and to the Industry Program of the College of Engineering for their help in the preparation of the manuscript.

TABLE OF CONTENTS

		Page
ACKNOWLEDGMENTS		ii
LIST OF FIGURES		v
CHAPTER		
I	INTRODUCTION	1
II	THE RESPONSE OF A LAMINAR FREE CONVECTION BOUNDARY LAYER TO TRANSVERSE WALL VIBRATION	3
	Statement of the Problem	3
	The Basic Mechanism	5
	Fundamental Equations and Transformation of Coordinates	5
	Recombination of Equations and Non-dimensionalization	11
	Perturbation of Equations	14
	Asymptotic Solutions for Large Values of $\omega\sqrt{4x}$	29
	Solutions for Low Values of $\omega\sqrt{4x}$	41
	Comparison of Solutions Based on the Wall Shear Stress and Temperature Gradient	61
	Further Discussion of Results	62
	List of Symbols for Chapter II	70
III	THE POTENTIAL FLOW AND BOUNDARY LAYER RESPONSE TO TRANSVERSE VIBRATION OF A THIN PLATE OF FINITE LENGTH	74
	Statement of the Problem	74
	The Potential Flow Response	74
	The Boundary Layer Response	92
	List of Symbols for Chapter III	108
IV	EXPERIMENTAL WORK	111
	Introduction	111
	Description of the Test Apparatus	111
	Observations Made in Connection with a Free Convection Boundary Layer Subjected to Transverse Wall Vibration	133
	Procedure and Results for the Case of Transverse Vibration of a Plate of Finite Length	140
	List of Symbols for Chapter IV	177
V	SUMMARY OF RESULTS	179
LIST OF REFERENCES		181

TABLE OF CONTENTS CONT'D

		Page
APPENDIX		
I	TABULATED VALUES FOR CHAPTER II	184
	I-a Ostrach's Results	185
	I-b The Forcing Function $\zeta(\eta)$	189
	I-c The Temperature Function $\eta H'(\eta)$	193
	I-d Values of the Parameters Defined by Equations (2.66)	195
	I-e Values of the Parameters Defined by Equations (2.72)	197
	I-f Values of the Coefficients R_n	198
	I-g Values of the Coefficients S_n	199
II	EXPRESSIONS FOR THE MAGNITUDE AND PHASE OF THE TEMPERATURE PERTURBATIONS FOR LARGE VALUES OF $\omega\sqrt{4x}$ (CHAPTER II)	200
III	AN ALTERNATE METHOD OF OBTAINING SOLUTIONS FOR LOW VALUES OF $\omega\sqrt{4x}$ (CHAPTER II)	203
IV	SUMMARY OF EXPERIMENTAL DATA	209
	IV-a Summary of Data From Potential Flow Measurements Along the Wall of a Vibrating Plate	209
	IV-b Summary of Data From Velocity Measurements Made in the Boundary Layer on a Vibrating Plate	211
	IV-c Summary of Heat Transfer Measurements Made Under Vibratory Conditions	212

LIST OF FIGURES

Figure		Page
1	Laminar Free Convection Boundary Layer Adjacent to a Heated Wall with Transverse Vibration.....	4
2	Sketch Showing a Section of the Boundary Layer and Illustrating the Basic Mechanism Being Investigated....	6
3	Sketch Illustrating the Stationary and Moving Coordinate Systems.....	8
4	Velocity Profiles for Laminar Free Convection Boundary Layers as Reproduced from Ostrach's Report (23).....	18
5	Temperature Profiles for Laminar Free Convection Boundary Layers as Reproduced from Ostrach's Report(23)	19
6	Velocity Measurements of Schmidt and Beckman(27) and Comparison with Theory as Reproduced from Ostrach's Report(23).....	20
7	Temperature Measurements of Schmidt and Beckman(27) and Comparison with Theory as Reproduced from Ostrach's Report(23).....	21
8	Velocity Measurements of Schmidt and Beckman(27) and Comparison with Theory as Reproduced from Ostrach's Report(23).....	22
9	Temperature Measurements of Schmidt and Beckman(27) and Comparison with Theory as Reproduced from Ostrach's Report(23).....	23
10	The Forcing Function.....	27
11	Magnitude and Phase of the Velocity Perturbations for $\gamma = 5$.....	32
12	Magnitude and Phase of the Velocity Perturbations for $\gamma = 10$.....	33
13	Magnitude and Phase of the Temperature Perturbations for $\gamma = 5$.....	39
14	Magnitude and Phase of the Temperature Perturbations for $\gamma = 10$.....	40
15	Sketch Illustrating Wall Acceleration at Zero Frequency.....	44

LIST OF FIGURES CONT'D

Figure		Page
16	Sketch Illustrating Wall Acceleration at Zero Frequency	45
17	The Temperature Function	47
18	Magnitude and Phase of the Oscillating Stream Function for Small Values γ	59
19	Magnitude and Phase of the Temperature Perturbations for Small Values of γ	60
20	Magnitude of the Oscillating Wall Shear Stress for High and Low Values of γ	63
21	Magnitude of the Oscillating Wall Temperature Gradient for High and Low Values of γ	64
22	Sketch Showing a Thin Plate of Finite Length Vibrating Transversely in an Infinite Incompressible Fluid at Rest	75
23	Sketch Showing the Boundary of a Solid Body Moving in a Fluid	81
24	The Oscillating Potential Flow Streamline Pattern for a Plate Vibrating Transversely	85
25	The Oscillating Potential Flow Velocity Distribution for a Plate Vibrating Transversely	87
26	The Oscillating Potential Flow Velocity Distribution for a Plate Vibrating Transversely	88
27	The Oscillating Potential Flow Velocity Distribution for a Plate Vibrating Transversely	89
28	The Oscillating Potential Flow Velocity Distribution for a Plate Vibrating Transversely	90
29	The Oscillating Potential Flow Along a Plate Vibrating Transversely	91
30	Magnitude and Phase of the First Approximation to the Oscillating Velocity Distribution in the Boundary Layer	98
31	Magnitude and Phase of the Second Approximation to the Oscillating Velocity Distribution in the Boundary Layer	103

LIST OF FIGURES CONT'D

Figure		Page
32	The Steady Velocity Distribution.....	105
33	General View of the Experimental Apparatus.....	112
34	Rear View of the Experimental Apparatus.....	112
35	Sketch Showing the Arrangement of the Vibratory Components of the Apparatus.....	115
36	View of the Test Plate.....	116
37	Construction of the Test Plate.....	117
38	Electrical Circuit for Measurement of Energy Input and Control of Heater Elements.....	118
39	View of Some of the Instruments.....	119
40	View of Some of the Instruments.....	119
41	Galvanometer Circuit for Controlling Guard Heater Elements.....	124
42	Linear Differential Transformer Circuit for Measurement of Vibration Amplitude.....	126
43	Output Signal of the Linear Differential Transformer with the Core Displaced from the Null Position as Displayed on an Oscilloscope.....	128
44	Output Signal of the Linear Differential Transformer Under Vibratory Conditions as Displayed on an Oscilloscope.....	128
45	Hot Wire Anemometer Circuit for Measurement of Oscillating Velocities.....	131
46	View Showing the Hot Wire Probe and Mounting System....	132
47	View Showing the Enclosure for Preventing Potential Flow.....	132
48	Sketch Showing the Hot Wire Probe Inserted into the Boundary Layer and the Enclosure for Preventing Potential Flow.....	134

LIST OF FIGURES CONT'D

Figure		Page
49	Output signal of the Hot Wire During the Measurement of Oscillating Velocity as Displayed on an Oscilloscope.....	142
50	A Typical Set of Calibration Curves for Measuring Oscillating Velocities with a Hot Wire Anemometer.....	143
51-68	Experimental Potential Flow Velocity Measurements Made Along a Plate Vibrating Transversely and the Comparison with Theory.....	145-162
69-71	Experimental Velocity Measurements Made in the Boundary Layer on a Plate Vibrating Transversely and the Comparison with Theory.....	163-165
72	Sketch Showing One of the Four Rods Attached to the Corners of the Heated Section.....	168
73	Correlation of Free Convection Heat Transfer Data Under Non-Vibratory Conditions.....	171
74	Correlation of Data Showing the Vibratory Effect on the Convection Heat Transfer Coefficient.....	174

CHAPTER I

INTRODUCTION

During recent years an increased interest has been focused on oscillatory phenomena associated with problems of fluid flow and convection heat transfer. An important contribution to this subject was made by Lighthill[16] who analyzed the laminar boundary layer and temperature distribution for a two dimensional body when the oncoming stream velocity oscillates sinusoidally with small amplitudes about a steady mean value.

Glauert[10] and Rott[25] have considered the case of a two dimensional laminar boundary layer on an infinite flat plate normal to an oncoming stream when the plate vibrates sinusoidally in its own plane. An interesting aspect of this problem is that the temperature distribution, and therefore the heat transfer, is not affected by the vibration for the case of a constant temperature plate.

Stuart[30] has obtained an exact solution of the Navier-Stokes equations for fluctuating flow past an infinite plane wall with constant suction. The corresponding temperature distribution is also given under the condition that no heat transfer occurs between the wall and the fluid.

The use of successive approximations for calculating boundary layer flows resulting from oscillations in the free stream has been discussed by Schlichting[26], Lin[17], and Gibson[9]. Rosenblat[24], Carrier and DiPrima[5], and Kestin and Persen[13] have investigated rotational vibration of bodies in viscous fluids.

Experimental measurements of heat transfer to air from vibrating wires have been made by Lemlich[15] and also by Anantanaraynan and Ramachandran.[1] The influence of sound waves on the heat transfer from heated bodies has been studied by several investigators including Fand and Kaye[8], Jackson, Harrison, and Boteler[12] and Holman and Mott-Smith[11]. Shine[28] has obtained interferometer photographs of a free convection boundary layer on a vertical heated plate vibrating normal to its own plane. Approximate values for the increase due to vibration in the convection heat transfer coefficient are also given.

The effect of transverse wall vibration on laminar free convection boundary layers has received no analytical treatment so far, and a start is made on this subject as a part of the present study. In addition, the case of a thin plate of finite length vibrating transversely in an ambient fluid at rest is considered, and the corresponding potential and boundary layer flows are investigated. An experimental program has been conducted along the lines suggested by these problems. Measurements of velocity and heat transfer are given and the results are discussed in terms of the analtyical work.

CHAPTER II

THE RESPONSE OF A LAMINAR FREE CONVECTION BOUNDARY LAYER TO TRANSVERSE WALL VIBRATION

Statement of the Problem

Consider an infinite plane wall in contact with an ambient fluid of temperature Θ_∞. The fluid has constant viscosity μ, constant thermal diffusivity κ, and constant coefficient of thermal expansion β. The wall is heated to a constant temperature Θ_o for $X > 0$ where X is the linear distance along the wall. The wall temperature for $X < 0$ is Θ_∞. A uniform force field g acts in the negative X direction inducing buoyancy forces on the lower density fluid adjacent to the wall. This action in turn causes a free convection boundary layer to develop along the wall.

The wall is now vibrated normal to its own plane with velocity $V_o = a_o\Omega \sin \Omega\tau$ where a_o is the amplitude of vibration and Ω is the frequency. A sketch of the physical system is shown in Figure 1. The problem is to find the boundary layer response to the transverse vibration described above. The analysis will be restricted to an investigation of the two dimensional incompressible boundary layer. These restrictions require that the system be uniform in the Z direction and that the boundary layer thickness δ be small compared with the acoustic wavelength $c/2\pi\Omega$. As normally done in the case of free convection systems, thermally induced density variations are considered in the momentum equations, but are neglected elsewhere.

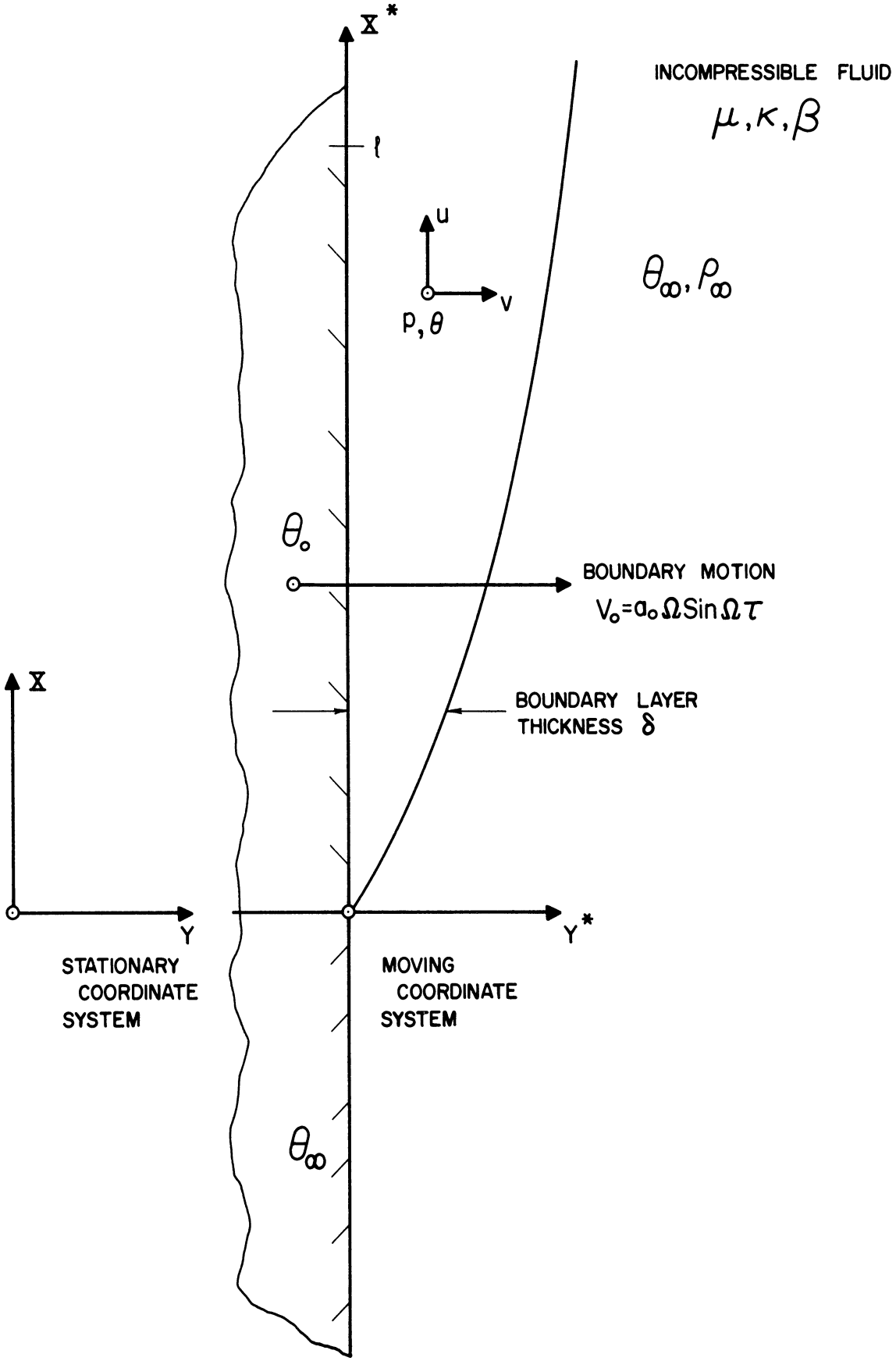

Figure 1. Laminar Free Convection Boundary Layer Adjacent to a Heated Wall with Transverse Vibration.

The Basic Mechanism

The basic mechanism under investigation can be qualitatively understood by the following explanation. Consider the sketch in Figure 2 which shows a section of the boundary layer. It is known that the boundary layer thickness δ grows with increasing distance downstream. In the absence of vibration pressure p_1 exceeds p_2 by the same amount that p_3 exceeds p_4, that is, by an amount corresponding to the hydrostatic head produced by force field g.

In the presence of vibration, however, the system accelrates with a periodic motion. Consider an instant of time during the cycle when the system is accelerating to the right. Since the boundary layer is thicker along line 2-4 than along 1-3, a greater proportion of low density fluid lies between 2 and 4 than between 1 and 3. Therefore, the mechanical inertia of the fluid between 1 and 3 exceeds that between 2 and 4 so that the pressure rise at 1 exceeds that at 2. This in turn causes a negative component of pressure gradient with respect to distance downstream. Acceleration of the system to the left likewise produces a positive component of pressure gradient.

As the acceleration of the system oscillates periodically, the induced pressure gradient in the boundary layer follows in phase. The detailed analysis of the magnitudes involved together with the effects on the velocity and temperature profiles will now be given a more rigorous treatment.

Fundamental Equations and Transformation of Coordinates

Considering the fixed axis system XY, the equations of momentum, continuity, and energy can be written as

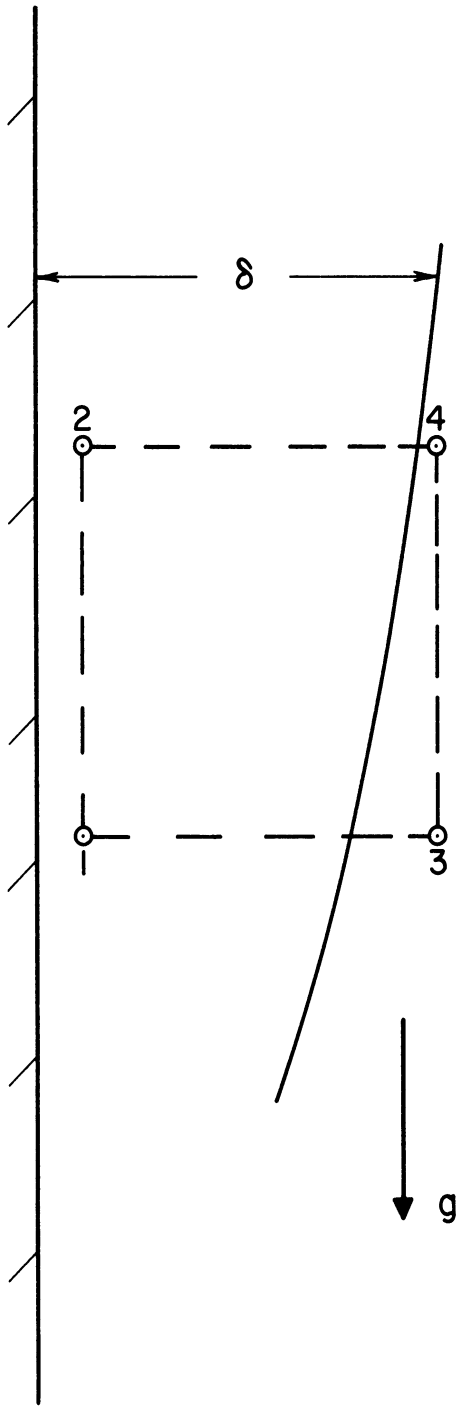

Figure 2. Sketch Showing a Section of the Boundary Layer and Illustrating the Basic Mechanism Being Investigated.

$$\rho \frac{Du}{D\tau} = -\frac{\partial p}{\partial X} + B_x + \mu \nabla^2 u \tag{2.1a}$$

$$\rho \frac{Dv}{D\tau} = -\frac{\partial p}{\partial Y} + B_y + \mu \nabla^2 v \tag{2.1b}$$

$$\frac{\partial u}{\partial X} + \frac{\partial v}{\partial Y} = 0 \tag{2.1c}$$

$$\frac{D\theta}{D\tau} = K \nabla^2 \theta \ . \tag{2.1d}$$

$D/D\tau$ is the substantial derivative operator $\frac{\partial}{\partial \tau} + u \frac{\partial}{\partial X} + v \frac{\partial}{\partial Y}$, and ∇^2 is the Laplacian operator $\frac{\partial^2}{\partial X^2} + \frac{\partial^2}{\partial Y^2}$.

For mathematical convenience these equations are transformed to a new coordinate system X* Y* which is fixed in the boundary so that $X = X^*$, $Y = Y^* + Y_o$, $u = u^*$, and $v = v^* + V_o$. The two operators are invarient with respect to the transformation and the description of continuity remains unchanged. Velocities parallel to the wall, temperatures, pressure gradients, and body forces are also independent of the transformation. The second Navier-Stokes equation is altered, however, since there is relative acceleration between the two systems in the Y direction.

Consider the sketch in Figure 3 which shows the stationary element dX dY in the fixed system XY and the moving element dX* dY* fixed with respect to the moving system X*Y*. The right hand sides of (2.1a) and (2.1b) comprise the forces acting on element dX dY.

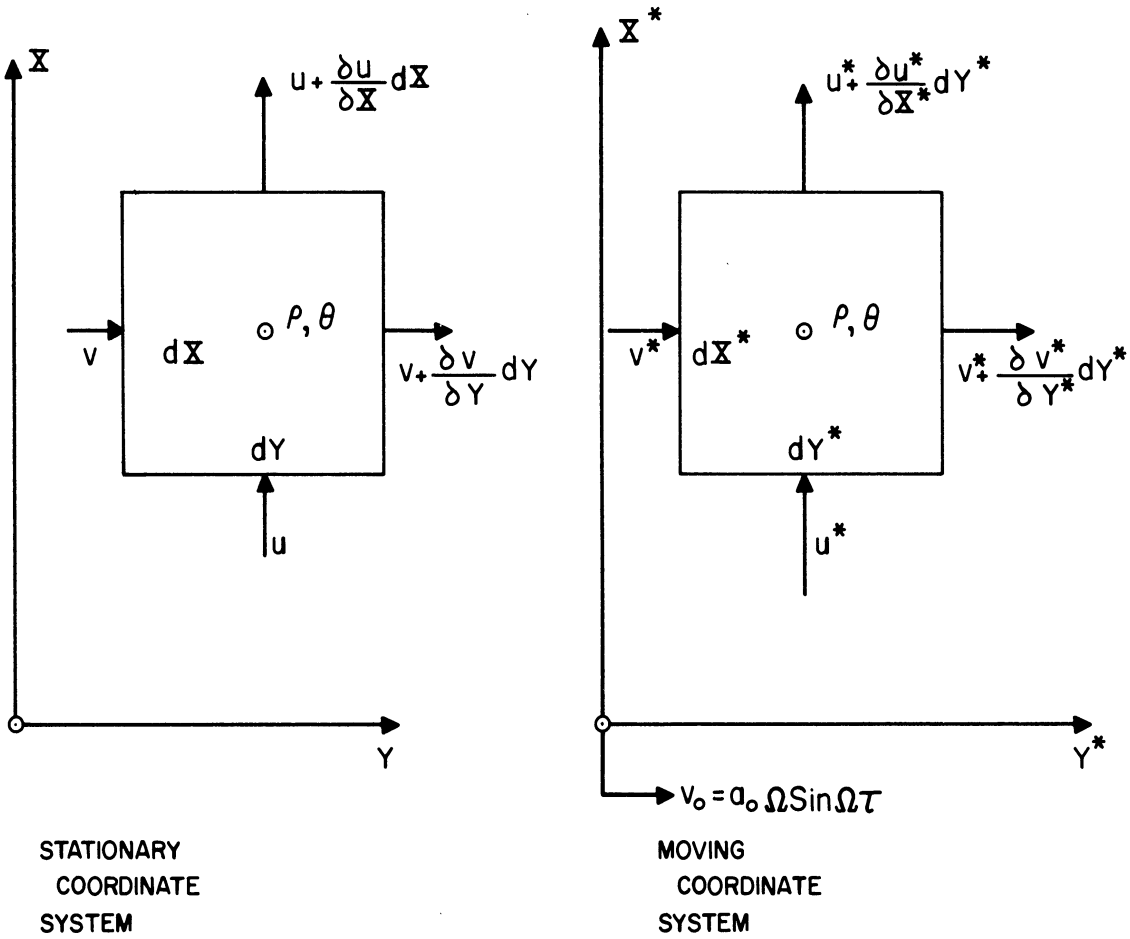

Figure 3. Sketch Illustrating the Stationary and Moving Coordinate Systems.

These consist of pressure forces, body forces, and viscous forces. The viscous forces depend only on relative changes in velocities. It is clear that all these quantities will appear in exactly the same form when written for the element dX* dY* since they are independent of whether the coordinate system is moving or not. The left hand sides of (2.1a) and (2.1b) represent the time rate of change of momentum within the element dX dY plus the net momentum flux leaving the element. The corresponding relations can now be written for the element dX* dY* as follows.

In the X* direction,

$$\frac{\partial}{\partial \tau}(\rho\, u^* dX^* dY^*) + \frac{\partial}{\partial X^*}(\rho\, u^* \cdot u^*\, dY^*)\, dX^* + \frac{\partial}{\partial Y^*}(\rho\, u^* \cdot v^*\, dX^*)\, dY^*$$

$$= \left[-\frac{\partial p}{\partial X^*} + B_x + \mu \nabla^{*2} u^* \right] dX^*\, dY^* \tag{2.2}$$

$$= \left\{ \rho \left[\frac{\partial u^*}{\partial \tau} + u^* \frac{\partial u^*}{\partial X^*} + v^* \frac{\partial u^*}{\partial Y^*} \right] + u^* \left[\frac{\partial \rho}{\partial \tau} + \frac{\partial(\rho u^*)}{\partial X^*} + \frac{\partial(\rho v^*)}{\partial Y^*} \right] \right\} dX^* dY^* .$$

By continuity,

$$\frac{\partial \rho}{\partial \tau} + \frac{\partial(\rho u^*)}{\partial X^*} + \frac{\partial(\rho v^*)}{\partial Y^*} = 0 , \tag{2.3}$$

so that the result is

$$\rho \left[\frac{\partial u^*}{\partial \tau} + u^* \frac{\partial u^*}{\partial X^*} + v^* \frac{\partial u^*}{\partial Y^*} \right] = -\frac{\partial p}{\partial X^*} + B_x + \mu \nabla^{*2} u^* . \tag{2.4}$$

The form of this equation is exactly the same as that of (2.1a).

In the Y* direction,

$$\frac{\partial}{\partial \tau}\left[\rho(V_0+v^*)\,dX^*dY^*\right]+\frac{\partial}{\partial X^*}\left[\rho(V_0+v^*)\,u^*dY^*\right]dX^*$$

$$+\frac{\partial}{\partial Y^*}\left[\rho(V_0+v^*)\,v^*dX^*\right]dY^* = \left[-\frac{\partial p}{\partial Y^*}+B_y+\mu\nabla^{*2}v^*\right]dX^*dY^*$$

$$= \left\{\rho\left[\frac{\partial v^*}{\partial \tau}+u^*\frac{\partial v^*}{\partial X^*}+v^*\frac{\partial v^*}{\partial Y^*}\right]\right. \tag{2.5}$$

$$\left.+(V_0+v^*)\left[\frac{\partial \rho}{\partial \tau}+\frac{\partial(\rho u^*)}{\partial X^*}+\frac{\partial(\rho v^*)}{\partial Y^*}\right]+\rho\frac{\partial V_0}{\partial \tau}\right\}dX^*dY^*,$$

or,

$$\rho\left[\frac{\partial v^*}{\partial \tau}+u^*\frac{\partial v^*}{\partial X^*}+v^*\frac{\partial v^*}{\partial Y^*}\right]=-\frac{\partial p}{\partial Y^*}+B_y+\mu\nabla^{*2}v^*-\rho\frac{dV_0}{d\tau} \tag{2.6}$$

This equation is in the same form as (2.1b) with the exception of the inertial force term.

Applying the law of conservation of energy to the volume dX* dY* in a way analogous to the treatment of momentum above yields the energy relation in the same form as that given in Equation (2.1d). Using this result together with Equations (2.3), (2.4), and (2.6), the transformed equations are now written as

$$\rho\frac{D^*u^*}{D\tau}=-\frac{\partial p}{\partial X^*}+B_x+\mu\nabla^{*2}u^* \tag{2.7a}$$

$$\rho\frac{D^*v^*}{D\tau}=-\frac{\partial p}{\partial Y^*}+B_y+\mu\nabla^{*2}v^*-\rho\frac{dV_0}{d\tau} \tag{2.7b}$$

$$\frac{\partial u^*}{\partial X^*}+\frac{\partial v^*}{\partial Y^*}=0 \tag{2.7c}$$

$$\frac{D^*\theta}{D\tau}=K\nabla^{*2}\theta\,. \tag{2.7d}$$

$D^*/D\tau$ is the substantial derivative operator in the moving system $\frac{\partial}{\partial \tau} + u^* \frac{\partial}{\partial X^*} + v^* \frac{\partial}{\partial Y^*}$; and correspondingly, $\nabla^{*2} = \frac{\partial^2}{\partial X^{*2}} + \frac{\partial^2}{\partial Y^{*2}}$.

In this problem $B_x = -\rho g$, $B_y = 0$, and $dV_o/d\tau = g_o \cos \Omega\tau$, although the problem may be interpreted as the case of a stationary boundary with $B_y = -\rho g_o \cos \Omega\tau$. Effectively then, the vibration produces a d'Alembert or body force due to the vibratory acceleration of the fluid coupled with its own inertia.

Recombination of Equations and Non-Dimensionalization

Pressure can be eliminated as a variable by cross differentiation of Equations (2.7a) and (2.7b) yielding

$$\frac{\partial}{\partial X^*}\left(\rho \frac{D^* v^*}{D\tau}\right) - \frac{\partial}{\partial Y^*}\left(\rho \frac{D^* u^*}{D\tau}\right) + \mu\left[\frac{\partial}{\partial Y^*}\left(\nabla^{*2} u^*\right) - \frac{\partial}{\partial X^*}\left(\nabla^{*2} v^*\right)\right] \tag{2.8}$$

$$= \frac{\partial}{\partial Y^*}(\rho g) - \frac{\partial}{\partial X^*}\left(\rho \frac{dV_o}{d\tau}\right).$$

In accordance with boundary layer theory,

$$\left|\frac{\partial}{\partial X^*}\left(\rho \frac{D^* v^*}{D\tau}\right)\right| \ll \left|\frac{\partial}{\partial Y^*}\left(\rho \frac{D^* u^*}{D\tau}\right)\right|,$$

$$\left|\frac{\partial}{\partial X^*}\left(\nabla^{*2} v^*\right)\right| \ll \left|\frac{\partial}{\partial Y^*}\left(\nabla^{*2} u^*\right)\right|, \text{ and } \left|\frac{\partial^2 u^*}{\partial X^{*2}}\right| \ll \left|\frac{\partial^2 u^*}{\partial Y^{*2}}\right|.$$

Making these approximations and integrating Equation (2.8) with respect to Y* from infinity to any finite value gives

$$\frac{D^* u^*}{D\tau} = g\left(\frac{\rho_\infty - \rho}{\rho}\right) + \frac{g_o}{\rho}\int_\infty^{Y^*} \frac{\partial \rho}{\partial X^*}\, dY^* \cos \Omega\tau + \frac{\mu}{\rho}\frac{\partial^2 u^*}{\partial Y^{*2}} \tag{2.9}$$

This result can also be obtained by applying boundary layer approximations to Equation (2.7b) and solving for pressure p. (Within this approximation the inertial force term is balanced by $\partial p/\partial Y^*$.) Entering p into

the boundary layer form of (2.7a) then gives the result in Equation (2.9).

From the definition of the thermal expansion coefficient β, $\rho = \rho_\infty[1 - \beta(\theta - \theta_\infty]$ so that Equation (2.9) becomes

$$\frac{D^* u^*}{D\tau} = \frac{\rho_\infty}{\rho} g\beta(\theta - \theta_\infty) + \frac{\rho_\infty}{\rho} g_0 \beta \int_{Y^*}^{\infty} \frac{\partial \theta}{\partial X^*} dY^* \cos \Omega \tau + \frac{\mu}{\rho} \frac{\partial^2 u^*}{\partial Y^*} . \tag{2.10}$$

As long as fractional changes in density are small the coefficient ρ_∞/ρ will be close to unity and μ/ρ can be replaced by $\nu = \mu/\rho_\infty$. Entering these conditions into Equation (2.10) and applying to Equation (2.7d) the boundary layer approximation that $\frac{\partial^2 \theta}{\partial X^{*2}} << \frac{\partial^2 \theta}{\partial Y^{*2}}$, the system of Equations (2.7) is now rewritten as

$$\frac{\partial u^*}{\partial \tau} + u^* \frac{\partial u^*}{\partial X^*} + v^* \frac{\partial u}{\partial Y^*} = g\beta(\theta - \theta_\infty) + g_0 \beta \int_{Y^*}^{\infty} \frac{\partial \theta}{\partial X^*} dY^* \cos \Omega \tau + \nu \frac{\partial^2 u^*}{\partial Y^{*2}} \tag{2.11a}$$

$$\frac{\partial u^*}{\partial X^*} + \frac{\partial v^*}{\partial Y^*} = 0 \tag{2.11b}$$

$$\frac{\partial \theta}{\partial \tau} + u^* \frac{\partial \theta}{\partial X^*} + v^* \frac{\partial \theta}{\partial Y^*} = K \frac{\partial^2 \theta}{\partial Y^{*2}} . \tag{2.11c}$$

The boundary conditions are $u_W = v_W = 0$ and $\theta_W = \theta_0$ at the wall, while $u_\infty = 0$ and $\theta = \theta_\infty$ at large distances from the wall.

The effect of the vibration can be seen from Equation (2.11a). The driving force for fluid motion is $\frac{1}{\rho}\left[B_x - \frac{\partial p}{\partial X^*}\right]$ which is given by $g\beta(\theta - \theta_\infty) + g_0 \beta \int_{Y^*}^{\infty} \frac{\partial \theta}{\partial X^*} dY^* \cos \Omega \tau$. In the absence of vibration ($g_0 = 0$) this quantity consists of the usual buoyancy term. In the presence of vibration, however, an additional time varying pressure

gradient is produced by the variation of density with X* coupled together with the vibratory acceleration of the fluid. It is the response of the boundary layer to this additional pressure gradient that will be of interest in the work that follows.

Equation (6) can be made non-dimensional by introducing the following relationships.

$$X^* = x\ell \qquad u^* = \frac{\nu\sqrt{G}}{\ell}\frac{\partial\psi}{\partial y}$$

$$Y^* = \frac{y\ell}{\sqrt[4]{G}} \qquad v^* = \frac{-\nu\sqrt[4]{G}}{\ell}\frac{\partial\psi}{\partial x}$$

$$\tau = \frac{\ell^2 t}{\nu\sqrt{G}} \qquad T = \frac{\theta-\theta_\infty}{\theta_0-\theta_\infty}$$

$$\sigma = \nu/K \qquad G = \frac{g\,\ell^3\beta(\theta_0-\theta_\infty)}{\nu^2}$$

$$\Omega = \frac{\nu\sqrt{G}\,\omega}{\ell^2} \qquad \epsilon = \frac{g_0/g}{\sqrt[4]{G}}$$

ψ is the stream function which is defined in such a way that u* and v* automatically satisfy the continuity condition (2.11b). Equations (2.11a) and (2.11c) now become

$$\frac{\partial^2\psi}{\partial y\partial t} + \frac{\partial\psi}{\partial y}\frac{\partial^2\psi}{\partial x\partial y} - \frac{\partial\psi}{\partial x}\frac{\partial^2\psi}{\partial y^2} - \frac{\partial^3\psi}{\partial y^3} = T + \epsilon\int_y^\infty \frac{\partial T}{\partial x}\,dy\,\cos\omega t \qquad (2.12a)$$

$$\frac{\partial T}{\partial t} + \frac{\partial\psi}{\partial y}\frac{\partial T}{\partial x} - \frac{\partial\psi}{\partial x}\frac{\partial T}{\partial y} = \frac{1}{\sigma}\frac{\partial^2 T}{\partial y^2} \qquad (2.12b)$$

The boundary conditions are

$$\left(\frac{\partial\psi}{\partial y}\right)_w = \left(\frac{\partial\psi}{\partial x}\right)_w = \left(\frac{\partial\psi}{\partial y}\right)_\infty = 0 \qquad , T_w = 1, \text{ and } T_\infty = 0.$$

Solutions are now desired in the form of $\psi(x,y,t,\epsilon,\omega,\sigma)$ and $T(x,y,t,\epsilon,\omega,\sigma)$.

Perturbation of Equations

The complexity of the system under investigation is due mainly to the following three factors. First, since free convection is involved, the momentum and energy relationships are coupled together making it necessary to consider both simultaneously. That is, it is not possible to solve the momentum problem independently and then use the resulting velocity distribution in the energy equation to obtain temperature as is done in the case forced convection systems.

Secondly, both the momentum and energy equations are non-linear as indicated by products of the derivatives of ψ and T in Equations (2.12a) and (2.12b). Third, the system involves quantities which vary with time in addition to space so that the problem is transient in nature.

Due to these complexities, a perturbation technique will be used. The functions $\psi_o(x,y,\sigma)$ and $T_o(x,y,\sigma)$ are defined to be solutions of Equations (2.12) when $\epsilon = 0$, that is, when no vibration is present. In the case of a vibrating wall, $\epsilon > 0$, but if the effect of the vibration is small compared with the free convection effect, then the vibratory effects can be represented as perturbations about ψ_o and T_o. In other words, if ϵ is small, then the following expressions are valid.

$$\psi(x,y,t,\epsilon,\omega,\sigma) \approx \psi_0(x,y,\sigma) + \epsilon\psi_1(x,y,t,\omega,\sigma) \tag{2.13a}$$

$$T(x,y,t,\epsilon,\omega,\sigma) \approx T_0(x,y,\sigma) + \epsilon T_1(x,y,t,\omega,\sigma) \tag{2.13b}$$

Equations (2.13) are now substituted into Equations (2.12) to obtain

$$\left[\frac{\partial\psi_0}{\partial y}\frac{\partial^2\psi_0}{\partial x\partial y}-\frac{\partial\psi_0}{\partial x}\frac{\partial^2\psi_0}{\partial y^2}-\frac{\partial^3\psi_0}{\partial y^3}-T_0\right]\epsilon^0$$
$$+\left[\frac{\partial^2\psi_1}{\partial y\partial t}+\left(\frac{\partial\psi_0}{\partial y}\frac{\partial^2\psi_1}{\partial x\partial y}+\frac{\partial^2\psi_0}{\partial x\partial y}\frac{\partial\psi_1}{\partial y}\right)-\left(\frac{\partial\psi_0}{\partial x}\frac{\partial^2\psi_1}{\partial y^2}+\frac{\partial^2\psi_0}{\partial y^2}\frac{\partial\psi_1}{\partial x}\right)\right. \tag{2.14a}$$
$$\left.-\frac{\partial^3\psi_0}{\partial y^3}-T_1\right]\epsilon+\left[\frac{\partial\psi_1}{\partial y}\frac{\partial^2\psi_1}{\partial x\partial y}-\frac{\partial\psi_1}{\partial x}\frac{\partial^2\psi_1}{\partial y^2}\right]\epsilon^2$$
$$=\epsilon\int_y^\infty\frac{\partial T_0}{\partial x}\,dy\,\cos\omega t+\epsilon^2\int_y^\infty\frac{\partial T_1}{\partial x}\,dy\,\cos\omega t.$$

$$\left[\frac{\partial\psi_0}{\partial y}\frac{\partial T_0}{\partial x}-\frac{\partial\psi_0}{\partial x}\frac{\partial T_0}{\partial y}\right]\epsilon^0+\left[\frac{\partial T_1}{\partial t}+\left(\frac{\partial\psi_0}{\partial y}\frac{\partial T_1}{\partial x}+\frac{\partial T_0}{\partial x}\frac{\partial\psi_1}{\partial y}\right)\right. \tag{2.14b}$$
$$\left.-\left(\frac{\partial\psi_0}{\partial x}\frac{\partial T_1}{\partial y}+\frac{\partial T_0}{\partial y}\frac{\partial\psi_1}{\partial x}\right)\right]\epsilon+\left[\frac{\partial\psi_1}{\partial y}\frac{\partial T_1}{\partial x}-\frac{\partial\psi_1}{\partial x}\frac{\partial T_1}{\partial y}\right]\epsilon^2=\frac{1}{\sigma}\frac{\partial^2T_0}{\partial y^2}+\frac{\epsilon}{\sigma}\frac{\partial^2T_1}{\partial y^2}$$

Since ϵ is assumed small, terms involving ϵ are retained, but those involving the squares of the perturbations are neglected by comparison. The coefficients of the zeroth power of ϵ in (2.14) yield

$$\frac{\partial\psi_0}{\partial y}\frac{\partial^2\psi_0}{\partial x\partial y}-\frac{\partial\psi_0}{\partial x}\frac{\partial^2\psi_0}{\partial y^2}-\frac{\partial^3\psi_0}{\partial y^3}-T_0=0 \tag{2.15a}$$

$$\frac{\partial\psi_0}{\partial y}\frac{\partial T_0}{\partial x}-\frac{\partial\psi_0}{\partial x}\frac{\partial T_0}{\partial y}=\frac{1}{\sigma}\frac{\partial^2T_0}{\partial y^2} \tag{2.15b}$$

The boundary conditions are

$$\left(\frac{\partial\psi_0}{\partial y}\right)_w=\left(\frac{\partial\psi_0}{\partial x}\right)_w=\left(\frac{\partial\psi_0}{\partial y}\right)_\infty=0\ ,\ (T_0)_w=1\ ,\ and\ (T_0)_\infty=0.$$

The coefficients of the first power of ϵ yield

$$\frac{\partial^2 \psi_1}{\partial y \partial t} + \left(\underline{\frac{\partial \psi_0}{\partial y}} \frac{\partial^2 \psi_1}{\partial x \partial y} + \underline{\frac{\partial^2 \psi_0}{\partial x \partial y}} \frac{\partial \psi_1}{\partial y} \right) - \left(\underline{\frac{\partial \psi_0}{\partial x}} \frac{\partial^2 \psi_1}{\partial y^2} + \underline{\frac{\partial^2 \psi_0}{\partial y^2}} \frac{\partial \psi_1}{\partial x} \right)$$

$$- \frac{\partial^3 \psi_1}{\partial y^3} - T_1 = \int_y^\infty \underline{\frac{\partial T_0}{\partial x}} \, dy \cos \omega t \tag{2.16a}$$

$$\frac{\partial T_1}{\partial t} + \left(\underline{\frac{\partial \psi_0}{\partial y}} \frac{\partial T_1}{\partial x} + \underline{\frac{\partial T_0}{\partial x}} \frac{\partial \psi_1}{\partial y} \right) - \left(\underline{\frac{\partial \psi_0}{\partial x}} \frac{\partial T_1}{\partial y} + \underline{\frac{\partial T_0}{\partial y}} \frac{\partial \psi_1}{\partial x} \right) = \frac{1}{\sigma} \frac{\partial^2 T_1}{\partial y^2}. \tag{2.16b}$$

Since the boundary conditions for (2.15) satisfy those of (2.12), the boundary conditions for (2.16) are all zero. Thus,

$$\left(\frac{\partial \psi_1}{\partial y} \right)_w = \left(\frac{\partial \psi_1}{\partial x} \right)_w = \left(\frac{\partial \psi_1}{\partial y} \right)_\infty = (T_1)_w = (T_1)_\infty = 0.$$

Equations (2.15) and (2.16) represent successive approximations of Equations (2.12). Equations (2.15) do not contain ψ_1 or T_1 and can be treated independently of these quantities. Equations (2.15) can be handled more conveniently by using the similarity variable $\eta = y/\sqrt[4]{4x}$. They can be changed to ordinary differential equations by taking

$$\psi_0 = (4x)^{3/4} F(\eta) \tag{2.17a}$$

$$T_0 = H(\eta). \tag{2.17b}$$

Introducing the above relationships into (2.15) gives

$$F'''(\eta) + 3F''(\eta)F(\eta) - 2F'^2(\eta) + H(\eta) = 0 \tag{2.18a}$$

$$\frac{1}{\sigma} H''(\eta) + 3F(\eta) H'(\eta) = 0. \tag{2.18b}$$

The boundary conditions are

$$F(0) = F'(0) = F'(\infty) = 0, \qquad H(0) = 1, \text{ and } H(\infty) = 0$$

Equations (2.18) were solved numerically by Schmidt and Beckman[27] for air and also more recently by Ostrach[23] for a wide range of Prandtl numbers. Ostrach's results were obtained by programming Equations (2.18) for an IBM 650 computer. These results are tabulated in Appendix Ia and are shown in Figures 4 and 5 which give the velocity and temperature distributions in the free convection boundary layer adjacent to a stationary wall.

Experimental verification of the theory of free convection from a stationary wall has been established by measurements made in air by Schmidt and Beckman[27], and also later by Eckert and Soehngen[7]. Schmidt and Beckman used a quartz-filament anemometer for measuring velocities and manganese-constantan thermocouples for obtaining the temperature profiles. Some of their data are shown in Figures 6 through 9 as reproduced from Ostrach's report. The data in Figures 6 and 7 were obtained using a short heated vertical plate 12 centimeters in length, while that in Figures 8 and 9 were obtained using a longer plate 50 centimeters in length. It is apparent that the temperature data show more consistent agreement with the theory. Eckert and Soehngen have also obtained similarly consistent data on the temperature profiles with the use of a Zehnder-Mach interferometer. The velocity data shows considerable deviation from the theory near the outer edge of the boundary layer where slight room turbulence disturbed the measurements to some degree. Eckert and Soehngen also observed this effect. The deviation is more pronounced far downstream from the leading edge of the larger plate where large oscillations in the flow were detected. These oscillations were due to the fact that the boundary layer was

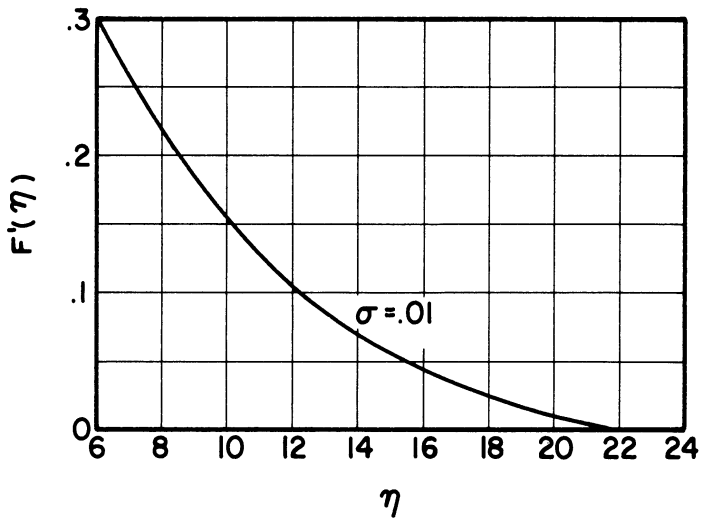

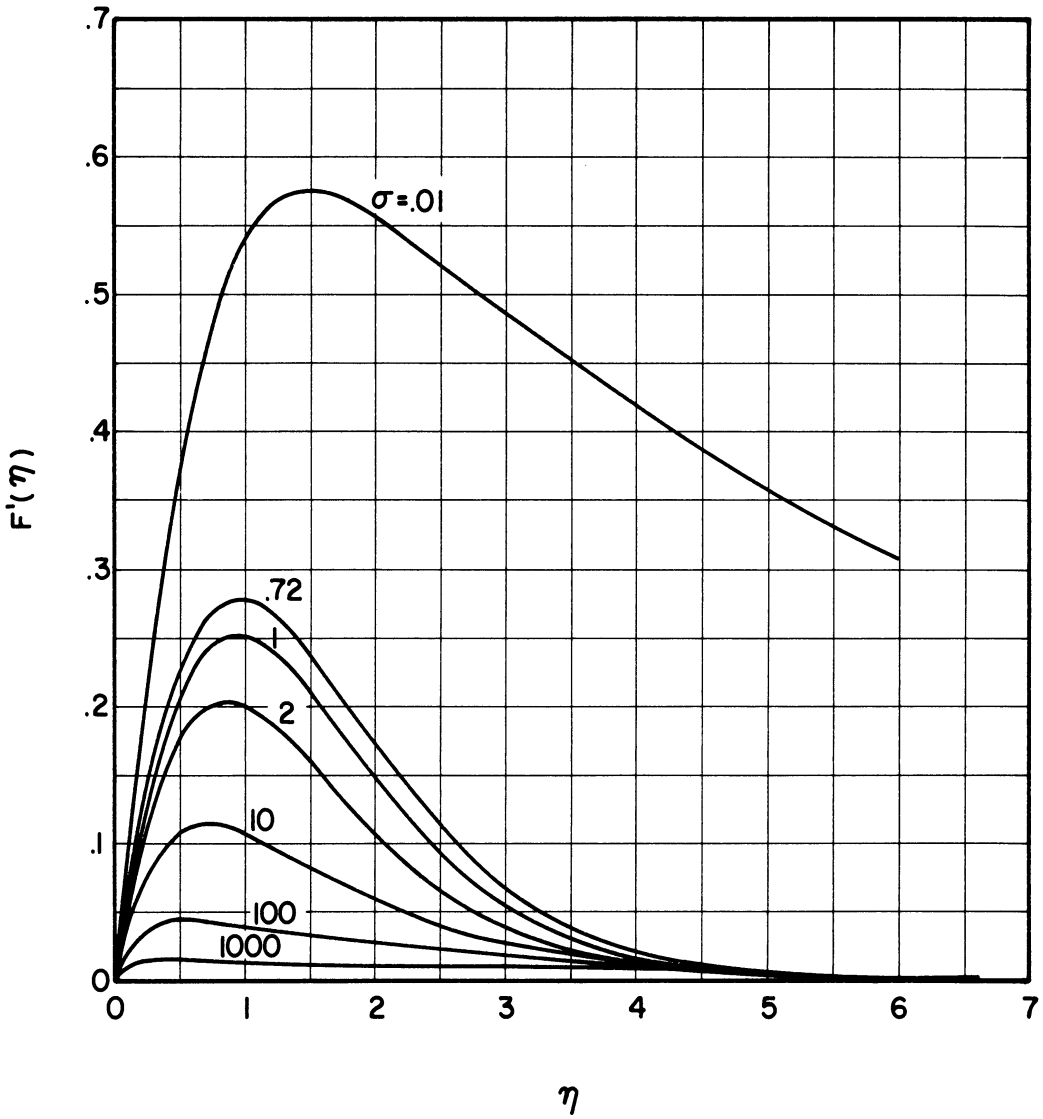

Figure 4. Velocity Profiles for Laminar Free Convection Boundary Layers as Reproduced from Ostrach's Report.[23]

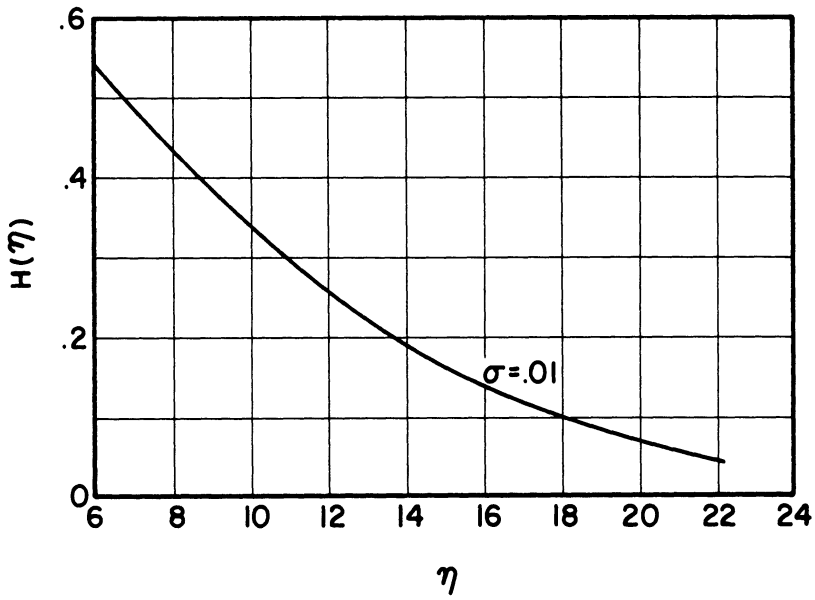

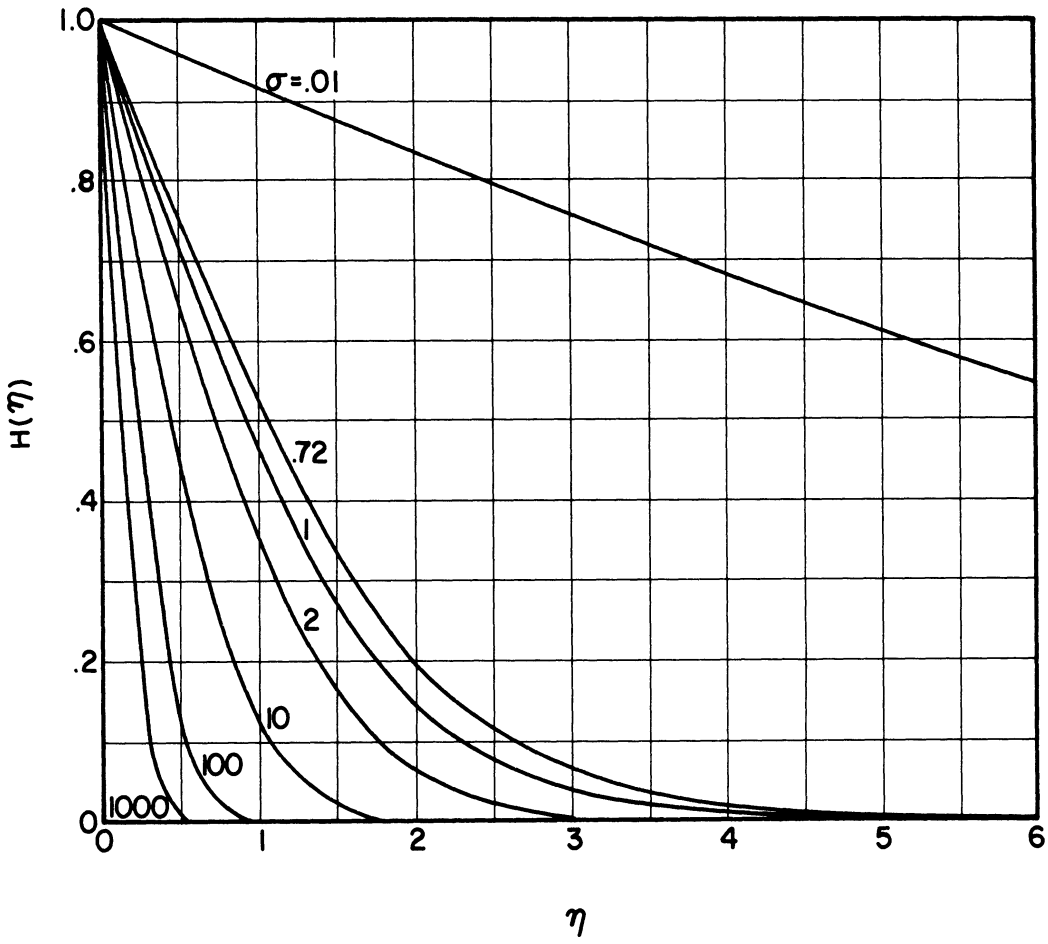

Figure 5. Temperature Profiles for Laminar Free Convection Boundary Layers as Reproduced from Ostrach's Report.[23]

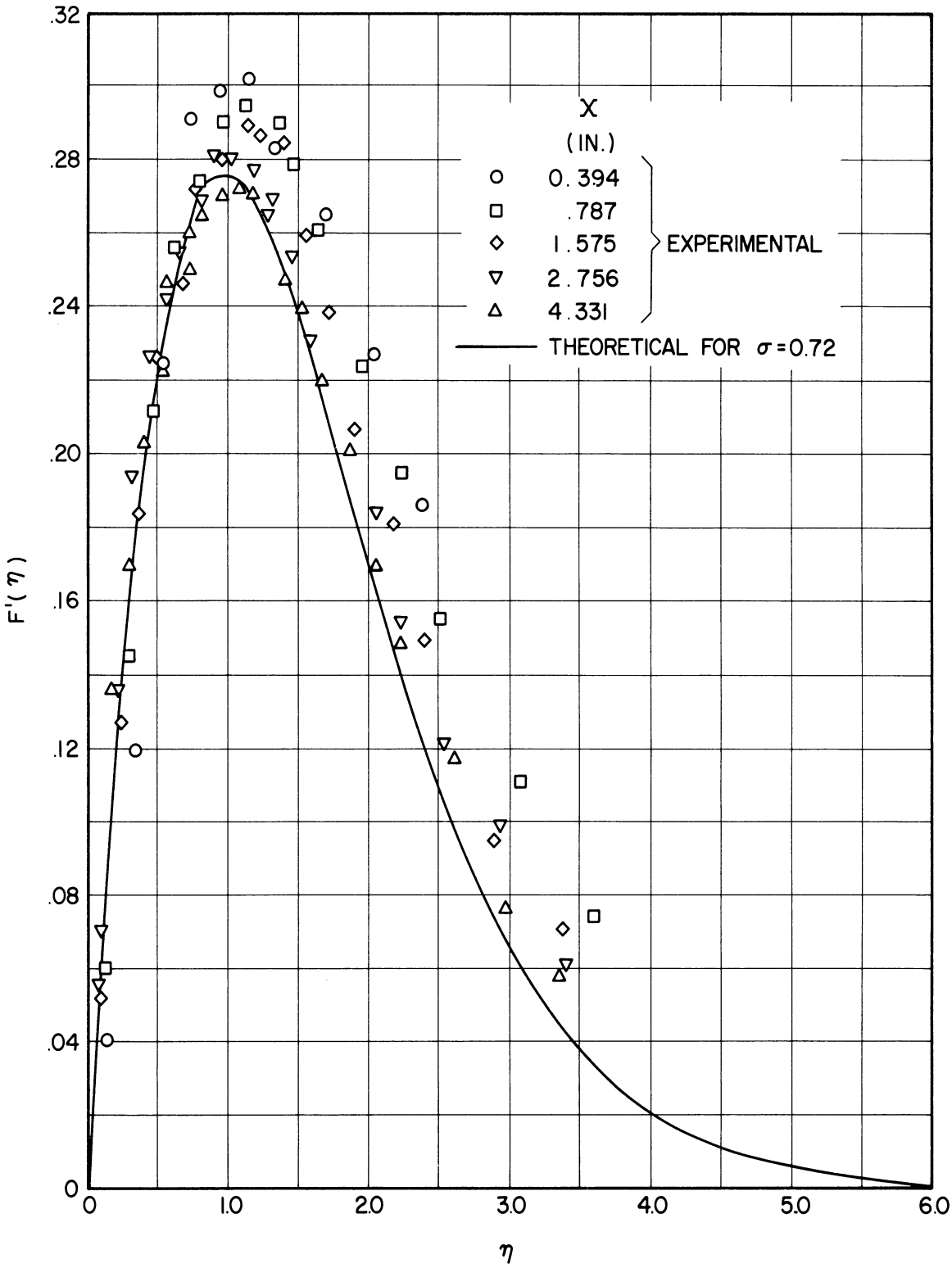

Figure 6. Velocity Measurements of Schmidt and Beckman[27] and Comparison with Theory as Reproduced from Ostrach's Report.[23]

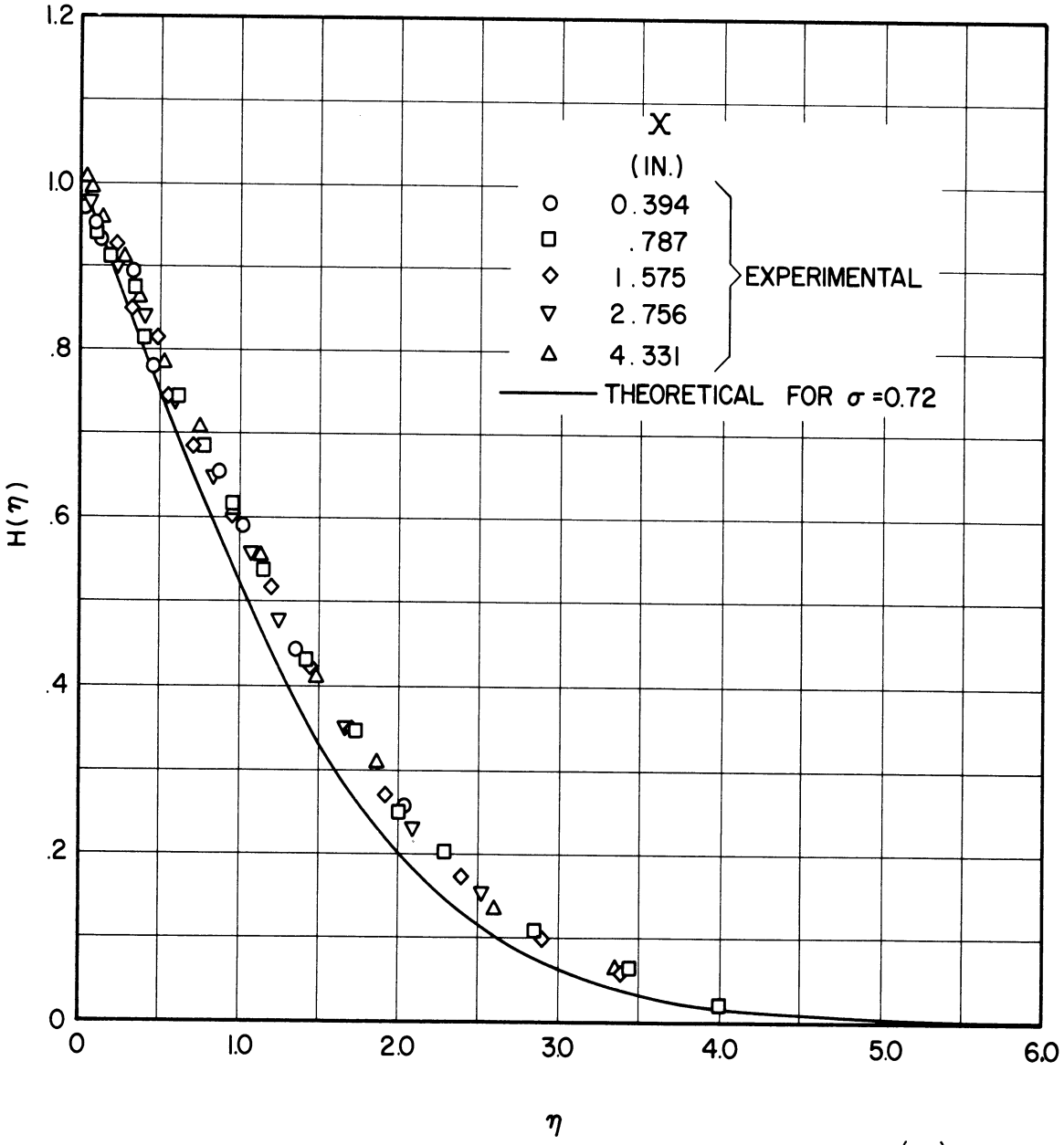

Figure 7. Temperature Measurements of Schmidt and Beckman[27] and Comparison with Theory as Reproduced from Ostrach's Report.[23]

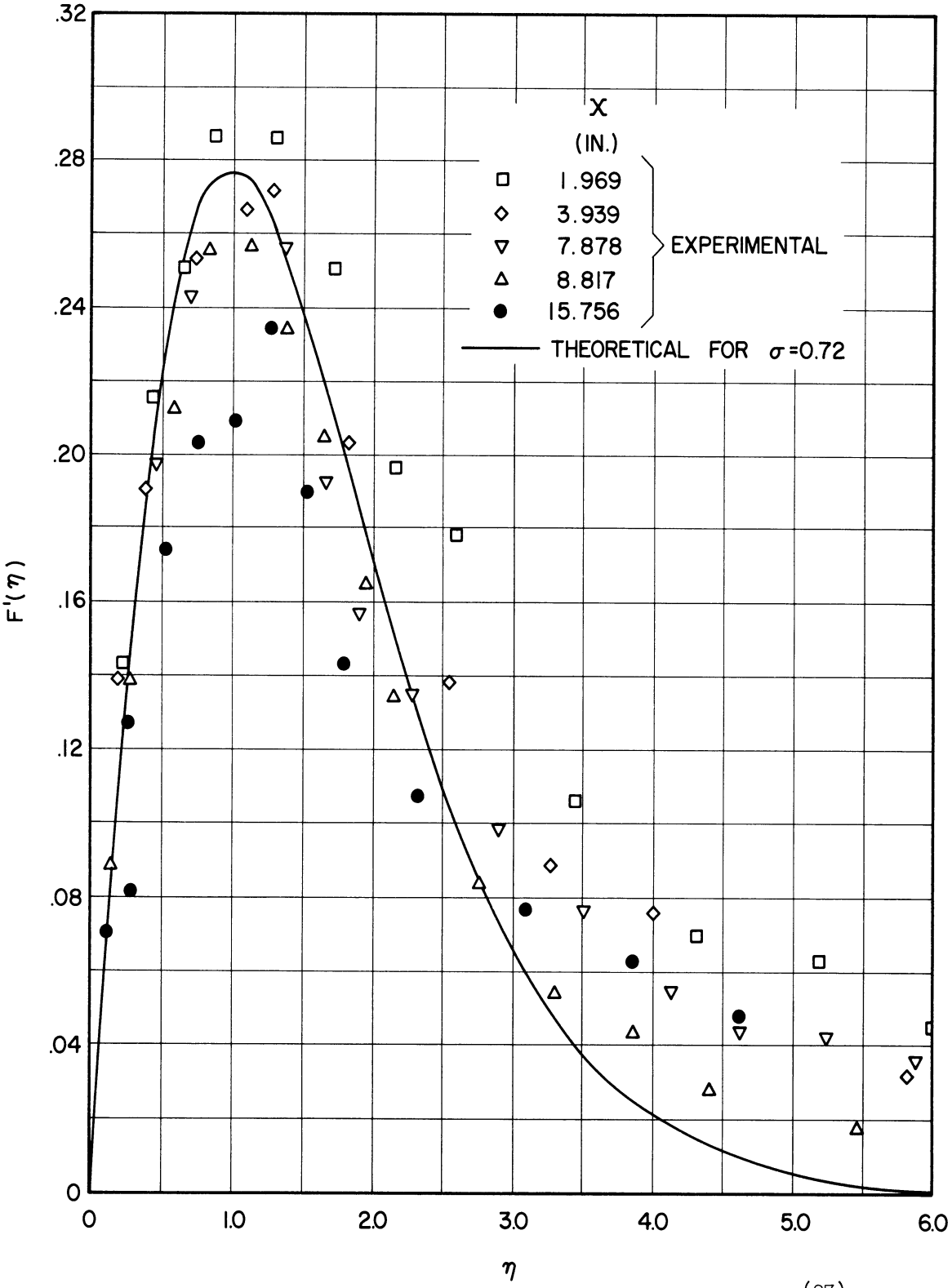

Figure 8. Velocity Measurements of Schmidt and Beckman[27] and Comparison with Theory as Reproduced from Ostrach's Report.[23]

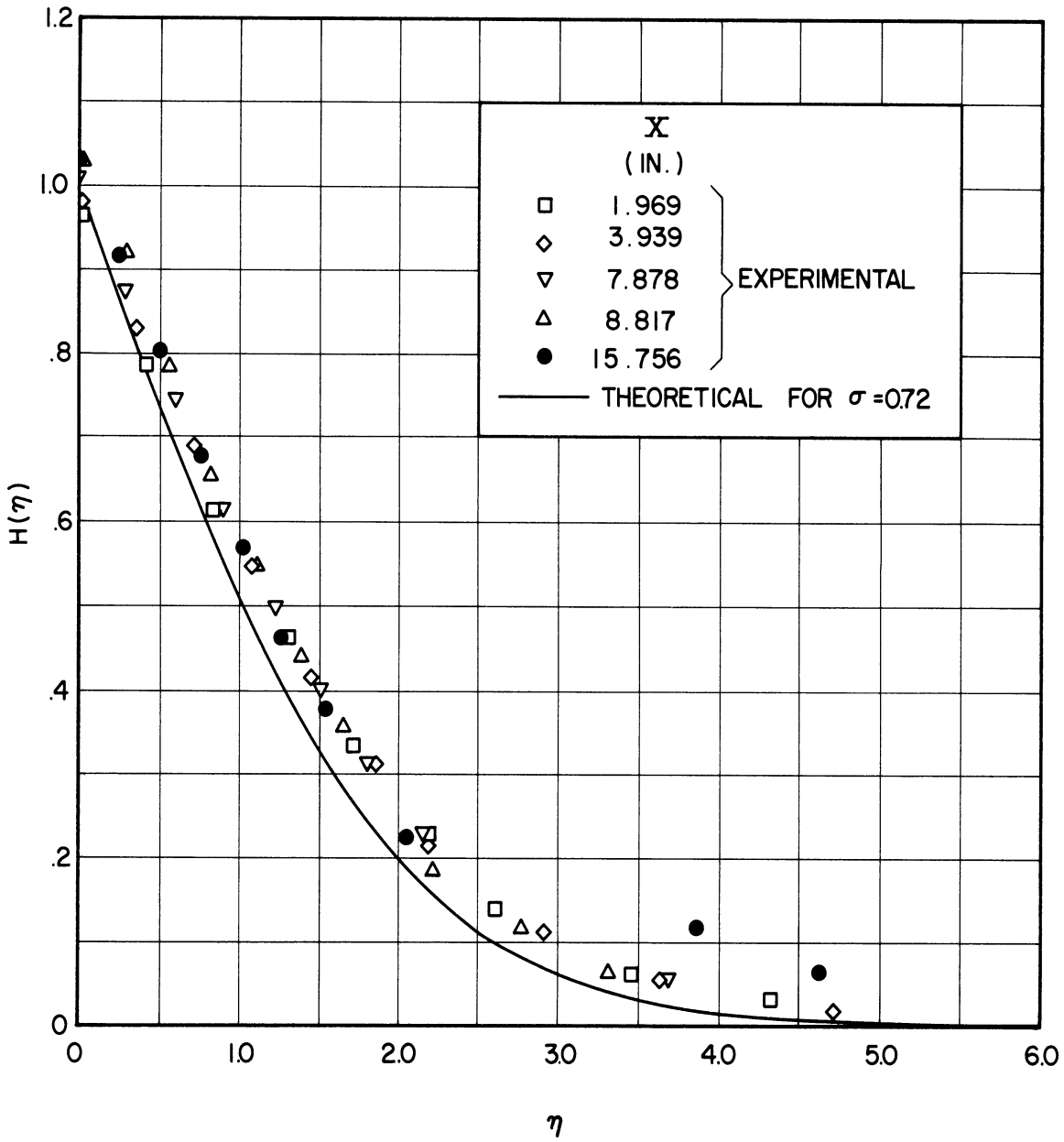

Figure 9. Temperature Measurements of Schmidt and Beckman[27] and Comparison with Theory as Reproduced from Ostrach's Report.[23]

approaching a turbulent condition in this region so that the laminar theory can not be expected to predict the results accurately here. The limiting Grashof Number for stability of laminar flow is known to be about 10^9. The velocity data from the short plate is more consistent due to the more stable condition of the boundary layer, especially close to the wall where the room turbulence had a smaller effect. The data from the short plate that are farthest from the theoretical solution were obtained very close to the leading edge. Here the boundary layer approximations made in the theoretical development are not satisfied very well so that some limitation of the theory may be expected in this region.

Although agreement of the experimental measurements is not perfect as pointed out in the previous paragraph, the general validity of the theory has been verified by these measurements. Of equal importance, the regions of limited applicability of the theory and the reasons for these limitations have been ascertained. It will be well to keep these limitations in mind when evaluating the vibratory effects on the boundary layer.

The vibratory perturbations are to be derived from Equations (2.16) and these will now be considered. The underlined terms in (2.16) are obtained from the solutions to (2.15) which are available from Ostrach's results. The derivatives of ψ_o and T_o appear in the form of variable coefficients, variable, that is, with respect to x and y. Although product terms are involved, each one consists of a variable coefficient which is known and a derivative of either ψ_1 and T_1 to the first power. Since the derivatives of ψ_1 and T_1 appear to the first power in every term, Equations (2.16) are linear. They are forced by a sinusoidal function of time by the term on the

right hand side of (2.16a), and the steady periodic solutions will oscillate at the same frequency.

In view of the above discussion it is possible to eliminate time from Equations (2.16) by taking

$$\psi_1(x,y,t,\omega,\sigma) = M(x,y,\omega,\sigma)\, e^{i\omega t} \tag{2.19a}$$

$$T_1(x,y,t,\omega,\sigma) = N(x,y,\omega,\sigma)\, e^{i\omega t} \tag{2.19b}$$

With this representation only the real parts of ψ_1 and T_1 have physical significance. M and N are complex functions and each will have associated with it a magnitude and a phase angle. Thus, the velocity oscillations parallel to the wall and the temperature oscillations are represented by the real parts of

$$\frac{\partial M}{\partial y} = \left|\frac{\partial M}{\partial y}\right| e^{i(\omega t+\phi)} \tag{2.20a}$$

$$N = |N|\, e^{i(\omega t+\alpha)}. \tag{2 20b}$$

The angles ϕ and α indicate by how much the perturbations either lead or lag the oscillating pressure gradient. An angle of 0° corresponds to the in phase condition, while positive angles indicate lead and negative angles indicate lag. As previously pointed out, the oscillating pressure gradient itself is in phase with the wall acceleration. Equations (2.16) now become

$$i\omega\frac{\partial M}{\partial y} + \left(\underline{\frac{\partial \psi_0}{\partial y}}\,\frac{\partial^2 M}{\partial x\,\partial y} + \underline{\frac{\partial^2 \psi_0}{\partial x\,\partial y}}\,\frac{\partial M}{\partial y}\right) - \left(\underline{\frac{\partial \psi_0}{\partial x}}\,\frac{\partial^2 M}{\partial y^2} + \underline{\frac{\partial^2 \psi_0}{\partial y^2}}\,\frac{\partial M}{\partial x}\right) - \frac{\partial^3 M}{\partial y^3} - N = \int_y^\infty \underline{\frac{\partial T_0}{\partial x}}\, dy \tag{2.21a}$$

$$i\omega N + \left(\underline{\frac{\partial \psi_0}{\partial y}}\,\frac{\partial N}{\partial x} + \underline{\frac{\partial T_0}{\partial x}}\,\frac{\partial M}{\partial y}\right) - \left(\underline{\frac{\partial \psi_0}{\partial x}}\,\frac{\partial N}{\partial y} + \underline{\frac{\partial T_0}{\partial y}}\,\frac{\partial M}{\partial x}\right) = \frac{1}{\sigma}\,\frac{\partial^2 N}{\partial y^2}\,. \qquad (2.21b)$$

The boundary conditions are

$$\left(\frac{\partial M}{\partial y}\right)_W = \left(\frac{\partial M}{\partial x}\right)_W = \left(\frac{\partial M}{\partial y}\right)_\infty = N_W = N_\infty = 0$$

The function on the right hand side of (2.21a) can be calculated as

$$\int_y^\infty \frac{\partial T_0}{\partial x}\,dy = (4x)^{-3/4}\int_\infty^\eta \eta\, H'(\eta)\,d\eta\,, \qquad (2.22)$$

where the function $\int_\infty^\eta \eta\, H'(\eta)\,d\eta$ is designated as $\zeta(\eta)$.

$\zeta(\eta)$ will be called the forcing function since it forces the momentum Equation (2.21a). This function has been calculated by numerical integration of Ostrach's results and the tabulated values are given in Appendix Ib. Plots of the forcing function are shown in Figure 10 for various Prandtl numbers. Its value at any point in the boundary layer indicates the amplitude of the oscillating pressure gradient produced by the wall vibration. Its value reaches a maximum value at the wall where a zero slope condition exists. The value drops off with increasing distance from the wall and becomes zero at the outer edge of the boundary layer.

An order of magnitude comparison can now be made between the free convection buoyancy effect due to density variations and the pressure gradient caused by the coupling of the density field with the wall vibration. In Equation (2.12a), the buoyancy term T can be approximated as $H(\eta)$ neglecting the higher order temperature perturbations. The first

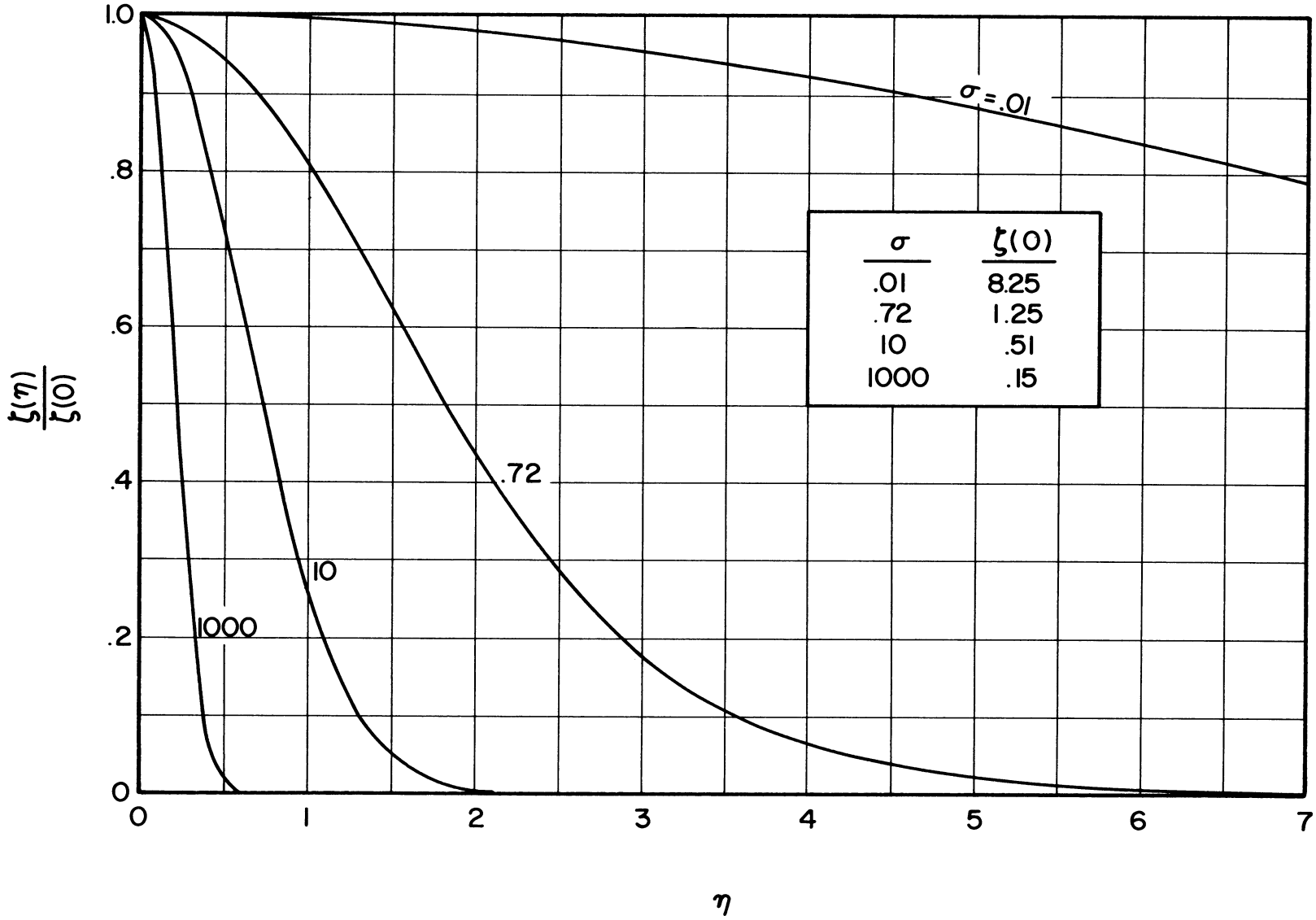

Figure 10. The Forcing Function.

approximation to the vibratory pressure gradient is $\epsilon(4x)^{-3/4}\zeta(\eta)\cos\omega t$. The approximate ratio of the peak to peak variation in pressure gradient to the steady buoyancy force is

$$2\epsilon(4x)^{-3/4}\zeta(\eta)/H(\eta) = \frac{g_0/g}{\sqrt{2}\,\sqrt[4]{G_x}}\,\zeta(\eta)/H(\eta) \tag{2.23}$$

This quantity can be rewritten as $\dfrac{g_0/g\,\sqrt{\nu/2}}{\sqrt[4]{g\beta\Delta\theta}\;X^{3/4}}\,\zeta(\eta)/H(\eta)$.

For air close to room temperatures with $\Delta\theta = 100°F$, the expression reduces to roughly $0.04\,\dfrac{g_0/g}{X^{3/4}}\,\zeta(\eta)/H(\eta)$, where X is in inches. From Figures 5 and 8 it can be seen that for $\sigma = 0.72$, $\zeta(\eta)/H(\eta)$ has a value of 1.25 at the wall and increases to slightly higher values farther out in the boundary layer. For example, at $\eta = 2$, $\zeta(2)/H(2) \approx 2.9$. For air with $\Delta\theta = 100°F$, the ratio of the vibratory variation in pressure gradient to the steady buoyancy force is roughly $0.05\,\dfrac{g_0/g}{X^{3/4}}$ at the wall. At a point two inches from the leading edge with $g_0 = 20g$, the value is about 60% at the wall, and becomes larger farther out in the boundary layer. This illustration with the nominal values given above will serve to indicate the order of magnitude of the oscillating pressure gradient.

Although the vibratory pressure gradients may be sizeable compared with the steady buoyancy forces, the corresponding velocity and temperature oscillations are not necessarily proportionate fractions of the steady velocity and temperature values. The reason for this is that if frequency is high, the induced vibratory forces are absorbed primarily by the local acceleration of the fluid, and not much time is available within a single cycle to accelerate the fluid to an appreciable velocity.

The details of these relationships will become clear in the next section where asymptotic solutions are obtained.

Asymptotic Solutions for Large Values of $\omega\sqrt{4x}$

Asymptotic solutions to Equations (2.21) can be obtained by considering large values of frequency. In this case the initial terms of (2.21a) and (2.21b) are expected to be of major importance since they contain the coefficient ω. The highest order derivatives must be retained in order that the boundary conditions be satisfied, but the convective and buoyancy terms are ignored. Under these conditions Equations (2.21) become

$$i\omega \frac{\partial M}{\partial y} - \frac{\partial^3 M}{\partial y^3} = (4x)^{-3/4} \underline{\zeta(\eta)} \tag{2.24a}$$

$$i\omega N - \frac{1}{\sigma}\frac{\partial^2 N}{\partial y^2} = \underline{\frac{\partial T_0}{\partial y}}\frac{\partial M}{\partial x} - \underline{\frac{\partial T_0}{\partial x}}\frac{\partial M}{\partial y} . \tag{2.24b}$$

A new variable is defined as $\gamma = \omega\sqrt{4X}$. Using this new variable together with the definition of η, Equations (2.24) are now rewritten as

$$\frac{\partial^3 M}{\partial \eta^3} - i\gamma\frac{\partial M}{\partial \eta} = -\underline{\zeta(\eta)} \tag{2.25a}$$

$$\frac{1}{\sigma}\frac{\partial^2 N}{\partial \eta^2} - i\gamma N = \left(\underline{\frac{\partial T_0}{\partial x}}\frac{\partial M}{\partial y} - \underline{\frac{\partial T_0}{\partial y}}\frac{\partial M}{\partial x}\right)\sqrt{4X} \tag{2.25b}$$

Since large values of ω are being considered here, not much additional restriction is caused if γ is taken to be large also. The corresponding asymptotic solutions will then be valid for large values of γ.

Equation (2.25a) does not contain N and can be solved independently of (2.25b). The particular solution of (2.25a) for large γ approaches $\zeta(\eta)/i\gamma$. An estimate of the error incurred for a given value of γ can be made by replacing $\partial M/\partial\eta$ by $\zeta(\eta)/i\gamma$ in Equation (2.25a). This results in

$$\frac{\zeta''(\eta)/\zeta(\eta)}{i\gamma} - 1 \approx -1. \tag{2.26}$$

The error incurred is then $\left| \frac{\zeta''(\eta)/\zeta(\eta)}{\gamma} \right|$ which approaches zero as γ becomes large. $\zeta''(\eta)/\zeta(\eta)$ varies throughout the boundary layer, but in general its value is fairly low for low Prandtl numbers and increases in magnitude as the Prandtl number increases. For a given tolerable error then, the allowable range of γ is smaller for the higher Prandtl numbers. For example, if $\sigma = 0.72$, $\zeta''(\eta)/\zeta(\eta)$ has a value of about unity or less throughout most of the boundary layer. For this Prandtl number then, an error of roughly 5% or less may be expected provided that γ is 20 or larger. This illustration will serve to show the range of validity of the particular asymptotic solution given above.

The homogeneous solution to (2.25a) is $c_1 e^{-\sqrt{i\gamma}\,\eta} + c_2 e^{\sqrt{i\gamma}\,\eta}$ The full solution is written as

$$\frac{\partial M}{\partial \eta} = \frac{\zeta(\eta)}{i\gamma} + C_1 e^{-\sqrt{i\gamma}\,\eta} + C_2 e^{\sqrt{i\gamma}\,\eta}. \tag{2.27}$$

Since $\left(\frac{\partial M}{\partial \eta}\right)_\infty = 0$, $C_2 = 0$, and C_1 is determined so that $\left(\frac{\partial M}{\partial \eta}\right)_w = 0$. Equation (2.27) now becomes

$$\frac{\partial M}{\partial \eta} = \frac{\zeta(0)}{i\gamma}\left[\frac{\zeta(\eta)}{\zeta(0)} - e^{-\sqrt{i\gamma}\,\eta}\right]. \tag{2.28}$$

Equation (2.28) is an asymptotic solution for the oscillating velocity profile and is valid for large values of γ. Expressions for the magnitude and phase of $\partial M/\partial\eta$ from (2.28) are written as

$$\left|\frac{\partial M}{\partial \eta}\right| = \sqrt{\left[\zeta(\eta)/\zeta(0) - e^{-\sqrt{\frac{\gamma}{2}}\eta}\cos\sqrt{\frac{\gamma}{2}}\eta\right]^2 + \left[e^{-\sqrt{\frac{\gamma}{2}}\eta}\sin\sqrt{\frac{\gamma}{2}}\eta\right]^2} \tag{2.29a}$$

$$\phi = -\operatorname{Arctan}\left[\frac{\zeta(\eta)/\zeta(0) - e^{-\sqrt{\frac{\gamma}{2}}\eta}\cos\sqrt{\frac{\gamma}{2}}\eta}{e^{-\sqrt{\frac{\gamma}{2}}\eta}\sin\sqrt{\frac{\gamma}{2}}\eta}\right] \tag{2.29b}$$

Figure 11 and 12 show the magnitude and phase of $\partial M/\partial\eta$ for two values of γ and for several Prandtl numbers.

It is apparent from (2.28) that the velocity oscillations approach asymptotically to zero as $\gamma \to \infty$. This is to be expected for two reasons. First, as X increases, the vibratory pressure gradient decreases. Second, as ω increases, the time within a given cycle during which the pressure gradient acts in a single direction is reduced. In this case there is not sufficient time for an appreciable velocity to be attained even though the local acceleration of the fluid may be fairly high.

As γ becomes larger the velocity oscillations tend to lag at 90° throughout most of the boundary layer since the oscillating pressure gradient is balanced primarily by local acceleration with viscosity having a negligible effect. Very close to the wall, however, viscosity becomes important since it causes the velocity to be zero at the wall no matter how large γ is. This causes the phase lag to be reduced to 45° as a limiting value at the wall. The in phase component of velocity disappears when $\eta = \pi\sqrt{2/\gamma}$ so that all velocity profiles have a phase lag of 90° at the same distance from the wall for a given value of γ.

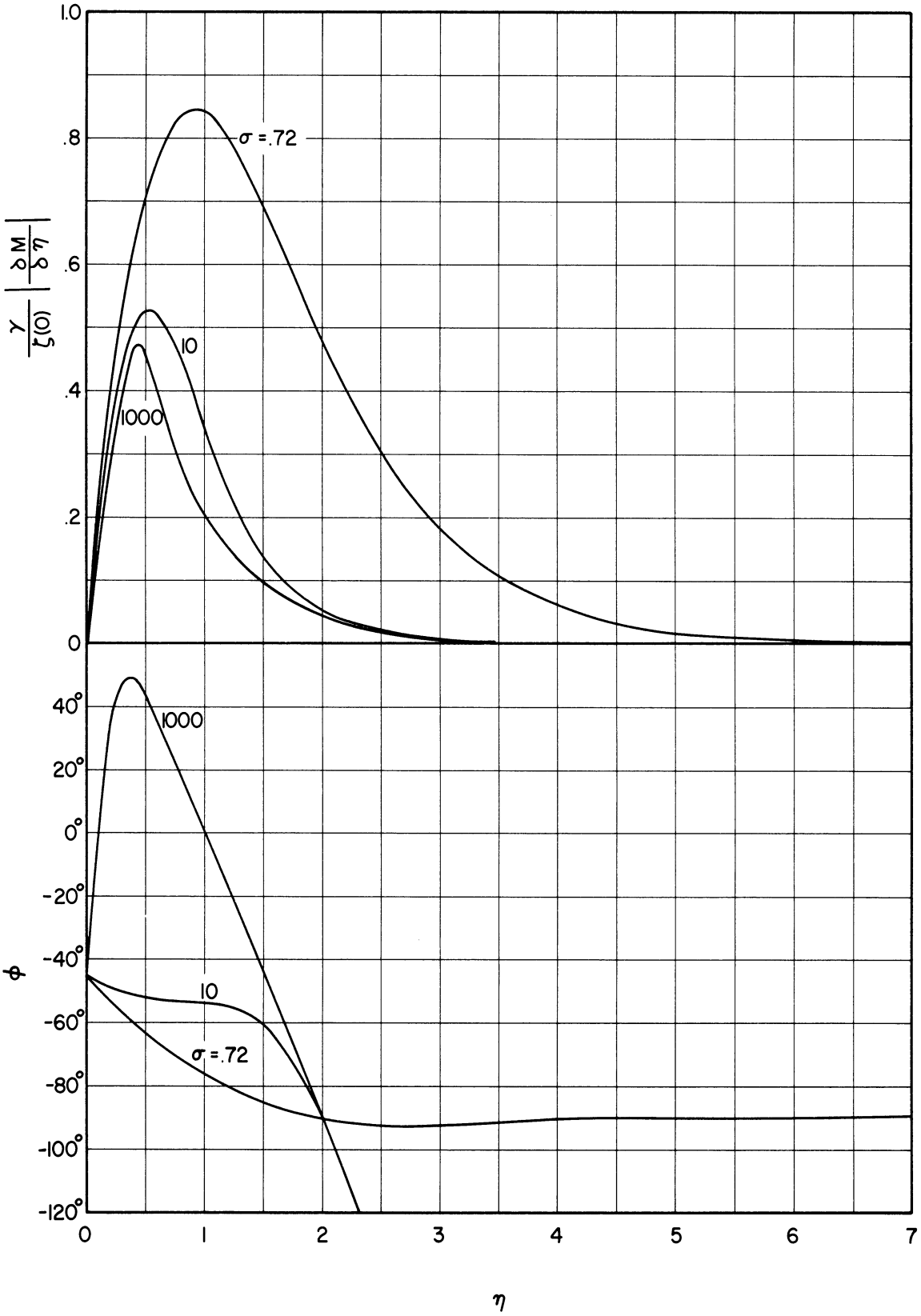

Figure 11. Magnitude and Phase of the Velocity Perturbations for $\gamma = 5$.

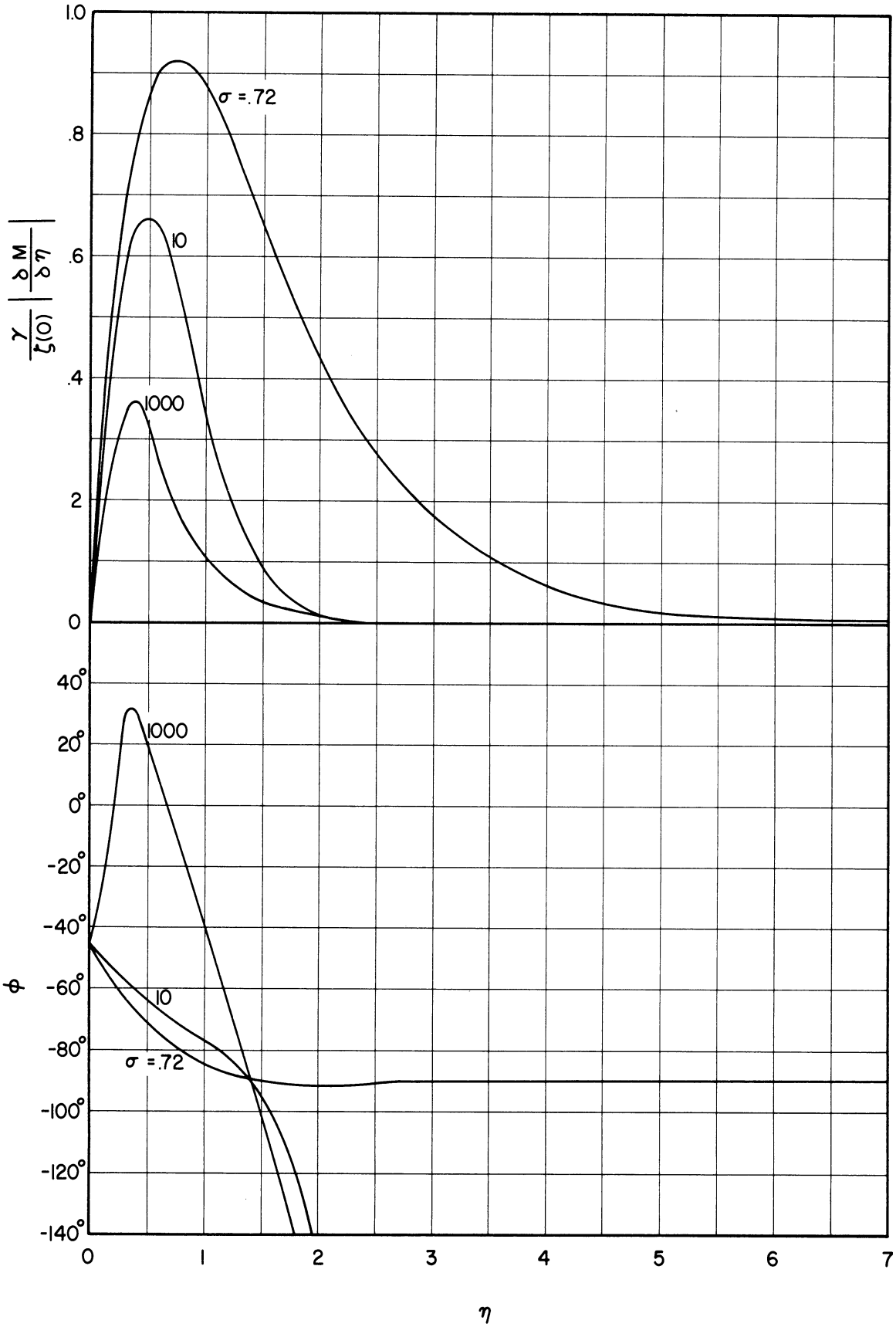

Figure 12. Magnitude and Phase of the Velocity Perturbations for γ = 10.

The oscillating shear stress is obtained by differentiating (2.28) which gives

$$\frac{\partial^2 M}{\partial y^2} = \frac{\zeta(0)}{i\gamma\sqrt{4x}}\left[\frac{\zeta'(\eta)}{\zeta(0)} + \sqrt{i\gamma}\; e^{-\sqrt{i\gamma}\,\eta}\right]. \tag{2.30}$$

At the wall $\zeta'(\eta) = 0$, so that the oscillating wall shear stress is proportional to

$$\left(\frac{\partial^2 M}{\partial y^2}\right)_W = \frac{\zeta(0)}{\sqrt{i\gamma}\sqrt{4x}}\;. \tag{2.31a}$$

The magnitude is

$$\left|\left(\frac{\partial^2 M}{\partial y^2}\right)_W\right| = \frac{\zeta(0)}{\sqrt{\gamma}\sqrt{4x}}\;, \tag{2.31b}$$

and the phase lag is 45° as expected since the velocity oscillations close to the wall lag by 45° also.

It is interesting to note at this point that the velocity oscillations close to the wall are a relatively larger fraction of the steady velocity values than is the case farther out in the boundary layer. This can be seen by considering the ratio of the peak to peak velocity variation to the steady velocity at the same point. This quantity is given by

$$\frac{2\epsilon\left|\frac{\partial M}{\partial y}\right|}{\partial \psi_0/\partial y} = \left|\frac{2\epsilon\,\zeta(0)}{i\gamma\,(4x)^{3/4}\,F'(\eta)}\left[\frac{\zeta(\eta)}{\zeta(0)} - e^{-\sqrt{i\gamma}\,\eta}\right]\right| \tag{2.32}$$

Since γ is large, the exponential will decay more rapidly than the functions of η. Thus, at distances removed from the wall,

$$2\epsilon\left|\frac{\partial M}{\partial y}\right| \Big/ \frac{\partial \psi_0}{\partial y} = \frac{2\epsilon}{\gamma\,(4x)^{3/4}}\;\frac{\zeta(\eta)}{F'(\eta)}\;. \tag{2.33}$$

On the other hand, close to the wall, the same quantity approaches the

ratio of the shear stresses. Therefore,

$$\frac{2\epsilon\left|\partial M/\partial y\right|}{\partial\psi_0/\partial y} = \frac{2\epsilon\left|\left(\frac{\partial^2 M}{\partial y^2}\right)_W\right|}{\left(\partial^2\psi_0/\partial y^2\right)_W} = \frac{2\epsilon}{\sqrt{\gamma}\,(4x)^{3/4}}\,\frac{S(0)}{F''(0)}\,. \tag{2.34}$$

Thus, the relative magnitude of the oscillations is proportional to $1/\gamma$ away from the wall, but is larger close to the wall where it is proportional to $1/\sqrt{\gamma}$.

In order to obtain the temperature perturbations the convective forcing terms on the right hand side of (2.25b) must be evaluated. The integration of (2.28) gives the oscillating stream function as

$$M = \frac{1}{i\gamma}\left[\int_0^\eta S(\eta)\,d\eta - \frac{S(0)}{\sqrt{i\gamma}}\left(1 - e^{-\sqrt{i\gamma}\,\eta}\right)\right]. \tag{2.35}$$

Differentiation of (2.35) gives the y component of the oscillating velocity as

$$\frac{\partial M}{\partial x} = \frac{S(0)}{4x\,i\gamma}\left[-\left(2\int_0^\eta \frac{S(\eta)}{S(0)}\,d\eta + \eta\,\frac{S(\eta)}{S(0)}\right) + \frac{3}{\sqrt{i\gamma}}\left(1 - e^{-\sqrt{i\gamma}\,\eta}\right)\right]. \tag{2.36}$$

Entering Equations (2.28) and (2.36) together with the derivatives of T_0 into the right hand side of (2.25b) results in

$$\frac{\partial^2 N}{\partial\eta^2} - i\gamma\sigma N = \frac{\sigma S(0)\,H'(\eta)}{i\gamma\,(4x)^{3/4}}\left[2\int_0^\eta \frac{S(\eta)}{S(0)}\,d\eta - \frac{3}{\sqrt{i\gamma}}\left(1 - e^{-\sqrt{i\gamma}\,\eta}\right) + \eta\,e^{-\sqrt{i\gamma}\,\eta}\right]. \tag{2.37}$$

Since asymptotic solutions for large γ are being considered, $\partial^2 N/\partial\eta^2$ can be neglected in comparison with $\gamma\sigma N$ throughout most of the boundary layer. If this approximation is made, the solution becomes

$$N = \frac{S(0)\,H'(\eta)}{\gamma^2\,(4x)^{3/4}}\left[2\int_0^\eta \frac{S(\eta)}{S(0)}\,d\eta - \frac{3}{\sqrt{i\gamma}}\left(1 - e^{-\sqrt{i\gamma}\,\eta}\right) + \eta\,e^{-\sqrt{i\gamma}\,\eta}\right]. \tag{2.38}$$

This expression is valid away from the wall where the exponential terms have small magnitudes. For small values of η, however, the approximation is not valid.

The physical significance of Equation (2.38) is that the temperature perturbations at a point occur mainly due to the velocity oscillations with conduction having a negligible effect. This is explained by the fact that for large values of γ there is little time for conduction to occur within a given cycle. The expression for N as given in Equation (2.38) satisfies the boundary condition that $N_\infty = 0$ so that no further consideration is necessary in that respect. Expressions for the magnitude and phase are given in Appendix II.

At the wall $N = 0$, and indeed, $N \to 0$ for $\eta \to 0$ from Equation (2.38). However, $(\partial^2 N/\partial\eta^2)_w \neq 0$ from (2.38). Therefore, close to the wall, $\partial^2 N/\partial\eta^2$ can not be neglected in comparison with $\gamma\sigma N$. On the other hand, if η is small, $H'(\eta)$ and $\int_0^\eta \zeta(\eta)\,d\eta$ can be expressed as

$$H'(\eta) = H'(0) + H''(0)\,\eta + H'''(0)\,\frac{\eta^2}{2} + \cdots , \tag{2.39a}$$

$$\int_0^\eta \zeta(\eta)\,d\eta = \zeta(0)\,\eta + \zeta'(0)\,\frac{\eta^2}{2} + \zeta''(0)\,\frac{\eta^3}{3} + \cdots . \tag{2.39b}$$

It can be noted, however, that the second term in each series is zero since $H''(0) = 0$ from (2.18b), while $\zeta'(\eta) = \eta H'(\eta)$ so that $\zeta'(0) = 0$ also. Close to the wall then, $H'(\eta) \approx H'(0)$ and $\int_0^\eta \zeta(\eta)\,d\eta \approx \zeta(0)\,\eta$ Equation (2.37) is now rewritten for small values of η as

$$\frac{\partial^2 N}{\partial\eta^2} - i\gamma\sigma N = \frac{\sigma\,\zeta(0)\,H'(0)}{i\gamma\,(4X)^{3/4}}\left[2\eta - \frac{3}{\sqrt{i\gamma}}\left(1 - e^{-\sqrt{i\gamma}\,\eta}\right) + \eta\, e^{-\sqrt{i\gamma}\,\eta}\right]. \tag{2.40}$$

The particular solution is of the form

$$N_p = b_0 + b_1\eta + b_2 e^{-\sqrt{i\gamma}\,\eta} + b_3\eta e^{-\sqrt{i\gamma}\,\eta} + b_4\eta^2 e^{-\sqrt{i\gamma}\,\eta} \tag{2.41}$$

By entering this expression into (2.40) and equating coefficients, the values of b_0, b_1, b_2, b_3, and b_4 are obtained. The particular solution is

$$N_p = \frac{S(0)\,H'(0)}{i\gamma\,(4x)^{3/4}}\left[\frac{3}{(i\gamma)^{3/2}} - \frac{2\eta}{i\gamma} - \frac{7}{4i\gamma}e^{-\sqrt{i\gamma}\,\eta} - \frac{\eta^2}{4\sqrt{i\gamma}}e^{-\sqrt{i\gamma}\,\eta}\right] \tag{2.42a}$$

if $\sigma = 1$, and

$$N_p = \frac{\sigma\,S(0)\,H'(0)}{i\gamma\,(4x)^{3/4}}\left[\frac{3}{(i\gamma)^{3/2}\sigma} - \frac{2\eta}{i\gamma\sigma} + \frac{(5-3\sigma)\,e^{-\sqrt{i\gamma}\,\eta}}{(1-\sigma)^2(i\gamma)^{3/2}} + \frac{\eta\,e^{-\sqrt{i\gamma}\,\eta}}{i\gamma(1-\sigma)}\right] \tag{2.42b}$$

if $\sigma \neq 1$.

The homogeneous solution is

$$N_h = C_1 e^{-\sqrt{i\gamma\sigma}\,\eta} + C_2 e^{\sqrt{i\gamma\sigma}\,\eta} \tag{2.43}$$

The total solution is $(N_p + N_h)$. The coefficients of η in the arguments of the exponentials in (2.38), (2.42), and (2.43) contain $\sqrt{\gamma}$. For large values of γ, the negative exponentials will decay fairly close to the wall while the positive exponential in (2.43) will grow indefinitely unless $C_2 = 0$. In order to make the solutions from (2.42) and (2.43) fit smoothly with (2.38) as the negative exponential terms become small, C_2 must be zero, while C_1 is determined so that $N = 0$ at the wall. The full solution is now

$$N = \frac{S(0)\,H'(0)}{\gamma^2(4x)^{3/4}}\left[2\eta - \frac{3}{\sqrt{i\gamma}}\left(1 - e^{-\sqrt{i\gamma}\,\eta}\right) + \frac{e^{-\sqrt{i\gamma}\,\eta}}{4}\left(7\eta + \sqrt{i\gamma}\,\eta^2\right)\right] \tag{2.44a}$$

if $\sigma = 1$, and

$$N = \frac{S(0)\,H'(0)}{\gamma^2(4x)^{3/4}}\left[2\eta - \frac{3}{\sqrt{i\gamma}}\left(1 - e^{-\sqrt{i\gamma\sigma}\,\eta}\right) + \frac{\sigma(5-3\sigma)}{(1-\sigma)^2\sqrt{i\gamma}}\left(e^{-\sqrt{i\gamma\sigma}\,\eta} - e^{-\sqrt{i\gamma}\,\eta}\right) - \frac{\sigma}{1-\sigma}\eta\,e^{-\sqrt{i\gamma}\,\eta}\right]$$

if $\sigma \neq 1$ (2.44b)

Expressions for the magnitude and phase of N from Equations (2.38) and (2.44) are given in Appendix II. Figures 13 and 14 show the magnitude and phase of N for two values of γ and for several Prandtl numbers. The curves at low values of η correspond to Equation (2.44b) while those at larger values of η correspond to (2.38). The dotted lines have been faired in to show how the solutions may be expected to behave in the intermediate region.

It may be noted at this point that the temperature perturbations are proportional to $1/\gamma^2$ and are therefore relatively smaller than the velocity perturbations which are proportional to $1/\gamma$ throughout most of the boundary layer. This fact adds support to the neglect of the buoyancy term of (2.21a) in the writing of (2.25a) as an asymptotic limit of (2.21a) for large values of γ. As expected, the temperature perturbations qualitatively follow the same pattern as those of velocity. That is, the magnitudes decrease with distance downstream and with frequency. The reasons for this behavior in the velocity perturbations have already been discussed. As γ becomes larger the temperature oscillations tend to approach a lag of 180° throughout the boundary layer, or 90° behind the velocity oscillations. In addition, the phase lag at the wall always approaches 180°.

The oscillating temperature gradient at the wall is obtained by differentiating Equations (2.44). Thus,

$$\left(\frac{\partial N}{\partial y}\right)_w = \frac{3}{4}\,\frac{\zeta(0)\,H'(0)}{\gamma^2\,(4x)} \tag{2.45a}$$

if $\sigma = 1$, and

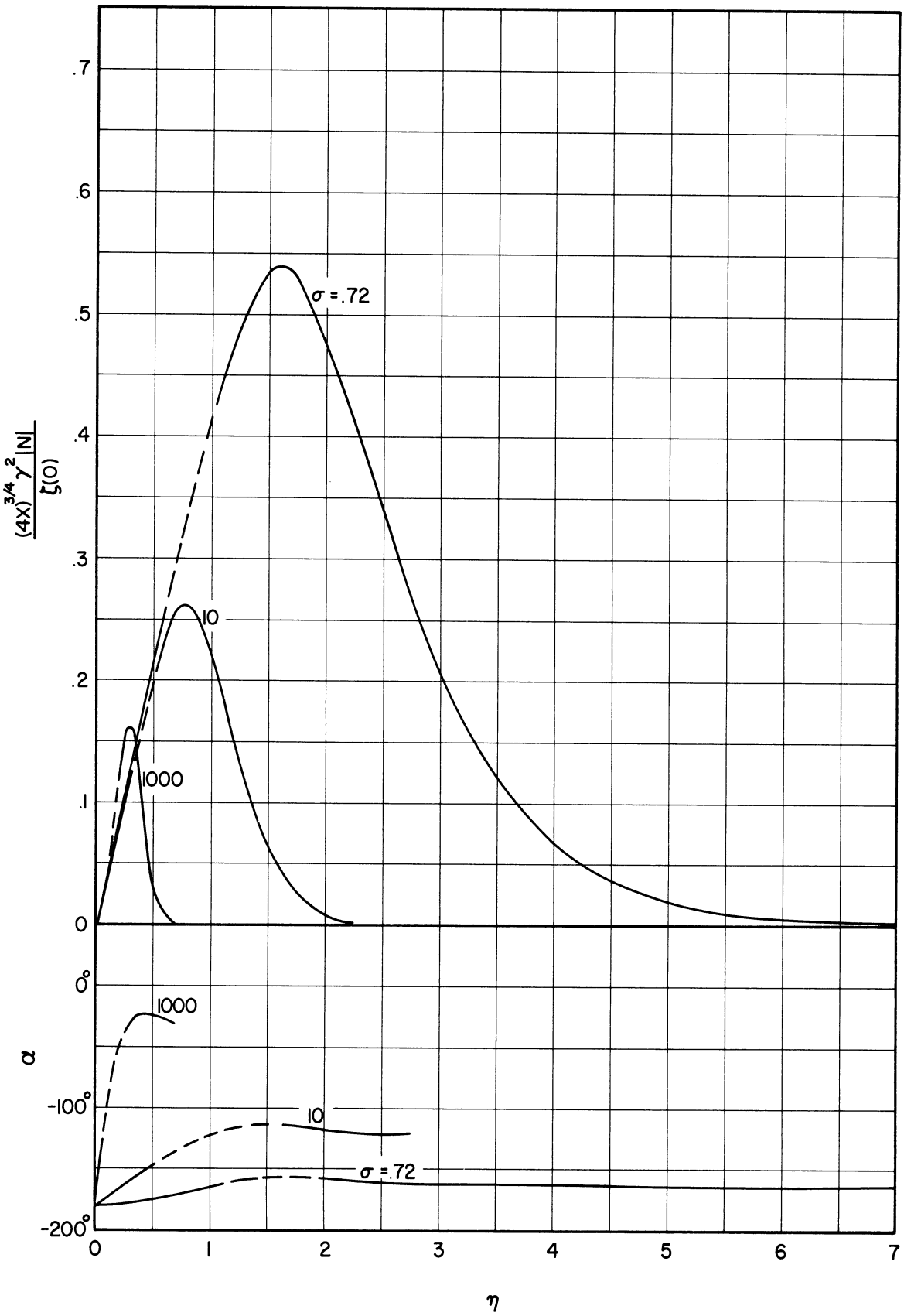

Figure 13. Magnitude and Phase of the Temperature Perturbations for $\gamma = 5$.

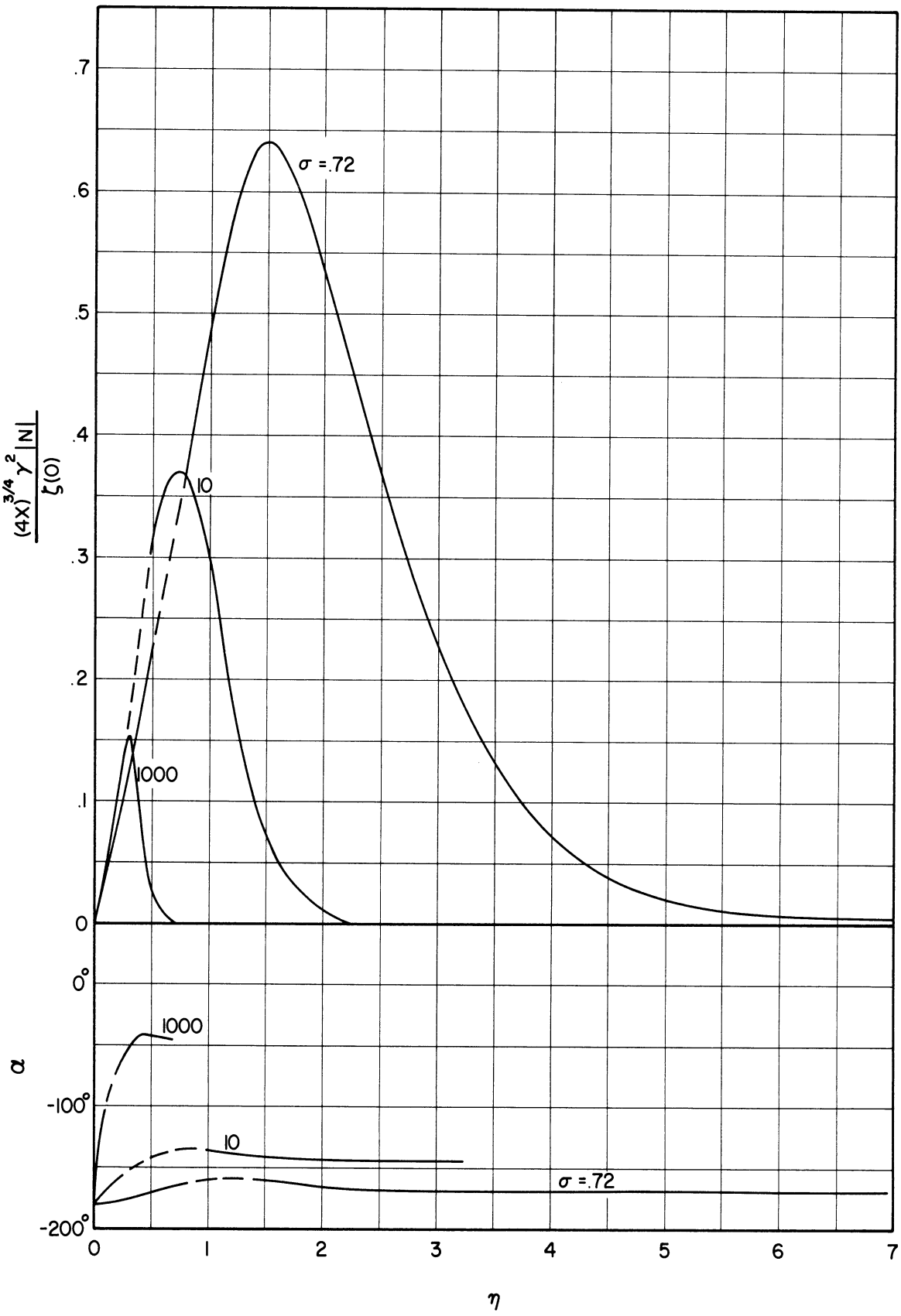

Figure 14. Magnitude and Phase of the Temperature Perturbations for $\gamma = 10$.

$$\left(\frac{\partial N}{\partial y}\right)_W = \frac{\zeta(0)\, H'(0)}{\gamma^2\,(4x)} \left[\frac{2-\sigma-\sqrt{\sigma}}{(1-\sigma)(1+\sqrt{\sigma})}\right] \tag{2.45b}$$

if $\sigma \neq 1$.

It can be seen from these equations that since $H'(0)$ is negative, $(\partial N/\partial y)_W$ is negative also for all Prandtl numbers. This is to be expected on the basis of the 180° phase lag in the temperature oscillations near the wall.

Solutions for Low Values of $\omega\sqrt{4x}$

The previous section was devoted to the finding of asymptotic solutions for large values of the variable $\gamma = \omega\sqrt{4x}$. In this section solutions will be obtained for low values of γ using the integral method. In order to do this some manipulations must be performed on Equations (2.21).

The terms $\left[\frac{\partial\psi_0}{\partial y}\frac{\partial^2 M}{\partial y\,\partial x} + \frac{\partial^2 M}{\partial x\,\partial y}\frac{\partial M}{\partial y}\right]$ are replaced by $\frac{\partial}{\partial x}\left(\frac{\partial\psi_0}{\partial y}\frac{\partial M}{\partial y}\right)$ and $\left[\frac{\partial\psi_0}{\partial y}\frac{\partial N}{\partial x} - \frac{\partial\psi_0}{\partial x}\frac{\partial N}{\partial y} + \frac{\partial T_0}{\partial x}\frac{\partial M}{\partial y} - \frac{\partial T_0}{\partial y}\frac{\partial M}{\partial x}\right]$ is rewritten as $\left[\frac{\partial}{\partial x}\left(N\,\partial\psi_0/\partial y + T_0\,\partial M/\partial y\right) - \partial/\partial y\left(N\,\partial\psi_0/\partial x + T_0\,\partial M/\partial x\right)\right]$. Making these replacements in Equations (2.21) and integrating with respect to y from the wall to infinity yields

$$i\omega M_\infty + \int_0^\infty \frac{\partial}{\partial x}\left(\frac{\partial\psi_0}{\partial y}\frac{\partial M}{\partial y}\right)dy - \int_0^\infty\left(\frac{\partial\psi_0}{\partial x}\frac{\partial^2 M}{\partial y^2} + \frac{\partial^2\psi_0}{\partial y^2}\frac{\partial M}{\partial x}\right)dy - \int_0^\infty N\,dy + \left(\frac{\partial^2 M}{\partial y^2}\right)_W = (4x)^{-3/4}\int_0^\infty \zeta(\eta)\,dy \tag{2.46a}$$

$$i\omega\int_0^\infty N\,dy + \frac{1}{\sigma}\left(\frac{\partial M}{\partial y}\right)_W + \int_0^\infty \frac{\partial}{\partial x}\left(N\frac{\partial\psi_0}{\partial y} + T_0\frac{\partial M}{\partial y}\right)dy - \int_0^\infty \frac{\partial}{\partial y}\left(N\frac{\partial\psi_0}{\partial x} + T_0\frac{\partial M}{\partial x}\right)dy = 0 \tag{2.46b}$$

Since $[N\,\partial\psi_0/\partial x + T_0\,\partial M/\partial x]$ is zero both at the wall and at infinity, the last integral in (2.46b) vanishes. The second integral in (2.46b) can be integrated by parts to give

$$-\int_0^\infty \left(\frac{\partial \psi_0}{\partial x} \frac{\partial^2 M}{\partial y^2} + \frac{\partial^2 \psi_0}{\partial y^2} \frac{\partial M}{\partial x} \right) dy = -\left[\frac{\partial \psi_0}{\partial x} \frac{\partial M}{\partial y} + \frac{\partial M}{\partial x} \frac{\partial \psi_0}{\partial y} \right]\Bigg|_0^\infty + \int_0^\infty \left(\frac{\partial \psi_0}{\partial y} \frac{\partial^2 M}{\partial x \partial y} + \frac{\partial M}{\partial y} \frac{\partial^2 \psi_0}{\partial x \partial y} \right) dy . \quad (2.47)$$

$\left[\frac{\partial \psi_0}{\partial x} \frac{\partial M}{\partial y} + \frac{\partial M}{\partial x} \frac{\partial \psi_0}{\partial y} \right]$ is zero both at the wall and at infinity while $\left(\partial\psi_0/\partial y \; \partial^2 M/\partial x \partial y + \partial M/\partial y \; \partial^2 \psi_0/\partial x \partial y \right)$ can be written as $\partial/\partial x \left(\partial\psi_0/\partial y \; \partial M/\partial y \right)$. Thus,

$$-\int_0^\infty \left(\frac{\partial \psi_0}{\partial x} \frac{\partial^2 M}{\partial y^2} + \frac{\partial^2 \psi_0}{\partial y^2} \frac{\partial M}{\partial x} \right) dy = \int_0^\infty \frac{\partial}{\partial x} \left(\frac{\partial \psi_0}{\partial y} \frac{\partial M}{\partial y} \right) dy . \quad (2.48)$$

Equations (2.46) now become

$$i\omega M_\omega + 2\int_0^\infty \frac{\partial}{\partial x}\left(\frac{\partial \psi_0}{\partial y} \frac{\partial M}{\partial y} \right) dy - \int_0^\infty N\, dy + \left(\frac{\partial^2 M}{\partial y^2} \right)_W = (4x)^{-3/4} \int_0^\infty S(\eta)\, dy \quad (2.49a)$$

$$i\omega \int_0^\infty N\, dy + \frac{1}{\sigma} \left(\frac{\partial N}{\partial y} \right)_W + \int_0^\infty \frac{\partial}{\partial x} \left(N \frac{\partial \psi_0}{\partial y} + T_0 \frac{\partial M}{\partial y} \right) dy = 0 . \quad (2.49b)$$

By Leibnitz's rule partial derivatives with respect to x can be taken outside the integral signs giving

$$i\omega M_\omega + 2\frac{\partial}{\partial x} \int_0^\infty \frac{\partial \psi_0}{\partial y} \frac{\partial M}{\partial y}\, dy - \int_0^\infty N\, dy + \left(\frac{\partial^2 M}{\partial y^2} \right)_W = (4x)^{-3/4} \int_0^\infty S(\eta)\, dy \quad (2.50a)$$

$$i\omega \int_0^\infty N\, dy + \frac{1}{\sigma} \left(\frac{\partial N}{\partial y} \right)_W + \frac{\partial}{\partial x} \int_0^\infty \left(N \frac{\partial \psi_0}{\partial y} + T_0 \frac{\partial M}{\partial y} \right) dy = 0 . \quad (2.50b)$$

Equations (2.50) represent the integral form of Equations (2.21).

Solutions have been obtained in the previous section for large values of γ which implies that ω is large also since $0 \leq x \leq 1$. Consider now the opposite extreme, that is, the case of $\omega = 0$. For this condition Equations (2.50) become

$$2\frac{\partial}{\partial x} \int_0^\infty \frac{\partial \psi_0}{\partial y} \frac{\partial M}{\partial y}\, dy - \int_0^\infty N\, dy + \left(\frac{\partial^2 M}{\partial y^2} \right)_W = (4x)^{-3/4} \int_0^\infty S(\eta)\, dy \quad (2.51a)$$

$$\frac{\partial}{\partial x}\int_0^\infty \left(N\frac{\partial u_0}{\partial y} + T_0\frac{\partial M}{\partial y}\right)dy + \frac{1}{\sigma}\left(\frac{\partial N}{\partial y}\right)_W = 0 . \qquad (2.51b)$$

It should be pointed out at this point that since Equations (2.51) are valid for $\omega = 0$, this also implies that γ is necessarily zero also. Solutions to Equations (2.51) will therefore be valid for $\gamma = 0$, the opposite extreme to the asymptotic solutions obtained for large values of γ in the previous section.

The present problem can be interpreted as a boundary layer subjected to a steady force field g_o acting either toward the wall or away from the wall depending on whether g_o is taken to be positive or negative. The first case can be realized physically in the case of a cylindrical tank with heated walls rotating about its axis at constant speed. The enclosed fluid would have a free convection boundary layer along the wall subjected to a transverse force field acting toward the wall due to centrifugal forces as shown by the sketch in Figure 15. One limitation is that the radius of the tank must be large compared with the boundary layer thickness δ in order that the force field g_o may be considered approximately constant across the entire width of the layer. The second case can be realized in the case of rotating cylindrical container with inner and outer concentric walls as shown in Figure 16. If the inner wall is heated, the boundary layer adjacent to its surface would be subjected to a force field acting normal to the wall in the direction away from the wall.

In both cases, in order to successfully simulate the problem, it is necessary that no rotational slippage occur between the fluid and the container walls. That is, the fluid must rotate with the container

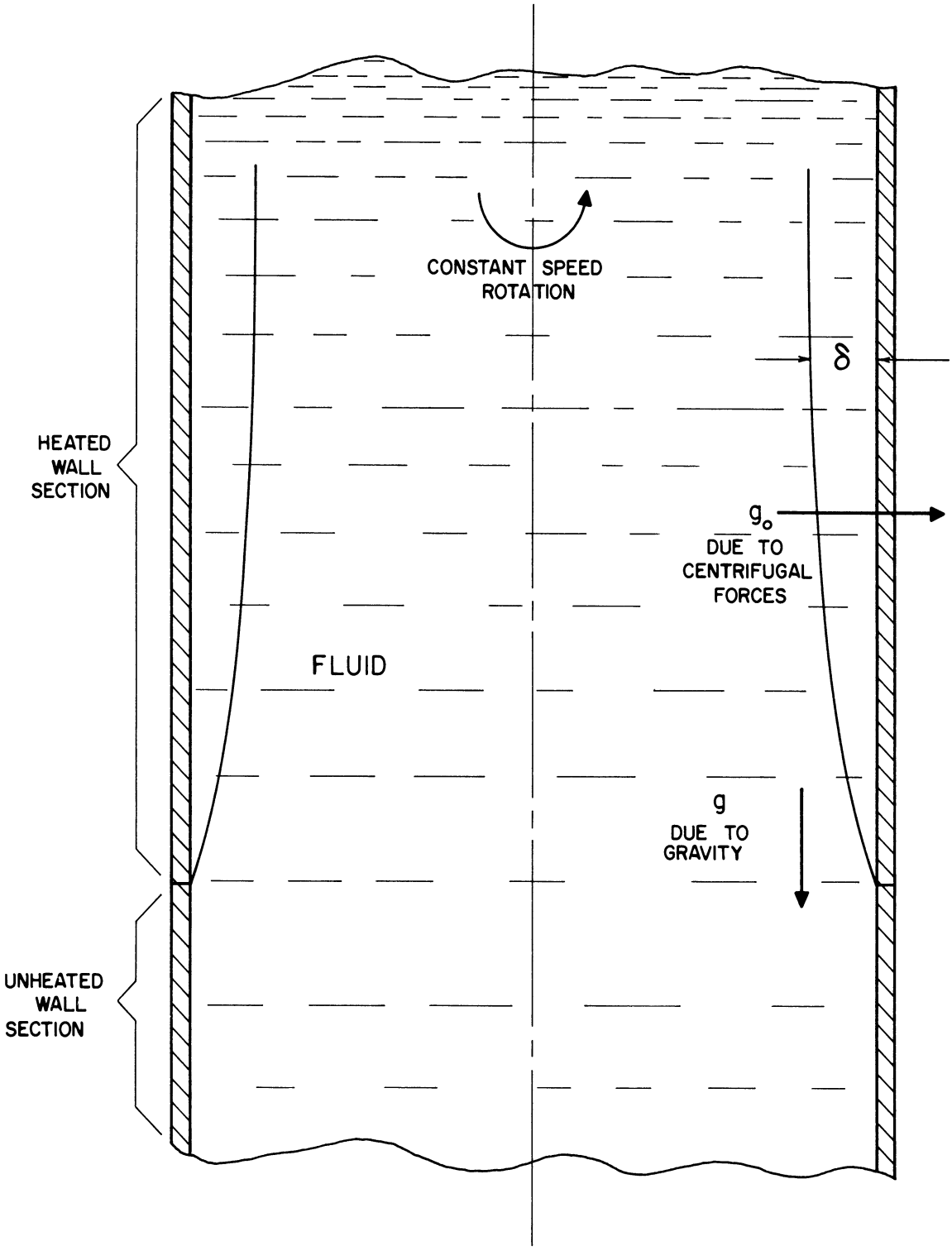

Figure 15. Sketch Illustrating Wall Acceleration at Zero Frequency.

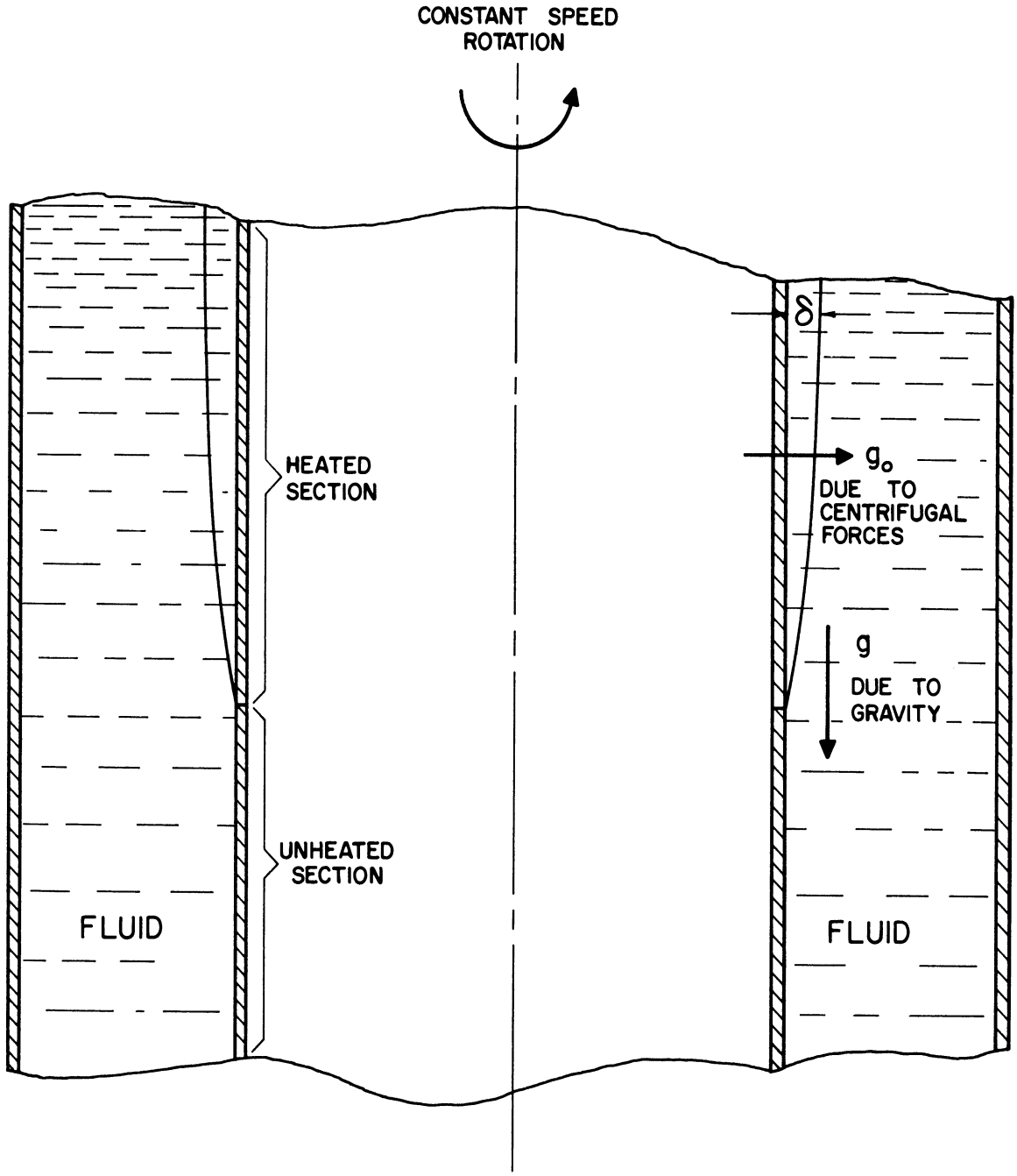

Figure 16. Sketch Illustrating Wall Acceleration at Zero Frequency.

at constant speed as a rigid body with the exception of the free convection boundary layer flow.

Solutions to this steady problem are now sought in the form

$$M = (4x)^r \; R_o \; F(\eta) \tag{2.52a}$$

$$N = (4x)^s \; S_o \; \eta \; H'(\eta) \tag{2.52b}$$

R_o, S_o, r, and s are constants to be determined. Plots of $F'(\eta)$ and $\eta H'(\eta)$ are given in Figures 4 and 17, and tabulated values are given in Appendices Ia and Ic respectively. The functions $F(\eta)$ and $\eta H'(\eta)$ satisfy all boundary conditions on M and N. In addition, these functions will give to the perturbations the proper range of η which is especially important when the Prandtl number is not close to unity. For example, it can be seen from Figures 4 and 5 that if $\sigma = 10$, the velocity boundary layer has thickness of about 5 while the temperature layer has a thickness of only about 2. For this Prandtl number then, the velocity perturbations may be expected to occur in the range $0 < \eta < 5$ while those of temperature may be expected to occur in the range $0 < \eta < 2$. The form of Equations (2.52) are in accordance with these observations. They can be illustrated more clearly, perhaps, by studying Figures 4 and 17 which show the velocity function $F'(\eta)$ and the temperature function $\eta H'(\eta)$ respectively. One additional point is worth mentioning concerning the fact that $(\partial^2 N/\partial y^2)_w = 0$ from Equation (2.21b). This condition is also satisfied by (2.52b) since

$$\frac{d}{d\eta^2}\left[\eta H'(\eta)\right] = \eta H'''(\eta) + 2 H''(\eta) \tag{2.53}$$

At the wall this quantity is zero since $H''(0) = 0$ from Equation (2.18b).

Equations (2.52), together with the functions $\psi_o = (4x)^{3/4} F(\eta)$ and $T_o = H(\eta)$, are now entered into Equations (2.51) to give

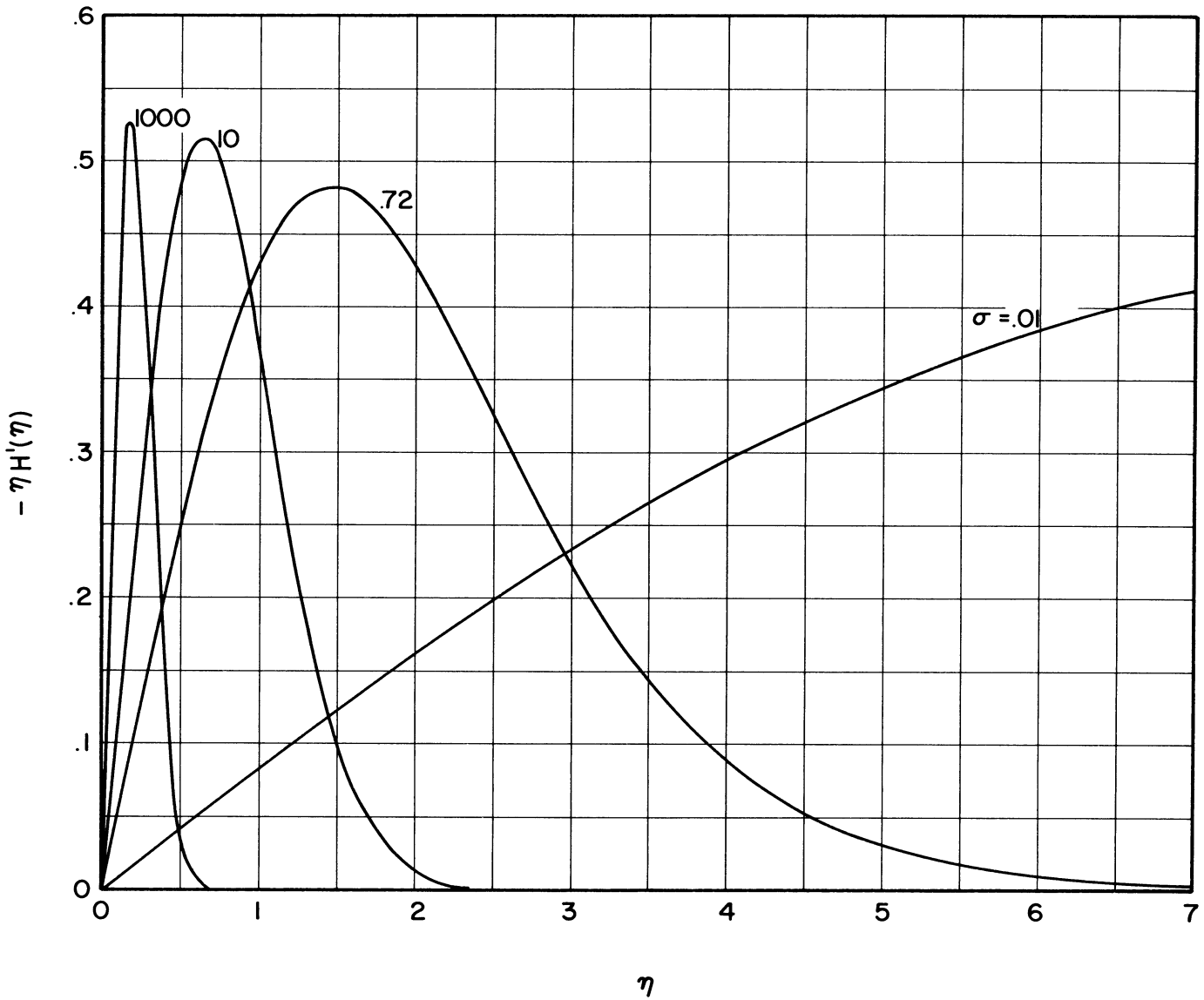

Figure 17. The Temperature Function.

$$2\frac{\partial}{\partial x}\int_0^\infty R_0\,(4x)^{r+\frac{1}{4}}\left[F'(\eta)\right]^2 dy - \int_0^\infty (4x)^s\, S_0\,\eta\, H'(\eta)\, dy$$
$$+\; R_0\,(4x)^{r-\frac{1}{2}}\, F''(0) \;=\; (4x)^{-3/4}\int_0^\infty \zeta(\eta)\, dy \tag{2.54a}$$

$$\frac{\partial}{\partial x}\int_0^\infty \left[(4x)^{s+\frac{1}{2}} S_0\,\eta\, H'(\eta) F'(\eta) + (4x)^{r-\frac{1}{4}} R_0\, H(\eta)\, F'(\eta)\right] dy$$
$$+\; \frac{1}{\sigma}\,(4x)^{s-\frac{1}{4}} S_0\, H'(0) \;=\; 0. \tag{2.54b}$$

Since the integrations are to be carried out with respect to y and with x held constant, dy can be replaced by $(4x)^{1/4}\,d\eta$, all powers of x can be taken outside the integral signs, and the integrations can be carried out with respect to η alone. Equations (2.54) now become

$$2R_0\int_0^\infty \left[F'(\eta)\right]^2 d\eta\,\frac{d}{dx}(4x)^{r+\frac{1}{2}} - S_0\int_0^\infty \eta\, H'(\eta)\, d\eta\,(4x)^{s+\frac{1}{4}}$$
$$+\; R_0\, F''(0)\,(4x)^{r-\frac{1}{2}} \;=\; (4x)^{-\frac{1}{2}}\int_0^\infty \zeta(\eta)\, d\eta \tag{2.55a}$$

$$S_0\int_0^\infty \eta\, H'(\eta)\, F'(\eta)\, d\eta\,\frac{d}{dx}(4x)^{s+3/4} + R_0\int_0^\infty H(\eta)\, F'(\eta)\, d\eta\,(4x)^r$$
$$+\; \frac{1}{\sigma}\, S_0\, H'(0)\,(4x)^{s-\frac{1}{4}} = 0. \tag{2.55b}$$

Carrying out the derivative operations yields

$$4R_0\,(2r+1)\,(4x)^{r-\frac{1}{2}}\int_0^\infty \left[F'(\eta)\right]^2 d\eta - S_0\,(4x)^{s+\frac{1}{4}}\int_0^\infty \eta\, H'(\eta)\, d\eta$$
$$+\; R_0\,(4x)^{r-\frac{1}{2}}\, F''(0) \;=\; (4x)^{-\frac{1}{2}}\int_0^\infty \zeta(\eta)\, d\eta \tag{2.56a}$$

$$S_0\,(4s+3)\,(4x)^{s-\frac{1}{4}}\int_0^\infty \eta\, H'(\eta)\, F'(\eta)\, d\eta$$
$$+\; 4R_0\, r\,(4x)^{r-1}\int_0^\infty H(\eta)\, F'(\eta)\, d\eta + S_0\,\frac{H'(0)}{\sigma}\,(4x)^{s-\frac{1}{4}} = 0. \tag{2.56b}$$

x can now be eliminated from both equations provided that $r = 0$ and $s = -3/4$. Entering these values into (2.56) gives

$$4R_0\int_0^\infty [F'(\eta)]^2 d\eta - S_0\int_0^\infty \eta\, H'(\eta)\, d\eta + R_0 F''(0) = \int_0^\infty \zeta(\eta)\, d\eta \tag{2.57a}$$

$$\frac{S_0 H'(0)}{\sigma} = 0 . \tag{2.57b}$$

Solving (2.57) for R_0 and S_0 gives the result that

$$R_0 = \frac{\int_0^\infty \zeta(\eta)\, d\eta}{F''(0) + 4\int_0^\infty [F'(\eta)]^2 d\eta} \tag{2.58a}$$

$$S_0 = 0. \tag{2.58b}$$

Finally Equations (2.52) are rewritten as

$$M = \left[\frac{\int_0^\infty \zeta(\eta)\, d\eta}{F''(0) + 4\int_0^\infty [F'(\eta)]^2 d\eta} \right] F(\eta) \tag{2.59a}$$

$$N = 0 . \tag{2.59b}$$

From (2.59b) it is seen that for the zero frequency case the temperature perturbations are zero everywhere even though the velocity field is altered in accordance with (2.59a). This can be easily reconciled, however, by the fact that the velocity perturbations occur along lines of constant η as shown by (2.59a), which are also lines of constant steady temperature by virtue of $T_0 = H(\eta)$. This argument gives strong support to the result given in (2.59b). It is recalled that Glauert[10] and Rott[25] obtained a similar result in their investigations as mentioned in Chapter I. The explanation in their case is essentially the same as that given here.

It is worth while to point out here that the large γ solutions given in the previous section represent the behavior of the boundary

layer when the perturbated convective effects are negligible in comparison with those of local acceleration and local time rate of change of energy. The solutions given by Equations (2.59) are valid when the reverse is true. This can be made more clear by recalling that Equations (2.59) satisfy Equations (2.51) which are the same as Equations (2.50) when time rates of change of velocity and temperature ignored. Consider now the case when these effects are small, but not negligible. It is clear that the magnitudes of these effects relative to the convective effects will depend on ω, and it is plausible that they will also depend on x. It is proposed that this dependency may be determined by a single variable now defined as $\lambda = \omega(4x)^m$ where m is a constant to be determined later.

It is obvious that the convective terms will dominate completely when $\lambda = 0$, and for this case the solutions are given by Equations (2.59). If λ is small, but not zero, it would seem reasonable to assume that solutions can be expressed as power series in λ expanded about $\lambda = 0$, a condition for which the solution is known. In this case Equations (2.52) are modified by power series in λ, and again taking $r = 0$ and $s = -3/4$, solutions are sought in the form

$$M = \left[R_0 + \sum_{n=1}^{\infty} R_n \lambda^n \right] F(\eta) \tag{2.60a}$$

$$N = (4x)^{-3/4} \left[S_0 + \sum_{n=1}^{\infty} S_n \lambda^n \right] \eta H'(\eta) . \tag{2.60b}$$

Entering these relations together with $\psi_0 = (4x)^{3/4} F(\eta)$ and $T_0 = H(\eta)$ into Equations (2.50) gives

$$i\omega F(\infty)\sum_{n=0}^{\infty} R_n \lambda^n + 2\frac{\partial}{\partial x}\int_0^{\infty}\sum_{n=0}^{\infty} R_n \lambda^n (4x)^{1/4}\left[F'(\eta)\right]^2 dy \tag{2.61a}$$

$$-\int_0^{\infty}(4x)^{-3/4}\sum_{n=0}^{\infty} S_n \lambda^n \eta\, H'(\eta)\, dy + (4x)^{-1/2}\sum_{n=0}^{\infty} R_n \lambda^n F''(0)$$

$$= (4x)^{-3/4}\int_0^{\infty}\zeta(\eta)\, dy$$

$$i\omega\int_0^{\infty}(4x)^{-3/4}\sum_{n=0}^{\infty} S_n \lambda^n \eta\, H'(\eta) dy + \frac{\partial}{\partial x}\int_0^{\infty}(4x)^{-1/4}\sum_{n=0}^{\infty} S_n \lambda^n \eta\, H'(\eta)\, F'(\eta)\, dy \tag{2.61b}$$

$$+\frac{\partial}{\partial x}\int_0^{\infty}(4x)^{-1/4}\sum_{n=0}^{\infty} R_n \lambda^n H(\eta)\, F'(\eta)\, dy + \frac{H'(0)}{\sigma}(4x)^{-1}\sum_{n=0}^{\infty} S_n \lambda^n = 0.$$

Since the integration is done with x held constant, dy can be replaced by $(4x)^{1/4}d\eta$, all powers of x and λ can be taken outside the integral signs, and the integrations can be carried out with respect to η. Equations (2.61) now become

$$i\omega F(\infty)\sum_{n=0}^{\infty} R_n \lambda^n + 2\int_0^{\infty}\left[F'(\eta)\right]^2 d\eta\, \frac{\partial}{\partial x}\left[\sqrt{4x}\sum_{n=0}^{\infty} R_n \lambda^n\right] \tag{2.62a}$$

$$-\int_0^{\infty}\eta\, H'(\eta)\, d\eta\, (4x)^{-1/2}\sum_{n=0}^{\infty} S_n \lambda^n + F''(0)\,(4x)^{-1/2}\sum_{n=0}^{\infty} R_n \lambda^n$$

$$= (4x)^{-1/2}\int_0^{\infty}\zeta(\eta)\, d\eta$$

$$i\omega\int_0^{\infty}\eta\, H'(\eta)\, d\eta\, (4x)^{-1/2}\sum_{n=0}^{\infty} S_n \lambda^n + \int_0^{\infty}\eta\, H'(\eta)\, F'(\eta)\, d\eta\, \frac{\partial}{\partial x}\sum_{n=0}^{\infty} S_n \lambda^n \tag{2.62b}$$

$$+\int_0^{\infty} H(\eta)\, F'(\eta)\, d\eta\, \frac{\partial}{\partial x}\sum_{n=0}^{\infty} R_n \lambda^n + \frac{H'(0)}{\sigma}(4x)^{-1}\sum_{n=0}^{\infty} S_n \lambda^n = 0$$

Since $\lambda = \omega(4x)^m$, $\dfrac{\partial\lambda}{\partial x} = 4m\omega(4x)^{m-1} = \dfrac{4m\lambda}{(4x)}$.

Now, $\dfrac{\partial}{\partial x}\displaystyle\sum_{n=0}^{\infty} R_n \lambda^n = \frac{\partial}{\partial\lambda}\left[\sum_{n=0}^{\infty} R_n \lambda^n\right]\frac{\partial\lambda}{\partial x} = \frac{4m}{(4x)}\sum_{n=0}^{\infty} n R_n \lambda^n$,

and similarly, $\dfrac{\partial}{\partial x}\displaystyle\sum_{n=0}^{\infty} S_n \lambda^n = \frac{4m}{4x}\sum_{n=0}^{\infty} n S_n \lambda^n$.

With this information the derivative operations in Equations (2.62) are carried out giving

$$
\begin{aligned}
& i F(\infty)(4x)^{-m} \sum_{n=0}^{\infty} R_n \lambda^{n+1} + 4\int_0^{\infty} [F'(\eta)]^2 d\eta \, (4x)^{-\frac{1}{2}} \sum_{n=0}^{\infty} R_n \lambda^n \\
& + 8m \int_0^{\infty} [F'(\eta)]^2 d\eta \, (4x)^{-\frac{1}{2}} \sum_{n=0}^{\infty} n R_n \lambda^n \\
& - \int_0^{\infty} \eta H'(\eta) d\eta \, (4x)^{-\frac{1}{2}} \sum_{n=0}^{\infty} S_n \lambda^n + F''(0)(4x)^{-\frac{1}{2}} \sum_{n=0}^{\infty} R_n \lambda^n = (4x)^{-\frac{1}{2}} \int_0^{\infty} \zeta(\eta) d\eta
\end{aligned}
\tag{2.63a}
$$

$$
\begin{aligned}
& i \int_0^{\infty} \eta H'(\eta) d\eta \, (4x)^{-m-\frac{1}{2}} \sum_{n=0}^{\infty} S_n \lambda^{n+1} + 4m(4x)^{-1} \int_0^{\infty} \eta H'(\eta) F'(\eta) d\eta \sum_{n=0}^{\infty} n S_n \lambda^n \\
& + 4m(4x)^{-1} \int_0^{\infty} H(\eta) F'(\eta) d\eta \sum_{n=0}^{\infty} n R_n \lambda^n + \frac{H'(0)}{\sigma} (4x)^{-1} \sum_{n=0}^{\infty} S_n \lambda^n = 0.
\end{aligned}
\tag{2.63b}
$$

It is readily seen that x can be eliminated from both (2.63a) and (2.63b) provided that m = 1/2. In this case $\lambda = \omega\sqrt{4x} = \gamma$ so that Equations (2.60) now become

$$M = F(\eta) \sum_{n=0}^{\infty} R_n \gamma^n \tag{2.64a}$$

$$N = (4x)^{-3/4} \eta H'(\eta) \sum_{n=0}^{\infty} S_n \gamma^n. \tag{2.64b}$$

The solutions are now expressed as power series expansions in γ about

$\gamma = 0$ so that Equations (2.64) can be expected to be valid for small values of γ.

The conditions that $m = 1/2$ and $\gamma = \lambda$ are now entered into Equations (2.63) giving

$$i F(\infty) \sum_{n=0}^{\infty} R_n \gamma^{n+1} + 4 \int_0^{\infty} \left[F'(\eta)\right]^2 d\eta \left[\sum_{n=0}^{\infty} R_n \gamma^n + \sum_{n=0}^{\infty} n R_n \gamma^n\right] \tag{2.65a}$$

$$- \int_0^{\infty} \eta H'(\eta)\, d\eta \sum_{n=0}^{\infty} S_n \gamma^n + F''(0) \sum_{n=0}^{\infty} R_n \gamma^n = \int_0^{\infty} \zeta(\eta)\, d\eta$$

$$i \int_0^{\infty} \eta H'(\eta)\, d\eta \sum_{n=0}^{\infty} S_n \gamma^{n+1} + 2 \int_0^{\infty} \eta H'(\eta) F'(\eta)\, d\eta \sum_{n=0}^{\infty} n S_n \gamma^n \tag{2.65b}$$

$$+ 2 \int_0^{\infty} H(\eta) F'(\eta)\, d\eta \sum_{n=0}^{\infty} n R_n \gamma^n + \frac{H'(0)}{\sigma} \sum_{n=0}^{\infty} S_n \gamma^n = 0 .$$

For the sake of simplicity it is convenient to redefine some of the quantities appearing in Equations (2.65). These new definitions are

$$P_0 = \int_0^{\infty} \zeta(\eta)\, d\eta \tag{2.66a}$$

$$P_1 = F''(0) \tag{2.66b}$$

$$P_2 = \int_0^{\infty} \left[F'(\eta)\right]^2 d\eta \tag{2.66c}$$

$$P_3 = F(\infty) \tag{2.66d}$$

$$P_4 = -2\int_0^\infty \eta\, H'(\eta)\, F'(\eta)\, d\eta \tag{2.66e}$$

$$P_5 = -H'(0)/3\sigma. \tag{2.66f}$$

In addition, it can be shown that $\int_0^\infty H(\eta)F'(\eta)d\eta = P_5$ and $-\int_0^\infty \eta H'(\eta)d\eta = (P_1 + 5P_2)$. The details of these relations are given in Appendix I-d along with tabulated values for different Prandtl numbers. Equations (2.65) are now rewritten as

$$i P_3 \sum_{n=0}^{\infty} R_n \gamma^{n+1} + 4 P_2 \sum_{n=0}^{\infty} (n+1) R_n \gamma^n + (P_1 + 5P_2) \sum_{n=0}^{\infty} S_n \gamma^n + P_1 \sum_{n=0}^{\infty} R_n \gamma^n = P_0 \tag{2.67a}$$

$$-i (P_1 + 5P_2) \sum_{n=0}^{\infty} S_n \gamma^{n+1} - P_4 \sum_{n=0}^{\infty} n S_n \gamma^n + 2 P_5 \sum_{n=0}^{\infty} n R_n \gamma^n - 3 P_5 \sum_{n=0}^{\infty} S_n \gamma^n = 0 \; . \tag{2.67b}$$

The quantities $\sum_{n=0}^{\infty} R_n\gamma^{n+1}$ and $\sum_{n=0}^{\infty} S_n\gamma^{n+1}$ can be replaced by $\sum_{n=1}^{\infty} R_{n-1}\gamma^n$ and $\sum_{n=1}^{\infty} S_{n-1}\gamma^n$. Also, since R_n and S_n do not exist for $n<0$, the lower indices of the summations can be changed from one to zero resulting in

$$\sum_{n=0}^{\infty} R_n \gamma^{n+1} = \sum_{n=0}^{\infty} R_{n-1} \gamma^n \quad \text{and} \quad \sum_{n=0}^{\infty} S_n \gamma^{n+1} = \sum_{n=0}^{\infty} S_{n-1} \gamma^n .$$

Making these modifications in (2.67) yields

$$\sum_{n=0}^{\infty}\left\{\left[P_1+4(n+1)P_2\right]R_n+i\,P_3\,R_{n-1}+(P_1+5P_2)S_n\right\}\gamma^n=P_0 \qquad (2.68a)$$

$$\sum_{n=0}^{\infty}\left\{(3P_5+P_4\,n)S_n+i\,(P_1+5P_2)\,S_{n-1}-2n\,P_5\,R_n\right\}\gamma^n=0 \qquad (2.68b)$$

The coefficients of all powers of γ must be zero except for that of γ° in Equation (2.68a) which must be equal to P_0. These conditions can be restated as

$$\left[P_1+4(n+1)P_2\right]R_n+i\,P_3\,R_{n-1}+(P_1+5P_2)S_n=\delta_{no}\,P_0 \qquad (2.69a)$$

$$(3P_5+P_4\,n)\,S_n+i\,(P_1+5P_2)S_{n-1}-2\,P_5\,n\,R_n=0\,. \qquad (2.69b)$$

δ_{no} is the Kronecker Delta δ_{ij} defined so that $\delta_{ij}=1$ if $i=j$, and $\delta_{ij}=0$ if $i\neq j$. Solution of (2.69a) for S_n gives

$$S_n=\frac{\delta_{no}P_0-\left\{\left[P_1+4(n+1)P_2\right]R_n+i\,P_3\,R_{n-1}\right\}}{P_1+5P_2}\,. \qquad (2.70a)$$

This expression can also be written as

$$S_{n-1}=\frac{\delta_{n1}\,P_0-\left\{\left[P_1+4P_2\,n\right]R_{n-1}+i\,P_3\,R_{n-2}\right.}{P_1+5P_2}\,. \qquad (2.70b)$$

Substituting (2.70a) and (2.70b) into (2.69b) and solving for R_n gives the recursion formula for R_n as

$$R_n=\frac{\left\{\begin{array}{l}3P_0P_5\delta_{no}+i\,P_0(P_1+5P_2)\delta_{n1}+P_3(P_1+5P_2)R_{n-2}\\ -i\left\{\left[P_3P_4+4P_2(P_1+5P_2)\right]n+\left[3P_3P_5+P_1(P_1+5P_2)\right]\right\}R_{n-1}\end{array}\right\}}{4P_2P_4\,n^2+\left[P_1P_4+4P_2P_4+12P_2P_5+2P_5(P_1+5P_2)\right]n+3P_5(P_1+4P_2)}\,. \qquad (2.71)$$

It can be seen from Equation (2.71) that $R_o = P_o/(P_1 + 4P_2) = \int_0^\infty \zeta(\eta)\, d\eta \Big/ \left[F''(0) + 4\int_0^\infty [F'(\eta)]^2 d\eta\right]$ which agrees with (2.58a). Entering this value of R_o into (2.70a) gives $S_o = 0$ which agrees with (2.58b). Equation (2.71) can be written in a more concise form by defining the following parameters.

$$Q_0 = \frac{3 P_0 P_5}{4 P_2 P_4} \tag{2.72a}$$

$$Q_1 = \frac{P_0 (P_1 + 5 P_2)}{4 P_2 P_4} \tag{2.72b}$$

$$Q_2 = \frac{P_3 (P_1 + 5 P_2)}{4 P_2 P_4} \tag{2.72c}$$

$$Q_3 = \frac{P_3 P_4 + 4 P_2 (P_1 + 5 P_2)}{4 P_2 P_4} \tag{2.72d}$$

$$Q_4 = \frac{3 P_3 P_5 + P_1 (P_1 + 5 P_2)}{4 P_2 P_4} \tag{2.72e}$$

$$Q_5 = \frac{P_1 P_4 + 12 P_2 P_5 + 2 P_5 (P_1 + 5 P_2)}{4 P_2 P_4} \tag{2.72f}$$

$$Q_6 = \frac{3 P_5 (P_1 + 4 P_2)}{4 P_2 P_4} \quad . \tag{2.72g}$$

Tabulated values of these parameters are given in Appendix Ie for several Prandtl numbers. In terms of these new definitions Equation (2.71) becomes

$$R_n = \frac{\delta_{n0} Q_0 + i Q_1 \delta_{n1} + Q_2 R_{n-2} - i (Q_3 n + Q_4) R_{n-1}}{n^2 + (Q_5 + 1) n + Q_6} \quad . \tag{2.73}$$

The limiting form of (2.73) as n increases without limit is

$$R_n = -i\, Q_3\, R_{n-1}/n \quad , \tag{2.74}$$

and the ratio of the n-th term to the preceding term in the series $\sum_{n=0}^{\infty} R_n\gamma^n$ is $-\, iQ_3\gamma/n$. Now, taking the limit as n increases gives

$$\lim_{n\to\infty} \left| i\, Q_3\, \gamma/n \right| = 0 \tag{2.75}$$

for $0 \leq \gamma < \infty$. Thus, the series $\sum_{n=0}^{\infty} R_n\gamma^n$ converges for all values of γ. The limiting forms of (2.70a) and (2.70b) as n increases are

$$S_n = \frac{-\left[4\, P_2\, n\, R_n + i\, P_3\, R_{n-1}\right]}{P_1 + 5P_2} \tag{2.76a}$$

$$S_{n-1} = \frac{-\left[4P_2\, n\, R_{n-1} + i\, P_3\, R_{n-2}\right]}{P_1 + 5P_2} \quad . \tag{2.76b}$$

Also, since $R_n \to \frac{-iP_3R_{n-1}}{n}$, $R_{n-1} \to \frac{-iP_3R_{n-2}}{n}$, and $R_n \to -(P_3/n)^2R_{n-2}$. Applying this information it is found that

$$\lim_{n\to\infty} \left| \frac{S_n\, \gamma^n}{S_{n-1}\, \gamma^{n-1}} \right| = \lim_{n\to\infty} \left| \frac{P_3\, \gamma}{i\, n} \right| = 0 \tag{2.77}$$

for $0 \leq \gamma < \infty$. Thus, the series $\sum_{n=0}^{\infty} S_n\gamma^n$ converges for all values of γ also.

Inspection of (2.73) shows that R_n is real if n is even, but imaginary if n is odd. Applying these conditions to (2.70a) shows that S_n behaves in the same way. This makes it possible to write the magnitude and phase of M as

$$|M| = F(\eta)\sqrt{\left(R_0 + R_2\gamma^2 + R_4\gamma^4 + \cdots\right)^2 + \left(\frac{R_1\gamma + R_3\gamma^2 + R_5\gamma^5 + \cdots}{i}\right)^2} \tag{2.78a}$$

$$\phi = \operatorname{Arc\,tan}\left[\frac{R_1\gamma + R_3\gamma^3 + R_5\gamma^5 + \cdots}{i\left(R_0 + R_2\gamma^2 + R_4\gamma^4 + \cdots\right)}\right] , \tag{2.78b}$$

while the magnitude and phase of N can be expressed as

$$N = -\frac{\omega \eta H'(\eta)}{(4x)^{1/4}\,\gamma}\sqrt{\left(S_2\gamma^2+S_4\gamma^4+S_6\gamma^6+\cdots\right)^2+\left(\frac{S_1\gamma+S_3\gamma^3+S_5\gamma^5+\cdots}{i}\right)} \quad (2.79a)$$

$$\alpha = \operatorname{Arc\,tan}\left[\frac{S_1\gamma+S_3\gamma^3+S_5\gamma^5+\cdots}{i\left(S_2\gamma^2+S_4\gamma^4+S_6\gamma^6+\cdots\right)}\right]-\pi \quad . \quad (2.79b)$$

In the next section some attention will be given to the oscillating wall shear stress and temperature gradient. These are obtained by differentiation of Equations (2.78a) and (2.79a) and are written as

$$\left|\left(\frac{\partial^2 M}{\partial \eta^2}\right)_W\right| = F''(0)\sqrt{\left(R_0+R_2\gamma^2+R_4\gamma^4+\cdots\right)^2+\left(\frac{R_1\gamma+R_3\gamma^3+R_5\gamma^5+\cdots}{i}\right)^2} \quad (2.80a)$$

$$\left|\left(\frac{\partial N}{\partial y}\right)_W\right| = -\frac{\omega H'(0)}{\sqrt{4x}\,\gamma}\sqrt{\left(S_2\gamma^2+S_4\gamma^4+S_6\gamma^6+\cdots\right)^2+\left(\frac{S_1\gamma+S_3\gamma^3+S_5\gamma^5+\cdots}{i}\right)^2} \quad (2.80b)$$

The first few values of the coefficients R_n and S_n have been calculated from Equations (2.73) and (2.70a) and are given in Appendices If and Ig for several Prandtl numbers. Using these values the magnitudes and phase angles of M and N have been calculated as functions of γ from Equations (2.78) and (2.79) above. Plots of these functions are given in Figures 18 and 19.

Figure 18 shows that the oscillating stream function exhibits a very slight peaking phenomena at small values of γ while approaching the value given in (2.58a) at $\gamma = 0$. This point represents the limiting condition when the local acceleration of the fluid has no effect, that is, either the steady or quasi-steady case. Here the velocity perturbations are completely in phase with the applied pressure gradient as expected.

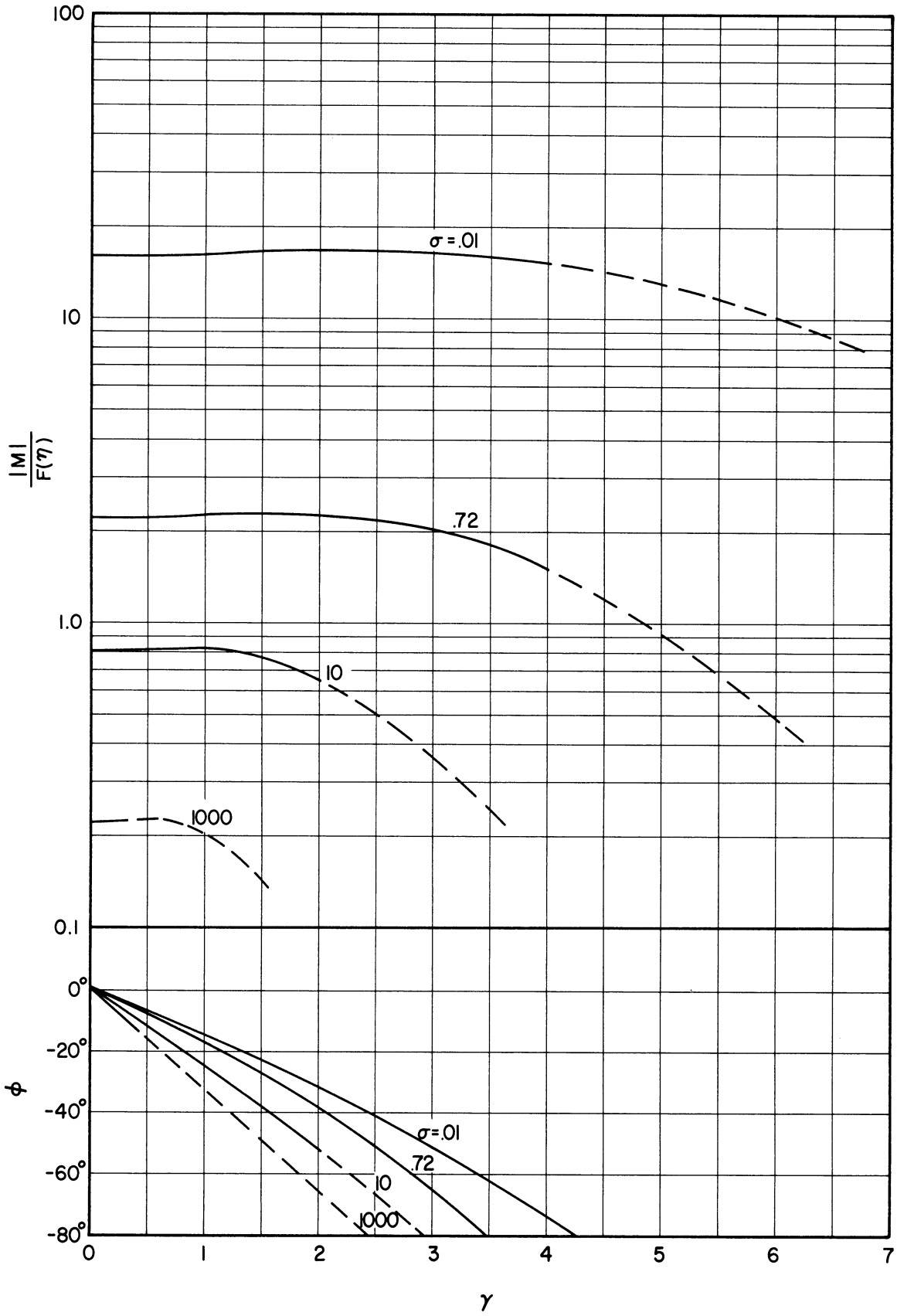

Figure 18. Magnitude and Phase of the Oscillating Stream Function for Small Values of γ.

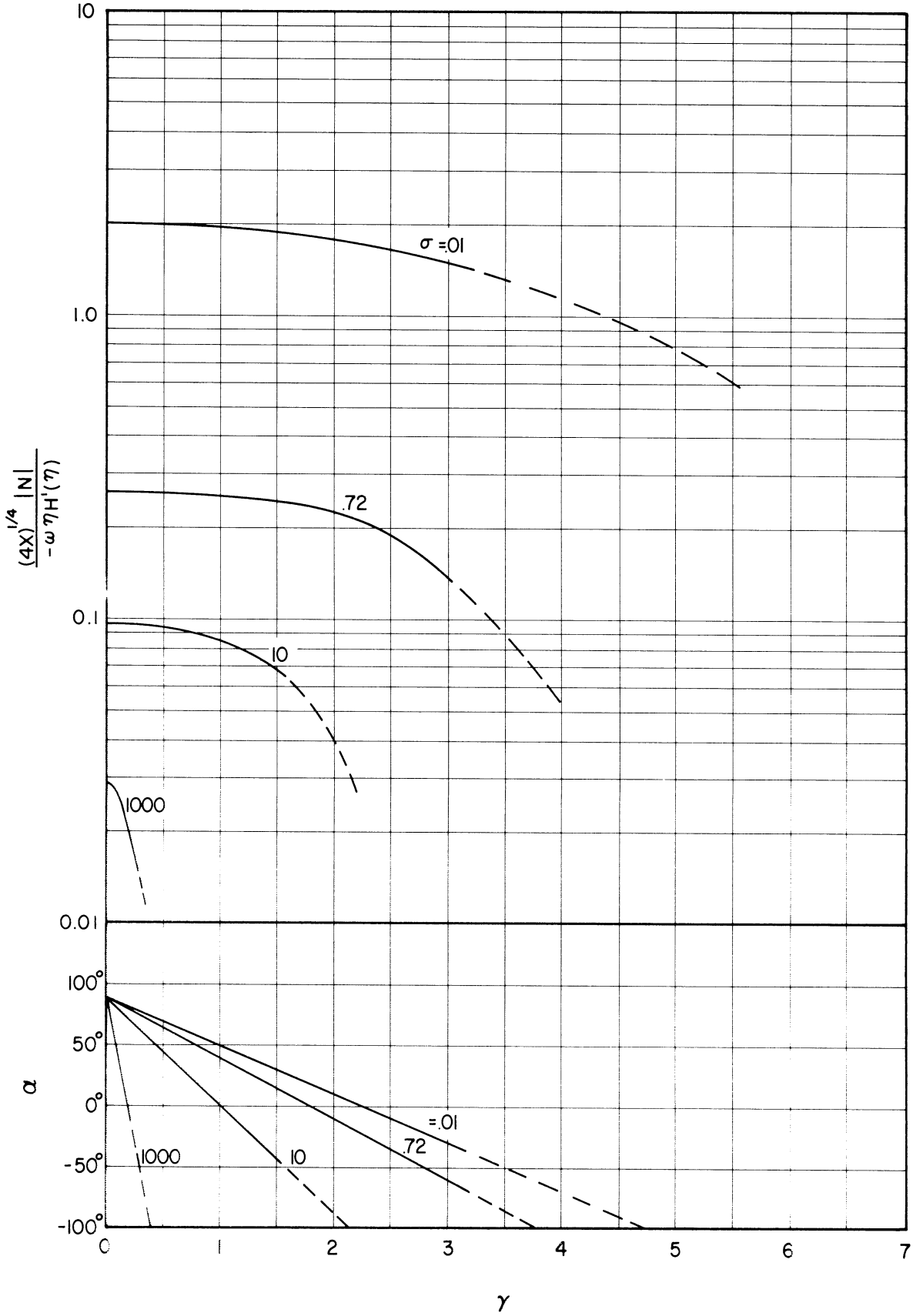

Figure 19. Magnitude and Phase of the Temperature Perturbations for Small Values of γ.

As γ increases, the convective processes have less effect so that the oscillating pressure gradient tends to be balanced more and more by local acceleration. This produces a phase lag and a decrease in the magnitude of the oscillating stream function. This behavior is to be expected on the basis of Equation (2.28) which shows that the stream function drops off with the reciprocal of γ and lags at about 90° at higher values of γ.

Figure 19 shows that the temperature perturbations are zero in the steady case as indicated by (2.59b). Since this is true, only the lagging component of velocity produces temperature perturbations so that their phase is 90° with respect to the oscillating pressure gradient in the limit as γ approaches zero. As γ increases, the tendency to lag with an eventual decrease in magnitude occurs. This behavior is to be expected since the local time rates of change of momentum and energy become relatively more important as γ becomes larger. It also is consistent with the high γ solutions which decrease with the reciprocal of γ^2 and lag at about 180° as γ becomes very large.

An integral method has been used in this section to obtain the velocity and temperature perturbations for low values of γ. An alternate method for obtaining the ocrresponding exact solutions is given in Appendix III.

Comparison of Solutions Based on the Wall Shear Stress and Temperature Gradient

The behavior of the solutions at high and low values of γ has been shown to be qualitatively consistent by the discussion in the latter part of the last section. It would be desirable, however, to plot the solutions as functions of γ to see if corresponding pairs of

solutions really approach each other in a satisfactory manner in the intermediate region of γ. This is not convenient in general since too many variables are involved, but η is eliminated if the oscillating wall shear stress and temperature gradient are considered. Fortunately, these quantities can be represented as functions of γ alone in each region. The oscillating wall shear stress is given by Equations (2.31b) and (2.80a) in the high and low regions respectively. Correspondingly, the fluctuating wall temperature gradient, and therefore the oscillating component of local heat transfer, is given by Equations (2.45) and (2.80b). Plots are given in Figures 20 and 21.

The solid lines were calculated from the equations while the dotted lines have been faired in to show the probable behavior in the intermediate region of γ. It can be seen that the solutions tend to approach each other, in a qualitative way at least, in this region. This graphical illustration adds more vivid support to the apparently consistent behavior of the two sets of solutions.

Further Discussion of Results

In connection with the velocity oscillations, it can be observed that the oscillating stream function takes on finite values when γ is small and decreases as γ becomes larger. Since the boundary layer is thin at the leading edge and becomes thicker downstream, the velocity oscillations are largest at the leading edge and decay to smaller values with increasing distance downstream. The temperature oscillations follow the same pattern, being largest at the leading edge and dropping off downstream. The decrease of the perturbations with x agrees with the fact

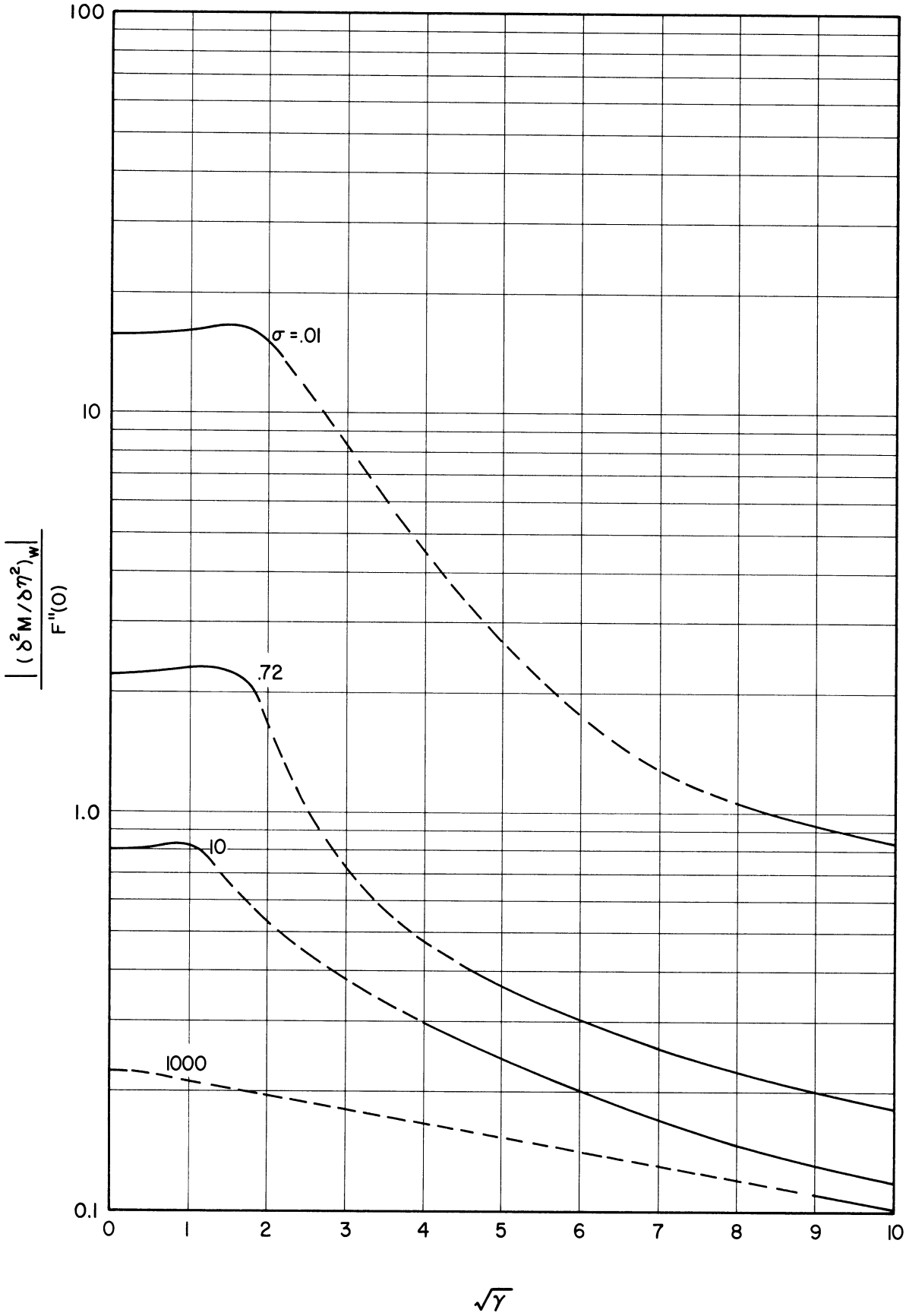

Figure 20. Magnitude of the Oscillating Wall Shear Stress for High and Low Values of γ.

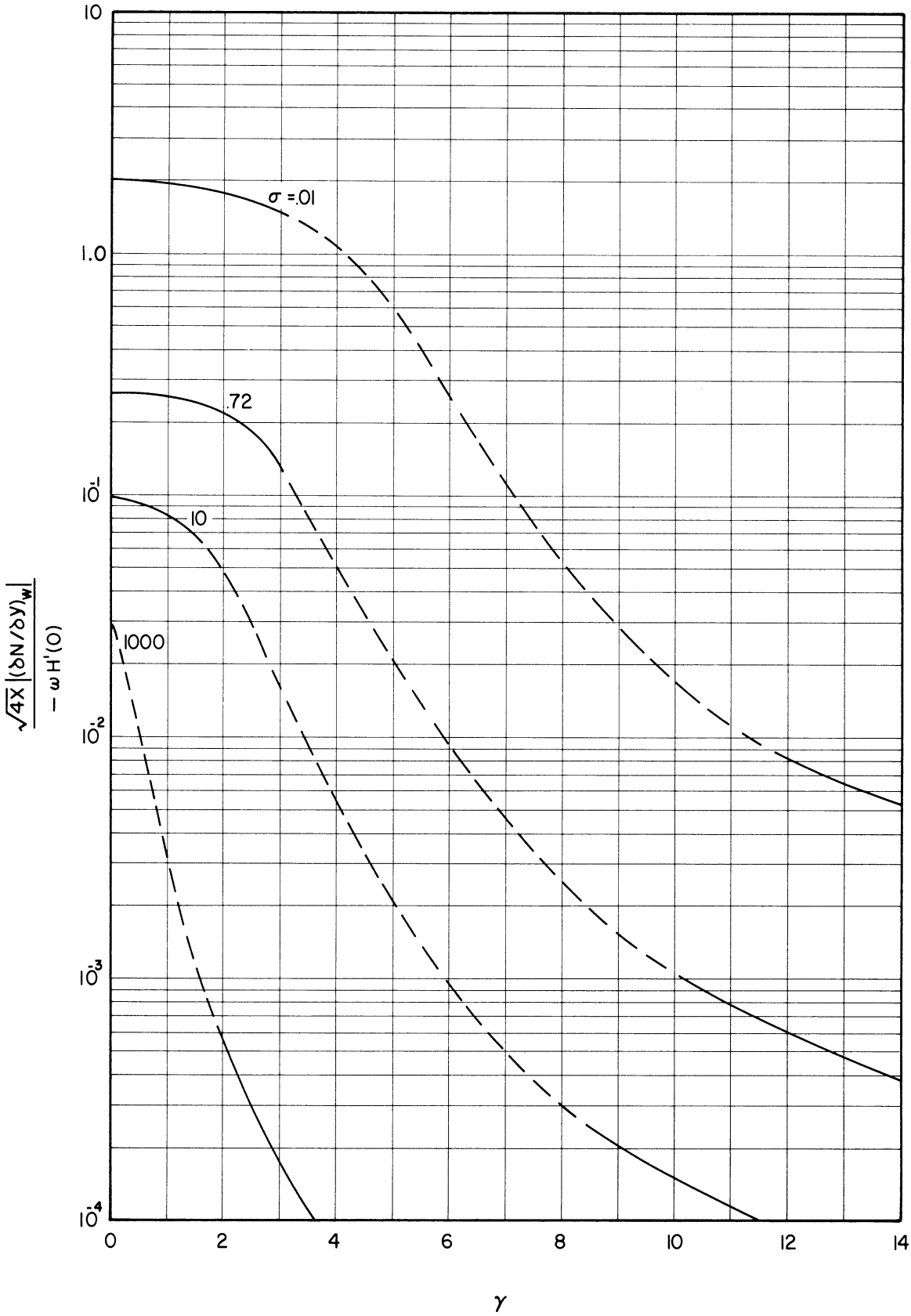

Figure 21. Magnitude of the Oscillating Wall Temperature Gradient for High and Low Values of γ.

that the oscillating pressure gradient also is large at the leading edge but decays with distance downstream. Both velocity and temperature show a tendency to lag with increasing x, the velocity osccilations being in phase at the leading edge. At low values of x, the velocity oscillations occur approximately along lines of constant temperature. Here only the lagging component causes oscillations in temperature so that their phase approaches 90° at the leading edge. The behavior of the perturbations near the leading edge indicates that the convective effects are dominant in this region while the time rates of change of momentum and energy are smaller by comparison even when the frequency is high. This can be explained by the fact that the magnitudes of the convective effects are dependent upon gradients in velocity and temperature. These gradients are high at the leading edge but decay downstream. Therefore, if the frequency is high, the convective effects dominate near the leading edge, while local acceleration and time rate of change of temperature dominate farther downstream.

It is clear from the analysis that the perturbations are proportional to ϵ. If ϵ is held constant it is implied that for a given physical system the vibratory acceleration $a_o\Omega^2$ is held constant also. Under these conditions the amplitude of the oscillating pressure gradient is constant at any given point in the boundary layer, but the frequency may vary. At zero frequency the velocity oscillations are in phase and occur along lines of constant η. At a given distance from the leading edge, except for the slight peaking phenomena shown in Figure 18, the velocity oscillations decrease with increasing frequency.

This behavior is due to the fact that although the oscillating pressure gradient is the same, less time is available within a given cycle for accelerating the fluid when frequency is high. At high values of $\omega\sqrt{4x}$ the velocity oscillations are proportional to the reciprocal of frequency except in the region very close to the wall where they are proportional to $1/\sqrt{\Omega}$. The temperature oscillations follow a slightly different pattern. In the quasi-steady case of $\omega \to 0$ the temperature perturbations are zero and approach a phase of 90° since the in phase components of velocity lie along lines of constant temperature. At a given distance from the leading edge the temperature perturbations at first increase linearly with frequency, then reach a maximum, and then decrease as frequency is varied from zero to increasingly higher values. At high values of $\omega\sqrt{4x}$ the temperature oscillations are porportional to the reciprocal of the square of frequency. Both temperature and velocity lag more and more with increasing frequency at a given distance from the leading edge. This behavior is due to the increasing importance of local acceleration and the time rate of change of temperature.

In regard to the phase of the perturbations it has been pointed out in the last two paragraphs that the tendency to lag becomes more predominate with increasing distance from the leading edge and with increasing frequency. This lag is primarily dependent on the variable $\gamma = \omega\sqrt{4x}$, although a fairly significant dependence on η may be expected at intermediate values of γ. The velocity and temperature oscillations have a phase of 0° and 90° respectively as either x or ω approaches zero. In the limiting case of very large values of the product $\omega\sqrt{4x}$, the temperature oscillations lag by 180° while those of velocity lag by 90°

throughout most of the boundary layer. Very close to the wall, however, viscosity becomes important so that the velocity phase lag is only 45° in this region when $\omega\sqrt{4x}$ is large.

The effect of frequency on the magnitudes of the velocity and temperature oscillations has been discussed previously in this section for the condition that ϵ, or in other words the acceleration $a_o\Omega^2$, be held constant for a given physical system. If this condition is now relaxed the effect of the amplitude a_o and the frequency Ω together can be observed. It is clear that if γ is very small, the velocity oscillations at a given distance from the leading edge are proportional to $a_o\Omega^2$, while those of temperature are proportional to $a_o\Omega^3$. If γ is large, however, the temperature oscillations are proportional to the amplitude a_o alone, while the velocity oscillations, except in the region very close to the wall, are proportional to the amplitude of vibrational velocity $a_o\Omega$. Very close to the wall the velocity perturbations vary with $a_o\Omega^{1.5}$.

The effect of the Prandtl number has not been discussed in any great detail here. However, it can be seen from all of the results presented that, with all other things being equal, the velocity and temperature perturbations are largest for the low Prandtl numbers. It is certainly reasonable that the temperature perturbations follow the same trend as those of velocity and it is to be expected that the velocity perturbations will have an inverse relationship with the Prandtl Number for the following reasons. First, the combating effect of viscosity is small if the Prandtl number is low. Also, the oscillating pressure gradient is larger and extends over a greater width as

shown in Figure 8. This is due to the fact that the thermal boundary layer is thick for low Prandtl numbers thus emphasizing the basic mechanism discussed at the beginning of this chapter. This follows a similar line of reasoning that can be applied to the steady velocity profiles. That is, the steady free convection velocities are larger for the low Prandtl numbers because the total buoyancy effect is large due to the greater thickness of the thermal layer. Conversely, for high Prandtl numbers the buoyancy effect is restricted to a very thin layer adjacent to the wall and is opposed by large viscous forces thus causing the total momentum to be small. In addition, high viscosity requires the the velocity layer to be relatively thicker than that of temperature. Therefore, the available momentum effect is distributed over a sizeable thickness causing the average velocity level to be low.

One additional parameter will be discussed here and that is the temperature difference $\Delta\theta = (\theta_o - \theta_\infty)$. The steady free convection flow velocities are proportional to $\sqrt{G}$, which indicates that they vary directly with the square root of the temperature difference. If γ is high, the velocity oscillations are proportional to $\Delta\theta^{3/4}$ except near the wall where they are proportional to $\Delta\theta^{1/2}$. Also, in the high γ region the temperature perturbations are proportional to $\Delta\theta^{3/4}$. Thus, the high γ oscillations show an increase with increasing temperature difference. In the region of very low γ the velocity oscillations are proportional to $\Delta\theta^{1/4}$, but those of temperature vary directly with $\Delta\theta^{-3/4}$. Here the temperature oscillations show a decrease with increasing temperature difference. It would seem in this case that very large temperature oscillations could be produced in the low γ

region by continually decreasing the temperature difference. This is not correct, however, since all of the analysis presumes the existence of a boundary layer type of flow which, as pointed out by Ostrach,[23] occurs only in cases where the Grashof Number is very large. It is also important to note when speaking of γ as being either large or small that γ itself varies in proportion to $\Delta\theta^{-1/2}$.

The problem discussed in this chapter involves the response of a free convection boundary layer on an infinite plane wall to transverse wall vibration. Due to the fact that the wall is infinite in extent, the fluid outside the boundary layer, just as in the non-vibrating case, remains stationary with respect to the wall. The boundary layer then responds to the pressure gradients distributed throughout its volume as a result of density variations. In the next chapter the problem of a finite plate will be considered when density variations are absent. In this case, however, potential flow exists outside the boundary layer and is directly attributable to the vibration. The response of the boundary layer is then determined on the basis of the potential flow existing at its outer edge.

List of Symbols for Chapter II

a_0	Amplitude of wall vibration
B_x	Body force per unit volume parallel to the wall
B_y	Body force per unit volume normal to the wall
b_0, b_1, b_2, b_3, b_4	Constants in Equation (2.41)
C_p	The specific heat per unit mass of the fluid
C_1, C_2	Constants in Equations (2.27) and (2.43)
C	Speed of sound in the fluid
$D/D\tau$	The substantial derivative operator in the stationary coordinate system, $\partial/\partial\tau + u\ \partial/\partial X + v\ \partial/\partial Y$
$D^*/D\tau$	The substantial derivative operator in the moving coordinate system, $\partial/\partial\tau + u^*\ \partial/\partial X^* + v^*\ \partial/\partial Y^*$
$E_n(\eta)$	Components of the oscillating stream function defined in Appendix III
e	Base of the natural logarithms
$F(\eta)$	Defines the steady velocity distribution $\psi_0 = (4x)^{3/4} F(\eta)$
G	The Grashof Number $g\beta\ell^3(\theta_0-\theta_\infty)/\nu^2$ based on the length ℓ
G_x	The Grashof Number $g\beta X^3(\theta_0-\theta_\infty)/\nu^2$ based on X.
g	Body force per unit mass acting parallel to the wall.
g_0	Amplitude of wall acceleration $a_0\Omega^2$.
$H(\eta)$	Defines the steady temperature distribution $T_0 = H(\eta)$
$(\ )_h$	Subscript indicating a homogenous solution
$I_n(\eta)$	Components of the oscillating stream function defined in Appendix III
i	The square root of -1
$J_n(\eta)$	Components of the oscillating temperature profile defined in Appendix III
k	Thermal conductivity of the fluid

$L_n(\eta)$	Components of the oscillating temperature profile defined in Appendix III
ℓ	Characteristic length along wall
M	The oscillating stream function defined by $\psi_1 = M\, e^{i\omega t}$
m	The exponent in the definition of $\lambda = \omega(4x)^m$
N	The oscillating temperature defined by $T_1 = N\, e^{i\omega t}$
n	Index on the summation $\sum_{n=0}^{\infty}$, on the coefficients R_n and S_n, and on the functions $E_n(\eta)$, $I_n(\eta)$, $J_n(\eta)$ and $L_n(\eta)$ in Appendix III
$P_0 \cdots P_5$	Parameters defined by Equations (2.66)
p	Pressure
$(\ )_p$	Subscript indicating a particular solution
$Q_0 \cdots Q_6$	Parameters defined by Equations (2.72)
R_0	The coefficient defined by Equation (2.52a)
R_n	Coefficients in the series $\sum_{n=0}^{\infty} R_n \lambda^n$ defined by Equation (2.60a)
r	The exponent of $(4x)$ defined by Equation (2.52a)
S_0	The coefficient defined by Equation (2.52b)
S_n	Coefficients in the series $\sum_{n=0}^{\infty} S_n \lambda^n$ defined by Equation (2.60b)
s	The exponent of $(4x)$ defined by Equation (2.52b)
T	Dimensionless temperature $\theta-\theta_\infty/\theta_0-\theta_\infty$
T_0, T_1	The steady and oscillating components of the temperature distribution, $T \approx T_0 + \epsilon T_1$.
t	Dimensionless time $(\nu\sqrt{G}\,/\ell^2) \cdot \tau$
u	Velocity in the direction parallel to the wall in the stationary coordinate system.
u^*	Velocity in the direction parallel to the wall in the moving coordinate system, $u^* = u$
V_0	Velocity of the wall, $V_0 = a_0\Omega \sin \Omega\tau$
v	Velocity in the direction normal to the wall in the stationary coordinate system

v^*	Velocity in the direction normal to the wall in the moving coordinate system, $v^* = v - V_o$
$(\ )_w$	Subscript denoting a condition at the wall
X	Distance in the direction parallel to the wall in the stationary coordinate system
X^*	Distance in the direction parallel to the wall in the moving coordinate system, $X^* = X$
x	Dimensionless distance in the direction parallel to the wall, $x = X^*/\ell$
Y	Distance in the direction normal to the wall in the stationary coordinate system
Y^*	Distance in the direction normal to the wall in the moving coordinate system, $Y^* = Y - Y_o$
Y_o	Motion of the wall normal to its own plane, $Y_o = -a_o \cos \Omega\tau$
y	Dimensionless distance in the direction normal to the wall in the moving coordinate system, $y = \frac{Y^*}{\ell} \sqrt[4]{G}$
Z	Coordinate normal to the XY plane
∞	Indicates a condition far away from the wall

Greek Letters

α	Phase angle of the temperature oscillations defined by $N = \lvert N \rvert e^{i\alpha}$
β	Coefficient of thermal expansion of the fluid defined by $\rho = \rho_\infty [1 - \beta(\theta - \theta_\infty)]$
γ	Defined by $\omega\sqrt{4x}$
$\Delta\theta$	The temperature difference $(\theta_o - \theta_\infty)$
∇^2	The Laplacian Operator in the stationary coordinate system $\partial^2/\partial X^2 + \partial^2/\partial Y^2$
∇^{*2}	The Laplacian Operator in the moving coordinate system $\partial^2/\partial X^{*2} + \partial^2/\partial Y^{*2}$
δ	The boundary layer thickness

δ_{n0}, δ_{n1}	The Kronecker Delta, $\delta_{ij} = 1$ if $i = j$, and $\delta_{ij} = 0$ if $i \neq j$
ϵ	Defined by $\epsilon = \frac{g_0/g}{\sqrt[4]{G}}$
$\zeta(\eta)$	The forcing function, $\zeta(\eta) = \int_{\infty}^{\eta} \eta H'(\eta) d\eta$
η	The similarity variable, $\eta = y/(4x)^{1/4}$
θ	Temperature
θ_0	The wall temperature for $X > 0$
θ_∞	The fluid temperature far from the wall
K	The thermal diffusivity of the fluid $k/\rho C_p$
λ	Defined by $\lambda = \omega(4x)^m$
μ	The absolute viscosity of the fluid
ν	The kinematic viscosity of the fluid μ/ρ_∞
ρ	The density of the fluid
ρ_∞	The density of the fluid far from the wall
$\sum_{n=0}^{\infty}$	Denotes a summation operation
σ	The Prandtl Number of the fluid, $\sigma = \nu/\kappa$
τ	Time
ϕ	Phase angle of the velocity oscillations defined by $\frac{\partial M}{\partial y} = \left\lvert\frac{\partial M}{\partial y}\right\rvert e^{i\phi}$
ψ	The stream function defined by $u^* = \frac{\nu\sqrt{G}}{\ell} \frac{\partial\psi}{\partial y}$ and $v^* = -\frac{\nu\sqrt[4]{G}}{\ell} \frac{\partial\psi}{\partial x}$
ψ_0, ψ_1	The steady and oscillating components of the stream function, $\psi \approx \psi_0 + \epsilon\psi_1$
Ω	The frequency of wall vibration defined by $V_0 = a_0\Omega \sin \Omega\tau$
ω	Dimensionless frequency of wall vibration, $\omega = \ell^2\Omega/\nu\sqrt{G}$

CHAPTER III

THE POTENTIAL FLOW AND BOUNDARY LAYER RESPONSE TO TRANSVERSE VIBRATION OF A THIN PLATE OF FINITE LENGTH

Statement of the Problem

Consider a thin plate of length 2c immersed in an infinite ambient fluid and vibrating normal to its own plane with a sinusoidal motion of amplitude a_o and frequency ω. The velocity of the plate is $V_o \cos \omega t$ where $V_o = a_o\omega$. A sketch of the physical system in Figure 22. The analysis will be restricted to the two dimensional incompressible flow pattern. This requires that the system be uniform in the direction normal to the xy plane, and that the velocity of the plate be small compared with the speed of sound in the fluid.

A boundary layer will form adjacent to the wall, but its behavior will depend on the potential flow at the outer edge of the layer. Therefore, the potential flow pattern will be considered first, and its effect on the viscous layer will be discussed later.

The Potential Flow Response

For bodies moving with translational motion in a constant density fluid it is immaterial whether the problem is analyzed with respect to a stationary frame of reference or a coordinate system fixed in the body. It is usually more convenient to fix the coordinates in the body, and this procedure will be used here. With respect to this frame of reference the velocity of the fluid at large distances from the plate is $-V_o \cos \omega t$ in the y direction. The y component of velocity along the plate is zero.

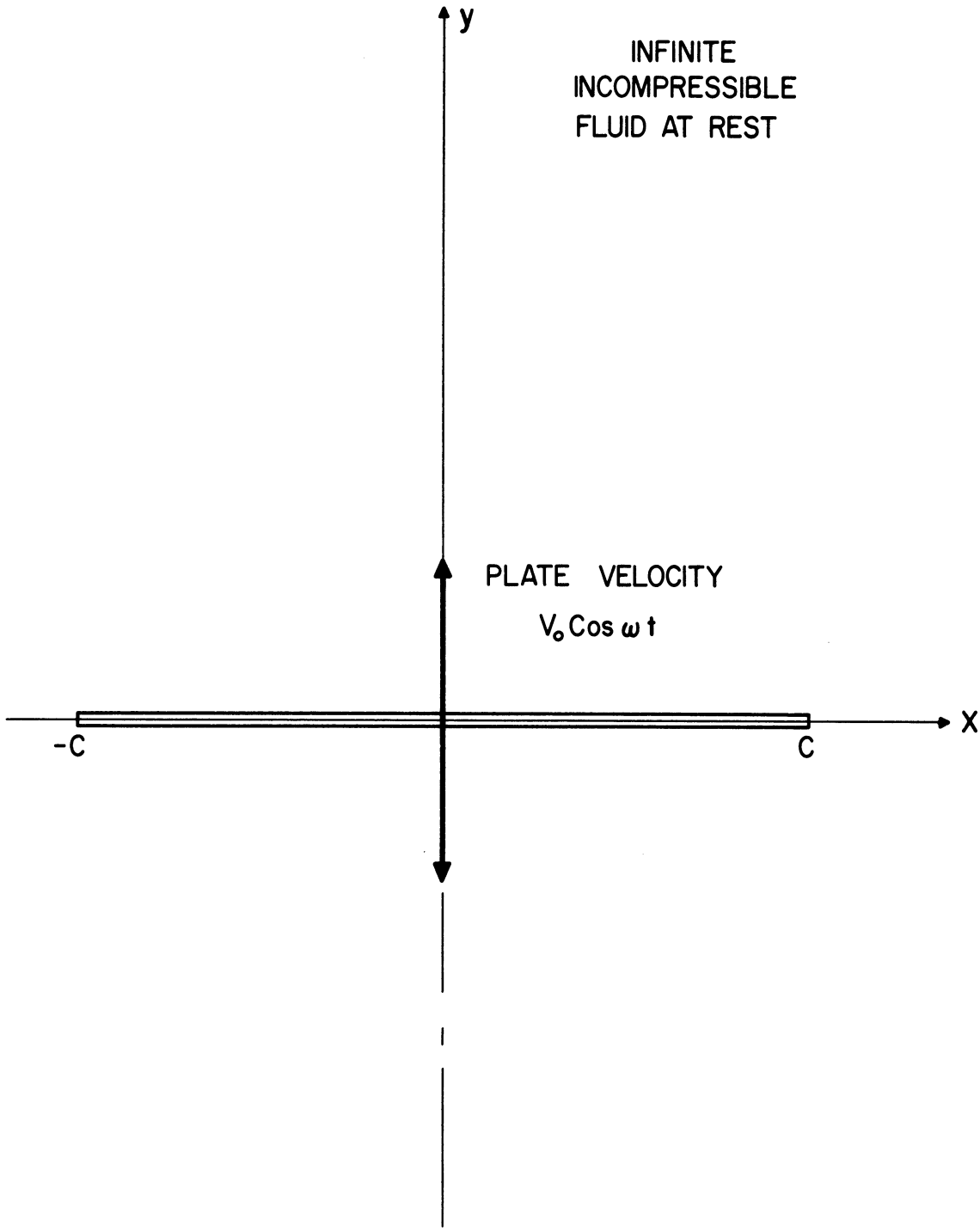

Figure 22. Sketch Showing a Thin Plate of Finite Length Vibrating Transversely in an Infinite Incompressible Fluid at Rest.

The equations governing the behavior of a frictionless incompressible fluid are the continuity relation

$$\frac{\partial U}{\partial x} + \frac{\partial V}{\partial y} = 0 \ , \tag{3.1a}$$

and the condition for irrotational flow that

$$\frac{\partial U}{\partial y} - \frac{\partial V}{\partial x} = 0 \ . \tag{3.1b}$$

The stream function and velocity potential are related by the Cauchy-Riemann equations written as

$$U = -\frac{\partial \Psi}{\partial y} = -\frac{\partial \Phi}{\partial x} \tag{3.2a}$$

$$V = \frac{\partial \Psi}{\partial x} = -\frac{\partial \Phi}{\partial y} \ . \tag{3.2b}$$

Substituting the stream function from (3.2) into (3.1a) gives

$$\left(-\frac{\partial^2 \Psi}{\partial x \partial y} + \frac{\partial^2 \Psi}{\partial x \partial y} \right) = 0 \ .$$

Entering the velocity potential from (3.2) into (3.1b) gives

$$\left(-\frac{\partial^2 \Phi}{\partial x \partial y} + \frac{\partial^2 \Phi}{\partial x \partial y} \right) = 0 \ .$$

Therefore, Equations (3.2) automatically satisfy the conditions prescribed by Equations (3.1). Two additional relations are obtained, however, by entering the velocity potential and stream function respectively into (3.1a) and (3.1b). These relations are

$$\nabla^2 \Phi = 0 \tag{3.3a}$$

$$\nabla^2 \Psi = 0 \ . \tag{3.3b}$$

Solutions to the problem must satisfy Laplace's equation as given by Equations (3.3) compatible with the boundary conditions that

$$U_\infty = -\left(\partial\Psi/\partial y\right)_\infty = -\left(\partial\Phi/\partial x\right)_\infty = 0$$

$$V_\infty = \left(\partial\Psi/\partial x\right)_\infty = -\left(\partial\Phi/\partial y\right)_\infty = -V_0 \cos\omega t$$

$$\left(V\right)_{y=0} = \left(\partial\Psi/\partial x\right)_{y=0} = -\left(\partial\Phi/\partial y\right)_{y=0} = 0 \qquad \text{for } -c<x<c$$

The infinity subscript indicates conditions far removed from the plate. Due to the linearity of Laplace's equation, time can be eliminated as a variable in the equations and solutions can be expressed as

$$\Phi(x,y,t) = \phi(x,y)\, e^{i\omega t} \tag{3.4a}$$

$$\Psi(x,y,t) = \psi(x,y)\, e^{i\omega t}. \tag{3.4b}$$

Correspondingly, the velocities are represented as

$$U = \bar{U}\, e^{i\omega t} = -\partial\psi/\partial y\; e^{i\omega t} = -\partial\phi/\partial x\; e^{i\omega t} \tag{3.4c}$$

$$V = \bar{V}\, e^{i\omega t} = \partial\psi/\partial x\; e^{i\omega t} = -\partial\phi/\partial y\; e^{i\omega t}. \tag{3.4d}$$

Equations (3.3) now become

$$\nabla^2\phi = 0 \tag{3.5a}$$

$$\nabla^2\psi = 0\,. \tag{3.5b}$$

The boundary conditions are

$$\bar{U}_\infty = -\left(\partial\psi/\partial y\right)_\infty = -\left(\partial\phi/\partial x\right)_\infty = 0$$

$$\bar{V}_\infty = \left(\partial\psi/\partial x\right)_\infty = -\left(\partial\phi/\partial x\right)_\infty = -V_0$$

$$\left(\bar{V}\right)_{y=0} = \left(\partial\psi/\partial x\right)_{y=0} = -\left(\partial\phi/\partial y\right)_{y=0} = 0 \qquad \text{for } -c<x<c\,.$$

The problem is now equivalent to that of finding the potential flow pattern around a stationary plate immersed in an infinite fluid moving with constant velocity V_o in the negative y direction.

Complex variable theory offers a convenient means of handling many potential flow problems and it will be used here. A function of a complex variable is defined as

$$w(z) = R(x, y) + i\, I(x, y) \tag{3.6}$$

where z = x + iy, and R and I represent the real and imaginary components of the function. The function w(z) is said to be analytic in a region if for every point in the region w(z) and its derivative are single valued, and the value of the function is finite. Points in the xy plane where w(z) is not analytic are called singular points. If the derivative of w(z) is to be single valued, it must be independent of the direction of the element dz. For example,

$$\frac{dw}{dz} = \lim_{\Delta z \to 0} \frac{w(z+\delta z) - w(z)}{\Delta z} = \lim_{\substack{\Delta x \to 0 \\ \Delta y \to 0}} \frac{w(z+\delta z) - w(z)}{\Delta x + i\,\Delta y}$$

$$= \lim_{\Delta x \to 0} \frac{w(z+\delta z) - w(z)}{\Delta x} = \frac{\partial w}{\partial x} = \lim_{\Delta y \to 0} \frac{w(z+\delta z) - w(z)}{i\,\Delta y} = \frac{1}{i}\,\frac{\partial w}{\partial y}\,.$$

Thus, if w(z) is an analytic function, then

$$\frac{\partial w}{\partial x} = \frac{1}{i}\,\frac{\partial w}{\partial y}\,. \tag{3.7}$$

Substituting Equation (3.6) into (3.7) gives

$$\left(\frac{\partial R}{\partial x} - \frac{\partial I}{\partial y}\right) + i\left(\frac{\partial I}{\partial x} + \frac{\partial R}{\partial y}\right) = 0\,. \tag{3.8}$$

Both the real and imaginary parts of Equation (3.8) are zero so that

$$\frac{\partial R}{\partial x} - \frac{\partial I}{\partial y} = 0 \tag{3.9a}$$

$$\frac{\partial R}{\partial y} + \frac{\partial I}{\partial x} = 0 . \tag{3.9b}$$

Differentiating (3.9a) with respect to x and (3.9b) with respect to y and adding gives

$$\nabla^2 R = 0 . \tag{3.10a}$$

Differentiating (3.9a) with respect to y and (3.9b) with respect to x and subtracting gives

$$\nabla^2 I = 0 , \tag{3.10b}$$

Therefore, both the real and imaginary components of an analytic function w(z) satisfy Laplace's equation. If $R = \phi$ and $I = \psi$, Equation (3.6) becomes

$$W(z) = \phi(x,y) + i\,\psi(x,y). \tag{3.11}$$

w(z) is called the complex potential. As long as w(z) is an analytic function it represents the solution to a potential flow problem since Equations (3.5) will be satisfied automatically. One additional point will be made here in connection with the calculation of the velocity vector from the complex potential. Since w(z) is analytic, $dw/dz = \partial w/\partial x = \partial\phi/\partial x + i\ \partial\psi/\partial x$. Therefore, using the relations given in Equations (3.4c) and (3.4d), the velocity vector is written as

$$\frac{\partial W}{\partial z} = -\bar{U} + i\,\bar{V} . \tag{3.12}$$

Methods for obtaining potential flow patterns associated with various geometric configurations are given in classical books on the subject such as Lamb's <u>Hydrodynamics</u>.[14] The potential flow about an

elliptic cylinder will be redeveloped here. The reason for introducing this work is that by allowing the semi-minor axis to approach zero, the steady potential flow about a thin plate can be approximated.

By introducing the elliptic coordinate transformation

$$z = c \cosh \zeta \tag{3.13a}$$

where $\zeta = \xi + i\beta$, the original coordinates are represented as

$$x = c \cosh \xi \cos \beta \tag{3.13b}$$

$$y = c \sinh \xi \sin \beta . \tag{3.13c}$$

Consider now the complex potential function

$$W(z) = i K e^{-\zeta} . \tag{3.14}$$

The corresponding velocity potential and stream function are

$$\phi = K e^{-\xi} \sin \beta \tag{3.15a}$$

$$\psi = K e^{-\xi} \cos \beta . \tag{3.15b}$$

For a body moving with constant velocity V_o in the y direction, the velocity of the body normal to its own surface is given by

$$\partial\psi/\partial s = V_0 \frac{dx}{ds} , \tag{3.16}$$

where s is the distance along the surface of the body. An illustrative sketch is shown in Figure 23. Integrating around the periphery gives the result that along the surface of the body,

$$\psi = V_o x + \text{constant}. \tag{3.17}$$

The constant is arbitrary and can be taken as zero. Equating the expressions in (3.15b) and (3.17) gives

$$K e^{-\xi} = V_0 c \cosh \xi \tag{3.18}$$

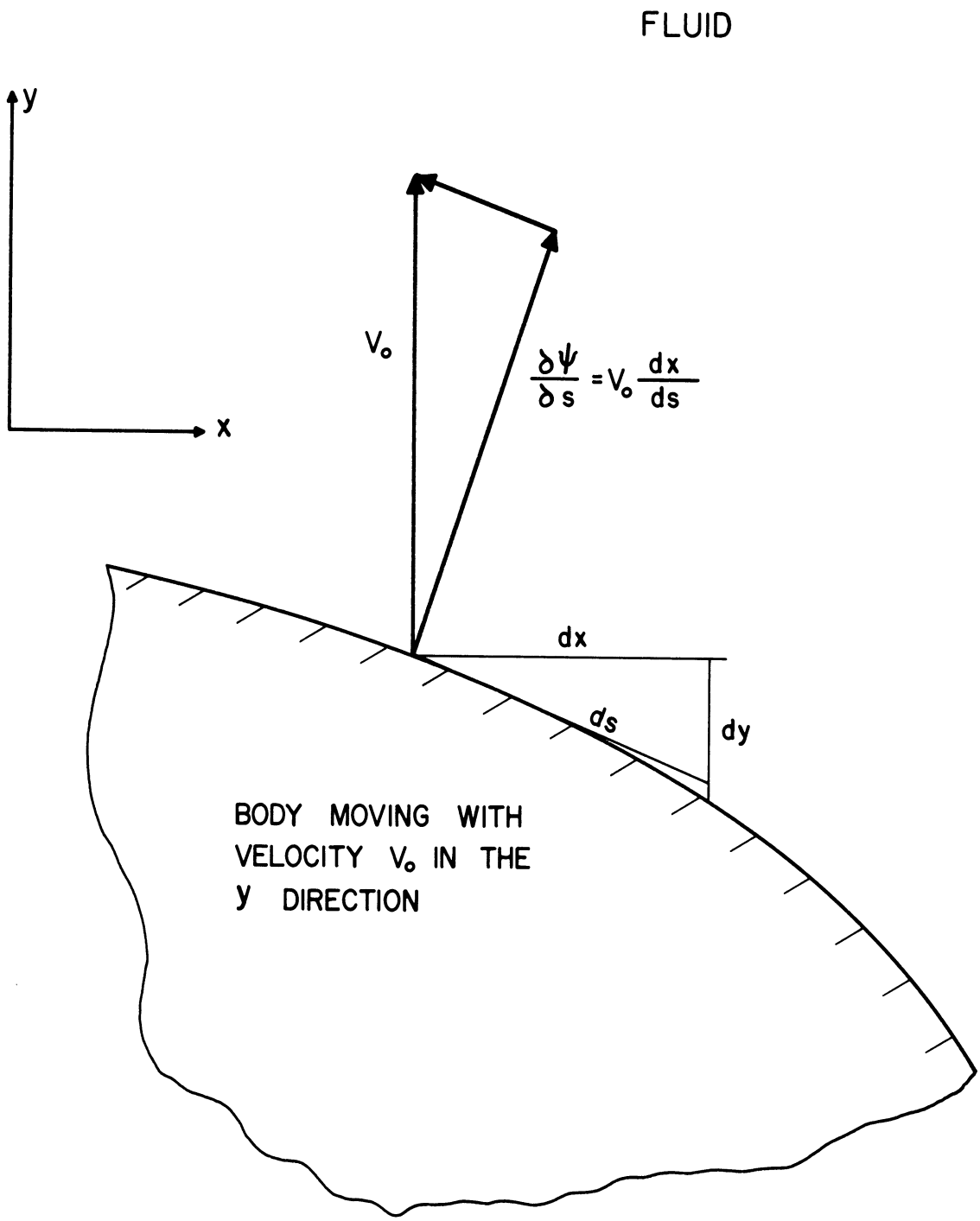

Figure 23. Sketch Showing the Boundary of a Solid Body Moving in a Fluid.

along the body. This relation is satisfied by only one value of ξ designated as ξ_o. But $\xi = \xi_o$ = constant is the equation of an ellipse of semi-major and semi-minor axis a and b respectively, where

$$a = c \cosh \xi_o \tag{3.19a}$$

$$b = c \sinh \xi_o \, . \tag{3.19b}$$

c can now be expressed in terms of a and b by

$$c = \sqrt{a^2 - b^2} \, . \tag{3.20}$$

Solving Equations (3.19) for ξ_o yields

$$\xi_0 = \ln \sqrt{\frac{a+b}{a-b}} \, . \tag{3.21}$$

Entering (3.20) and (3.21) into (3.18) gives

$$K = V_0 \, a \sqrt{\frac{a+b}{a-b}} \, . \tag{3.22}$$

Equation (3.14) now becomes

$$W(z) = i \, V_0 \, a \sqrt{\frac{a+b}{a-b}} \; e^{-\zeta} \, . \tag{3.23}$$

Correspondingly, Equations (3.15) become

$$\phi = V_0 \, a \sqrt{\frac{a+b}{a-b}} \; e^{-\xi} \cos \beta \tag{3.24a}$$

$$\psi = V_0 \, a \sqrt{\frac{a+b}{a-b}} \; e^{-\xi} \sin \beta \, . \tag{3.24b}$$

Differentiation of (3.24a) shows that $\left(\frac{\partial \phi}{\partial \xi}\right)_{\xi \to \infty} = \left(\frac{\partial \phi}{\partial \beta}\right)_{\xi \to \infty} = 0$. From Equation (3.13), $x \to \infty$ as $\xi \to \infty$ except for $\beta = \pm \pi/2$ which is the y axis. Also, $y \to \infty$ for $\xi \to \infty$ except for $\beta = 0$ or $\beta = \pi$ which is the x axis. Therefore, the fluid is at rest at large distances from the body. Thus, Equations (3.23) and (3.24) give the steady potential flow pattern

for an ellipse moving broadside with constant velocity V_o in the y direction in a fluid otherwise at rest.

By superposing a flow of V_o in the negative y direction the steady flow about a stationary ellipse is obtained. In accordance with Equation (3.12), this is done by subtracting $i\,V_o\,z$ in Equation (3.23) which gives

$$W = i\,V_o\,a\sqrt{\frac{a+b}{a-b}}\;e^{-\zeta} - i\,V_o\sqrt{a^2-b^2}\;\cosh\zeta\,. \tag{3.25}$$

The corresponding velocity potential and stream function are

$$\phi = V_o\left[a\sqrt{\frac{a+b}{a-b}}\;e^{-\xi} + \sqrt{a^2-b^2}\;\sinh\xi\right]\sin\beta \tag{3.26a}$$

$$\psi = V_o\left[a\sqrt{\frac{a+b}{a-b}}\;e^{-\xi} - \sqrt{a^2-b^2}\;\cosh\xi\right]\cos\beta\,. \tag{3.26b}$$

Equations (3.25) and (3.26) give the flow pattern about a stationary ellipse immersed in an infinite fluid of velocity V_o in the negative y direction. $\psi = 0$ for $\beta = \pm\,\pi/2$ which is the y axis, and also for $\xi = \xi_o = \ln\sqrt{\frac{a+b}{a-b}}$ which is along the surface of the ellipse. Now that the potential flow about an ellipse is available from Equations (3.25) and (3.26), the case of a thin plate can be investigated.

By letting b approach zero, in which case a = c and $\xi_o = 0$, Equation (3.25) becomes

$$W(z) = -\,i\,V_o\,c\,\sinh\zeta\,, \tag{3.27}$$

and Equations (3.26) become

$$\phi = V_o\,c\,\cosh\xi\,\sin\beta \tag{3.28a}$$

$$\psi = -V_o\,c\,\sinh\xi\,\cos\beta\,. \tag{3.28b}$$

Equations (3.27) and (3.28) give the flow pattern about a thin plate immersed in an infinite fluid of velocity V_o in the negative y direction. The streamline pattern has been obtained by plotting Equation (3.28b) for constant values of ψ/V_oC and is shown in Figure 24.

Equations (3.28) satisfy Equations (3.5) and also the corresponding boundary conditions so that the solution to the oscillating plate problem is now determined by Equations (3.4).

Equation (3.27) can be rewritten as

$$W(z) = V_o\sqrt{c^2 - z^2} \quad . \tag{3.29}$$

Differentiation of (3.29) gives

$$\frac{dW}{dz} = -\frac{V_o z}{\sqrt{c^2-z^2}} = -\frac{V_o(x+iy)}{\sqrt{c^2-x^2+y^2-2ixy}} \quad . \tag{3.30}$$

By virtue of Equation (3.12), Equation (3.30) shows that

$$\bar{U} =$$

$$\frac{V_o}{\sqrt{2}}\left\{\frac{x}{c}\sqrt{\frac{\sqrt{\left[1-(x/c)^2+(y/c)^2\right]^2+4(x/c)^2(y/c)^2}+\left[1-(x/c)^2+(y/c)^2\right]}{\left[1-(x/c)^2+(y/c)^2\right]^2+4(x/c)^2(y/c)^2}}\right. \tag{3.31a}$$

$$\left.-\frac{y}{c}\sqrt{\frac{\sqrt{\left[1-(x/c)^2+(y/c)^2\right]^2+4(x/c)^2(y/c)^2}-\left[1-(x/c)^2+(y/c)^2\right]}{\left[1-(x/c)^2+(y/c)^2\right]^2+4(x/c)^2(y/c)^2}}\right\} .$$

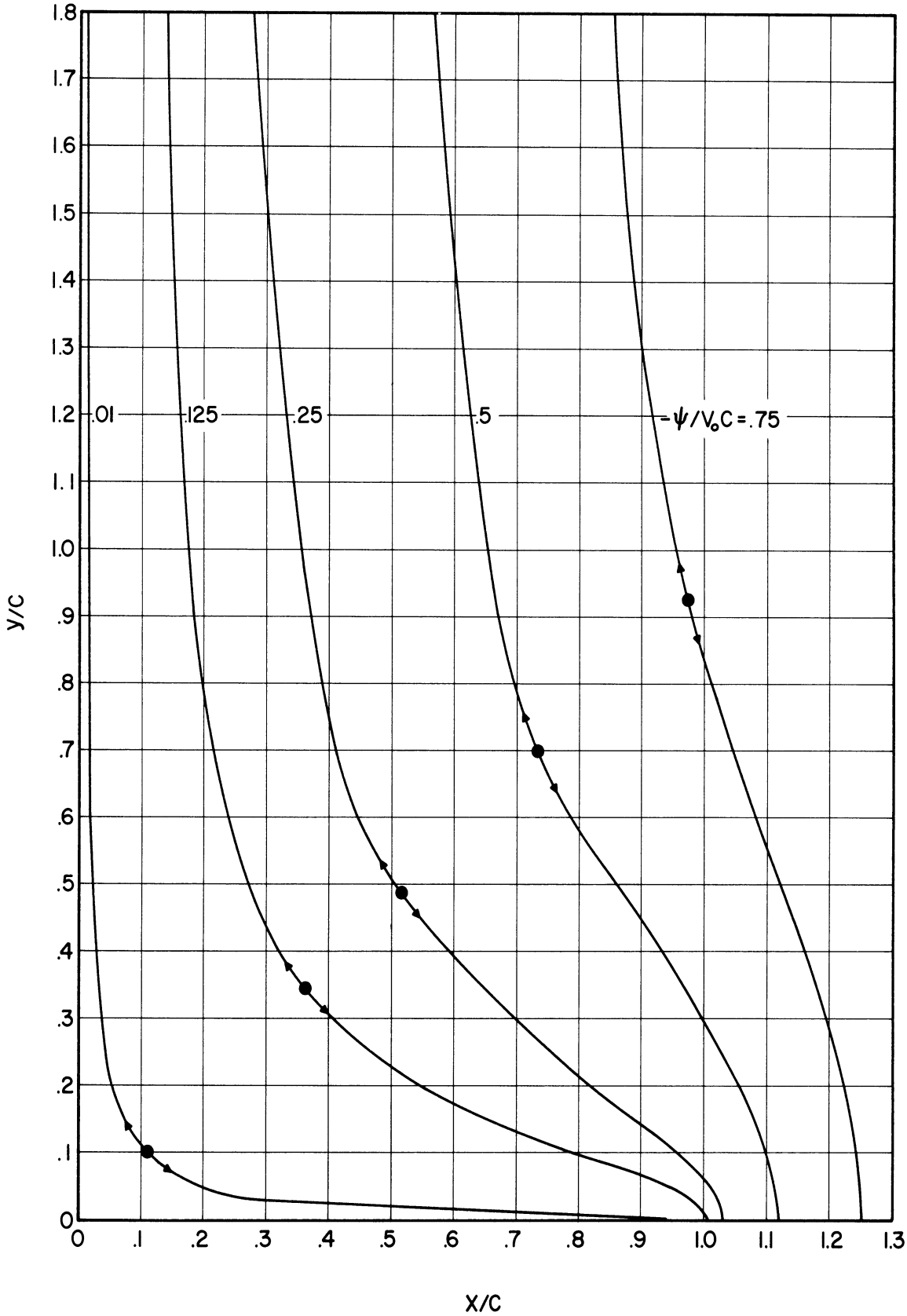

Figure 24. The Oscillating Potential Flow Streamline Pattern for a Plate Vibrating Transversely.

$$\bar{V} =$$

$$-\frac{V_0}{\sqrt{2}}\left\{\frac{x}{c}\sqrt{\frac{\sqrt{\left[1-(x/c)^2+(y/c)^2\right]^2+4(x/c)^2(y/c)^2}-\left[1-(x/c)^2+(y/c)^2\right]}{\left[1-(x/c)^2+(y/c)^2\right]^2+4(x/c)^2(y/c)^2}}\right. \tag{3.31b}$$

$$\left.+\frac{y}{c}\sqrt{\frac{\sqrt{\left[1-(x/c)^2+(y/c)^2\right]^2+4(x/c)^2(y/c)^2}+\left[1-(x/c)^2+(y/c)^2\right]}{\left[1-(x/c)^2+(y/c)^2\right]^2+4(x/c)^2(y/c)^2}}\right\}.$$

Plots of the velocity profiles $\bar{U}$ and $\bar{V}$ are shown as functions of x/c and y/c in Figures 25 through 28. Equations (3.31) show that close to the stagnation point where $x/c \ll 1$ and $y/c \ll 1$, the velocity is given by

$$\bar{U} = V_0 \; x/c \tag{3.32a}$$

$$\bar{V} = -V_0 \; y/c \tag{3.32b}$$

Along the y axis, of course, $\bar{U} = 0$ due to symmetry, but the y component of velocity is given by

$$(\bar{V})_{x=0} = -V_0 \frac{y/c}{\sqrt{1+(y/c)^2}} \tag{3.33}$$

Along the plate, y = 0 so that $(\bar{V})_{y=0} = 0$ and

$$U_0 = V_0 \frac{x/c}{\sqrt{1-(x/c)^2}} \tag{3.34}$$

where U_0 designates $(\bar{U})_{y=0}$.

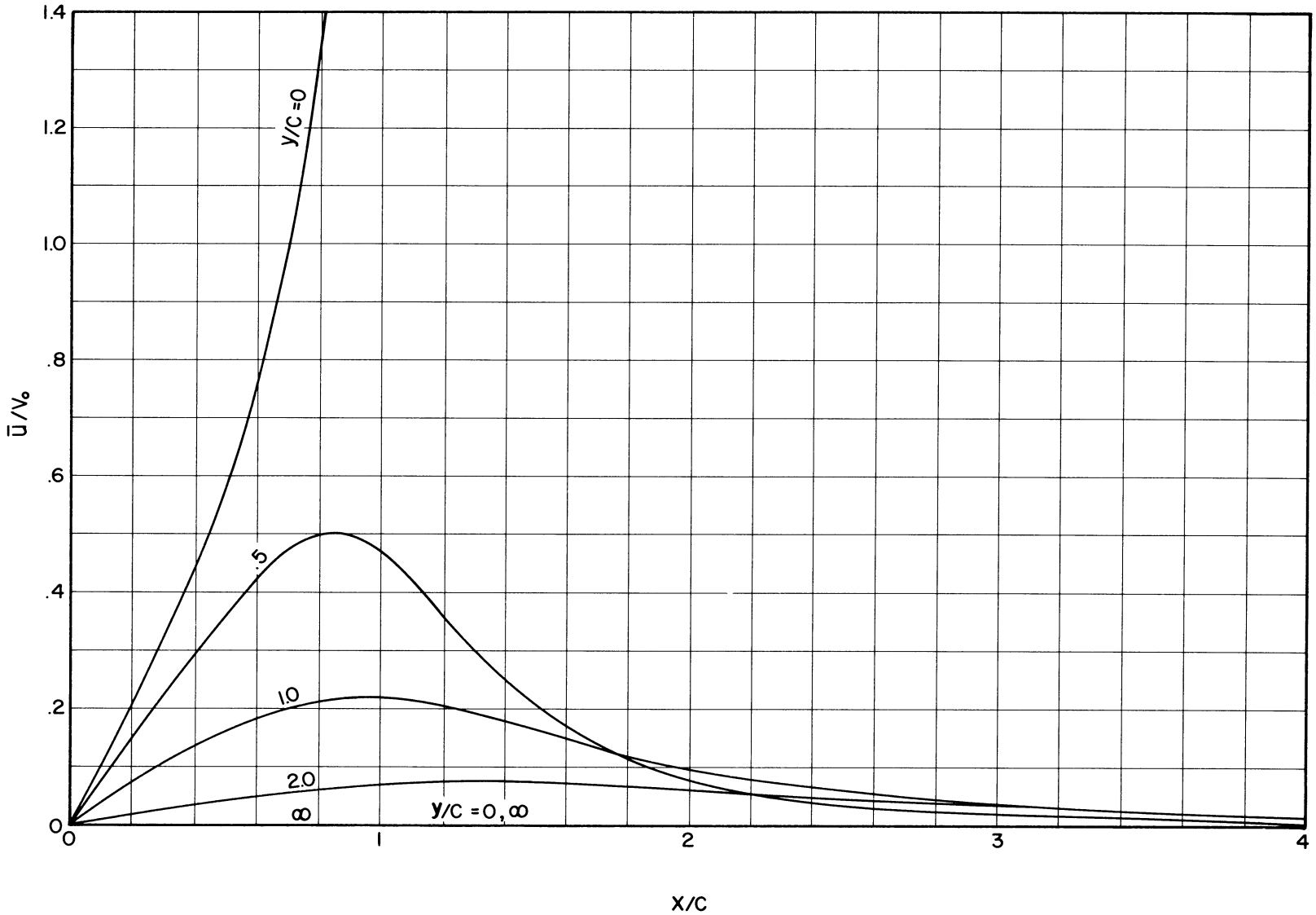

Figure 25. The Oscillating Potential Flow Velocity Distribution for a Plate Vibrating Transversely.

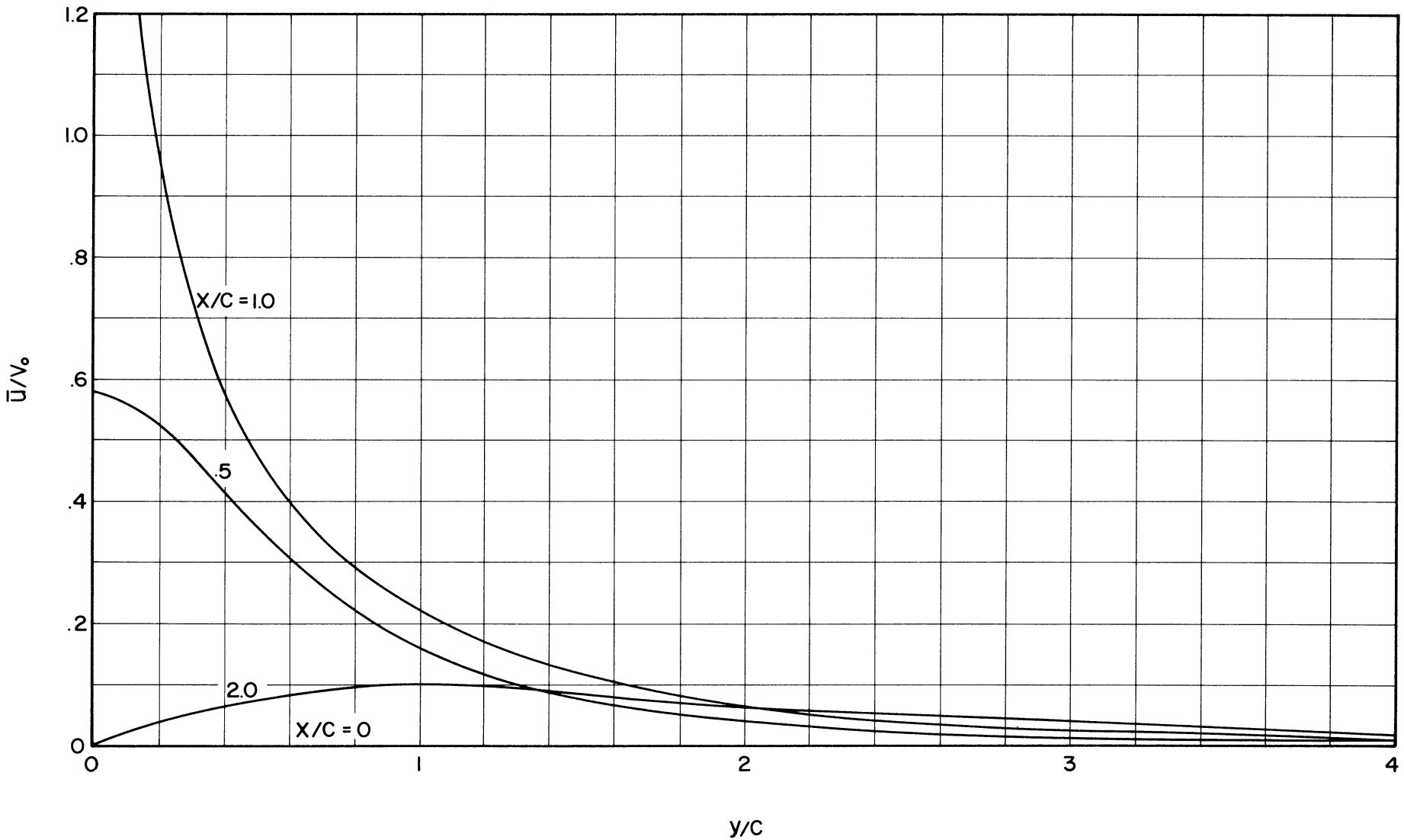

Figure 26. The Oscillating Potential Flow Velocity Distribution for a Plate Vibrating Transversely.

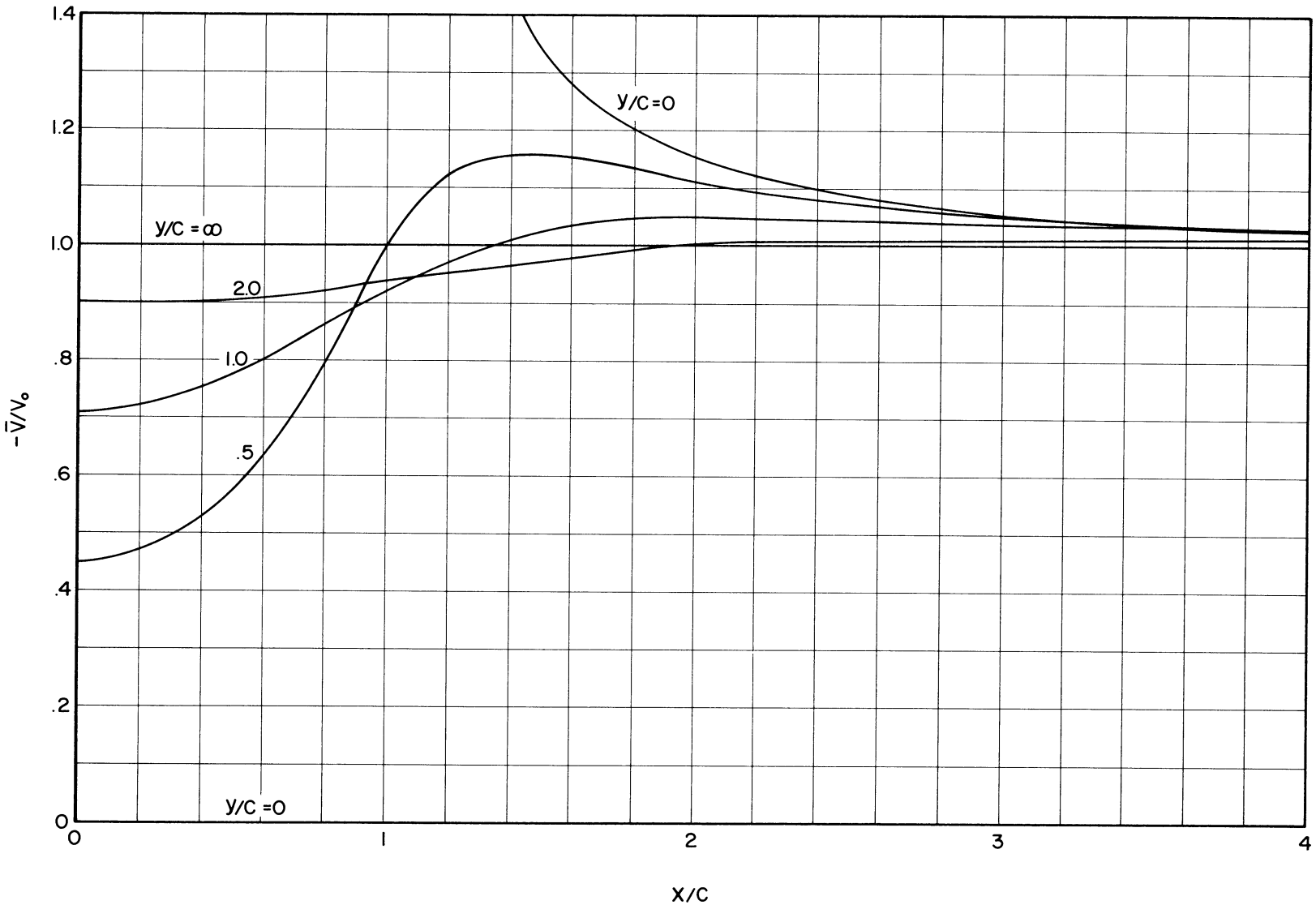

Figure 27. The Oscillating Potential Flow Velocity Distribution for a Plate Vibrating Transversely.

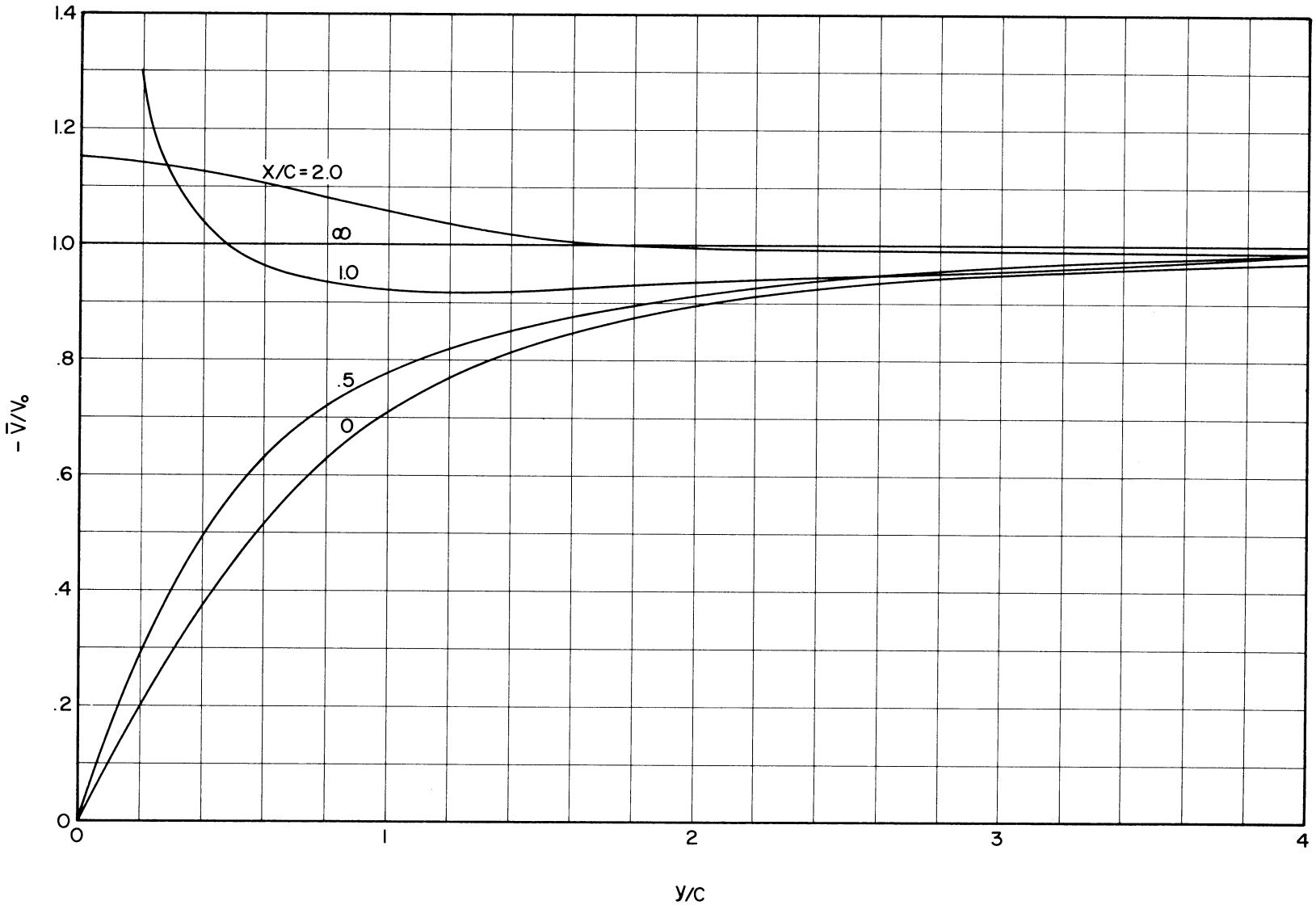

Figure 28. The Oscillating Potential Flow Velocity Distribution for a Plate Vibrating Transversely.

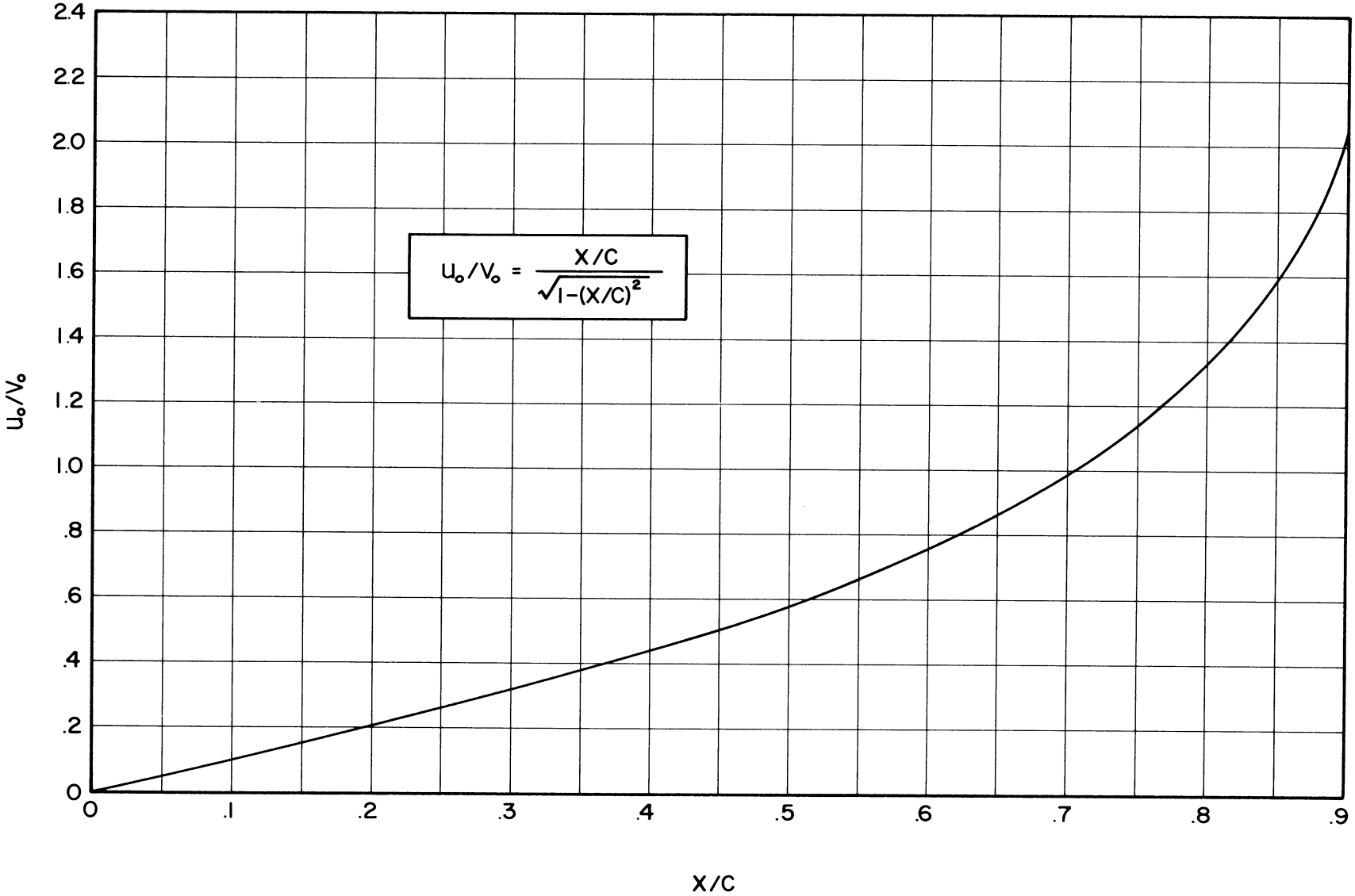

Figure 29. The Oscillating Potential Flow Along a Plate Vibrating Transversely.

Equation (3.34) gives the potential flow at the outer edge of the boundary layer and it will be used in the next section where the boundary layer response is discussed. A plot of Equation (3.34) is given in Figure 29. Close to the center of the plate U_0 varies directly with distance along the plate. Farther out toward the edge the value increases at a faster rate. At x/c = .707 the amplitude of the oscillating velocity along the wall is equal to the amplitude of velocity of vibration. The velocities increase indefinitely as the edges of the plate are approached. These points are singular points. In this region the theory can not be expected to accurately describe the behavior of an actual fluid. This is due to the fact that viscosity becomes important in this region so that the condition of irrotational flow used in the analysis is not valid. Within this limitation, however, the potential flow field has been determined and the potential flow along the wall can now be used to investigate the boundary layer.

The Boundary Layer Response

The potential flow at the outer edge of the boundary layer has been given in the last section as

$$U = V_0 \frac{x/c}{\sqrt{1-(x/c)^2}} \cos \omega t . \tag{3.35}$$

Due to this velocity distribution, the pressure gradient imposed upon the boundary layer is given by

$$-\frac{1}{\rho}\frac{\partial p}{\partial x} = \frac{\partial U}{\partial t} + U\frac{\partial U}{\partial x} . \tag{3.36}$$

The relations governing the boundary layer are the equations of momentum and continuity written as

$$\frac{\partial u}{\partial t} + u\frac{\partial u}{\partial x} + v\frac{\partial v}{\partial y} = -\frac{1}{\rho}\frac{\partial p}{\partial x} + \nu\frac{\partial^2 u}{\partial y^2} \tag{3.37a}$$

$$\frac{\partial u}{\partial x} + \frac{\partial v}{\partial y} = 0 \ , \tag{3.37b}$$

where the pressure gradient is given by Equation (3.36).

The method of successive approximations will be used so that

$$u = u_0 + u_1 + \cdots \tag{3.38a}$$

$$v = v_0 + v_1 + \cdots \ . \tag{3.38b}$$

u_o and v_o represent initial approximations to the actual exact values of u and v, while the additional terms can be taken as correction terms thus achieving a successively higher degree of accuracy as more terms are taken. This should be a useful method provided that it can be shown that $|u_1| < |u_o|$, $|v_1| < |v_o|$, $|u_2| < |u_1|$, and so on. The use of successive approximations for calculating periodic boundary layer flows has been discussed by Schlichting[26], Lin[17], Gibson[9], and others.[2,3] Some of the more recent work has been done in connection with problems of acoustics.[2,3] Schlichting has applied his work to the case of a cylinder vibrating in a fluid at rest. This will be discussed further at the latter part of this section.

Only the first two approximations will be discussed here and the probable accuracy will be indicated during the discussion. Entering Equations (3.38) into Equations (3.37) gives

$$\underline{\left(\frac{\partial u_0}{\partial t} - \nu \frac{\partial^2 u_0}{\partial y^2}\right)} + \left[\frac{\partial u_1}{\partial t} - \nu \frac{\partial^2 u_1}{\partial y^2} + u_0 \frac{\partial u_0}{\partial x} + v_0 \frac{\partial u_0}{\partial y}\right] \tag{3.39a}$$

$$+\left[\left(u_0 \frac{\partial u_1}{\partial x} + u_1 \frac{\partial u_0}{\partial x}\right) + \left(v_0 \frac{\partial u_1}{\partial y} + v_1 \frac{\partial u_0}{\partial y}\right)\right] + \left(u_1 \frac{\partial u_1}{\partial x} + v_1 \frac{\partial u_1}{\partial y}\right)$$

$$+ \cdots = \underline{\frac{\partial U}{\partial t}} + U \frac{\partial U}{\partial x}$$

$$\underline{\left(\frac{\partial u_0}{\partial x} + \frac{\partial v_0}{\partial y}\right)} + \left(\frac{\partial u_1}{\partial x} + \frac{\partial v_1}{\partial y}\right) + \cdots = 0. \tag{3.39b}$$

For a first approximation only the underlined terms are retained giving

$$\frac{\partial u_0}{\partial t} - \nu \frac{\partial^2 u_0}{\partial y^2} = \frac{\partial U}{\partial t} \tag{3.40a}$$

$$\frac{\partial u_0}{\partial x} + \frac{\partial v_0}{\partial y} = 0. \tag{3.40b}$$

Equation (3.40a) would appear to be a valid first approximation to Equation (3.37a) provided that the local acceleration effects are larger than the convective effects. For example, the solution to (3.40a) will satisfy (3.37a) except for the error caused by the neglect of the terms $\left(u_0 \frac{\partial u_0}{\partial x} + v_0 \frac{\partial u_0}{\partial y}\right)$ and $U \frac{\partial U}{\partial x}$. A comparison of the terms $U \frac{\partial U}{\partial x}$ and $\partial U/\partial t$ can be made directly since U is known from Equation (3.35). The order of magnitude of the terms $(u_0 \, \partial u_0/\partial x + v_0 \, \partial u_0/\partial y)$ relative to $\partial u_0/\partial t$ cannot be given directly, since u_0 and v_0 are not known at this point. However, the velocities in the boundary layer may be expected to follow, in a qualitative way at least, the potential flow existing at the outer edge. For this reason, a fair idea of the magnitude of

the convective effects relative to those of local acceleration in the boundary layer can be obtained by considering the ratio of the convective term $U \frac{\partial U}{\partial x}$ to the local acceleration $\frac{\partial U}{\partial t}$ in the potential flow. The convective acceleration of the potential flow is calculated from (3.35) as

$$U \frac{\partial U}{\partial x} = \frac{V_0^2}{c} \frac{x/c}{[1-(x/c)^2]^2} \cos^2 \omega t \quad , \tag{3.41}$$

and the local acceleration is given by

$$\frac{\partial U}{\partial t} = - \omega V_0 \frac{x/c}{\sqrt{1-(x/c)^2}} \sin \omega t \quad . \tag{3.42}$$

Thus, $U \frac{\partial U}{\partial x}$ oscillates from zero to $\frac{V_0^2}{c} \frac{x/c}{[1-(x/c)^2]^2}$, while $\frac{\partial U}{\partial t}$ oscillates between plus and minus $\omega V_0 \frac{x/c}{\sqrt{1-(x/c)^2}}$. The importance of the convective term $U \frac{\partial U}{\partial x}$ relative to $\frac{\partial U}{\partial t}$ can now be found by computing the ratio

$$\frac{[U \, \partial U/\partial x]_{MAXIMUM}}{[|\partial U/\partial t|]_{MAXIMUM}} = \frac{a_0/c}{[1-(x/c)^2]^{3/2}} \tag{3.43}$$

Thus, the method can be expected to yield useful results if the amplitude of vibration is small compared with the length of the plate, except in the regions very close to the edges. Here the potential flow may be expected to be in error anyway, as pointed out in the last section, indicating a pressure distribution in the boundary layer quite different from that given by the expressions used in this analysis. Except in the edge region, however, the ratio given in (3.43) may be small in many cases. For example, consider a plate 10 inches long vibrating with an amplitude of .050 inches. The ratio given in (3.43) has a value of .01 at x/c = 0, .02 at x/c = .6, and .05 at x/c = .8. It should be pointed out that even when the ratio is not negligibly small Equations (3.40)

can still be used to obtain a useful first approximation since the overall error can be reduced to a smaller value by carrying the second approximation.

Now that the validity of neglecting the convective terms in comparison with local acceleration for a first approximation has been demonstrated, Equations (3.40) will be considered. Although convective terms are ignored in the first approximation, it is necessary that the viscous term be retained in order to satisfy the boundary condition of zero velocity at the wall. Physically this means that although convective effects may be small compared with local acceleration, viscosity must eventually become important very close to the wall and completely dominate at the wall. This is because both local and convective acceleration are zero at the wall leaving only viscosity to balance the pressure gradient corresponding to $\partial U/\partial t$. Equation (3.40a) can be satisfied by

$$U_0 = V_0 \frac{x/c}{\sqrt{1-(x/c)^2}} f'(\eta)\, e^{i\omega t}, \tag{3.44}$$

where $\eta = y\sqrt{\omega/\nu}$. Equation (3.40a) now becomes

$$f_0'''(\eta) - i\, f_0'(\eta) = -i \,. \tag{3.45}$$

Since the velocity must be zero at the wall and must approach $V_0 \frac{x/c}{\sqrt{1-(x/c)^2}}$ at the other edge of the boundary layer, the boundary conditions are $f_0'(0) = 0$ and $f_0'(\infty) = 1$. The solution to (3.45) is

$$f_0'(\eta) = 1 + C_1 e^{-\sqrt{i}\,\eta} + C_2 e^{\sqrt{i}\,\eta} \,. \tag{3.46}$$

In order to satisfy the boundary conditions, $C_2 = 0$ and $C_1 = -1$ so that the result is

$$f_0'(\eta) = 1 - e^{-\sqrt{i}\,\eta}. \tag{3.47}$$

The function $f_0'(\eta)$ is complex and has associated with it a magnitude and a phase angle. Therefore, it can be represented in the form $|f_0'(\eta)|e^{i\alpha_0}$. The magnitude and phase of $f_0'(\eta)$ are expressed as

$$\left|f_0'(\eta)\right| = \sqrt{\left[1 - e^{-\eta/\sqrt{2}} \cos \eta/\sqrt{2}\right]^2 + \left[e^{-\eta/\sqrt{2}} \sin \eta/\sqrt{2}\right]^2} \tag{3.48a}$$

$$\alpha_0 = \operatorname{Arc\,tan}\left[\frac{e^{-\eta/\sqrt{2}} \sin \eta/\sqrt{2}}{1 - e^{-\eta/\sqrt{2}} \cos \eta/\sqrt{2}}\right]. \tag{3.48b}$$

Plots of Equations (3.48) are shown in Figure 30. The amplitude of the oscillating velocity close to the outer edge of the boundary layer exceeds that of the potential flow outside the layer. The oscillations are in phase in the outer regions of the boundary layer, but the effect of viscosity causes a phase lead close to the wall that approaches a limiting value of 45° at the wall. The boundary layer thickness is given by $\eta/\sqrt{2} \approx 4$, or $\delta \approx 4\sqrt{2\nu/\omega}$, although most of the velocity variation occurs between the wall and $y = 1.5\sqrt{2\nu/\omega}$. As frequency increases the boundary layer becomes very thin. For air at 80°F, $\nu \approx 1.7 \times 10^{-4}$ ft^2/sec so that if the frequency is 50 cycles per second, the boundary layer thickness is about .050 inches. As the boundary layer becomes thinner with increasing frequency it can be expected that the wall shear stress will increase. This is verified by differentiation of (3.44) which yields

$$\left(\frac{\partial u_0}{\partial y}\right)_w = V_0 \frac{x/c}{\sqrt{1-(x/c)^2}} \sqrt{\frac{\omega}{\nu}}\; e^{i(\omega t + \pi/4)} \tag{3.49}$$

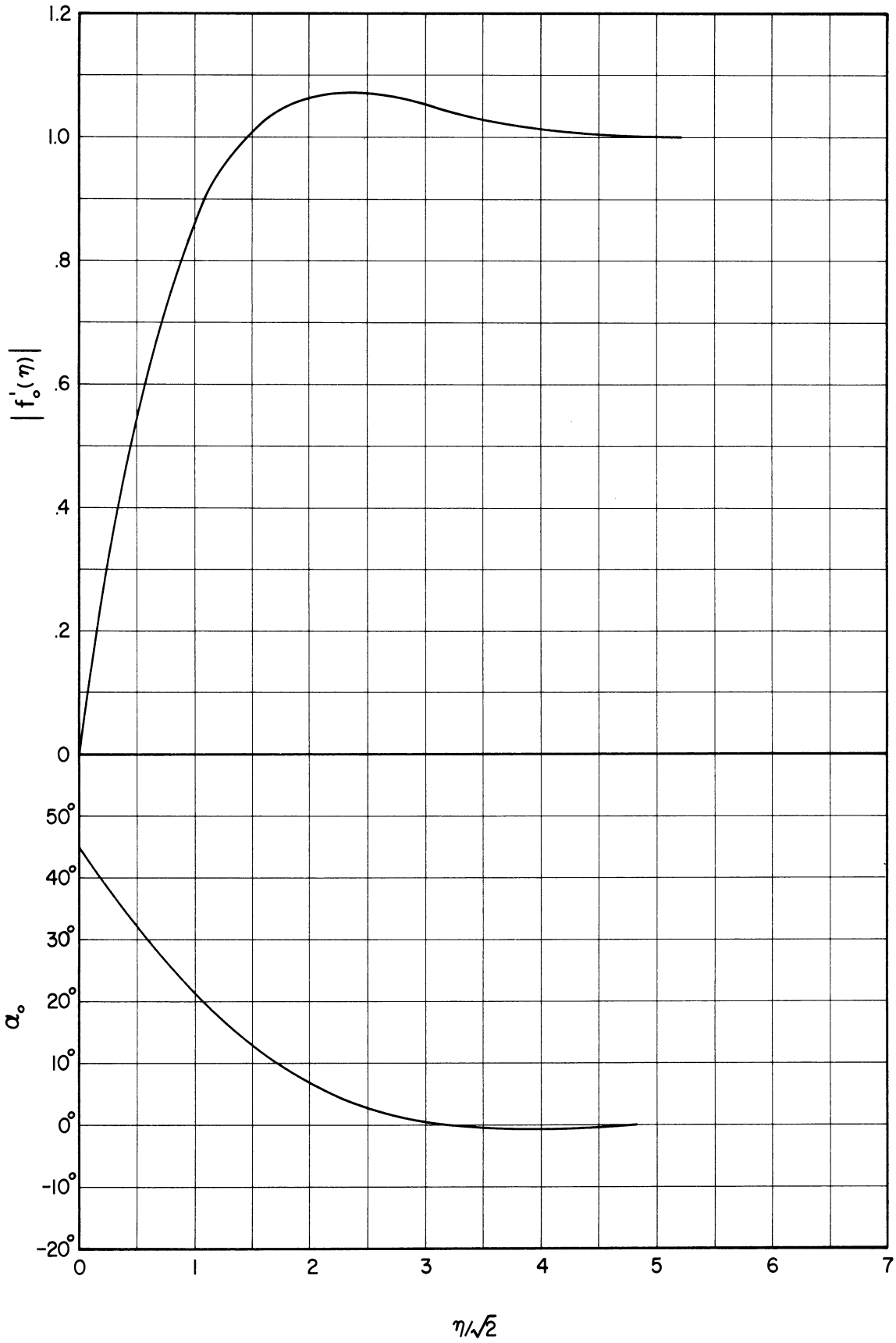

Figure 30. Magnitude and Phase of the First Approximation to the Oscillating Velocity Distribution in the Boundary Layer.

The shear stress has a phase lead of 45°, the same as that of the velocity oscillations close to the wall.

The y component of velocity in the first approximation is obtained by entering Equation (3.44) into Equation (3.40b) and integrating. The result is

$$v_0 = -\sqrt{\frac{\nu}{\omega}}\ \frac{V_0/c}{\left[1-(x/c)^2\right]^{3/2}}\ f_0(\eta)\ e^{i\omega t}, \tag{3.50}$$

where $f_0(\eta)$ is obtained by integrating (3.47) to give

$$f_0(\eta) = \eta - \frac{1}{\sqrt{i}}\left(1 - e^{-\sqrt{i}\,\eta}\right). \tag{3.51}$$

Writing $f_0(\eta)$ as a complex number $f_{0r}(\eta) + i\, f_{0i}(\eta)$ makes it possible to write the convective terms of the first approximation as

$$\left(u_0 \frac{\partial u_0}{\partial x} + v_0 \frac{\partial u_0}{\partial y}\right) = \frac{1}{2}\frac{V_0^2}{c}\frac{x/c}{\left[1-(x/c)^2\right]^2}\Big\{\Big[\left(f_{0r}'^2 + f_{0i}'^2\right) - \left(f_{0r} f_{0r}'' + f_{0i} f_{0i}''\right)\Big] + \Big[\left(f_{0r}'^2 - f_{0i}'^2\right) - \left(f_{0r} f_{0r}'' - f_{0i} f_{0i}''\right)\Big]\cos 2\omega t + \Big[\left(f_{0r} f_{0i}'' + f_{0i} f_{0r}''\right) - 2 f_{0r}' f_{0i}'\Big]\sin 2\omega t\Big\}. \tag{3.52}$$

The same quantity expressed in complex notation is

$$\left(u_0 \frac{\partial u_0}{\partial x} + v_0 \frac{\partial u_0}{\partial y}\right) = \frac{1}{2}\frac{V_0^2}{c}\frac{x/c}{\left[1-(x/c)^2\right]^2}\Big\{\Big[f_0' \bar{f}_0' - \frac{1}{2}\left(f_0 \bar{f}_0'' + \bar{f}_0 f''\right)\Big] + \Big[f_0'^2 - f_0 f_0''\Big]\, e^{i2\omega t}\Big\}, \tag{3.53}$$

where the bar notation indicates the complex conjugate. The local acceleration of the first approximation is

$$\frac{\partial u_0}{\partial t} = i\omega V_0 \frac{x/c}{\sqrt{1-(x/c)^2}} f_0'(\eta) \; e^{i\omega t} \quad . \tag{3.54}$$

Since the function $f_0(\eta)$ and its derivatives have values whose order of magnitude is roughly unity, a comparison of $\left(u_0 \frac{\partial u_0}{\partial x} + v_0 \frac{\partial u_0}{\partial y}\right)$ relative to $\partial u_0/\partial t$ from Equations (3.53) and (3.54) is seen to give the ratio $\frac{a_0/c}{[1-(x/c)^2]^{3/2}}$ which agrees with the estimate given in Equation (3.43). This quantity gives a rough idea of the error involved in Equation (3.37a) by approximating it with Equation (3.40a). It can therefore be expected that the error involved in the solutions u and v will be about the same order of magnitude when only the first approximations u_0 and v_0 are used.

A second approximation can be obtained from Equations (3.39) by writing

$$\frac{\partial u_1}{\partial t} - \nu \frac{\partial^2 u_1}{\partial y^2} = U \frac{\partial U}{\partial x} - \left(u_0 \frac{\partial u_0}{\partial x} + v_0 \frac{\partial u_0}{\partial y}\right) \tag{3.55a}$$

$$\frac{\partial u_1}{\partial x} + \frac{\partial v_1}{\partial y} = 0 \quad . \tag{3.55b}$$

Terms involving products of the first and second approximations and also those involving products of the second approximations are neglected in Equation (3.39a) at this point, but these smaller effects could be accounted for by taking successively higher approximations. Using Equations (3.41) and (3.53), Equation (3.55a) is now rewritten as

$$\frac{\partial u_1}{\partial t} - \nu \frac{\partial^2 u_1}{\partial y^2} = \frac{1}{2} \frac{V_0^2}{c} \frac{x/c}{[1-(x/c)^2]^2} \left\{ \left[1 - f_0' \bar{f}_0' + \frac{1}{2}\left(f_0 \bar{f}_0'' + \bar{f}_0 f_0'' \right) \right] + \left[1 - f_0'^2 + f_0 f_0'' \right] e^{i2\omega t} \right\} . \tag{3.56}$$

It is clear that u_1 will have a time varying component of frequency 2ω and also a steady component. In view of this fact it is possible to write $u = u_{1t} + u_{1s}$, and

$$u_1 = \frac{a_0}{c} V_0 \frac{x/c}{\left[1-(x/c)^2\right]^2} \left[f_{1t}'(\eta)\, e^{i2\omega t} + f_{1s}'(\eta) \right]. \tag{3.57}$$

Entering this expression into (3.56) gives

$$f_{1t}'''(\eta) - 2i\, f_{1t}'(\eta) = -\frac{1}{2} + \frac{1}{2} f_0'^2 - \frac{1}{2} f_0 f_0'' \tag{3.58a}$$

$$f_{1s}'''(\eta) = -\frac{1}{2} + \frac{1}{2} f_0' \bar{f}_0' - \frac{1}{4}\left(f_0 \bar{f}_0'' + \bar{f}_0 f_0'' \right). \tag{3.58b}$$

Substituting the expression for $f_0(\eta)$ into Equations (3.58) yields

$$f_{1t}'''(\eta) - 2i\, f_{1t}'(\eta) = -\frac{1}{2} e^{-\sqrt{i}\,\eta}\left(1 + \sqrt{i}\,\eta\right) \tag{3.59a}$$

$$\begin{aligned} f_{1s}'''(\eta) = \frac{1}{4}\Big\{ & 2 e^{-\sqrt{2}\,\eta} - (2-i)\, e^{-\sqrt{i}\,\eta} - (2+i)\, e^{-\sqrt{-i}\,\eta} \\ & - \sqrt{i}\,\eta\, e^{-\sqrt{i}\,\eta} - \sqrt{-i}\,\eta\, e^{-\sqrt{-i}\,\eta} \Big\}. \end{aligned} \tag{3.59b}$$

The particular solution to (3.59a) is of the form

$$\left[f_{1t}'(\eta) \right]_p = b_0\, e^{-\sqrt{i}\,\eta} + b_1\, \eta\, e^{-\sqrt{i}\,\eta} \tag{3.60}$$

Entering this expression into Equation (3.59a) yields $b_0 = i/2$ and $b_1 = -i^{3/2}/2$. The homogeneous solution to (3.59a) is

$$\left[f_{1t}'(\eta) \right]_h = C_1\, e^{-\sqrt{2i}\,\eta} + C_2\, e^{\sqrt{2i}\,\eta} \tag{3.61}$$

The full solution to (3.59a) is $f_{1t}'(\eta) = [f_{1t}'(\eta)]_p + [f_{1t}'(\eta)]_h$. Since $f_{1t}'(0) = f_{1t}'(\infty) = 0$, $C_2 = 0$ and $C_1 = -i/2$, so that the full solution to (3.59a) is now

$$f_{1t}'(\eta) = \frac{i}{2}\left(e^{-\sqrt{i}\,\eta} - e^{-\sqrt{2i}\,\eta}\right) + \frac{1}{2}\sqrt{-i}\;\eta\, e^{-\sqrt{i}\,\eta}. \tag{3.62}$$

Since $f_{1t}'(\eta)$ is a complex function it is possible to represent it as $|f_{1t}'(\eta)|e^{i\alpha_1}$ where the magnitude and phase are given by

$$\left|f_{1t}'(\eta)\right| =$$

$$\frac{1}{2}\sqrt{\left\{e^{-\eta/\sqrt{2}}\left[\frac{\eta}{\sqrt{2}}\cos\frac{\eta}{\sqrt{2}} + \left(1-\frac{\eta}{\sqrt{2}}\right)\sin\frac{\eta}{\sqrt{2}}\right] - e^{-\eta}\sin\eta\right\}^2 + \left\{e^{-\eta/\sqrt{2}}\left[\left(1-\frac{\eta}{\sqrt{2}}\right)\cos\frac{\eta}{\sqrt{2}} - \frac{\eta}{\sqrt{2}}\sin\frac{\eta}{\sqrt{2}}\right] - e^{-\eta}\cos\eta\right\}^2} \tag{3.63a}$$

$$\alpha_1 = \operatorname{Arc\,tan}\left\{\frac{e^{-\eta/\sqrt{2}}\left[\left(1-\eta/\sqrt{2}\right)\cos\eta/\sqrt{2} - \eta/\sqrt{2}\,\sin\eta/\sqrt{2}\right] - e^{-\eta}\cos\eta}{e^{-\eta/\sqrt{2}}\left[\eta/\sqrt{2}\,\cos\eta/\sqrt{2} + \left(1-\eta/\sqrt{2}\right)\sin\eta/\sqrt{2}\right] - e^{-\eta}\sin\eta}\right\}. \tag{3.63b}$$

Plots of the magnitude and phase of $f_{1t}'(\eta)$ are given in Figure 31. The magnitude rises from zero at the wall, reaches a maximum and drops off to zero at the outer edge of the boundary layer. The phase shows a lag of 45° at the wall with an increasingly larger lag farther out in the boundary layer. The component of shear stress oscillating at frequency 2ω is obtained by differentiation of (3.62) which gives

$$\left(\frac{\partial u_1}{\partial y}\right)_w = \left(\frac{2-\sqrt{2}}{2}\right)\sqrt{\frac{\omega}{\nu}}\;\frac{a_0}{C}\;V_0\;\frac{x/c}{\left[1-(x/c)^2\right]^2}\;e^{i\left(2\omega t - \frac{\pi}{4}\right)}. \tag{3.64}$$

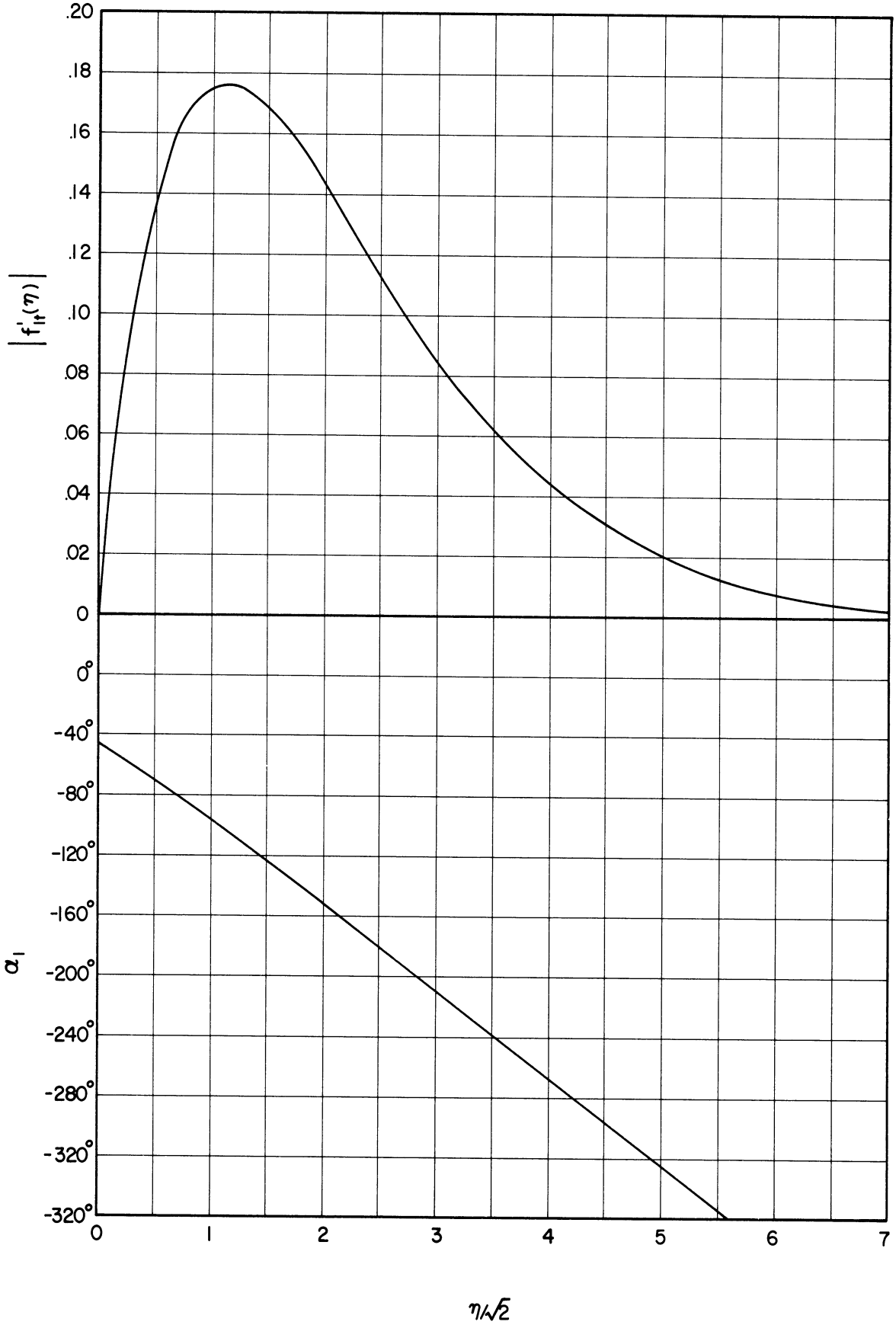

Figure 31. Magnitude and Phase of the Second Approximation to the Oscillating Velocity Distribution in the Boundary Layer.

The 45° lag in the wall shear stress agrees with the lag in the velocity oscillations near the wall as indicated by Figure 31.

The steady component u_{1s} is obtained by the double integration of Equation (3.59b) which gives

$$f_{1s}'(\eta) = \frac{1}{4}\left[e^{-2\eta} + (1+4i)\,e^{-\sqrt{i}\,\eta} + (1-4i)\,e^{-\sqrt{-i}\,\eta} - (1-i)\frac{\eta}{\sqrt{2}}\,e^{-\sqrt{i}\,\eta} - (1+i)\frac{\eta}{\sqrt{2}}\,e^{-\sqrt{-i}\,\eta}\right] + C_1\eta + C_2 \,, \tag{3.65}$$

where C_1 and C_2 are integration constants. It is clear that the velocity will increase indefinitely with increasing distance from the wall unless $C_1 = 0$. Also, $C_2 = -3/4$ in order to satisfy the no slip condition at the wall. All imaginary components cancel in Equation (3.65) so that the steady component of velocity is now written as

$$f_{1s}'(\eta) = -\frac{3}{4} + \frac{1}{4}\,e^{-\sqrt{2}\,\eta} + 2\,e^{-\eta/\sqrt{2}}\sin\eta/\sqrt{2} + \frac{1}{2}\,e^{-\eta/\sqrt{2}}\cos\eta/\sqrt{2} - \frac{1}{2}\,\frac{\eta}{\sqrt{2}}\,e^{-\eta/\sqrt{2}}\left(\cos\frac{\eta}{\sqrt{2}} - \sin\frac{\eta}{\sqrt{2}}\right). \tag{3.66}$$

A plot of Equation (3.66) is given in Figure 32. Close to the wall the steady motion is directed away from the stagnation point and toward the edges of the plate. At $\eta/\sqrt{2} \approx 1.15$, however, the direction reverses so that flow occurs from the edges toward the stagnation region farther out in the boundary layer. At the outer edge of the layer the steady flow does not go to zero but approaches a value of

$$u_{1s}(\infty) = -\frac{3}{4}\,\frac{a_0}{c}\,V_0\,\frac{x/c}{\left[1-(x/c)^2\right]^2} \,. \tag{3.67}$$

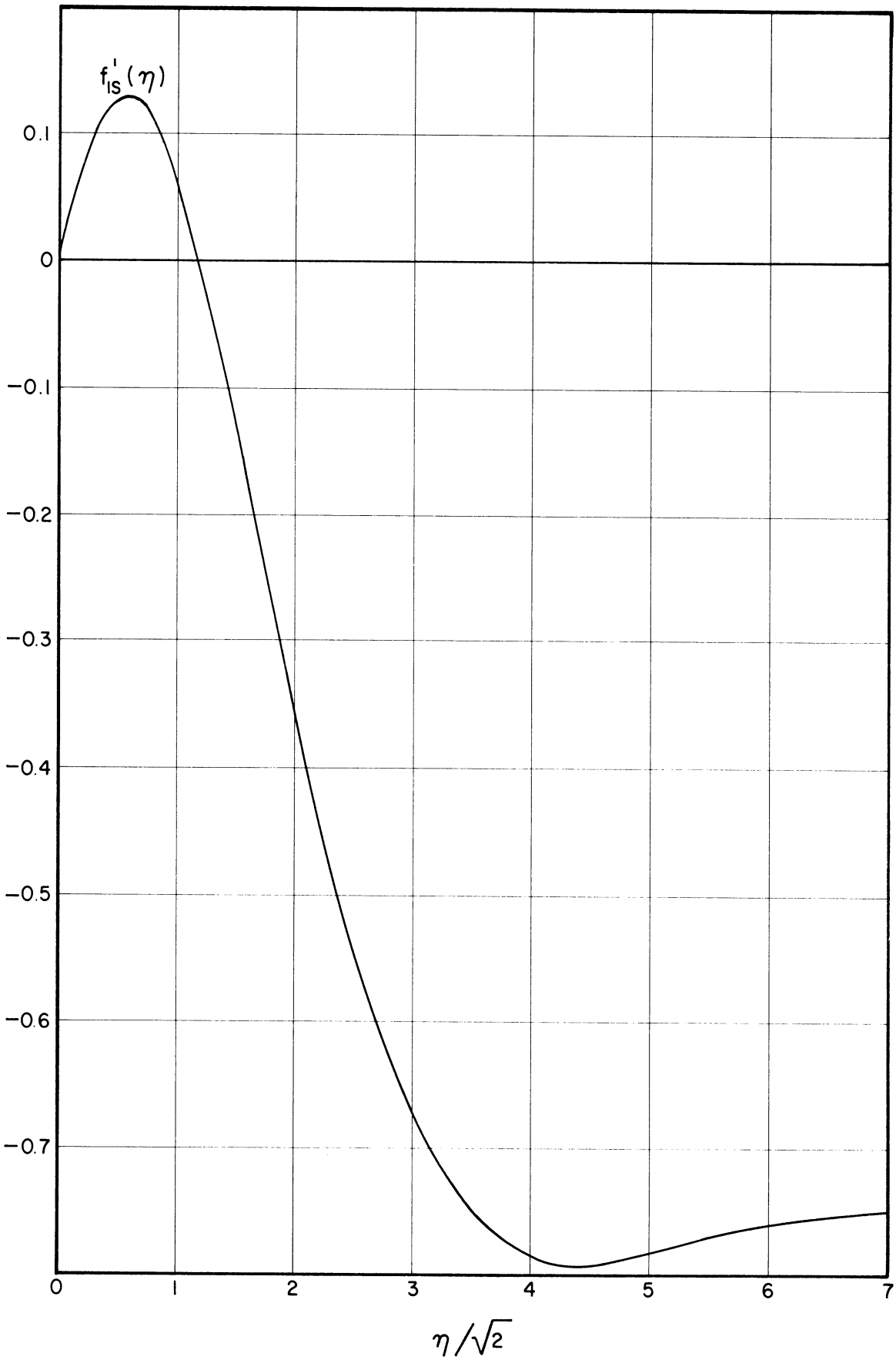

Figure 32. The Steady Velocity Distribution.

Thus, the effect of viscosity in the thin oscillating viscous layer is to produce a steady flow at the outer edge of the layer and beyond. This effect has been observed experimentally by Schlichting[26] who vibrated a circular cylinder in water. Fine metallic particles placed on the surface were photographed using long exposure times. The resulting photographs showed the trajectories followed by the particles. The particles far outside the boundary layer moved with a steady motion toward the stagnation region of the cylinder. This behavior agrees with the result given in Equation (3.67) in this analysis for a flat plate. Additional investigations of induced steady flow as a result of fluid oscillations have been made in connection with acoustics and some of these are given in the references.[2,3,4,18,20,21,22,31] The steady flow in these problems is called acoustic streaming. This phenomena occurs when a sound wave impinges upon a stationary object.

The steady component of shear stress is obtained by differentiating (3.65) which gives

$$\left(\frac{\partial u_{1s}}{\partial y}\right)_W = \left(\frac{\sqrt{2}-1}{2}\right)\sqrt{\frac{\omega}{\nu}}\ \frac{a_0}{c}\ V_0\ \frac{x/c}{\left[1-(x/c)^2\right]^2} \tag{3.68}$$

The oscillating and steady components of v_1 can be obtained if desired by integrating the expressions for u_1 in accordance with the continuity Equation (3.55b). The details of this operation will not be carried out here, but it can be verified that v_1 will have an order of magnitude given by $\sqrt{\frac{\nu}{\omega}}\ \frac{a_0}{c}\ \frac{V_0}{c}\ \frac{\left[1+3(x/c)^2\right]}{\left[1-(x/c)^2\right]^3}$. By comparison, v_0 is seen to have an order of magnitude given by $\sqrt{\frac{\nu}{\omega}}\ \frac{V_0/c}{\left[1-(x/c)^2\right]^{3/2}}$ from Equation (3.50). Therefore, v_1 has an order of magnitude that is smaller than that of v_0 by a factor of $\frac{a_0}{c}\ \frac{\left[1+3(x/c)^2\right]}{\left[1-(x/c)^2\right]^{3/2}}$. Similarly, since u_1 is proportional to

$\frac{a_0}{c} V_0 \frac{x/c}{[1-(x/c)^2]^2}$ from Equation (3.57), and u_0 is proportional to $V_0 \frac{x/c}{\sqrt{1-(x/c)^2}}$ from Equation (3.44), u_1 has an order of magnitude that is smaller than u_0 by a factor of $\frac{a_0/c}{[1-(x/c)^2]^{3/2}}$. Thus, both u_1 and v_1 are smaller than u_0 and v_0 respectively if the amplitude of vibration is small compared with the length of the plate except in the regions close to the edges.

The higher order terms not carried in this analysis can be expected to be somewhat smaller than the second approximation given here. In order to briefly summarize the results of this section the boundary layer velocity is now rewritten as

$$u = V_0 \frac{x/c}{\sqrt{1-(x/c)^2}} \left\{ \left| f_0'(\eta) \right| e^{i(\omega t + \alpha_0)} + \frac{a_0/c}{[1-(x/c)^2]^{3/2}} \left[\left| f_{1t}'(\eta) \right| e^{i(2\omega t + \alpha_1)} + f_{1s}'(\eta) \right] + \cdots \right\}, \tag{3.69}$$

where $f_0'(\eta)$, $f_{1t}'(\eta)$, and $f_{1s}'(\eta)$ are given in Figures 30, 31, and 32. This is the boundary layer response to an oscillating potential flow $U = V_0 \frac{x/c}{\sqrt{1-(x/c)^2}} e^{i\omega t}$. The potential flow oscillations increase with increasing distance from the stagnation point. The boundary layer responds with both oscillating and steady components whose magnitudes also increase with distance from the stagnation point.

List of Symbols for Chapter III

a	The semi-major axis of an ellipse defined by Equation (3.19a)
a_o	The amplitude of vibration of the plate
b	The semi-minor axis of an ellipse defined by Equation (3.19b)
b_o, b_1	Constants in Equation (3.60)
C_1, C_2	Constants in Equations (3.46), (3.61), and (3.65)
c	One half the length of the plate
e	Base of the natural logarithms
$f_o(\eta)$	First approximation to the boundary layer velocity profile defined by Equation (3.44)
$f_{oi}(\eta)$	The imaginary component of $f_o(\eta)$, $f_o(\eta) = f_{or}(\eta) + if_{oi}(\eta)$.
$f_{or}(\eta)$	The real component of $f_o(\eta)$, $f_o(\eta) = f_{or}(\eta) + if_{oi}(\eta)$.
$f_{1s}(\eta)$	The steady component of the second approximation to the boundary layer velocity profile defined by Equation (3.57)
$f_{1t}(\eta)$	The time varying component of the second approximation to the boundary layer velocity profile defined by Equation (3.57)
$(\ )_h$	Subscript indicating a homogeneous solution.
I	The imaginary component of w(z) defined by Equation (3.6)
i	The square root of (-1)
K	Constant in Equation (3.14)
p	Pressure
$(\ )_p$	Subscript indicating a particular solution
R	The real component of w(z) defined by Equation (3.6)
s	Distance along the surface of a solid body moving in a fluid
t	Time
U	Potential flow velocity in the direction parallel to the plate

$\bar{U}$	Amplitude of the potential flow velocity oscillations in the direction parallel to the plate, $U = \bar{U}\, e^{i\omega t}$
U_o	Amplitude of the potential flow velocity oscillations along the plate, $U_o = (\bar{U})_{y=o}$ for $0 < \lvert x/c \rvert < 1$
u	Boundary layer velocity in the direction parallel to the plate
u_o, u_1	The first two approximations to u defined by Equation (3.38a)
u_{1t}, u_{1s}	The time varying and steady components of u_1, where $u_1 = u_{1t} + u_{1s}$
V	Potential flow velocity in the direction normal to the plate
$\bar{V}$	Amplitude of the potential flow velocity oscillations in the direction normal to the plate, $V = \bar{V}\, e^{i\omega t}$
V_o	Amplitude of velocity of vibration of the plate, $V_o = a_o\omega$
v	Boundary layer velocity in the direction normal to the plate
v_o, v_1	The first two approximations to v defined by Equation (3.38b)
$W(z)$	A function of a complex variable defined by Equation (3.6) and also the complex potential defined by Equation (3.11)
x	The coordinate in the direction parallel to the plate
y	The coordinate in the direction normal to the plate
z	The complex variable $x + iy$
∞	Indicates a condition far from the plate

Greek Letters

α_o	The phase angle of the first approximation to the boundary layer velocity, $f_o'(\eta) = \lvert f_o(\eta) \rvert e^{i\alpha_o}$.
α_1	The phase angle of the oscillating component of the second approximation to the boundary layer velocity, $f_{1t}'(\eta) = \lvert f_{1t}'(\eta) \rvert e^{i\alpha_1}$
β	The imaginary component of ζ where $\zeta = \xi + i\beta$
Δ	Indicates an increment of a quantity such as Δx or Δy
∇^2	The Laplacian Operator $\partial^2/\partial x^2 + \partial^2/\partial y^2$.
δ	The boundary layer thickness

ζ	The elliptic coordinate defined by Equation (3.13a)
η	Dimensionless distance from the plate, $\eta = y\sqrt{\omega/\nu}$
ν	Kinematic viscosity of the fluid
ρ	The density of the fluid
ξ	The real component of ζ where $\zeta = \xi + i\beta$
ξ_0	A constant defining the equation of the ellipse in the elliptic coordinate system
Φ	The velocity potential defined by Equations (3.2)
ϕ	The amplitude of the velocity potential defined by Equation (3.4a)
Ψ	The stream function defined by Equations (3.2)
ψ	The amplitude of the stream function defined by Equation (3.4b)
ω	The frequency of vibration of the plate.

CHAPTER IV

EXPERIMENTAL WORK

Introduction

An experimental program has been carried out in the Heat Transfer and Thermodynamics Laboratory of the Department of Mechanical Engineering, and the results will be discussed primarily in relation to the phenomena described in Chapters II and III. These results involve data obtained from velocity measurements made with a hot wire anemometer, and also some data from heat transfer measurements made to determine the effect of wall vibration on the time averaged heat transfer rate. Air is used as the fluid for all of the experimental work reported here. Although the major emphasis of Chapters II and III is applied to fluid mechanics rather than heat transfer, it is extremely helpful to have experimental measurements of heat transfer so that the order of magnitude of the effects of vibration as predicted by the analysis may be verified. Also, future heat transfer work beyond that described in this report is contemplated as a part of the vibration research program being continued in the Heat Transfer and Thermodynamics Laboratory. For these reasons the construction of the test apparatus has been strongly oriented toward the problem of heat transfer measurement.

Description of the Test Apparatus

A general view of the test apparatus is shown in Figure 33. The main components are a 10 inch square plate 3/4 of an inch thick provided with a 6 inch square heated section, and a mechanical vibrator whose moving element is attached to the plate by a suitable mounting

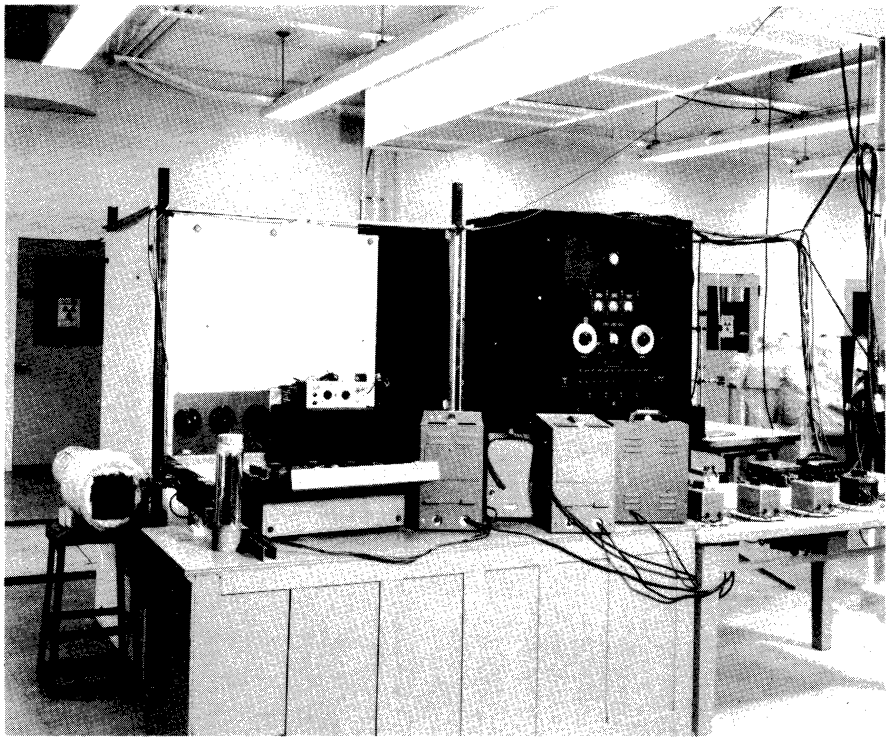

Figure 33. General View of the Experimental Apparatus.

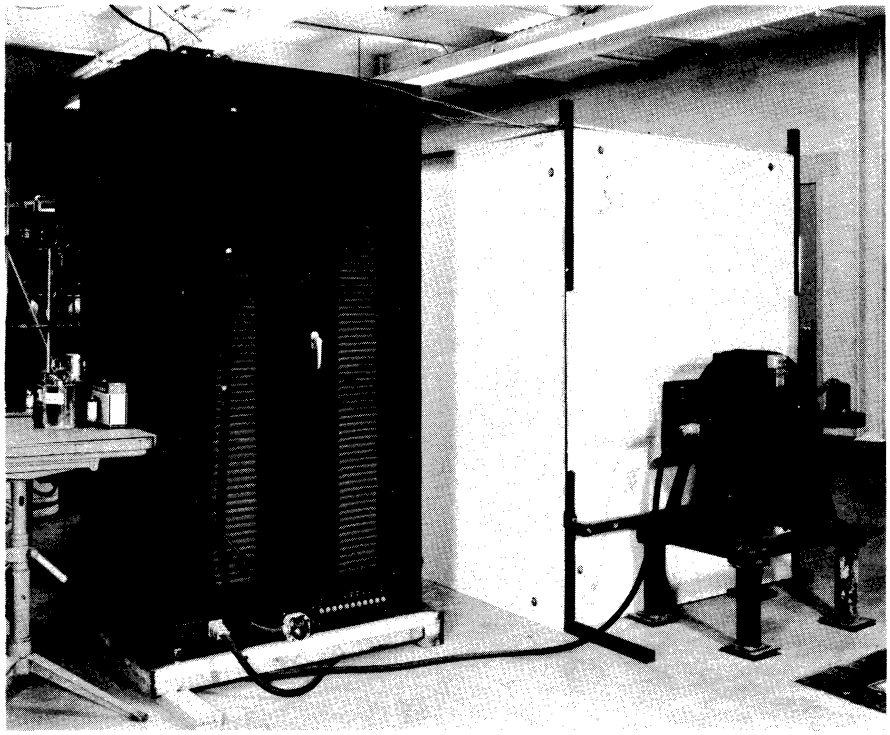

Figure 34. Rear View of the Experimental Apparatus.

system. This system consists of a set of rods 3/8 of an inch in diameter which fasten to the plate normal to its surface. The rods slide in teflon bushings mounted in a stationary bearing wall 2 inches thick, and connect to the moving element of the vibration exciter on the other side. A sketch of the physical arrangement described above is shown in Figure 35. The vibration equipment was built by the MB Manufacturing Company. The vibration exciter is a model C-5B and its control unit is a model T-51D. The vibrator together with its control unit can be seen in Figure 34. Also shown in this figure and in Figure 33 is the celotex enclosure surrounding the test area. Its function is to insure that the measurements are not influenced by drafts and stray air currents from the ventilating system of the building or the cooling fan on the vibrator. The plate inside the enclosure is shown in Figure 36. Further modifications, such as the bracket for mounting the hot wire anemometer probe, will be indicated later after the detailed construction of the test plate and the instruments associated with it have been discussed.

The construction of the test plate is shown in Figure 37. The center section of the plate consists of a heating element sandwiched between two aluminum plates 6 inches square and approximately 3/8 of an inch thick. These plates are clamped together by four hex nuts at the corners which attach to the ends of the four mounting rods that are threaded into one of the plates. The heating element was made by winding chromal ribbon 1/8 of an inch wide by .002 inches thick on a thin sheet of mica. Two additional mica sheets insulate the heating element from the aluminum plates. The energy input to the heater is controlled electrically by means of a variac, while the current and voltage drop

are measured with an ammeter and voltmeter respectively so that the energy rate can be determined. The heating element has an electrical resistance of about 30 ohms. A diagram of the electrical heating system is shown in Figure 38. The ammeter and voltmeter have been calibrated by the Calibration Laboratory of the Electrical Engineering Department. The heating circuits shown in Figure 38 in addition to the circuit described above are concerned with the four guard heaters which surround the heated aluminum plates in the center of the test plate. These heating elements consist of Chromal ribbon wound on transite strips whose ends are fastened to the outside section of the test plate as shown in Figure 37. A view showing the instruments discussed in this paragraph can be seen in Figure 39.

The purpose of the guard heaters is to prevent any of the measured energy input to the central section from being conducted away from the edges of the aluminum plates to the outside section of the test plate. Thin magnesium strips insulated from the guard heater elements by mica are glued to the transite strips facing toward the central heated section. An air gap of approximately 1/10 of an inch separates each magnesium strip from the edges of the aluminum plates in the center. With the exception of a few very small transite spacers for maintaining relative location, there is no mechanical contact within the test plate between the aluminum plates and the magnesium strips which surround them. The air gaps, therefore, provide a high thermal resistance between the two. Each magnesium strip, having low thermal resistance, achieves a uniform temperature which is determined by the controlled energy input to its respective guard heater element. By maintaining the temperature of

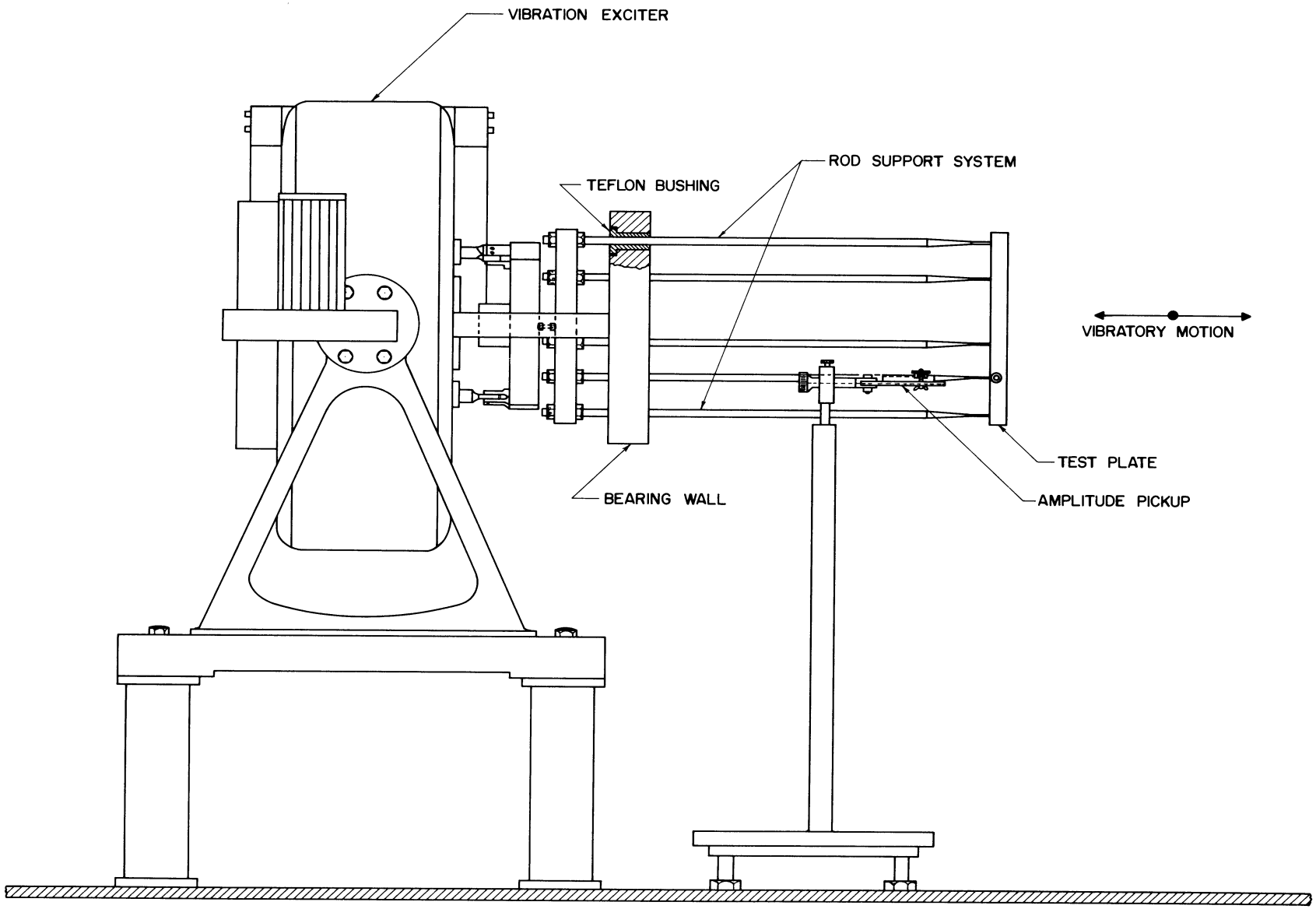

Figure 35. Sketch Showing the Arrangement of the Vibratory Components of the Apparatus.

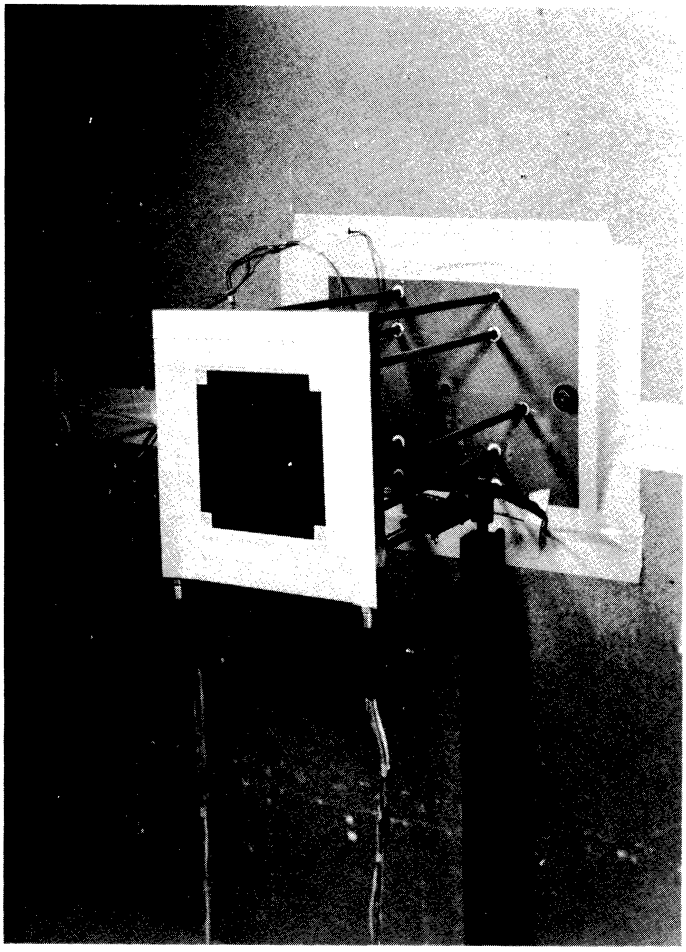

Figure 36. View of the Test Plate.

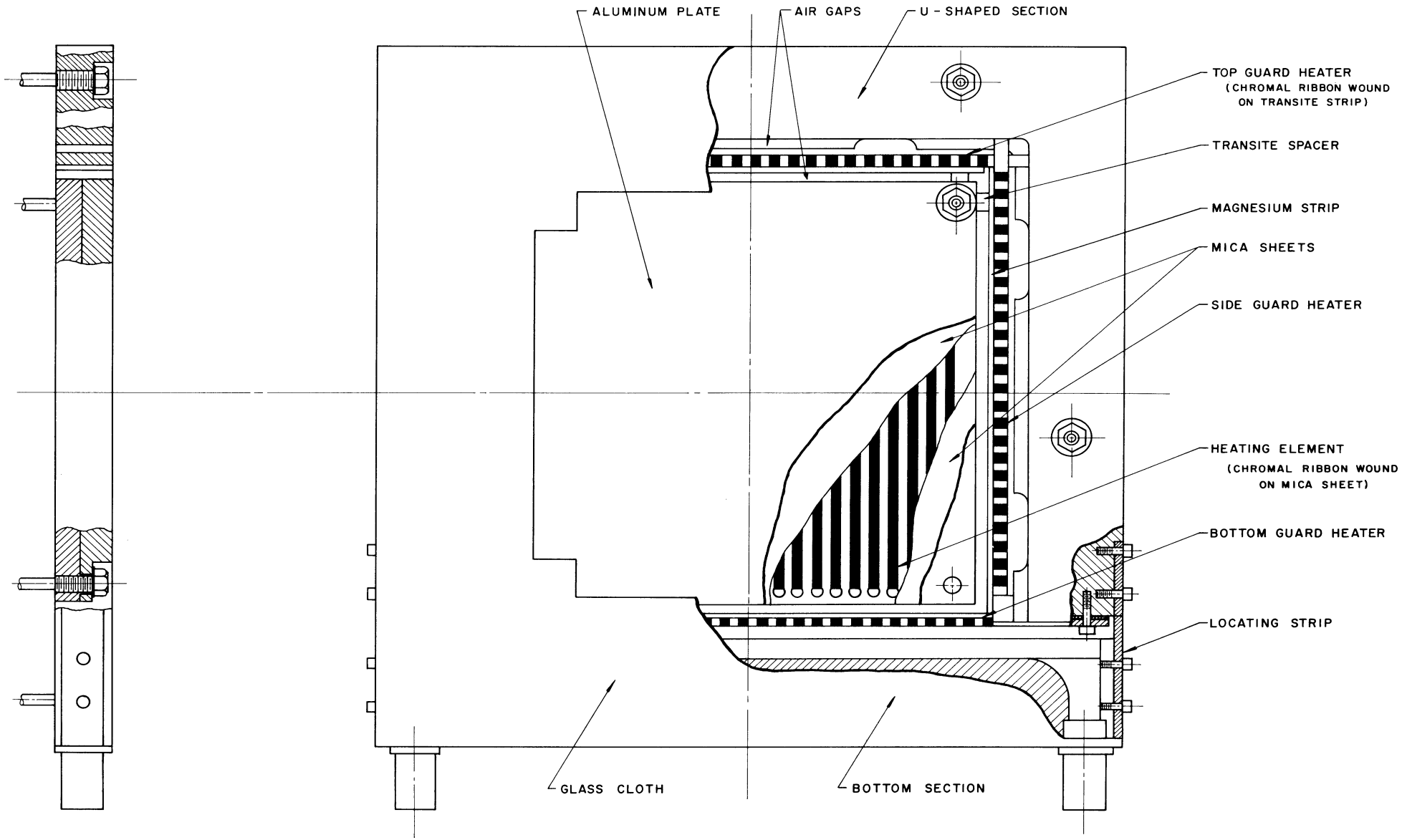

Figure 37. Construction of the Test Plate.

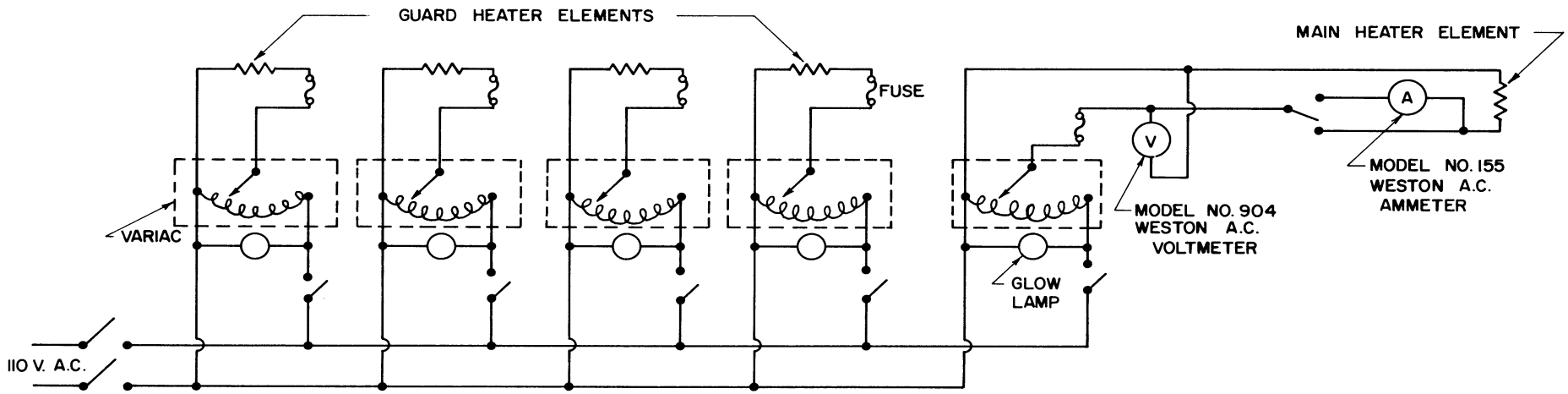

Figure 38. Electrical Circuit for Measurement of Energy Input and Control of Heater Elements.

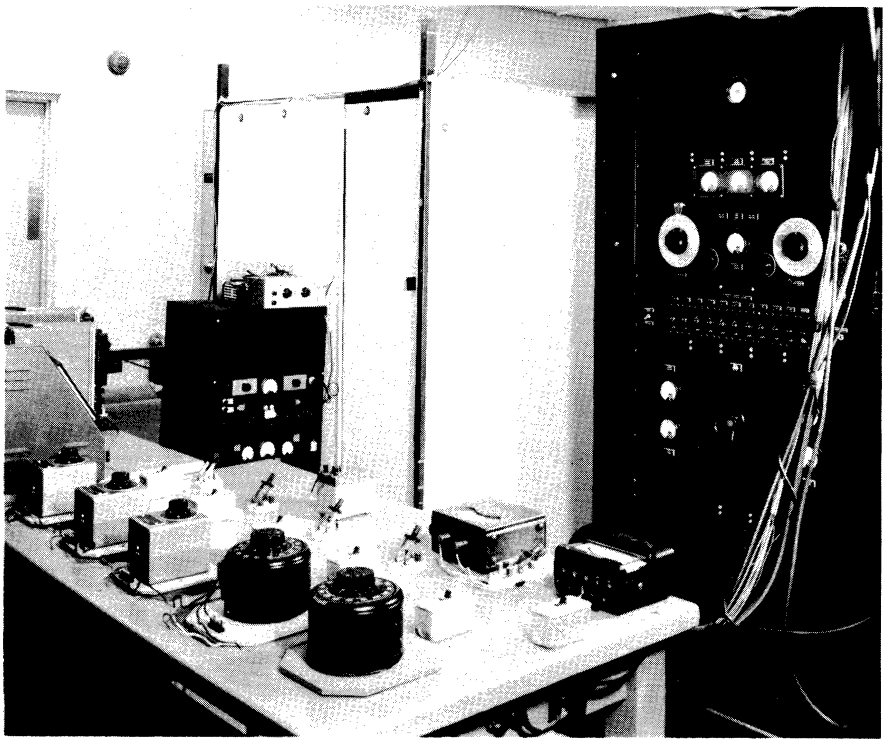

Figure 39. View of Some of the Instruments.

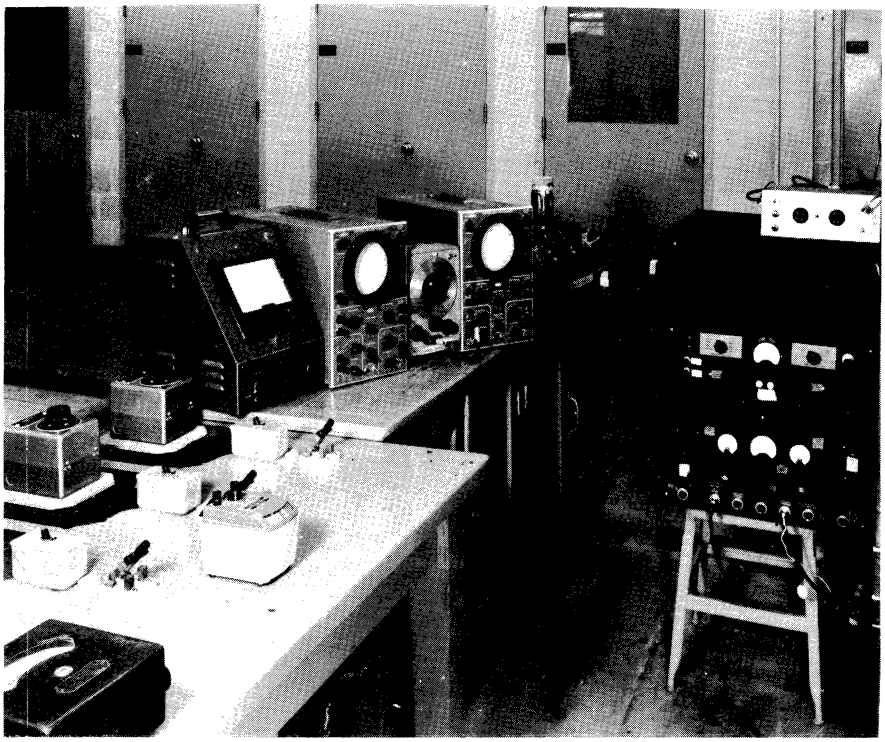

Figure 40. View of Some of the Instruments.

each strip at the same level as that of the aluminum plates, heat transfer from central section across the air gaps to the outer section of the test plate is prevented. The method of temperature measurement and control will be discussed after the description of the test plate construction has been completed.

Although the transite strips are fastened to the outer section of the test plate at the ends, no contact occurs along the length of each strip as air gaps are provided here also. This minimizes the heat transfer from the guard heaters to the outer edges of the test plate, but the top and side portions, which consist of a single U-shaped section, do heat up to some extent during operation since the ends of all four transite strips are fastened mechanically to this piece. The bottom portion of the outside section is separate and its only mechanical connection with the U-shaped section is provided by means of two small locating strips at the extreme outer edges of the test plate. This bottom section, therefore, is insulated fairly well from all sources of heat within the apparatus so that its temperature rise during operation is very slight. Ideally this portion should remain at ambient temperature for free convection studies so that the condition of a step change in wall temperature may be approached at the bottom edge of the heated section.

In order to provide a continuous flat surface over the entire area of the test plate and still maintain the high thermal resistance between the heated and outside sections provided by the air gaps, thin glass cloth with a thermosetting adhesive is extended between the two sections as shown in Figure 37. This conceals the guard heaters, the air gaps, and internal wiring from the view in Figure 36.

The reason for the large number of rods in the support system should now be apparent. The fact that the test plate consists of mechanically isolated sections to achieve proper thermal control requires that each section be supported independently by its own set of rods. Although the test plate is suspended about 16 inches beyond the bearing wall, no particular difficulty has been encountered due to the bending moment exerted on the rods by the weight of the test plate. The reason for this rather large overhang is that the test plate must be removed sufficiently far from the bearing wall so that the test plate and the air around it form a symmetrical system. This is especially important when investigating the problem discussed in Chapter III where it is desired to simulate the hydrodynamics of a finite plate vibrating in an infinite fluid at rest. Another instance when symmetry required is that of heat transfer measurement where it is necessary to assume that the measured energy input to the test section is transferred equally from the faces of the two aluminum plates. The rods are 3/8 of an inch in diameter, but are necked down in the region where they attach to the test plate. In this region the bending problem is not important and the smaller diameter of the rods here was intended to minimize any possible disturbance that the rods would exert on the flow pattern.

An attempt was made to keep the vibrating members of the apparatus as light as possible and to maintain a high degree of stiffness in most places. For this reason magnesium was used in fabricating the outside section of the test plate, the rods which support it, and the plate connecting all of the rods on the opposite side of the bearing

wall. The plates comprising the central section were made of aluminum, as previously mentioned, the reason for this being that radiation losses from this section are kept small by using highly polished aluminum for the heated surface. The rods supporting the heated section were made of stainless steel because of its low thermal conductivity, and these rods are necked down to a diameter of .140 inches for a distance of about one inch from the plate. The objective here was to minimize the conduction losses from the heated section through the rods supporting it. The radiation and conduction losses are important in those measurements involving heat transfer and will be more fully discussed later.

Now that the mechanical construction of the test plate, its mounting system, and its heater components have been explained, the problem of temperature measurement and control will be discussed. Thermocouples made from number 24 guage copper-constantan wire are used to indicate temperature. Seven thermocouples are imbedded at various points in each aluminum plate of the central section. This was accomplished by drilling small holes from the back side of each plate to within 3/32 of an inch of the polished surface, inserting the thermocouples so that they were in contact with the ends of the holes, and glueing them in place with epoxy thermosetting resin. Slots milled on the inside face of each aluminum plate from the holes to the lower edge provide space for leading the wires out into the bottom section of the test plate from which all wires emerge as shown in Figure 36. These thermocouple wires are connected to a system of rotary switches, shown on the wall of the celotex enclosure in Figure 33, making it possible to switch to any single thermocouple and read its indicated output voltage using a

Leeds and Northrup Model 8662 Portable Precision Potentiometer. An ice bath is used for the reference junction and the thermocouple wire has been calibrated in the laboratory. Due to the large therml inertia and low thermal resistance of the aluminum plates, and also the relatively low heat transfer coefficient at the surface, all thermocouples in both plates read very close to the same value at any given time during operation. This indicates a high degree of uniformity of temperature throughout the heated portion of the test section. The fact that essentially no temperature difference exists between the two plates indicates that the previously discussed symmetry condition has been achieved.

Four additional thermocouples are mounted in contact with the magnesium strips on the guard heaters. These are connected by means of the switching arrangement shown in Figure 41 with the leads coming from four other thermocouples imbedded in the aluminum plates near the edges. The resultant voltage difference from each pair of thermocouples is applied individually to a sensitive galvanometer by depressing the proper switch as shown in Figure 41. If the galvanometer does not deflect, both thermocouples are at the same temperature indicating that the particular magnesium strip in question has the same temperature as the aluminum plates. This means that the particular guard heater involved is adjusted properly so that no heat transfer can occur from that edge of the central heated section. A negative deflection of the galvanometer indicates that the variac controlling the current to the guard heater requires an increase in its setting. Correspondingly, a positive deflection indicates too high a setting that needs to be reduced. It is estimated that the magnesium strips

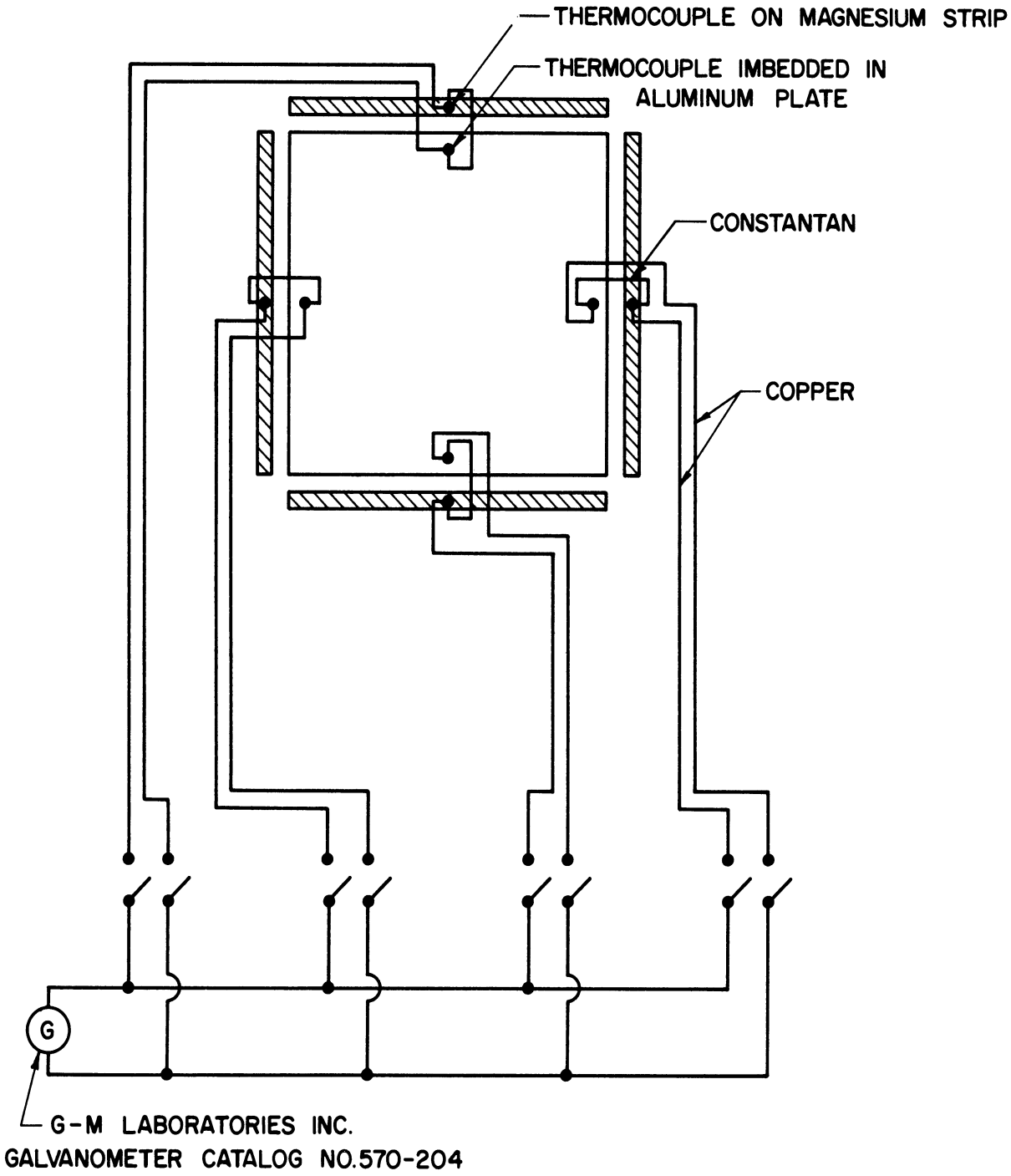

Figure 41. Galvanometer Circuit for Controlling Guard Heater Elements.

can be kept within 3°F of the temperature of the aluminum plates during operation of the system for measuring heat transfer if the galvanometer readings are sampled and the variacs properly adjusted periodically. The galvanometer and the four double switches used to connect it to each pair of thermocouples can be seen in Figure 39.

The operation of the vibrator is controlled by means of the control unit shown on the right in Figure 39. The desired frequency is set on frequency control dial of the oscillator whose signal is used as input to the power amplifier driving the vibrator. The amplitude is monitered by means of a Schaevitz Linear Differential Transformer Model 100-AS-L and a movable core attached to one edge of the test plate with a small brass rod. The transformer has a stationary mounting provided with fine position adjustment by means of a sliding member controlled by a threaded shaft. The transformer and movable core system can be seen just to the right of the test plate in Figure 36. A Hewlett-Packard Model 200 CD Audio Oscillator set at 10 kilocycles carrier frequency is used for an input to the transformer. The output is displayed on a Dumont Oscilloscope Type 304-H. A diagram of this system is shown in Figure 42. In order to calibrate the system the transformer is first placed in its null position with respect to core by moving it until a zero signal is shown on the scope. If it is desired to operate at an amplitude of .050 inches for example, the sliding member of the transformer mounting system is moved against a spacer .050 inches thick placed in a slot provided for that purpose. This displaces the transformer .050 inches with respect to the core away from the null position so that the high carrier frequency causes a blurred signal on the scope

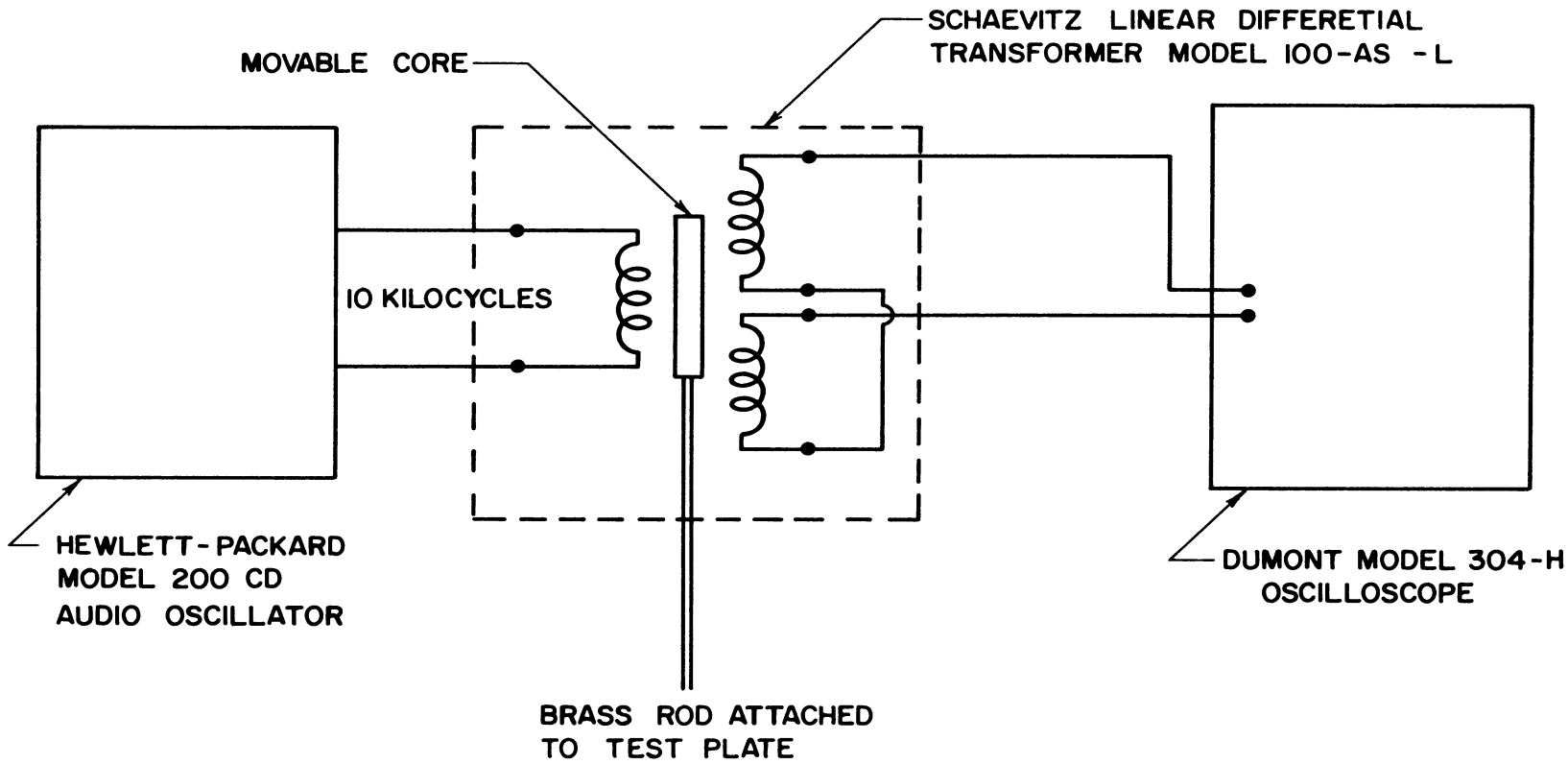

Figure 42. Linear Differential Transformer Circuit for Measurement of Vibration Amplitude.

as shown in Figure 43. The oscillator output or scope gain is then adjusted until the signal occupies the full scale of the scope screen. This calibrates the system so that full scale on the scope corresponds to a displacement of .050 inches. During vibratory conditions the sweep frequency on the scope is set equal to the frequency of vibration. The signal appears as the envelope of a sine wave as shown in Figure 44 when the transformer position adjustment is properly set so that motion occurs equally to either side of the null position. The region between the limits of the sine wave envelope is blurred by the sinusoidal signal corresponding to the 10 kilocycle carrier frequency. The amplitude of vibration is then increased by means of the power control on the control unit until the sine wave envelope occupies full scale on the scope screen. The amplitude of vibration is then known to be that for which the system was calibrated originally which is .050 inches in the example. In addition to the measurement of vibration amplitude described above, the uniformity of vibration of the test plate has been checked periodically using a Model 11-A Televiso Vibration Meter with a manual vibration pickup. The procedure is to hold the pickup on each of the four corners of the test plate under vibratory conditions to see if the meter readings are the same at each corner. The vibration meter, oscilloscope, and audio oscillator can be seen in Figure 40.

In evaluating heat transfer measurements it is important to know the magnitude of the radiation losses from the polished aluminum plates of the central heated section of the test plate. For this reason the emissivity of these plates was measured using a Model 810C69 Cenco Thermopile. The output of the thermopile was measured using a Leeds and

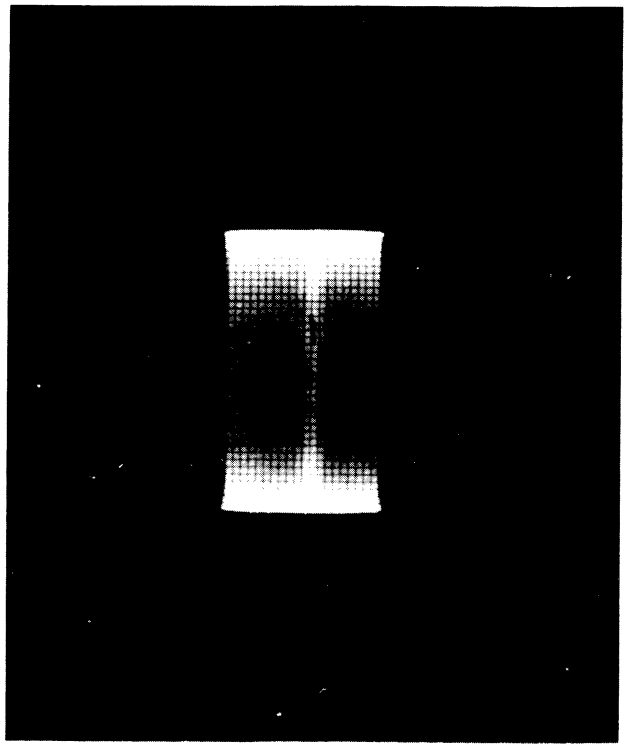

Figure 43. Output Signal of the Linear Differential Transformer with the Core Displaced from the Null Position as Displayed on an Oscilloscope.

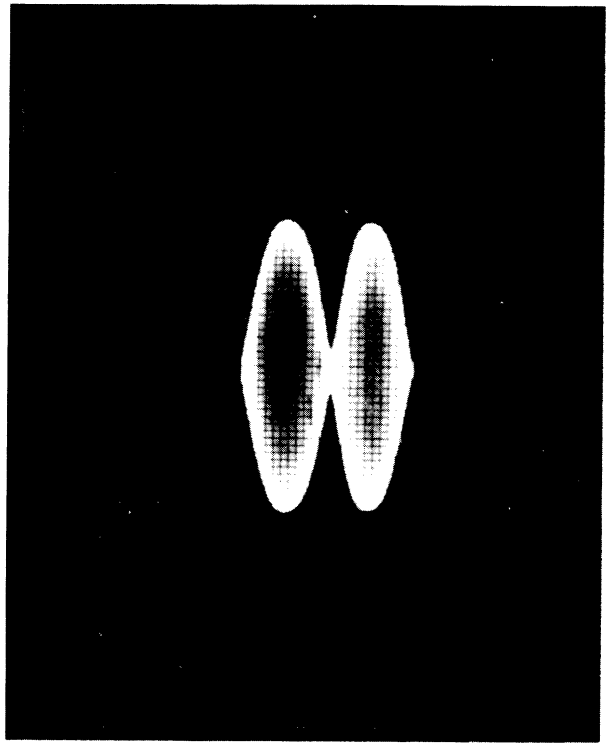

Figure 44. Output Signal of the Linear Differential Transformer Under Vibratory Conditions as Displayed on an Oscilloscope.

Northrup K-3 Universal Potentiometer. This instrument is capable of measuring voltages to an accuracy of about one microvolt. A black body was constructed of copper 1/8 of an inch thick formed into a cone of square crossection. Additional pieces of copper 1/4 of an inch thick were soldered on all four sides of the cone to increase temperature uniformity during operation. The open end is 6 inches square and the included angle at the apex is about 12°. The inside surface was blackened by means of an acetylene torch. This type of geometry is known to cause the open end of the cone to approach very closely the characteristics of a theoretical black body even when the surface emissivity inside is much lower than unity. The cone is insulated with a layer of asbestos paper and many turns of high resistance wire are wound around the cone over the paper. This wire is connected to a variac supplied with 110 volt AC power. The heating of the cone is controlled by means of this variac while the temperature of the cone is measured by means of several thermocouples imbedded in the copper. Heavy fiberglass insulation surrounds the cone and its heating element. Its purposes are to help maintain a uniform temperature throughout the cone, to keep the cone at a relatively stable temperature level thus preventing rapid temperature drops during operation when readings are being made, and to minimize the time necessary for heating the cone to a prescribed temperature by preventing losses that would otherwise occur. The constructed black body can be seen just to the left of the celotex enclosure in Figure 33.

The procedure for obtaining the emissivity of the aluminum plates was to focus the thermopile on one of the plates and to record

the output of the thermopile for various plate temperatures. This process was then repeated for the black body. The ratio of the voltages at a given temperature level gives the emissivity of the plate. For a more thorough discussion of emissivity measurement the reader is referred to papers on this subject such as those given in references 6 and 29. The emissivity of the polished aluminum plates was found to be very close to .05 over a temperature range of 20°F to 100°F above ambient.

For the purpose of making velocity measurements a hot wire anemometer system is used. All velocity measurements have been made with respect to the vibrating wall, that is, the hot wire probe is mounted to the moving plate under vibratory conditions. This was done in view of the moving coordinate systems used in Chapters II and III. The probe and its mounting system providing a means for changing the position of the probe are shown in Figure 46. Although the control unit contains a standard cell with bridge and potentiometer circuits for accurate measurements of resistance, current, and voltage, only the circuit used during operation for measuring oscillating velocities will be discussed here. This circuit is shown in Figure 45. The current is adjusted by means of the rheostats and remains constant during operation due to the relatively low resistance of the hot wire as compared with the other resistance in the circuit. The hot wire probe itself is made of .00015 inch diameter platinum etched Wollaston Process Wire. Velocity fluctuations cause the wire to alternately change its temperature and the resistance of the wire varies in response to these temperature changes. Since current is constant, a fluctuating

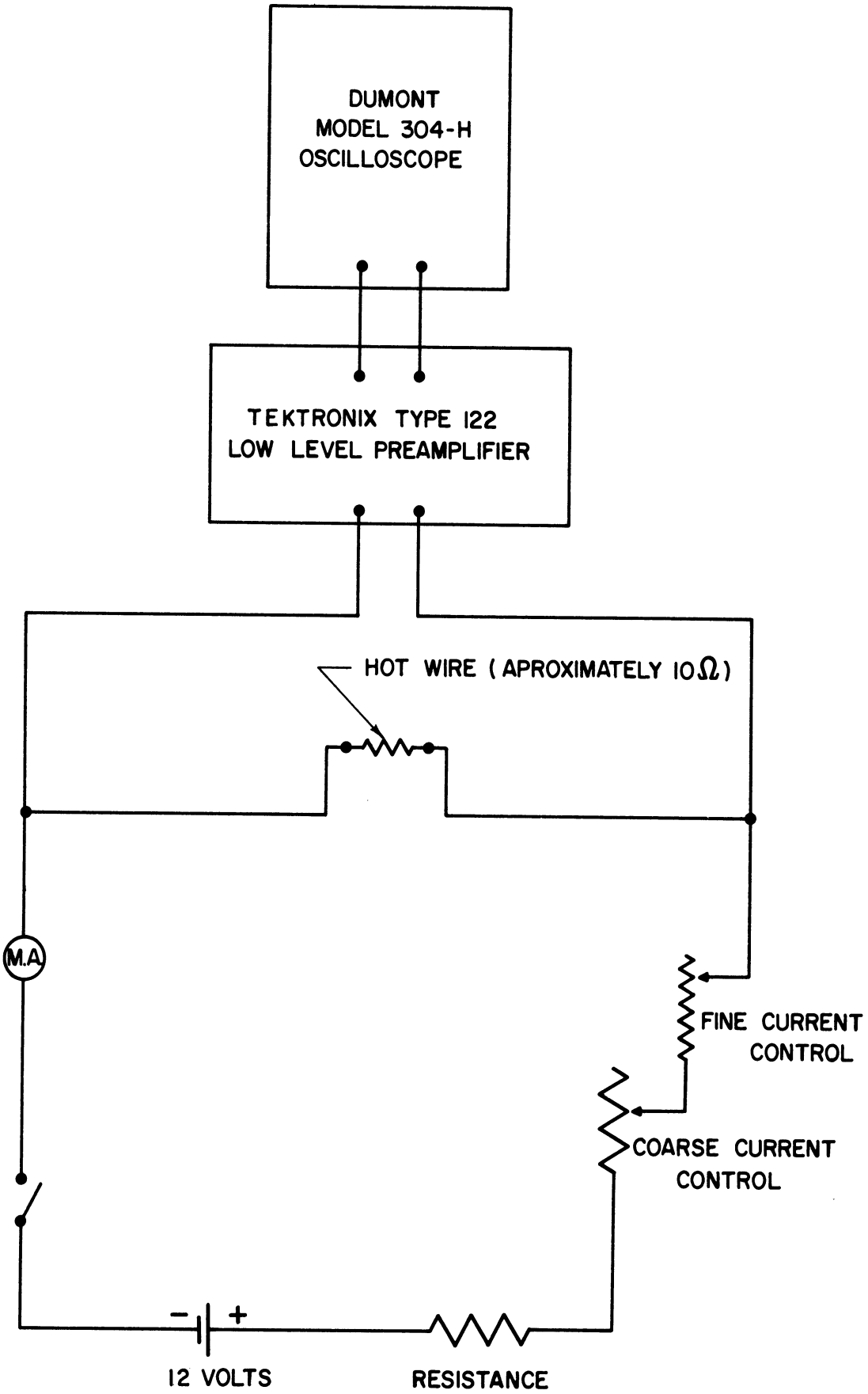

Figure 45. Hot Wire Anemometer Circuit for Measurement of Oscillating Velocities.

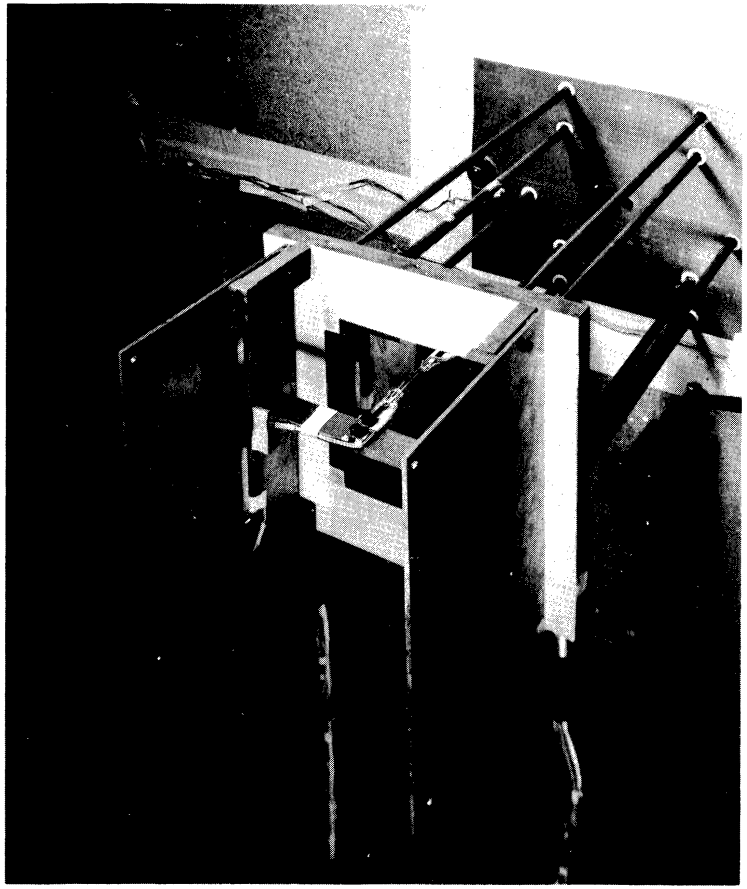

Figure 46. View Showing the Hot Wire Probe and Mounting System.

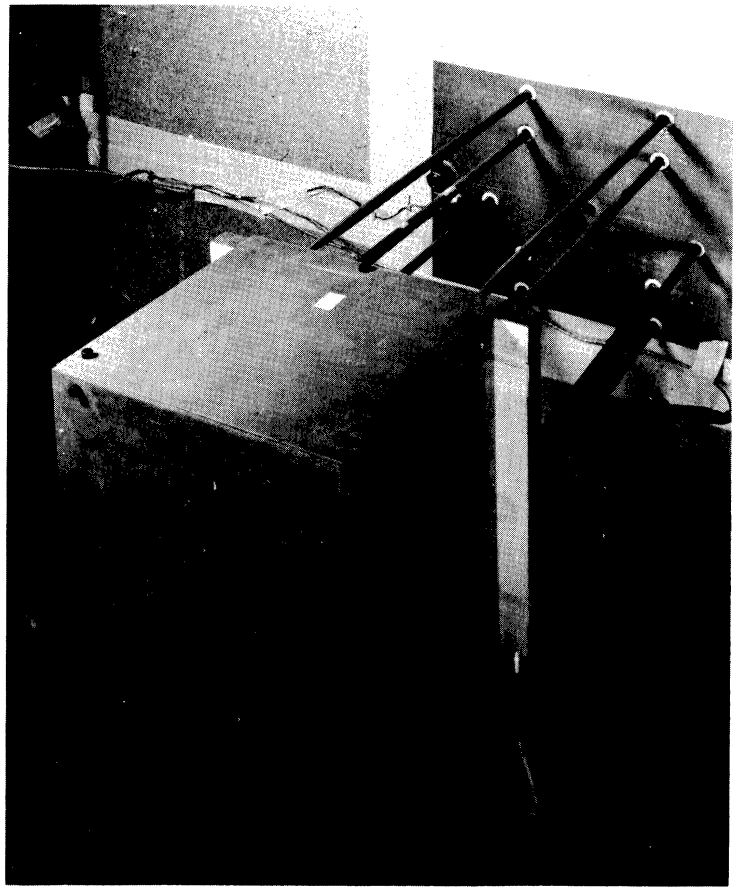

Figure 47. View Showing the Enclosure for Preventing Potential Flow.

voltage drop across the wire is obtained, and it is amplified by a Tektronix Type 122 Low Level Preamplifier. This signal is then displayed on a Dumont Oscilloscope Type 304-H. The hot wire control unit and preamplifier can be seen on the right in Figure 40 and the oscilloscope is just to the left. More details on the use of this equipment will be given later.

This concludes the description of the test apparatus, although some additional points will be mentioned in the following sections on procedure and results.

Observations Made in Connection with a Free Convection Boundary Layer Subjected to Transverse Wall Vibration

In order to properly simulate the problem discussed in Chapter II it is necessary to eliminate the potential flow that would otherwise occur due to the finite dimensions of the test plate. This is done by attaching additional plates to the test plate which completely enclose the air space adjacent to the test plate. This arrangement is shown in Figure 48 which also shows the hot wire probe inserted into the free convection boundary layer along the heated wall. The plates forming the enclosure were made of 1/8 inch thick magnesium. They prevent flow from occurring around the edges of the test plate thus eliminating the potential flow phenomena discussed in Chapter III. A photograph of this system is shown in Figure 47.

The attempt to measure the velocity oscillations discussed in Chapter II by means of the system described above was not successful. For this reason the exact procedure used will not be discussed here, but the two most probable causes of the difficulty will be reviewed.

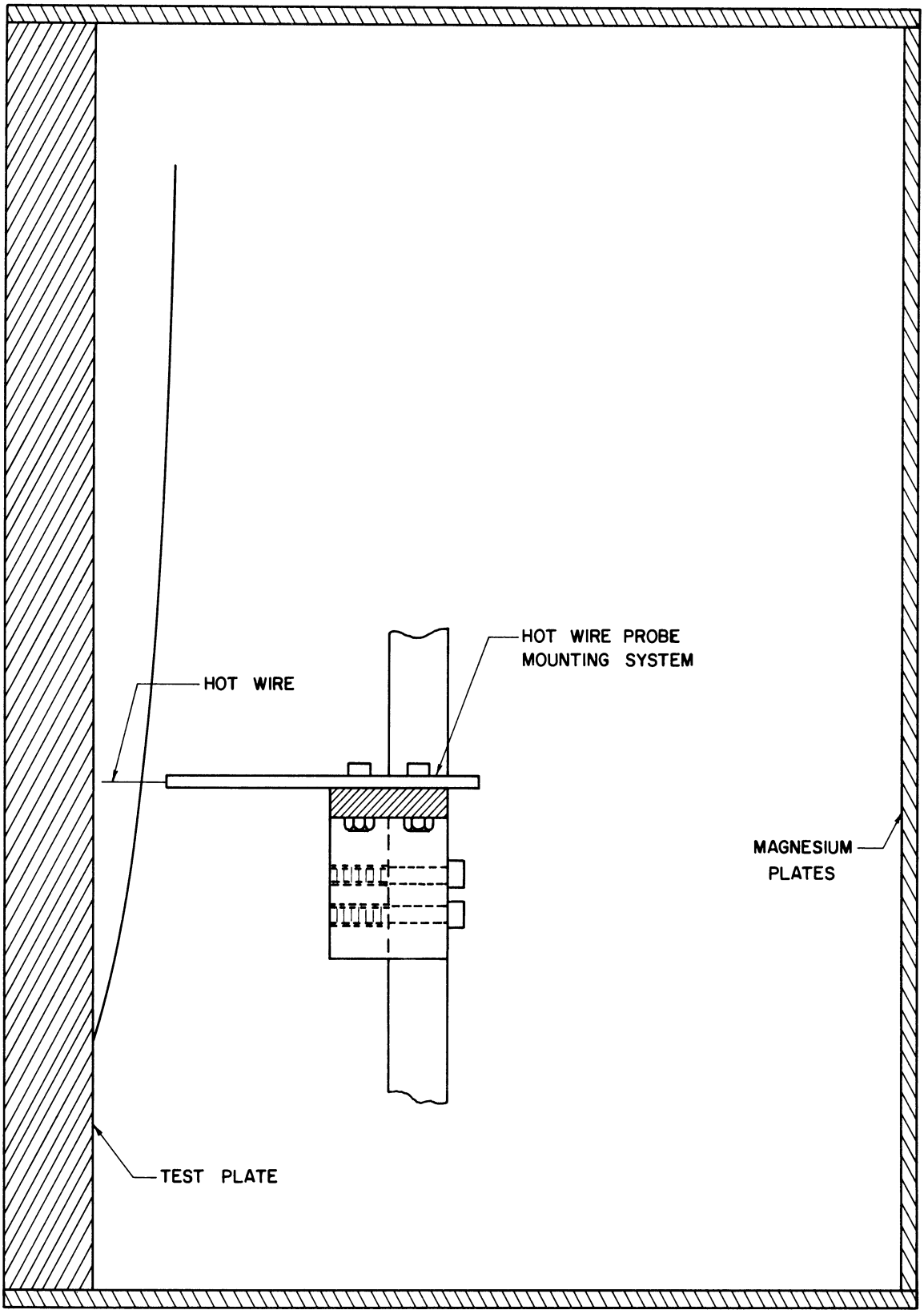

Figure 48. Sketch Showing the Hot Wire Probe Inserted into the Boundary Layer and the Enclosure for Preventing Potential Flow.

The first results from the small order of magnitude of the velocity perturbations. The second concerns the behavior of the hot wire probe under vibratory conditions when operating at necessarily high gain conditions. Both of these features will be discussed.

In regard to the order of magnitude of free convection velocities and their perturbations, reference is made to the analysis of Chapter II. In terms of the symbols used there the free convection velocity profile under non-vibratory conditions is obtained from Equation (2.17a) and is given by

$$u = 2\sqrt{g\beta\,\Delta\theta\,X}\;F'(\eta) \tag{4.1}$$

For air at ambient temperature or slightly above, $\beta \approx 1.7 \times 10^{-3}$ (°F.)$^{-1}$, and taking $\Delta\theta = 100$°F. for example, the expression becomes

$$u = 16.2\sqrt{X}\;F'(\eta) \qquad \text{inches per second} \tag{4.2}$$

where X is in inches. The maximum value of $F'(\eta)$ for air is .276 which occurs at $\eta = 1$. At 2 inches from the leading edge the maximum free convection velocity is therefore about 6.3 inches per second.

In Chapter II, referring now to the result in Equation (2.33), it was shown that for large values of γ the ratio of peak to peak velocity variation to the steady velocity at the same point is given approximately by $\dfrac{2\epsilon\,S(\eta)}{\gamma\,(4x)^{3/4}\,F'(\eta)}$ except in the region very close to the wall. This expression can be rewritten as

$$\frac{g_0/g\,\sqrt{\nu/2}}{2\,\Omega\,X^{5/4}}\,\sqrt[4]{g\beta\,\Delta\theta}\;\;\frac{S(\eta)}{F'(\eta)}\,.$$

For air at ambient temperature or slightly above, $\nu \approx 2 \times 10^{-4}$ ft^2/second, while $\Delta\theta = 100$°F, X = 2 inches, and $\eta = 1$ in this example. For these

conditions the ratio becomes .072 $\zeta(1)g_o/g \Big/ F'(1)\Omega$, or .265 g_o/g.

Consider now a vibration amplitude of 1/10 of an inch and a frequency of 50 cycles per second. The value of γ is given by $2\Omega\sqrt{\frac{X}{g\beta\,\Delta\theta}}$, or γ = 110 at 2 inches from the leading edge. This rather large value of γ justifies the use of the ratio discussed above. For the particular amplitude and frequency used in this example, Ω = 314 radians per second and g_o/g = 25.5. Thus, at a point 2 inches from the leading edge with η = 1, the peak to peak velocity variation is only 2.2% of the steady velocity at that point, or about .14 inches per second. This example illustrates the low order of magnitude of the oscillations for which measurement was attempted. The steady free convection velocities have values of only a few inches per second, while the perturbations are small percentages of these values at nominal ranges of frequency and amplitude available with the vibration equipment used.

It is interesting to note here that in the example above the varying component of velocity is only about 2% of the steady velocity, while the oscillating pressure gradient is much larger relative to the steady buoyancy force at the same point. From Equation (2.23) in Chapter II, the ratio of the oscillating pressure gradient to the steady buoyancy force is calculated approximately from $.04\,\frac{g_o/g\;\zeta(\eta)}{X^{3/4}\,H(\eta)}$, which gives a value of about 1.2 under the conditions given for the example discussed above. Thus, in this particular case the oscillating pressure gradient is 20% larger than the steady buoyancy force, but the oscillating velocity is only about 2% of steady velocity at the same point. The reason for the difference in the order of magnitude of each comparison is explained in Chapter II.

Although the velocity perturbations are small, it would appear feasible to measure them with a hot wire anemometer on the basis that this instrument can be made very sensitive by using a fairly high wire temperature together with large amplification of the output signal. When this was done under vibratory conditions, however, an oscillating signal was obtained from the probe, mounted inside the enclosure as shown in Figure 48, even when the test plate was not heated at all. Ideally no signal should be obtained since the air inside the enclosure may be expected to move as a rigid body under these isothermal conditions. The probe is fastened rigidly to the test plate so that no relative motion should occur between the air surrounding the hot wire and the wire itself. On the other hand, the wire must be heated in order to obtain a signal when making measurements, and this means that truly isothermal conditions in the immediate region of the wire are never achieved during operation. The most feasible explanation appears to be that the small free convection temperature field produced by heat from the wire interacts with the vibration to produce pressure gradients by the same type of mechanism as that discussed in Chapter II. These gradients could logically produce velocity oscillations causing alternate heating and cooling of the wire. In other words, if vibration causes oscillations in a free convection boundary layer on a flat plate, there is no reason to believe that similar oscillations will not occur in the free convection field around the heated hot wire when subjected to the same vibration.

No matter what the exact explanation is for the signal discussed in the preceding paragraph, it can be regarded as a noise signal in the system. The objective is to measure the oscillations in the boundary layer

along a heated plate, and therefore any signal obtained when the plate is not heated is caused by effects extraneous to the actual velocities whose measurement is desired. It has been estimated that the noise signal is several times larger than that expected from measurements in the free convection boundary layer along a heated flat plate. Thus, the noise signal obscures the latter and prevents its measurement.

It is possible in many instrumentation systems to isolate the desired signal from that of the so-called noise by means of certain techniques. The common methods of doing this are not feasible in this case, however. For example, the desired signal can be increased in this system by vibrating at higher amplitudes and frequencies. On the other hand, the noise signal also increases with an increase in amplitude or frequency. It is sometimes possible to use selective filtering to separate out the noise if its frequency spectrum is markedly different from that of the desired signal. In this case, however, both the desired and noise signals correspond to the frequency of vibration so that filtering is not possible.

In order to measure heat transfer, a set of plates similar to those shown in Figure 47 were fastened to the test plate forming another enclosure on the opposite side. This was necessary to achieve symmetry and prevent potential flow occurring on that side of the test plate since heat is transferred from both sides of the heated section. This section was allowed to come to a steady uniform temperature of about 100°F above ambient under non-vibratory conditions. The guard heaters were carefully adjusted by means of the galvanometer system described in the previous section so as to prevent edge losses. The test plate was then vibrated

at an amplitude of 1/10 of an inch and a frequency of 25 cycles per second. After a period of about an hour no significant change was observed in the temperature difference between the heated section and ambient. This indicated that no significant change in the free convection heat transfer coefficient was caused by the vibration. The result verifies that the oscillations in the boundary layer are small for frequencies and amplitudes available with the vibration equipment used. If the velocity oscillations were large fractions of the mean velocities, for example, a change in the heat transfer coefficient would most certainly be expected.

One important distinction should be made here in connection with the fact that the above discussion is related to the time averaged heat transfer coefficient. The instantaneous coefficient may be expected to have an oscillating component at the frequency vibration. Its magnitude, according to the perturbation in the wall temperature gradient given in Chapter II, is a small fraction of the steady coefficient under the vibratory conditions used in the experiment. The change in the time averaged coefficient is smaller and can be expected to have an order of magnitude of roughly the square of the oscillating component. For example, if a particular amplitude and frequency produces an oscillating component that is 10% of the steady value, the change in the steady coefficient can be expected to have an order of magnitude of roughly 1%.

The experimental observations discussed in this section are summed up by the following. The attempt to measure the free convection velocity perturbations was not successful, but the small magnitude of the perturbations at nominal values of frequency and amplitude was verified. This verification consists of the fact that no significant change due to vibration was observed in the time averaged heat transfer coefficient.

Procedure and Results for the Case of Transverse Vibration of a Plate of Finite Length

Experimental measurements of velocity and heat transfer have been made for the problem treated in Chapter III and these are discussed in this section.

For measuring oscillating velocities the test plate was not heated and the hot wire probe was mounted as shown in Figure 46. The vertical magnesium plates were intended to keep the flow pattern two dimensional to agree with the physical model used in Chapter III. The velocity oscillations measured in this problem are relatively larger at the same amplitude and frequency than those discussed in the previous section. For example, in terms of the symbols used in Chapter III, $U_0 = V_0$ at $x/c = .707$. In other words, the amplitude of the potential flow oscillations at this point is the same as the amplitude of velocity of plate vibration. This gives a value of 31.4 inches per second at a vibration amplitude and frequency of 1/10 of an inch and 50 cycles per second respectively. The order of magnitude of these oscillations is large enough so that high gain is not necessary for their measurement, and therefore the noise problem discussed in the previous section caused no difficulty here.

In order to calibrate a hot wire for making a particular set of measurements, the probe is removed from its mounting as shown in Figure 46 and attached to the side of the test plate. The probe is positioned so that the wire itself is far from the plate in a region of still ambient air essentially unaffected by the plate vibration. The plate is then vibrated thus causing the wire to move back and forth with respect to the stationary air surrounding it at a known amplitude and frequency. The hot wire current and preamplifier gain are held constant, but the oscilloscope gain

is varied corresponding to various velocity ranges. The wave form of the signal appears on the scope screen as shown in Figure 49. Since the hot wire is sensitive only to the magnitude of velocity, but not its direction, the signal on the scope has twice the frequency of vibration. The magnitude of the signal is determined by counting the number of grid lines on the scope screen included by the peak to peak wave form. A typical set of calibration curves is shown in Figure 50. The non-linearity of the instrument is apparent by the curvature of some of these lines. With the filter control knobs on the preamplifier properly set, the frequency response of the preamplifier-scope combination was found to be constant over the frequency range used in this investigation.

Once a set of calibration curves has been obtained, the actual desired velocity measurements can be made. After the completion of a particular set of measurements, a few points of the original calibration are rechecked. The object here is to insure that the characteristics of the system do not change between the time of the original calibration and the completion of the measurements.

Two sets of velocity measurements have been made in connection with the problem of Chapter III. The first involves measurements of the potential flow oscillations along the plate but outside the boundary layer, and the second involves measurements of the boundary layer oscillations made by probing in closer to the wall.

The potential flow oscillations were measured 1/10 of an inch from the plate at various values of x/c, a_o, and ω. The 1/10 inch distance from the plate is rather arbitrary, but it is slightly outside the boundary

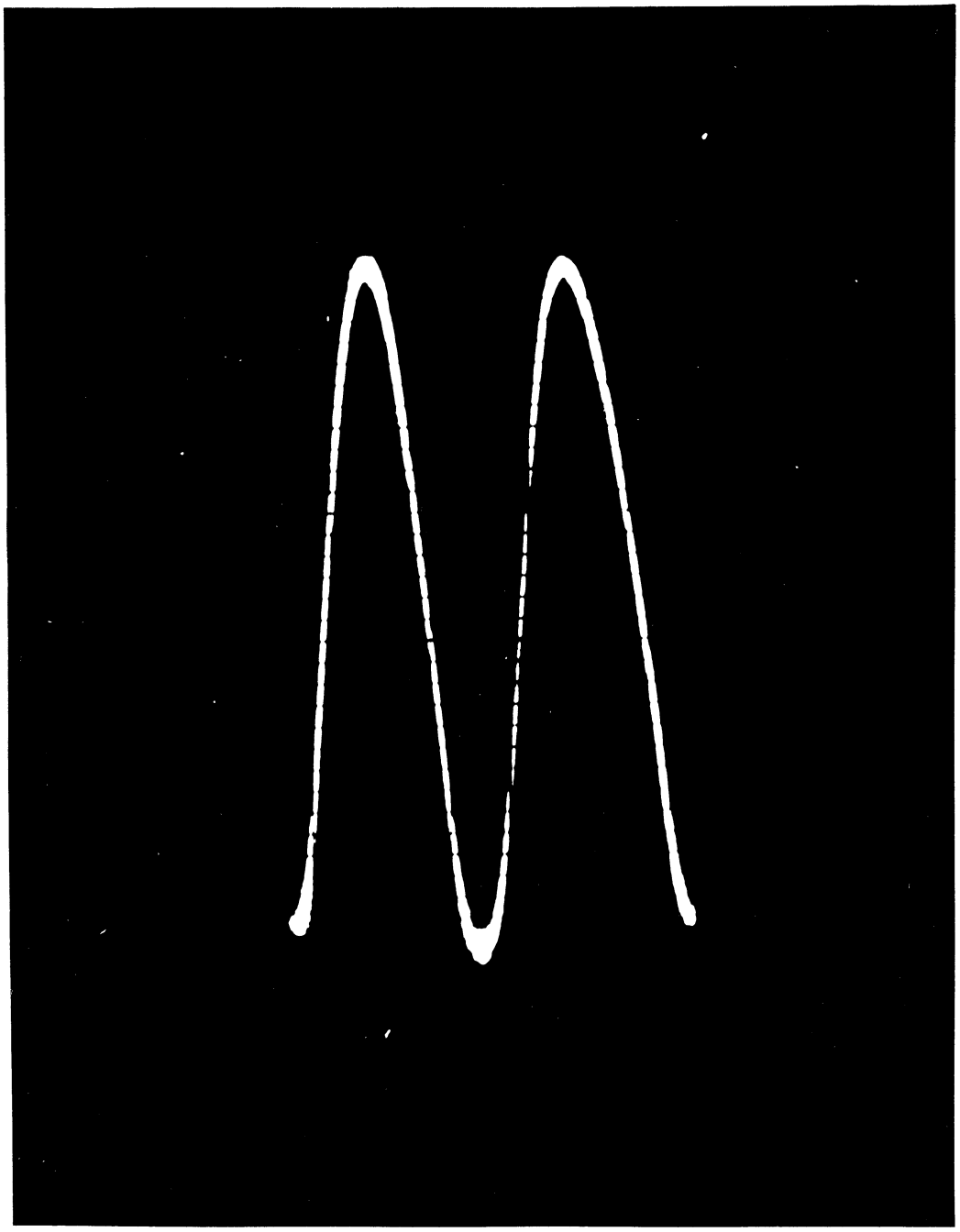

Figure 49. Output Signal of the Hot Wire During Measurement of Oscillating Velocity as Displayed on an Oscilloscope.

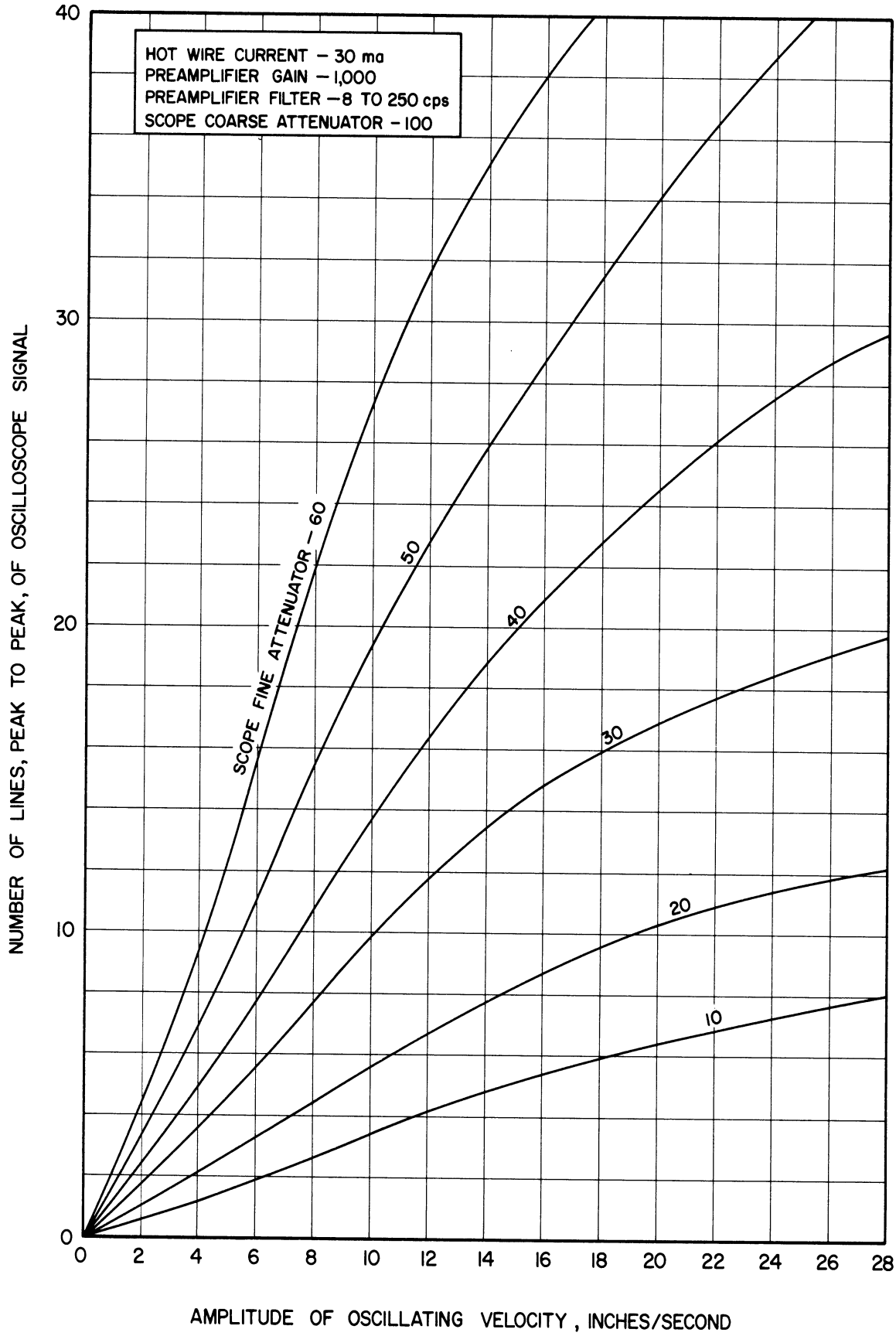

Figure 50. A Typical Set of Calibration Curves for Measuring Oscillating Velocities with a Hot Wire Anemometer.

layer in all cases, yet close enough to the wall so that the resulting data essentially correspond to $y = 0$ as far as the potential flow theory is concerned. This was verified experimentally by noting that the scope signal did not change as y was varied from about .070 inches to .200 inches while holding x/c, a_o, and ω constant.

A summary of the potential flow data is given in Appendix IVa. This data is plotted in Figures 51 through 68 and is compared with the theory as given in Chapter III. Agreement with the theory may be described as fair in view of the scatter involved. The experimental values are lower than those predicted at the highest frequencies used. A dropping off of the experimental points at high values of x/c can be seen in several cases.

It is probable that some of the discrepencies are due to the following four causes. First, the theory assumes an infinitely thin plate while the actual plate is 3/4 of an inch thick. Second, viscous effects probably have some importance near the edges of plate, but are neglected in the analysis. Third, the analysis was made assuming two dimensional flow, while the actual system may have three dimensional effects associated with it in the region where x/c is close to unity. Fourth, the probe and its mounting structure may have some effect on the flow pattern.

Measurements of the oscillating velocities in the boundary layer were made 2-3/4 inches from the stagnation point at a vibration frequency of 20 cycles per second and amplitudes of .050, .075, and .100 inches. This data is summarized in Appendix IVb and is plotted in Figures 69, 70, and 71 where comparison is made with the theory. The theoretical curve is based on only the first approximation $f_o'(\eta)$ as given in Chapter III. This is permissible since the second approximation has an order of magnitude

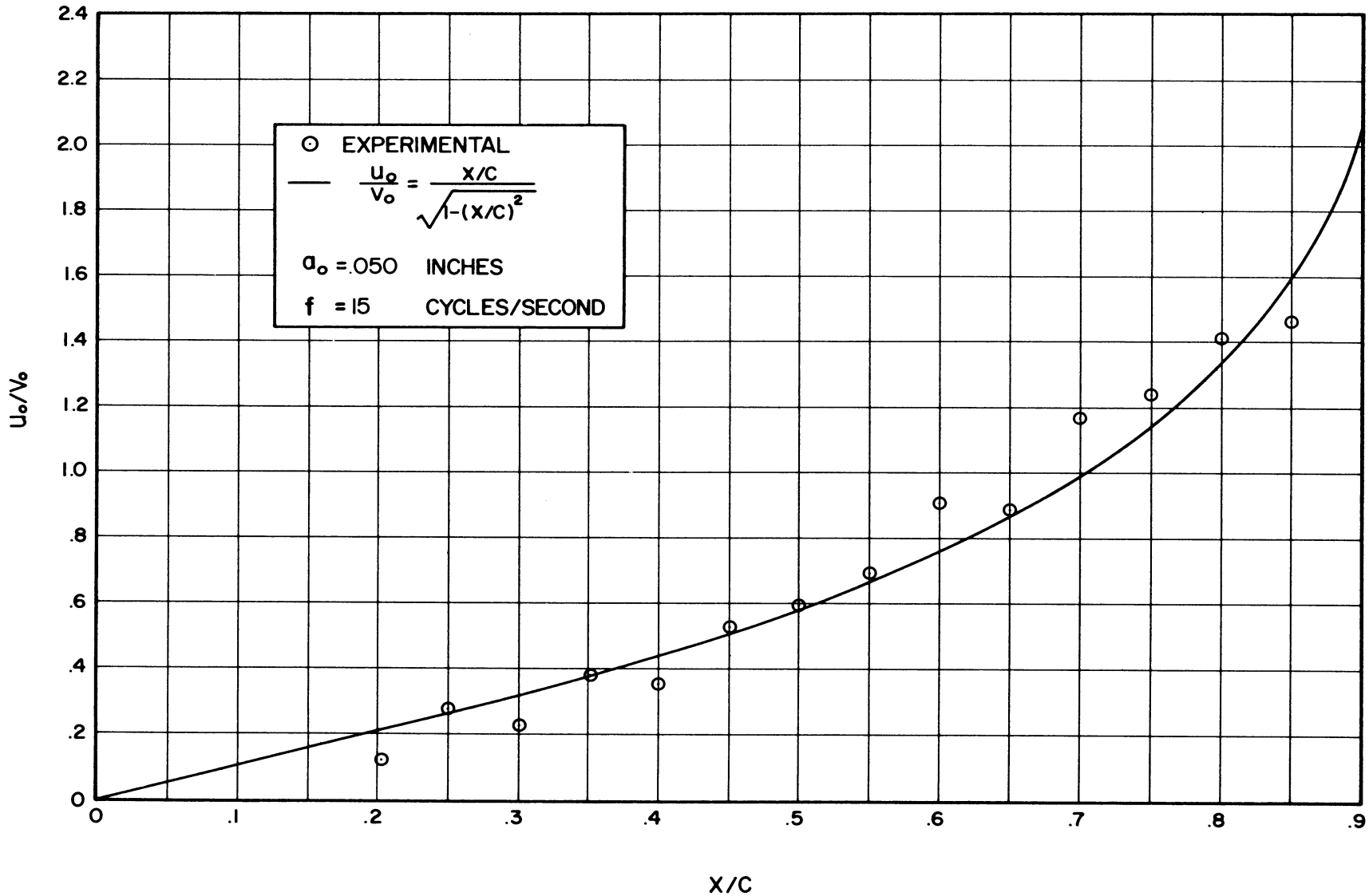

Figure 51. Experimental Potential Flow Velocity Measurements Made Along a Plate Vibrating Transversely and the Comparison with Theory.

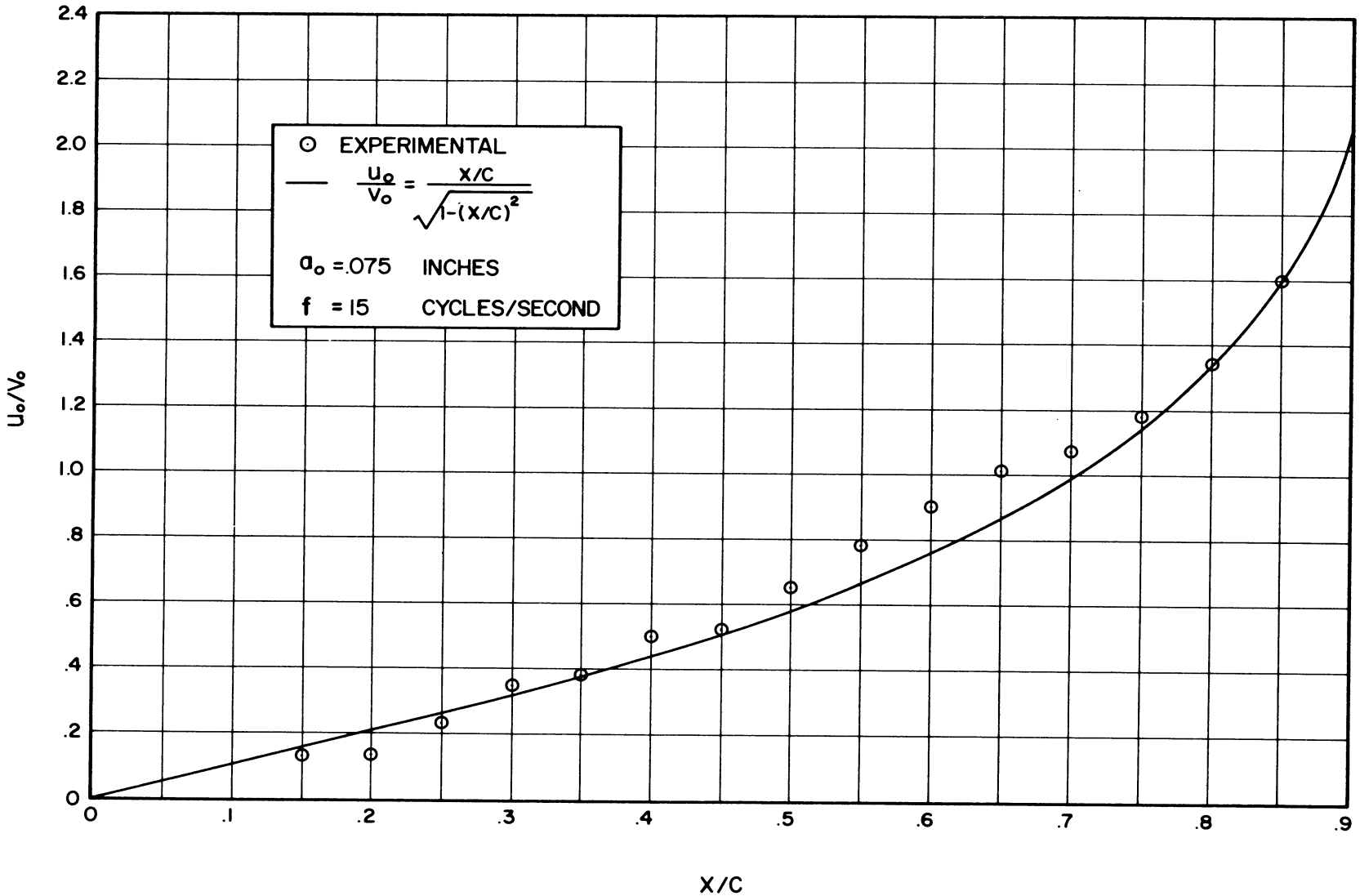

Figure 52. Experimental Potential Flow Velocity Measurements Made Long a Plate Vibrating Transversely and the Comparison with Theory.

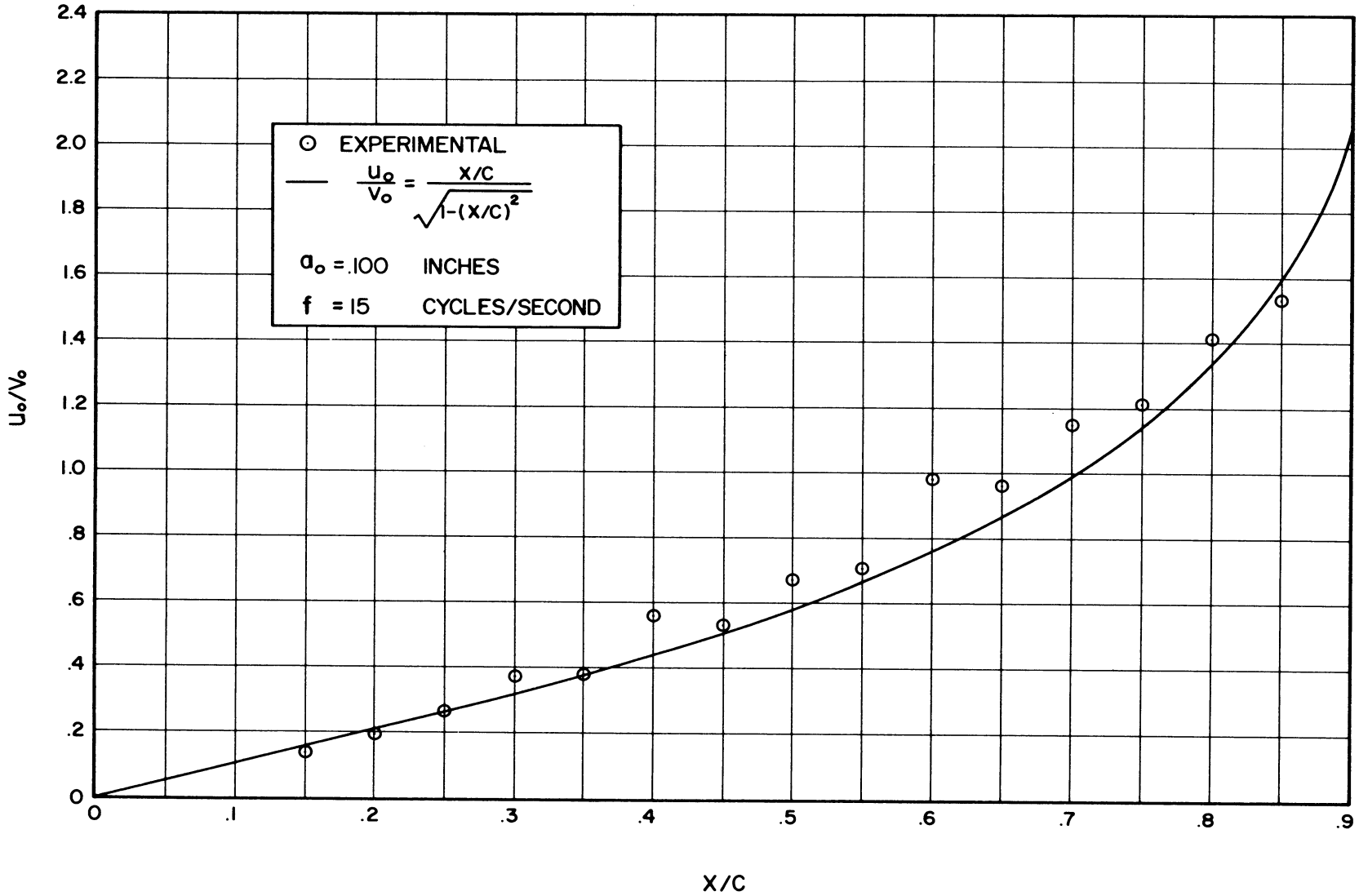

Figure 53. Experimental Potential Flow Velocity Measurements Made Along a Plate Vibrating Transversely and the Comparison with Theory.

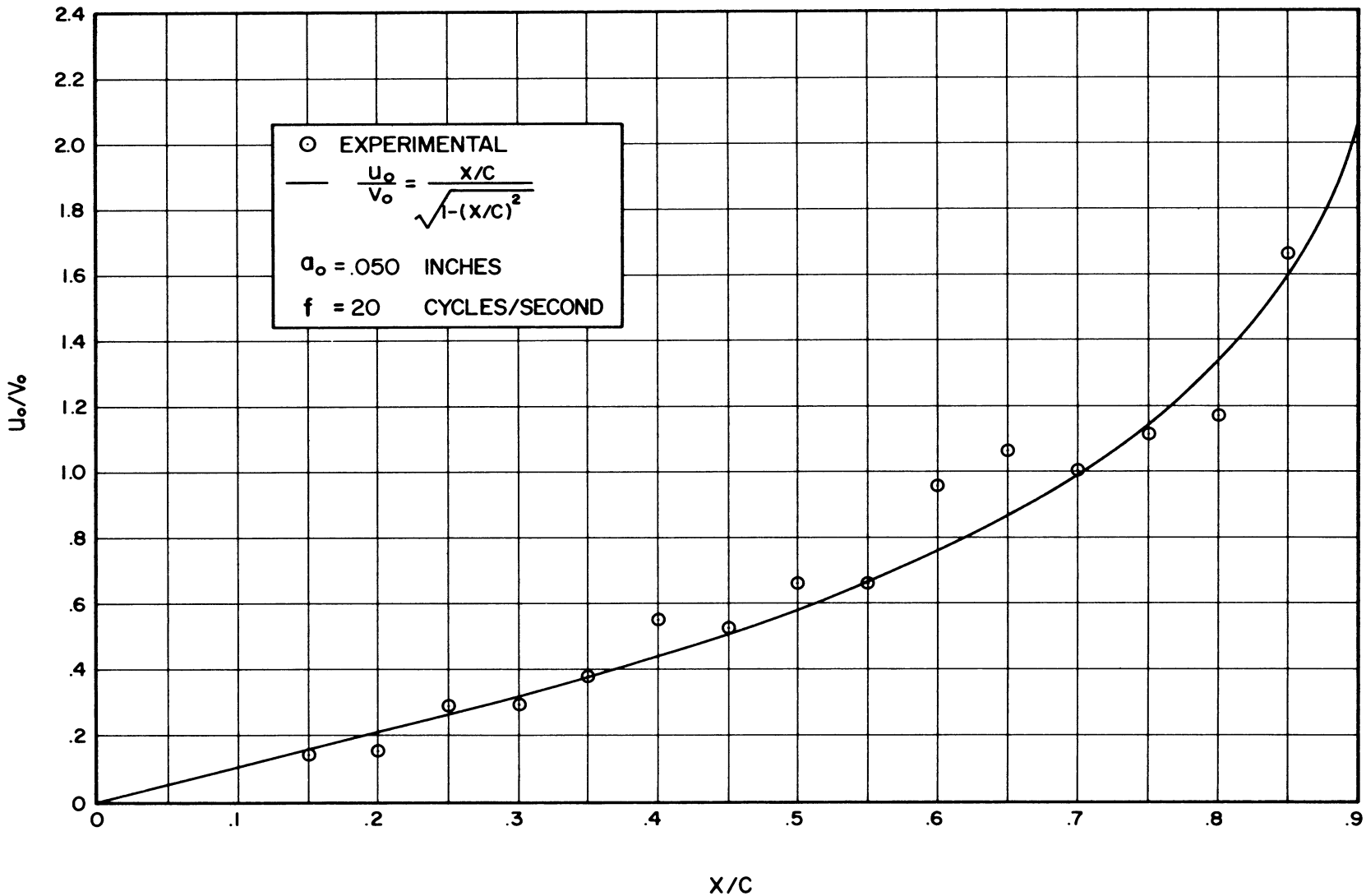

Figure 54. Experimental Potential Flow Velocity Measurements Made Along a Plate Vibrating Transversely and the Comparison with Theory.

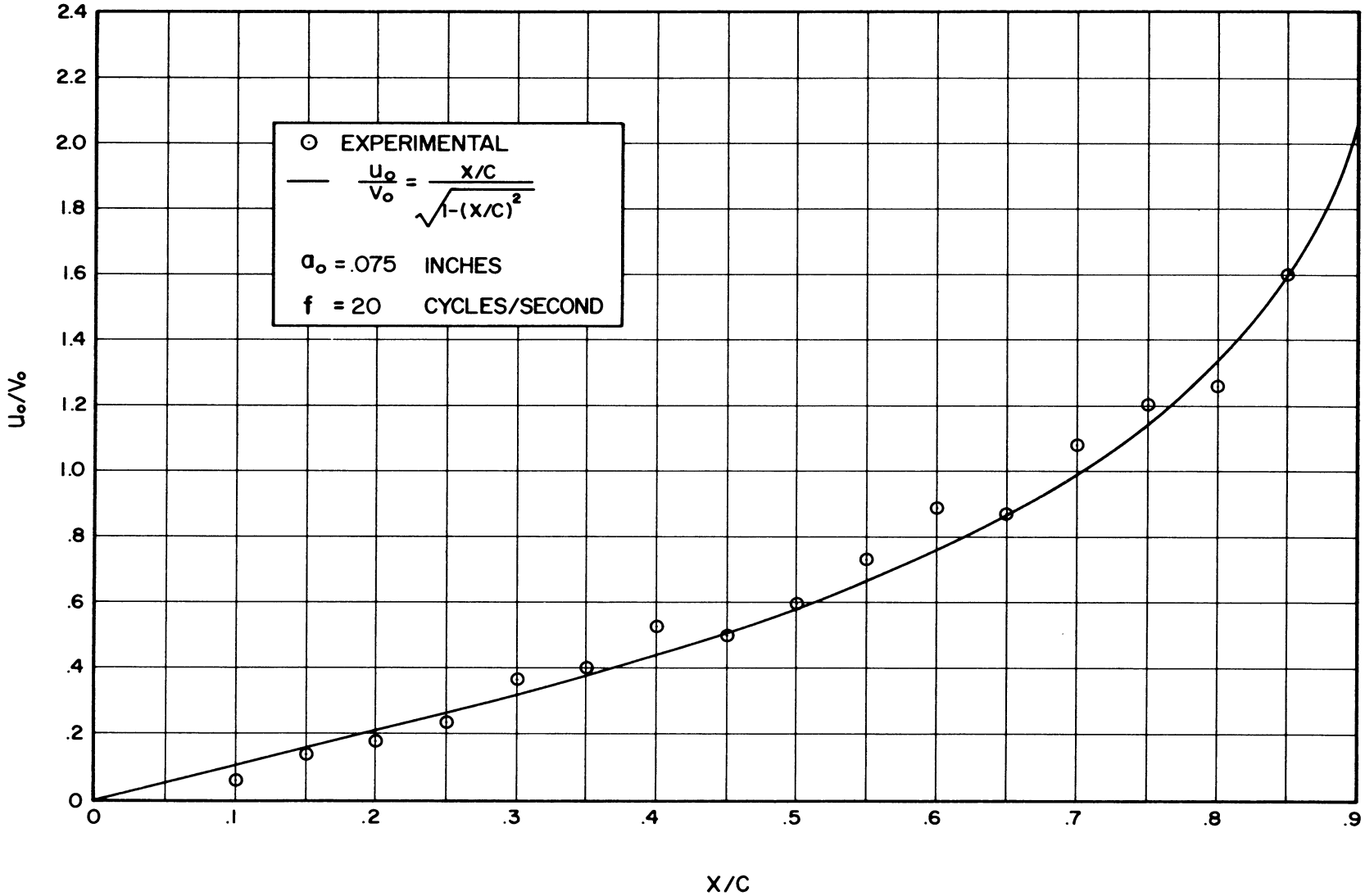

Figure 55. Experimental Potential Flow Velocity Measurements Made Along a Plate Vibrating Transversely and the Comparison with Theory.

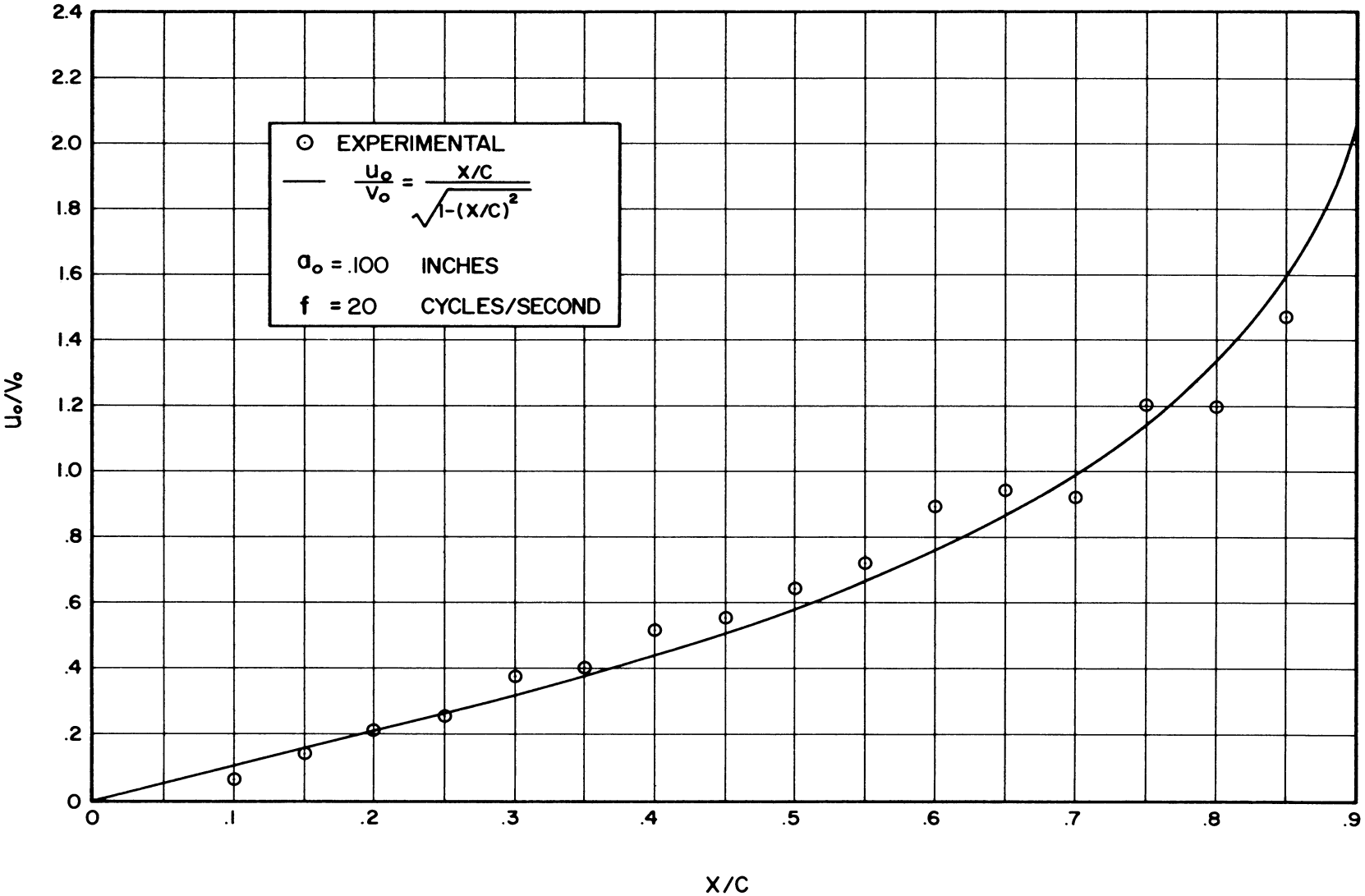

Figure 56. Experimental Potential Flow Velocity Measurements Made Along a Plate Vibrating Transversely and the Comparison with Theory.

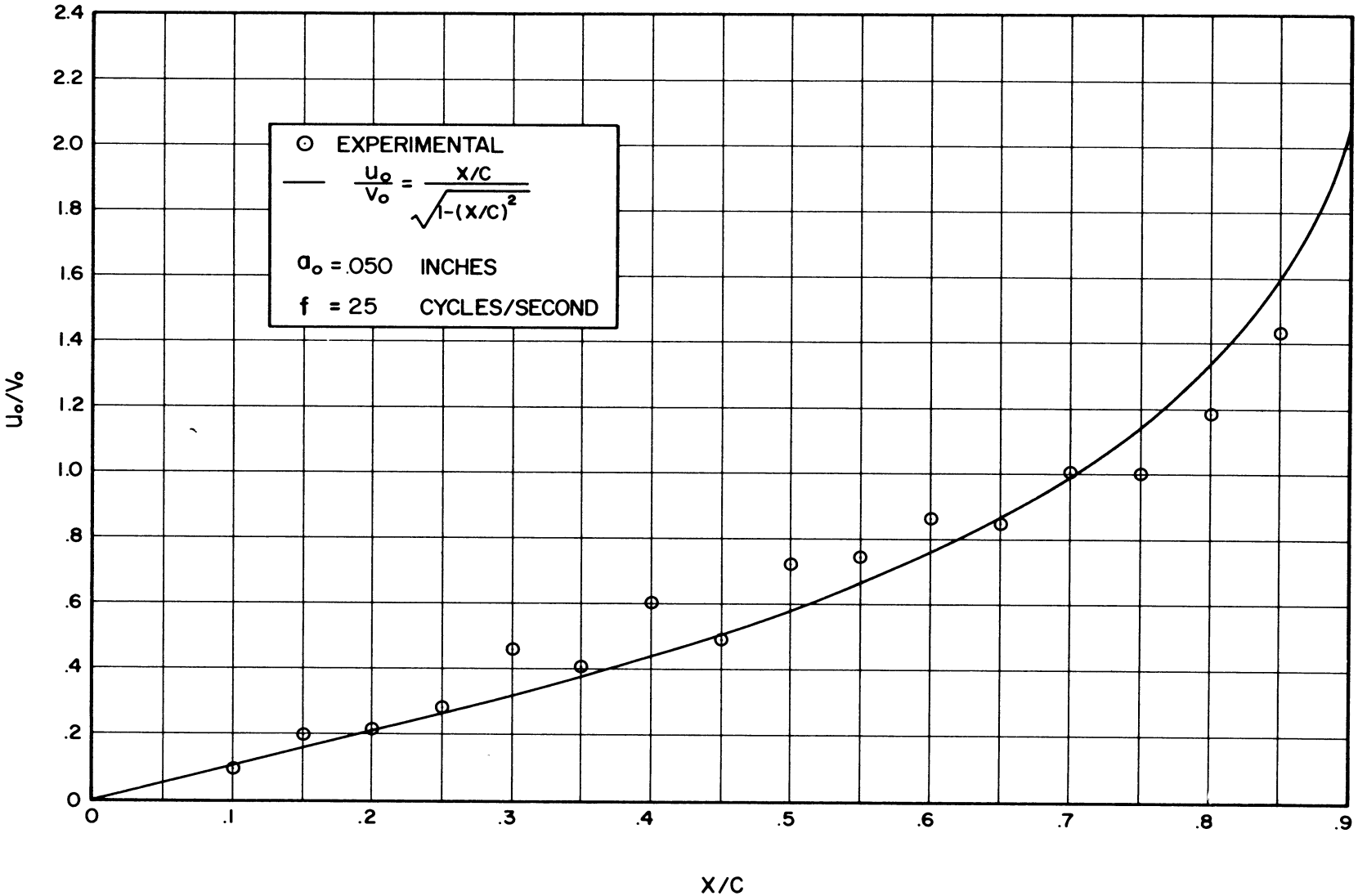

Figure 57. Experimental Potential Flow Velocity Measurements Made Along a Plate Vibrating Transversely and the Comparison with Theory.

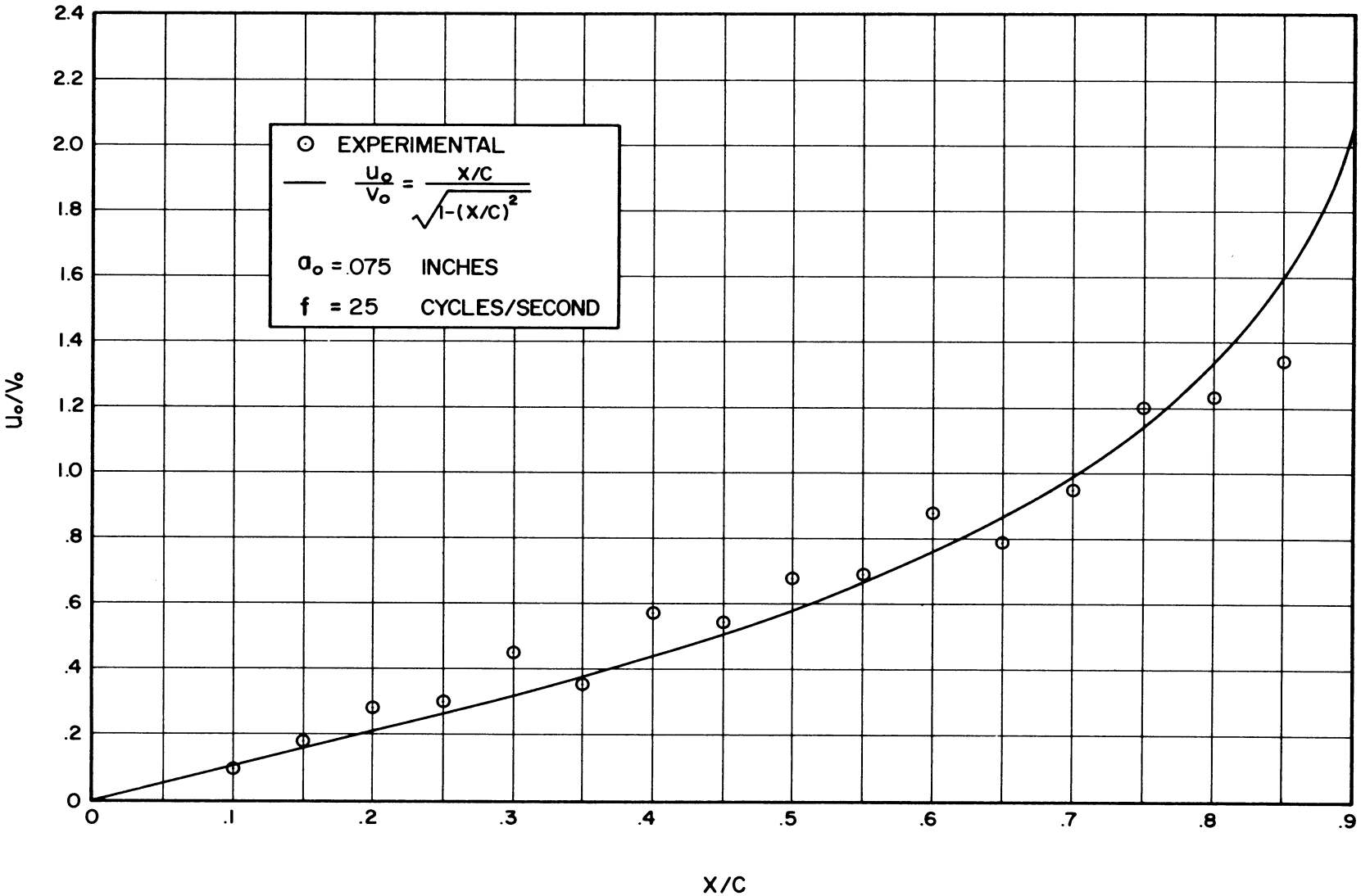

Figure 58. Experimental Potential Flow Velocity Measurements Made Along a Plate Vibrating Transversely and the Comparison with Theory.

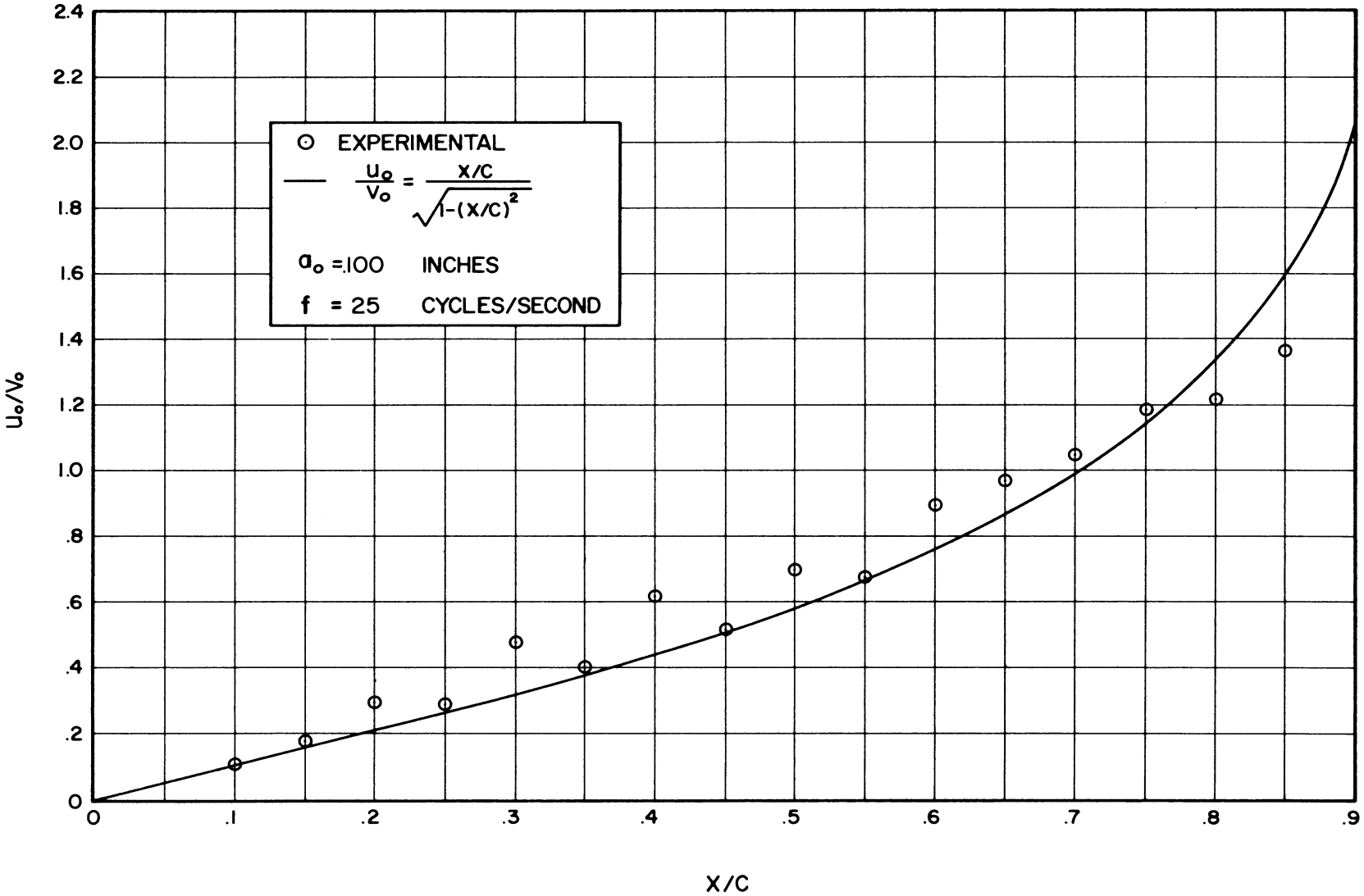

Figure 59. Experimental Potential Flow Velocity Measurements Made Along a Plate Vibrating Transversely and the Comparison with Theory.

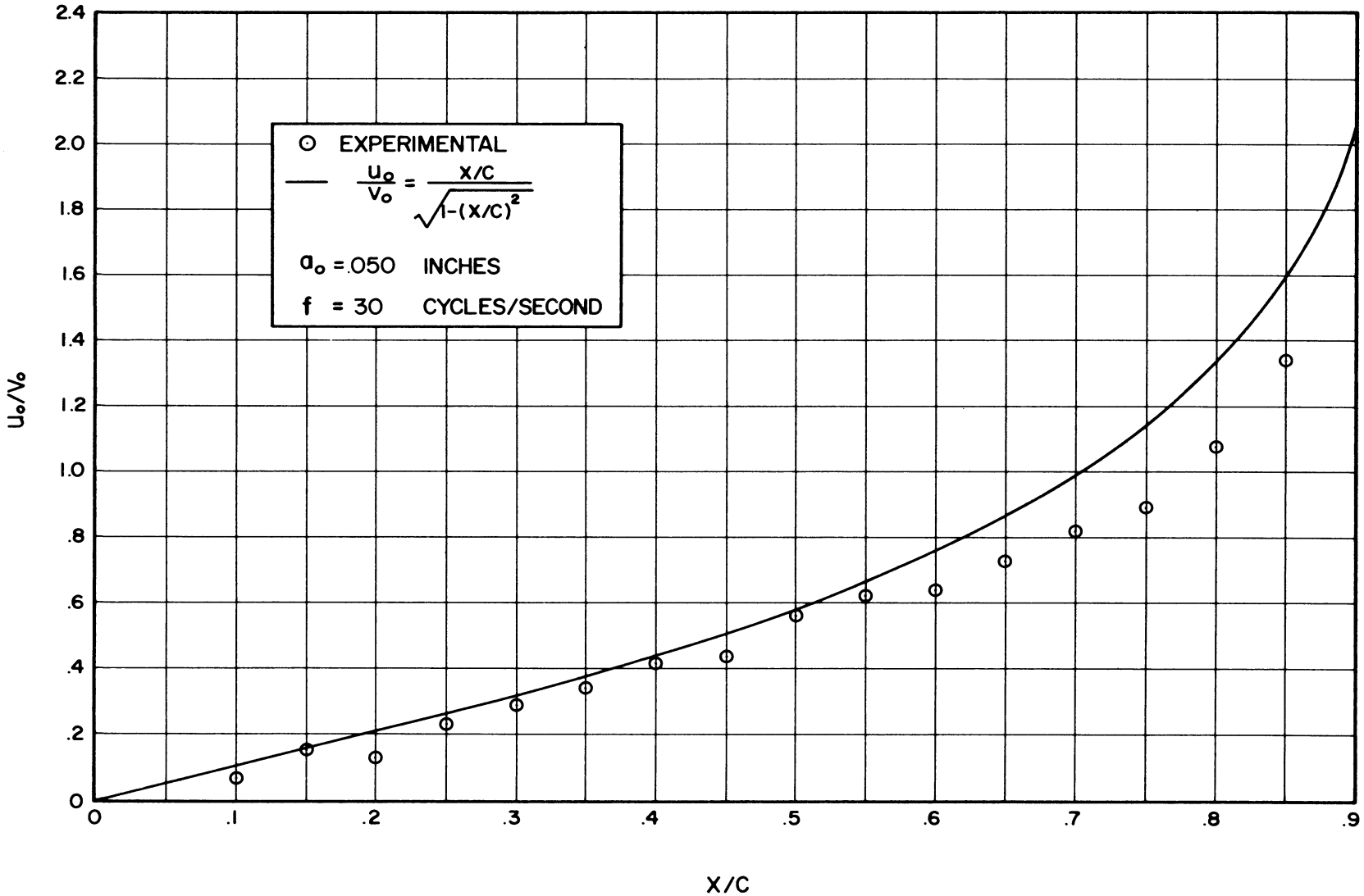

Figure 60. Experimental Potential Flow Velocity Measurements Made Along a Plate Vibrating Transversely and the Comparison with Theory.

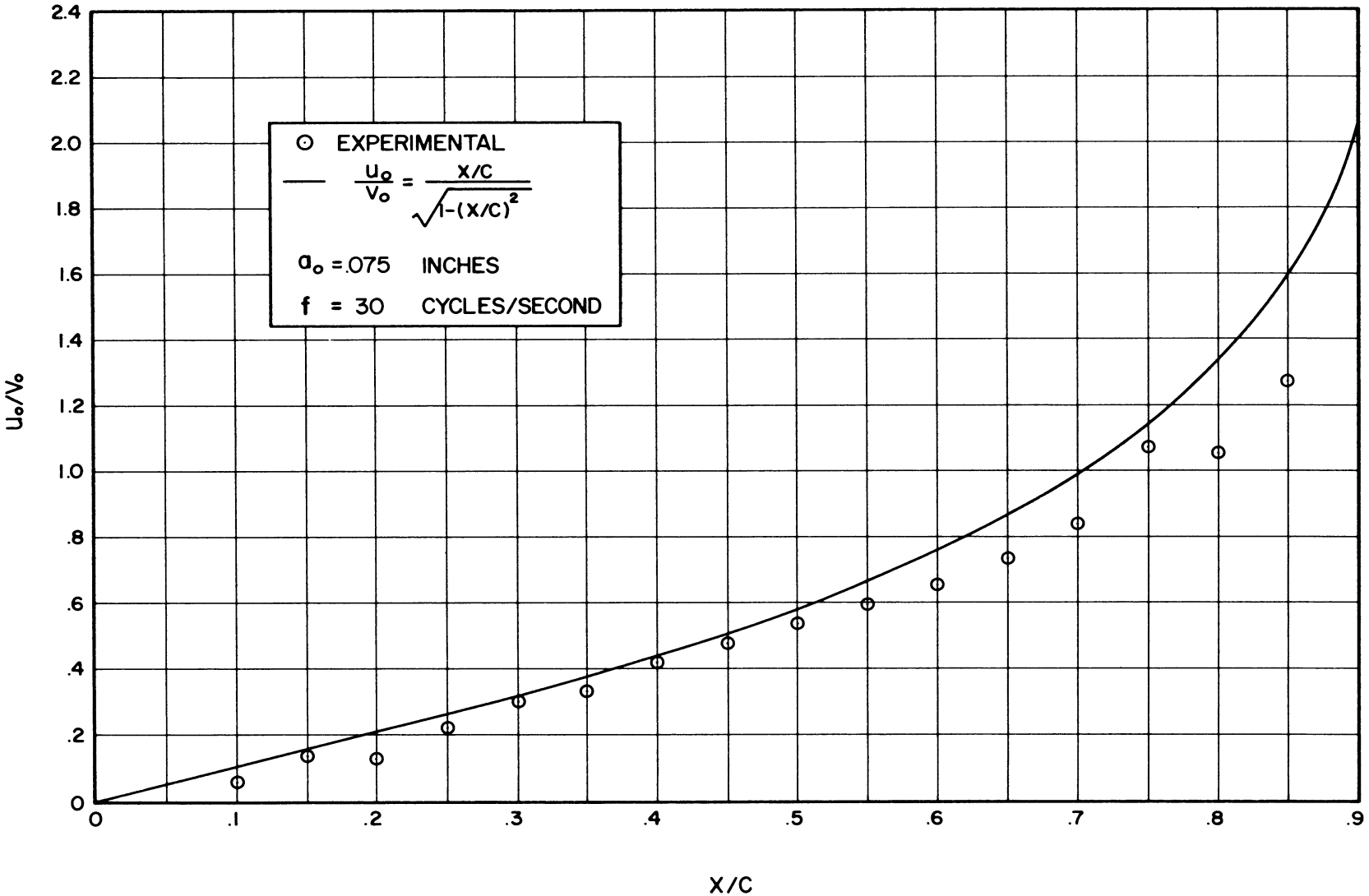

Figure 61. Experimental Potential Flow Velocity Measurements Made Along a Plate Vibrating Transversely and the Comparison with Theory.

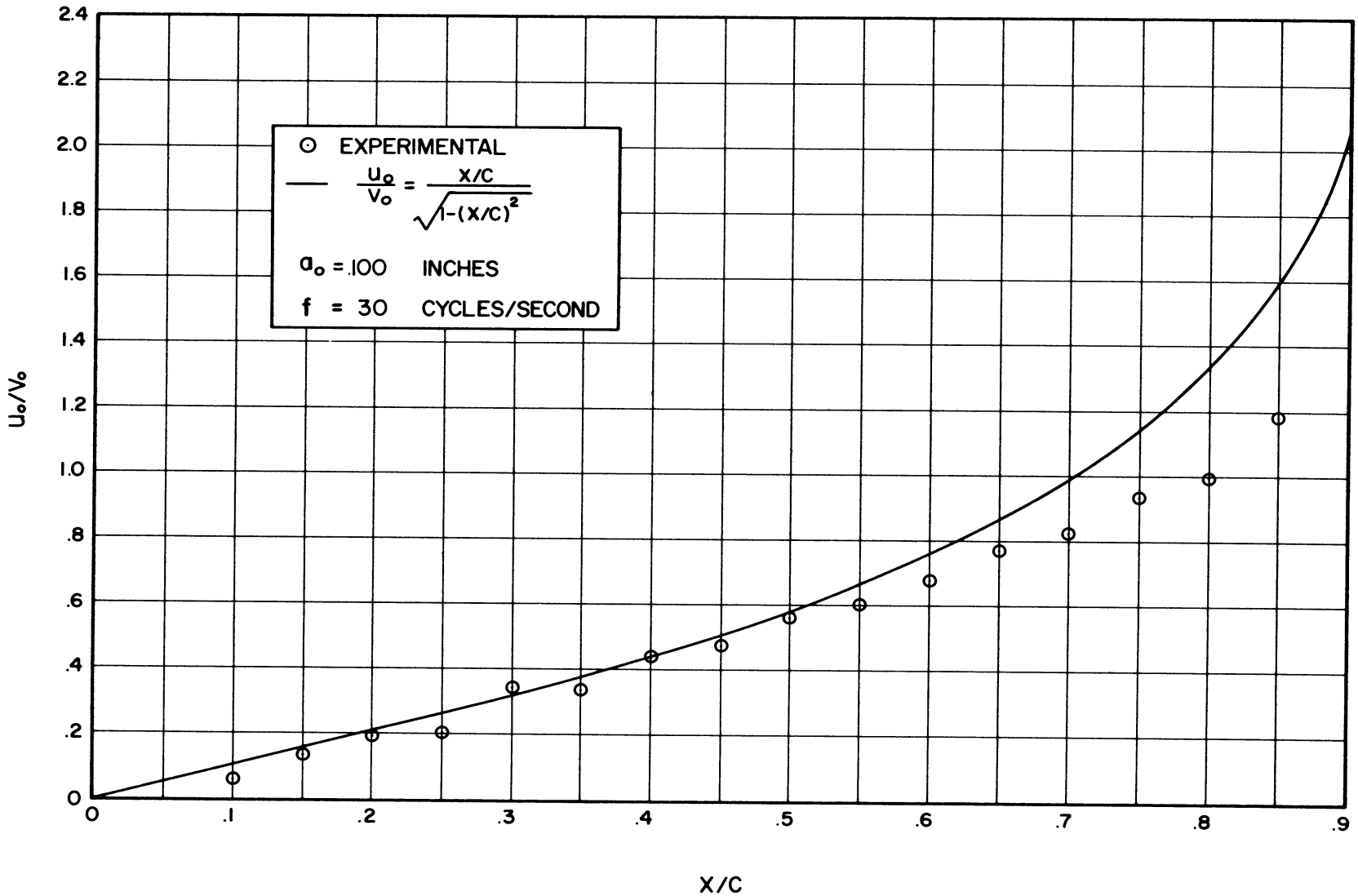

Figure 62. Experimental Potential Flow Velocity Measurements Made Along a Plate Vibrating Transversely and the Comparison with Theory.

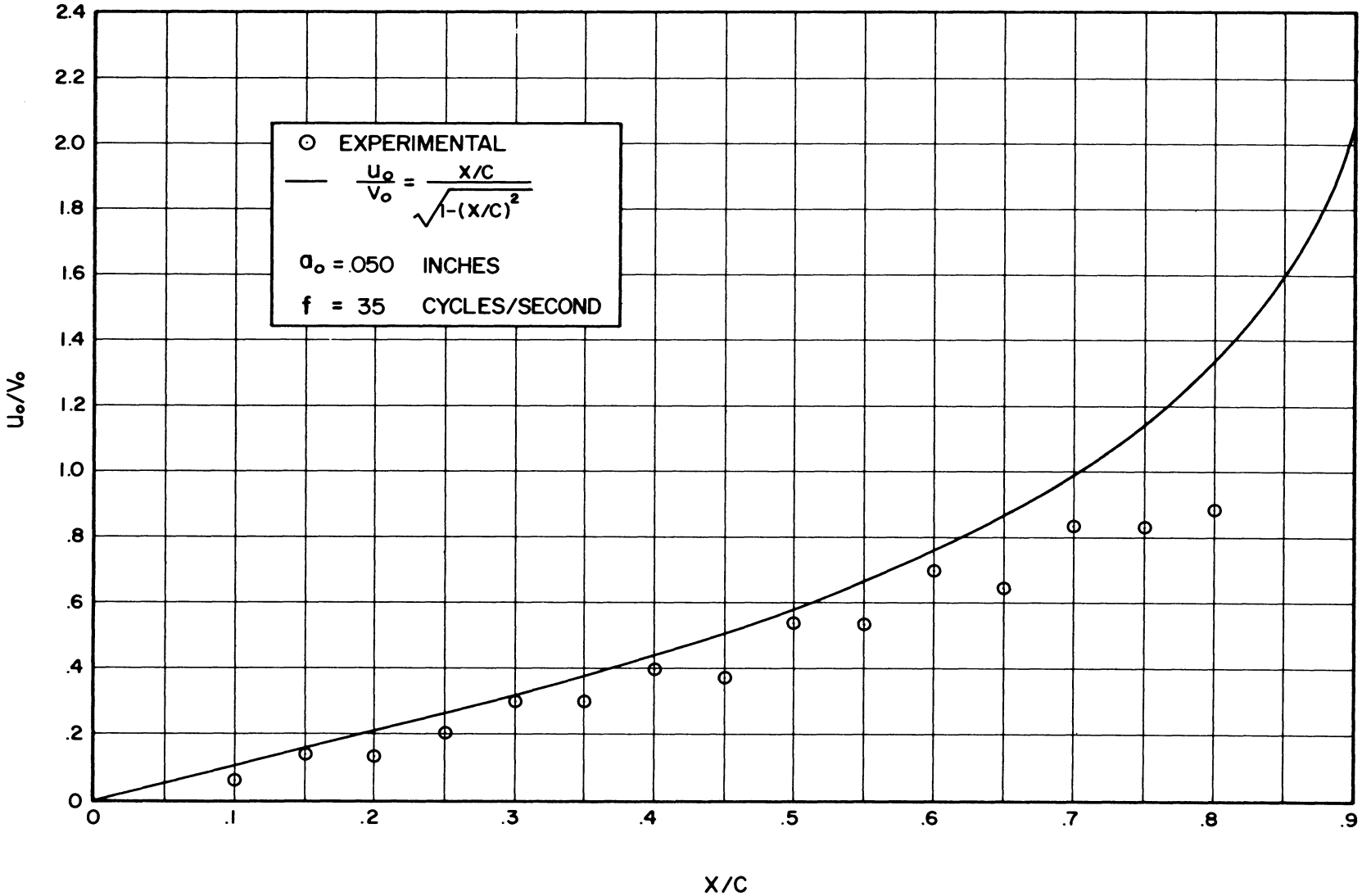

Figure 63. Experimental Potential Flow Velocity Measurements Made Along a Plate Vibrating Transversely and the Comparison with Theory.

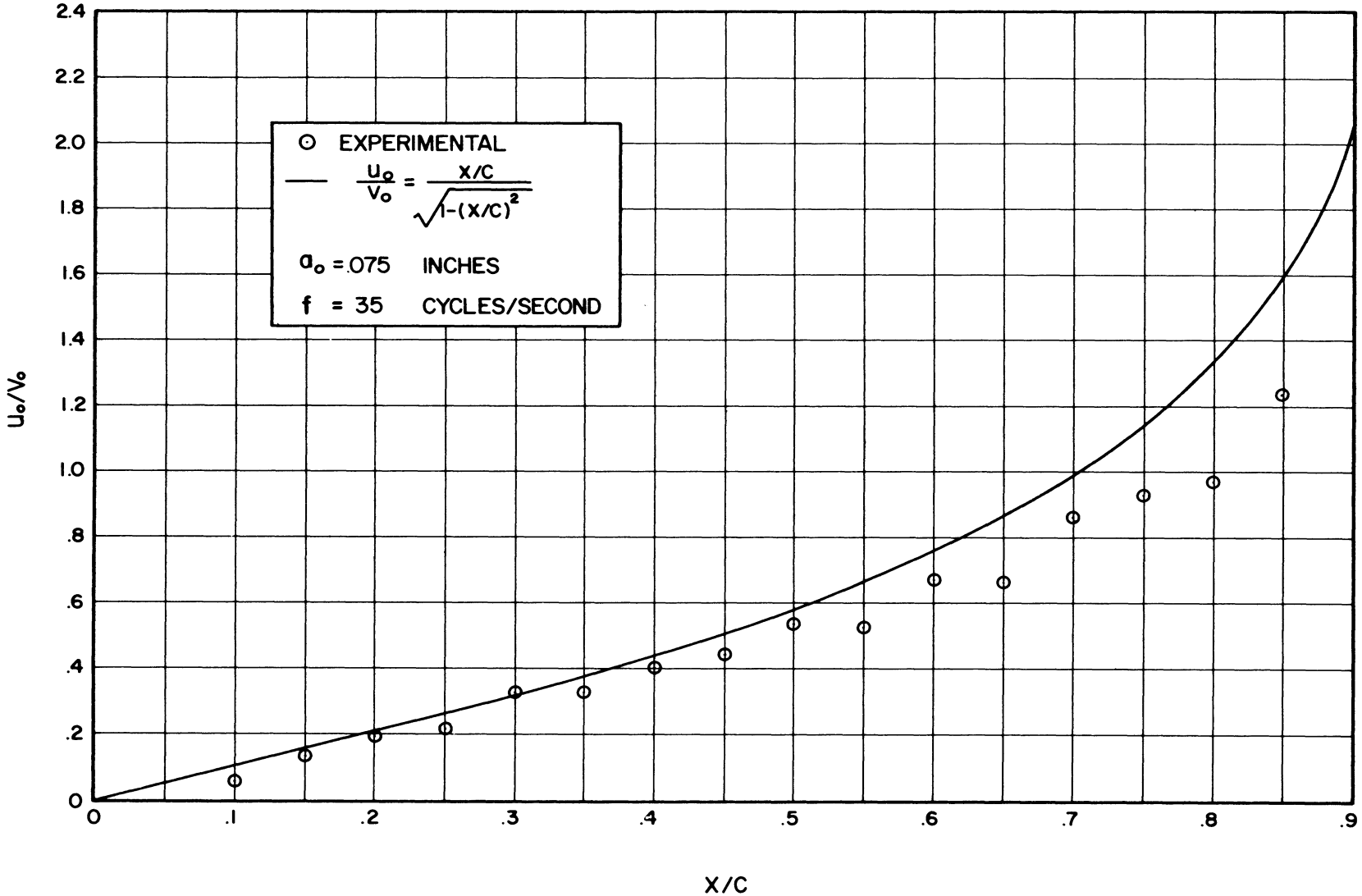

Figure 64. Experimental Potential Flow Velocity Measurements Made Along a Plate Vibrating Transversely and the Comparison with Theory.

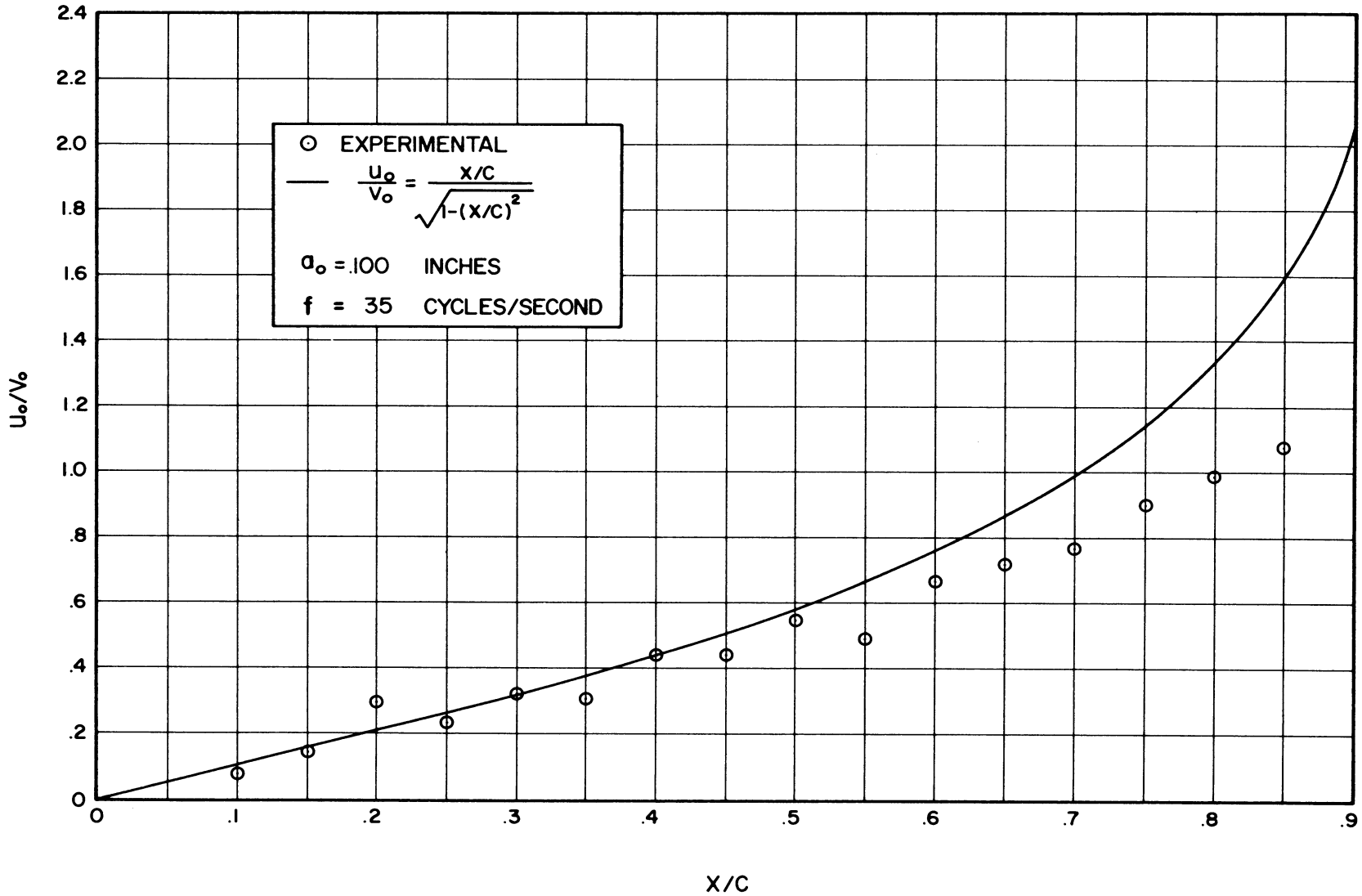

Figure 65. Experimental Potential Flow Velocity Measurements Made Along a Plate Vibrating Transversely and the Comparison with Theory.

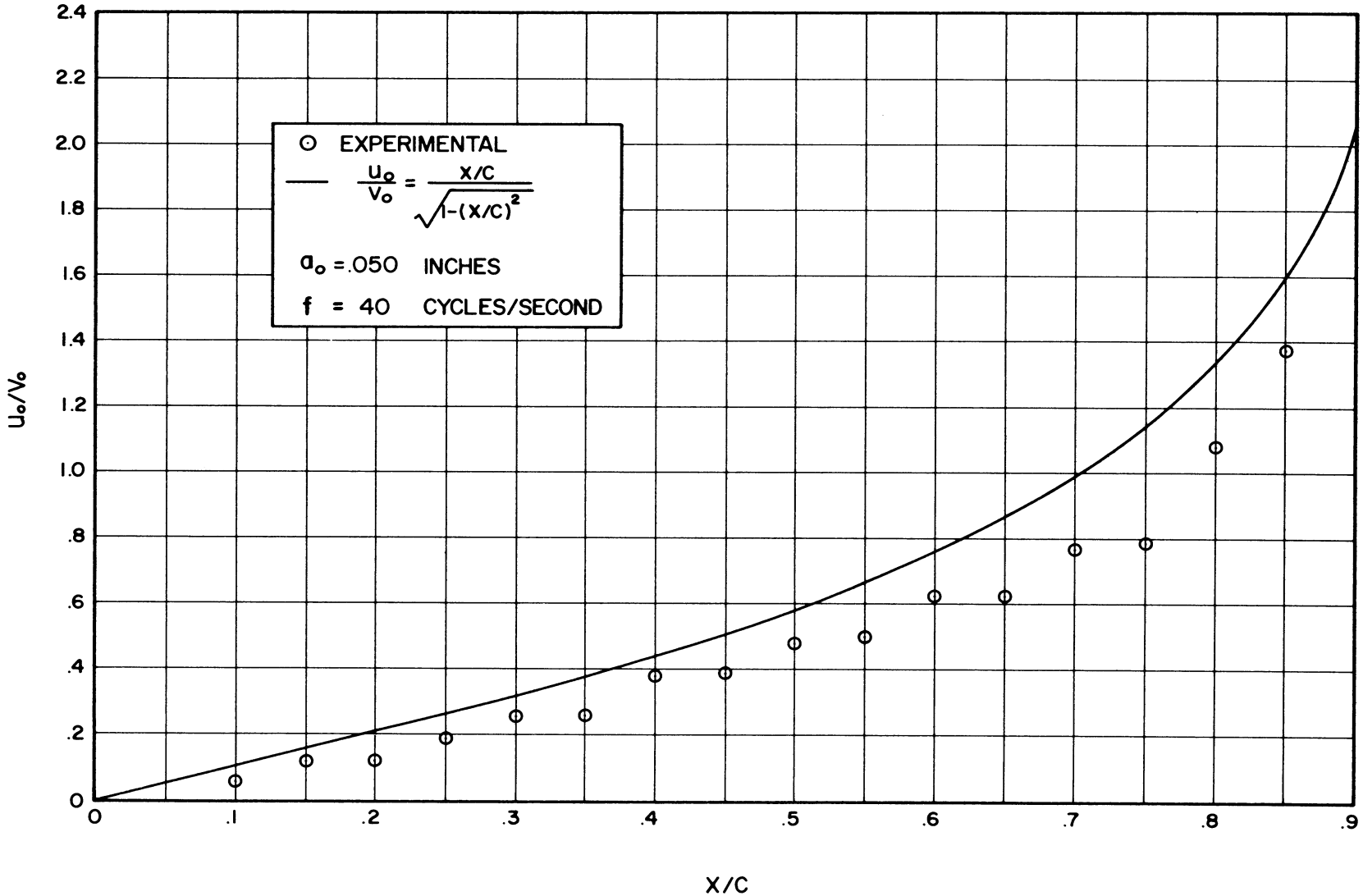

Figure 66. Experimental Potential Flow Velocity Measurements Made Along a Plate Vibrating Transversely and the Comparison with Theory.

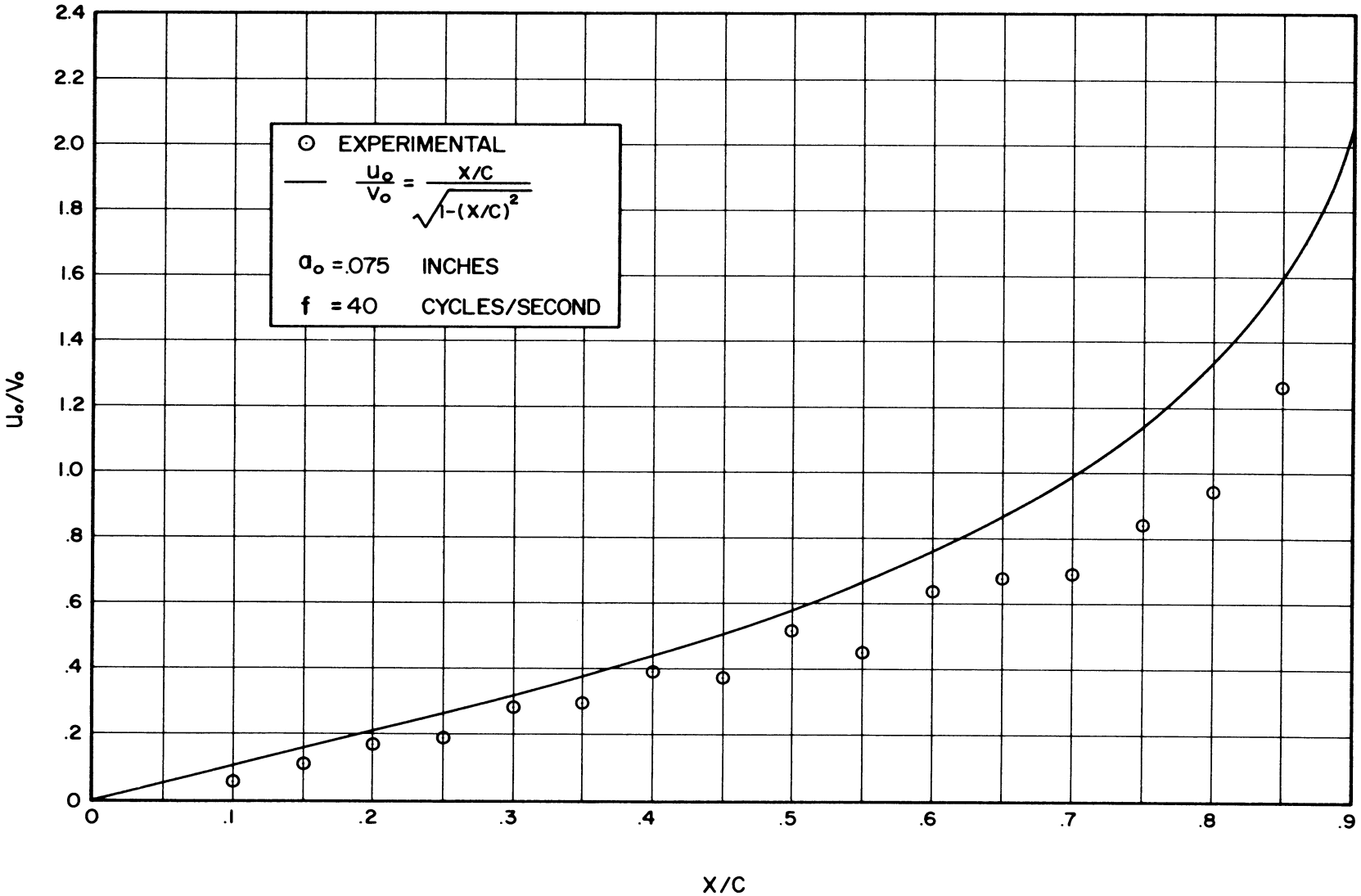

Figure 67. Experimental Potential Flow Velocity Measurements Made Along a Plate Vibrating Transversely and the Comparison with Theory.

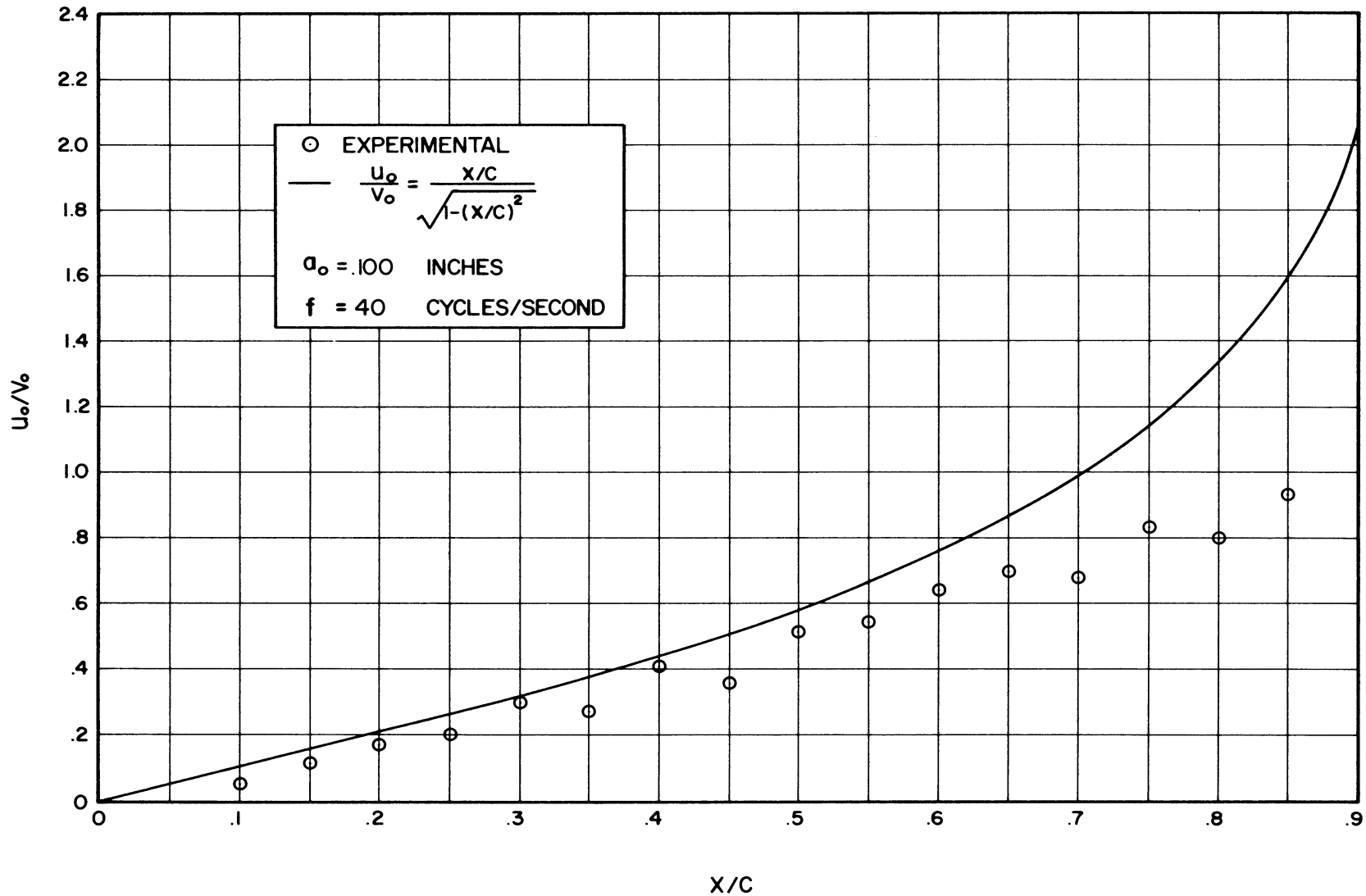

Figure 68. Experimental Potential Flow Velocity Measurements Made Along a Plate Vibrating Transversely and the Comparison with Theory.

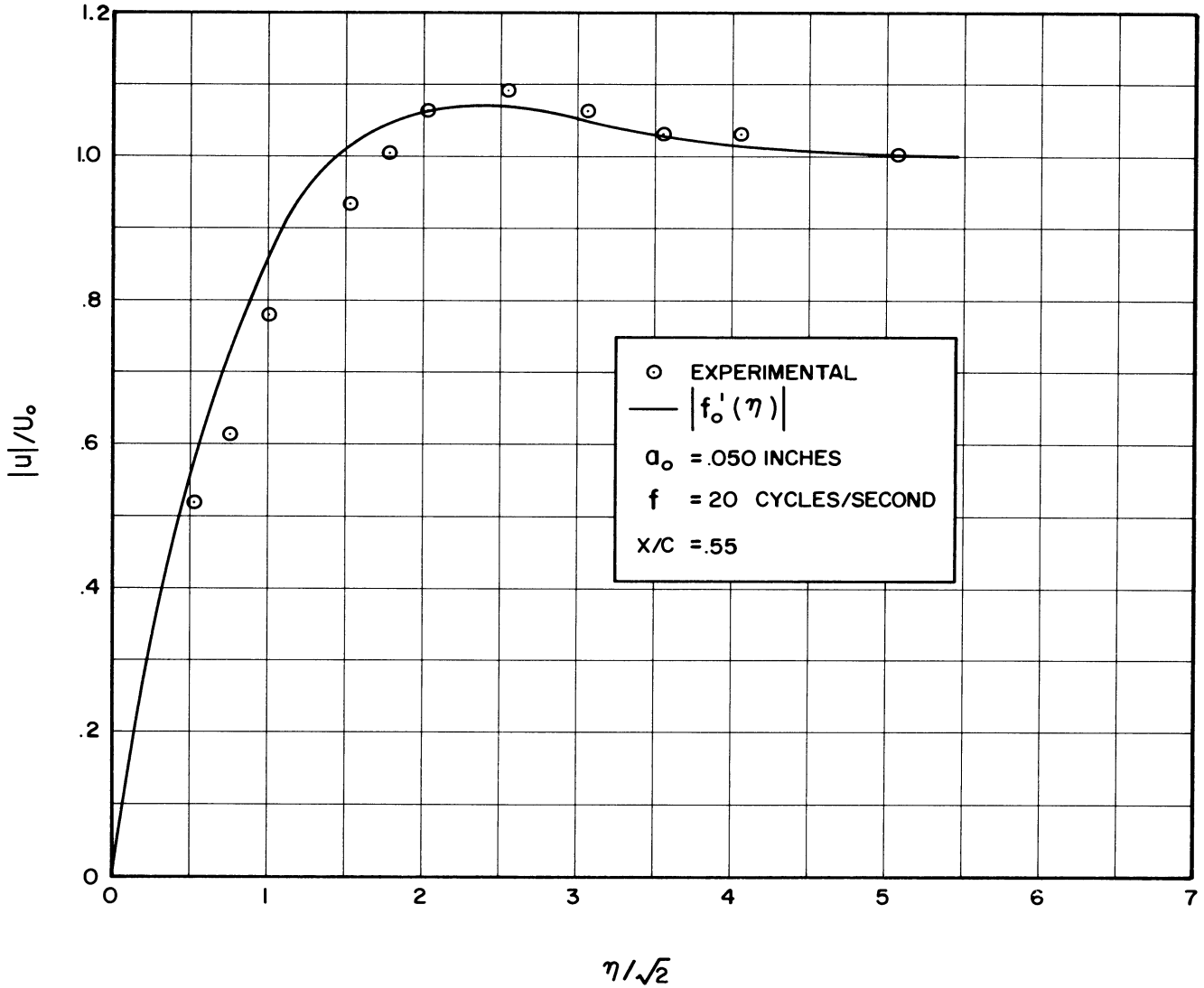

Figure 69. Experimental Velocity Measurements Made in the Boundary Layer on a Plate Vibrating Transversely and the Comparison with Theory.

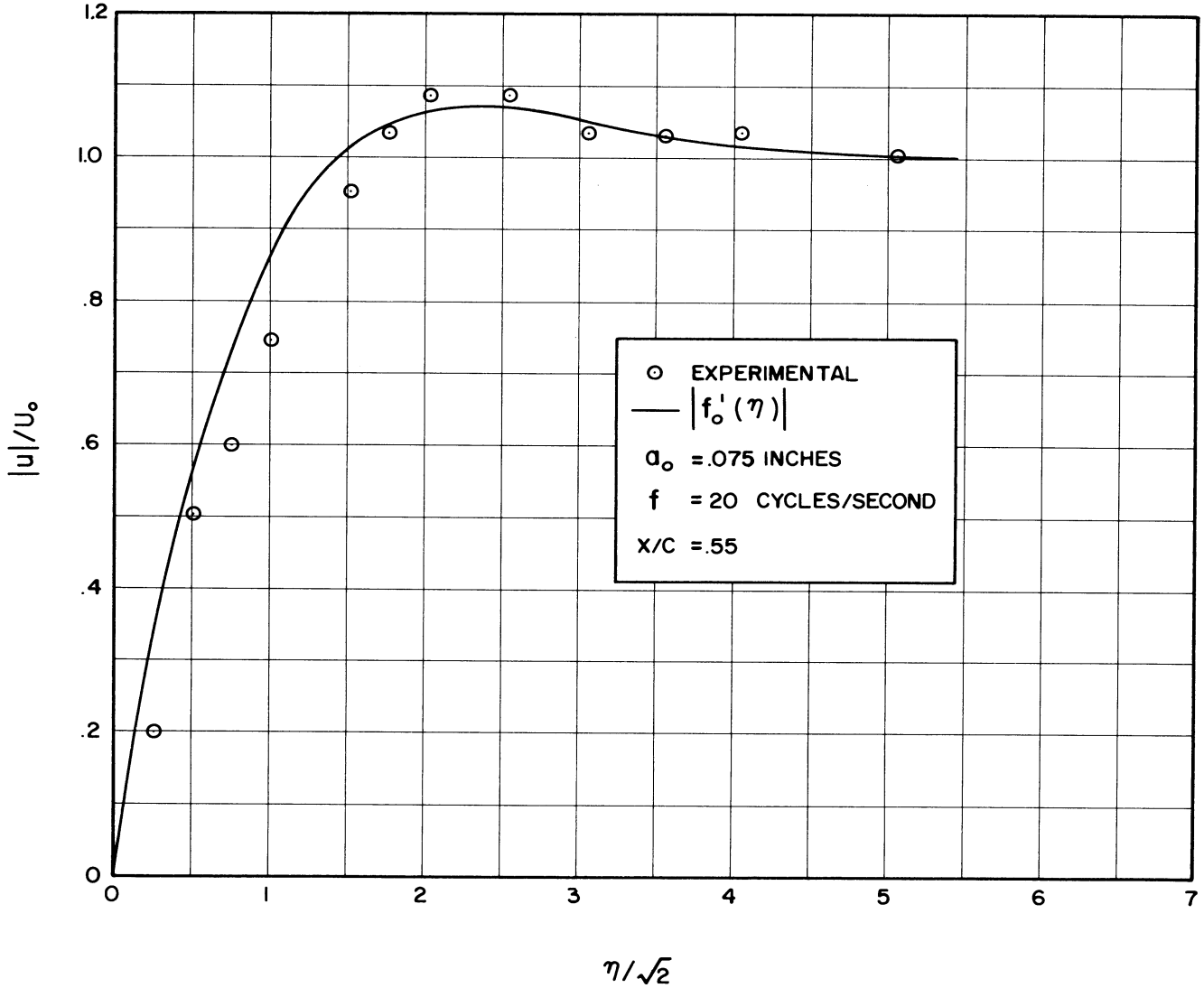

Figure 70. Experimental Velocity Measurements Made in the Boundary Layer on a Plate Vibrating Transversely and the Comparison with Theory.

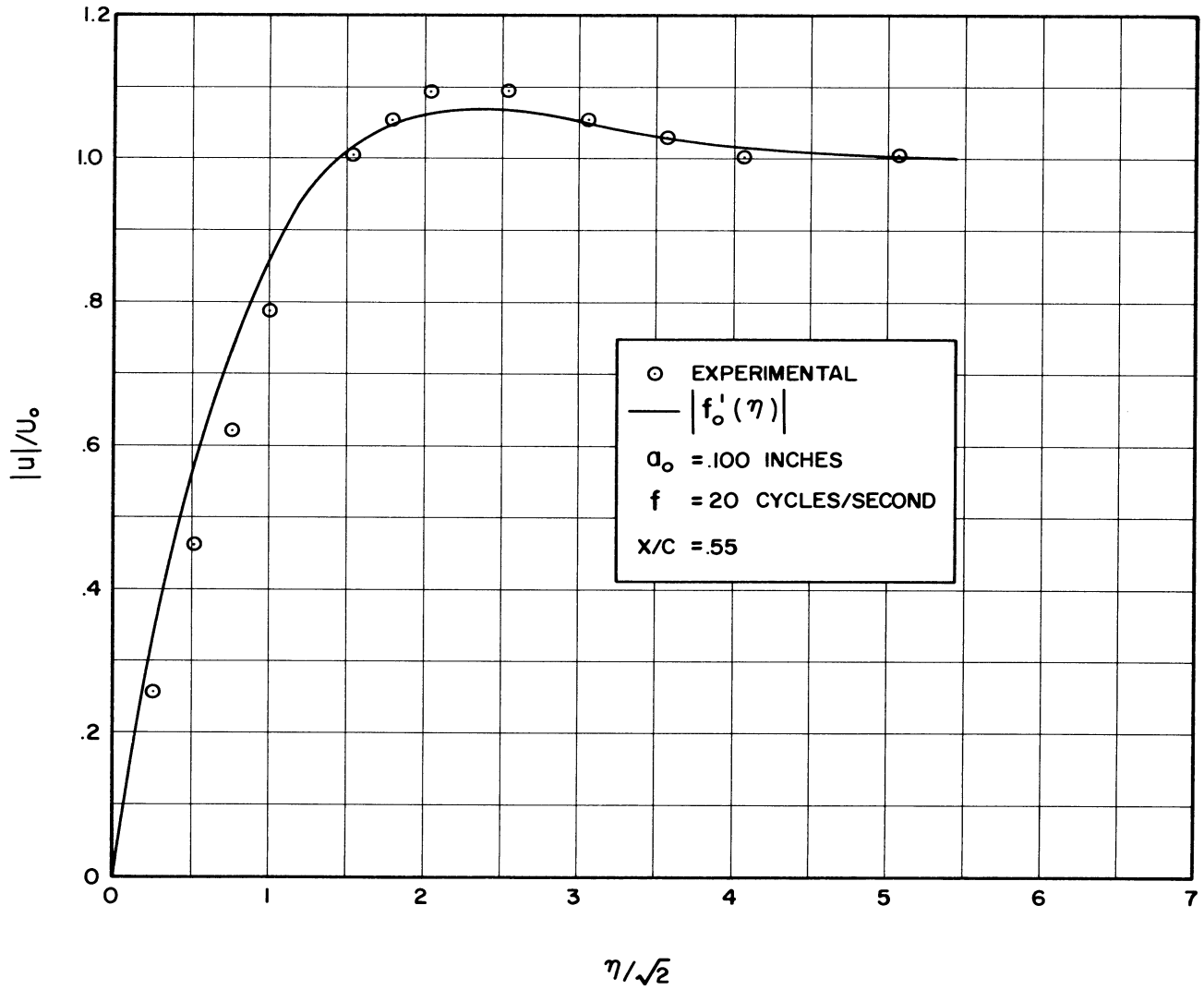

Figure 71. Experimental Velocity Measurements Made in the Boundary Layer on a Plate Vibrating Transversely and the Comparison with Theory.

close to $\frac{a_0/c}{[1-(x/c)^2]^{3/4}}$ as compared with the first. Since x/c = .55 and c = 5 inches, $\frac{a_0/c}{[1-(x/c)^2]^{3/2}}$ has values of .017, .026, and .034 for the three vibrational amplitudes used. Agreement with the theory is fairly good, although those measurements made close to the wall all show a tendency to be low. The theoretical prediction of boundary layer thickness shows excellent agreement with the measurements. Also, the peaking of the theoretical curve is definitely verified by the experimental data in all three figures.

The order of magnitude of the velocity oscillations discussed in Chapter III clearly indicates that a significant effect of vibration on the heat transfer from a heated plate may occur. This has been verified by data obtained from heat transfer measurements, and these will now be discussed.

It is true that heating the plate causes the occurrance of free convection velocities in addition to the oscillating components produced by the vibration and that the resulting system is very complicated. In spite of this complication, however, the vibration may be expected to produce velocity oscillations of roughly the same description as that given in Chapter III even in the presence of buoyancy effects. For a heated plate these oscillating velocity components, providing they are large enough, affect the temperature distribution and thus increase the heat transfer for a given wall temperature.

Before indicating the results of the measurements a discussion of the procedure is appropriate. The method of measuring the energy input to the heated section and also the operation of the guard heater system were discussed earlier in this chapter. Although the guard heaters prevent losses from the edges of the heated section, some of the measured

energy input is lost by radiation from the faces of the aluminum plates and also by conduction through the four rods extending from the corners of the heated section. When these two losses are subtracted from the measured energy input the result gives the convection heat transfer.

The emissivity of the polished aluminum plates has been measured using a thermopile as mentioned earlier. The emissivity of both plates was found to be very close to .05. The radiation losses are calculated from

$$q_r = \sigma_s \, \epsilon_m \, A \left(T_p^4 - T_a \right)^4. \tag{4.3}$$

For convenience a radiation heat transfer coefficient is defined by

$$q_r = h_r \, A \, \Delta\theta \, , \tag{4.4}$$

which results in

$$h_r = \frac{\sigma_s \, \epsilon_m}{\Delta\theta} \left(T_p^4 - T_a^4 \right). \tag{4.5}$$

For determining the conduction losses reference is made to Figure 72 which shows one of the rods where it attaches to the heated section. Thermocouples attached at points 1 and 2 give the temperatures at these points during operation. Applying conservation of energy to an element of the rod gives

$$\frac{\partial^2 \Delta\theta_r}{\partial x_r^2} - m_r^2 \, \Delta\theta_r = 0 \, , \tag{4.6}$$

where $\Delta\theta_r = (\theta_r - \theta_\infty)$ and $m_r^2 = \dfrac{4 h_s}{D k_r}$.

The solution is

$$\Delta\theta_r = C_1 \cosh m_r x_r + C_2 \sinh m_r x_r \, . \tag{4.7}$$

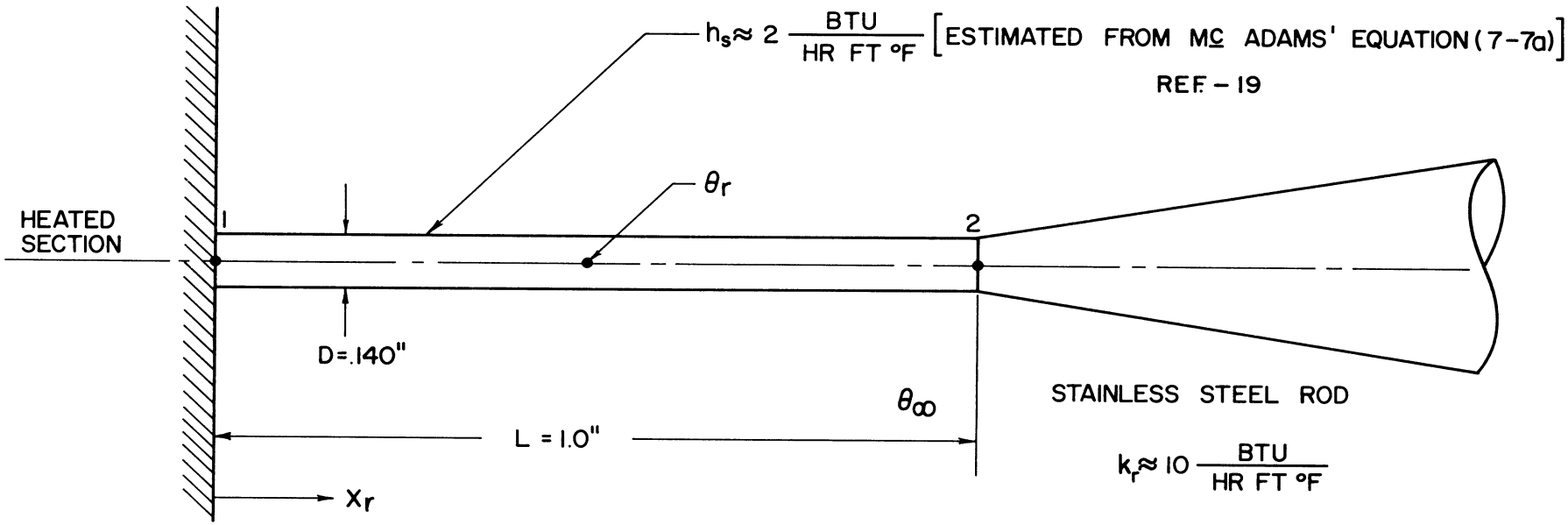

Figure 72. Sketch Showing One of the Four Rods Attached to the Corners of the Heated Section.

The two temperatures $(\theta_r)_1$ and $(\theta_r)_2$ are known from experimental measurements by means of thermocouples and these are used as boundary conditions to solve for the constants in Equation (4.7). The result is

$$\Delta\theta_r = (\Delta\theta_r)_1 \cosh m_r x_r + \left[\frac{(\Delta\theta_r)_2 - (\Delta\theta_r)_1 \cosh m_r L}{\sinh m_r L}\right] \sinh m_r x_r . \qquad (4.8)$$

The conduction heat transfer entering the rod at $x_r = 0$ is

$$-k_r \frac{\pi D^2}{4} \left(\frac{\partial\theta_r}{\partial x_r}\right)_{x_r=0} .$$

Since there are four rods this quantity is multiplied by four to give

$$q_k = 2\pi D \sqrt{h_s k_r D} \left[\frac{(\Delta\theta_r)_1 \cosh m_r L - (\Delta\theta_r)_2}{\sinh m_r L}\right] \qquad (4.9)$$

For convenience a conduction heat transfer coefficient is defined by

$$q_k = h_k A \Delta\theta , \qquad (4.10)$$

which results in

$$h_k = \frac{2\pi D \sqrt{h_s k_r D}}{A \Delta\theta} \left[\frac{(\Delta\theta_r)_1 \cosh m_r L - (\Delta\theta_r)_2}{\sinh m_r L}\right] . \qquad (4.11)$$

The total radiation and conduction losses are $q_\ell = (q_r + q_k)$, and correspondingly,

$$h_\ell = (h_r + h_k). \qquad (4.12)$$

The total measured energy input is now distributed according to

$$q = (h_c + h_v + h_\ell) A \Delta\theta . \qquad (4.13)$$

h_ℓ is defined by Equation (4.12), h_c is the free convection coefficient under non-vibratory conditions, and h_v is the increase in the convection coefficient caused by vibration at a particular value of $\Delta\theta$. Under non-vibratory conditions $h_v = 0$, and

$$h_c = \frac{q}{A \Delta\theta} - h_\ell . \qquad (4.14)$$

h_ℓ was found to be relatively constant over the temperature range used and h_c as a function of $\Delta\theta$ was obtained in accordance with Equation (4.14) from

measurements made of $\Delta\theta$ and q under steady state operation of the system. The results are shown by the graph in Figure 73 which has the equation

$$h_c = .40 \ \Delta\theta^{1/4} \ \frac{BTU}{HR - FT^2 - {}^\circ F} \ . \tag{4.15}$$

The result is slightly higher than that predicted by McAdams' Equation (7.5b) given as a simplified free convection correlation for air.[19]

In order to determine the vibratory effect on the convection coefficient at a particular vibration amplitude and frequency, the final temperature of the heated section for a given energy input is first estimated on the basis of an expected vibratory effect. The heated section is then brought to this estimated temperature after which the energy input, vibration amplitude, and frequency are adjusted to their proper values. A waiting period of about an hour or more is usually necessary to insure a steady state condition, that is, a condition where the temperature difference between the heated section and ambient does not change with time. This insures that the energy input to the system is being transferred away at the same rate so that the normal equations of steady heat transfer can be used to evaluate the convection heat transfer coefficient. During the waiting period the guard heaters are carefully controlled by means of the galvanometer system previously described, and the vibration amplitude is monitored by means of the output signal of the linear differential transformer displayed on the oscilloscope. Once steady state is achieved all temperatures together with the vibratory conditions and the energy input are recorded.

The information obtained by the procedure discussed in the previous paragraph is used to calculate the effect of vibration on the heat transfer in the following manner. For a particular energy input to the heated section the heat transfer under vibratory and non-vibratory

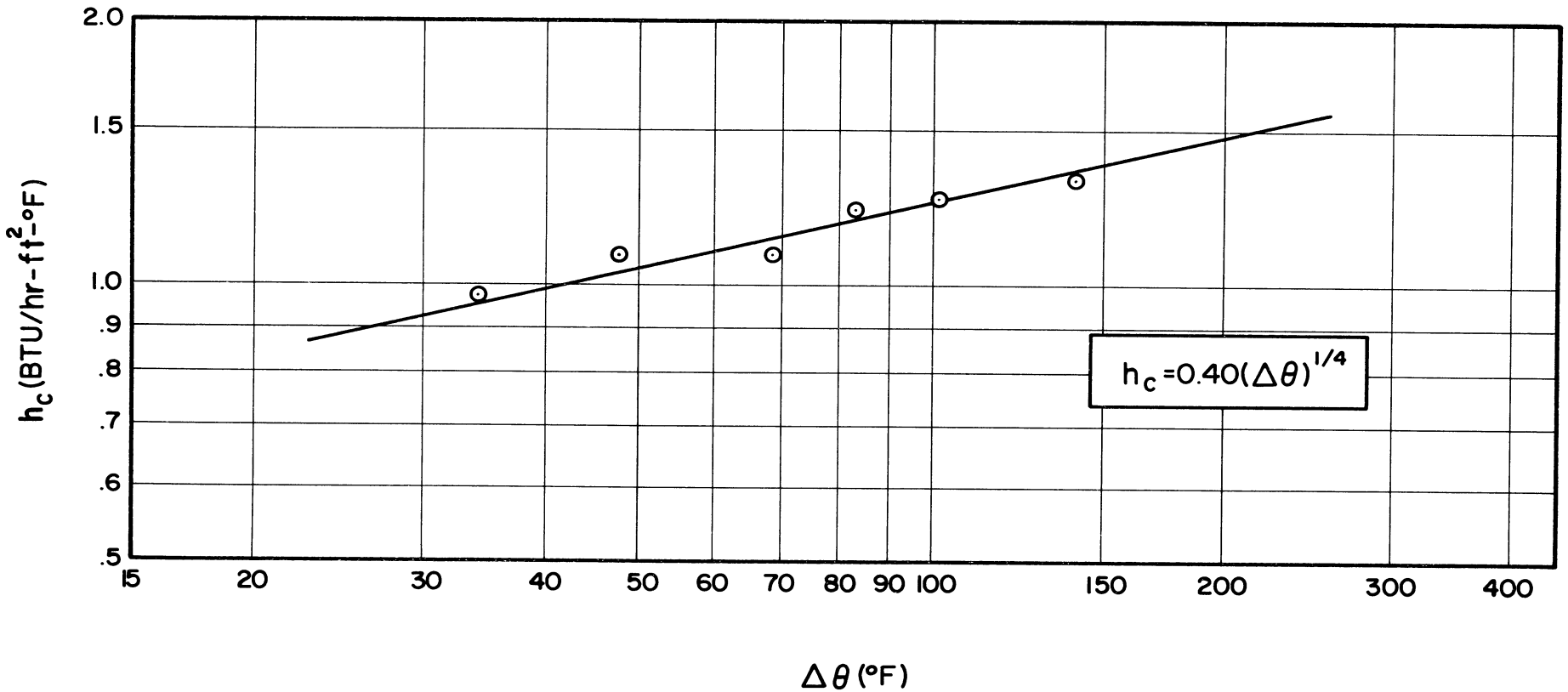

Figure 73. Correlation of Free Convection Heat Transfer Data Under Non-Vibratory Conditions.

conditions is the same. Thus,

$$(h_{co} + h_{\ell o})\, A\, \Delta\theta_o = (h_c + h_v + h_\ell)\, A\, \Delta\theta, \tag{4.16}$$

where the zero subscript indicates the non-vibratory condition. Dividing by h_c and noting that h_{co}/h_c is given by $(\Delta\theta_o/\Delta\theta)^{1/4}$ from (4.15), Equation (4.16) is rewritten as

$$\frac{h_v}{h_c} = \left[\left(\frac{\Delta\theta_o}{\Delta\theta}\right)^{5/4} - 1\right] + \frac{h_\ell}{h_c}\left[\frac{h_{\ell o}}{h_\ell}\,\frac{\Delta\theta_o}{\Delta\theta} - 1\right]. \tag{4.17}$$

Equation (4.17) gives the comparison of the vibratory effect on the convection coefficient with the value of the coefficient under non-vibratory conditions. This method places emphasis on the temperature measurement which can be done rather accurately. Results calculated in terms of the ratio h_v/h_c have a smaller error than that involved in the determination of the absolute values of h_ℓ and h_c. This can be seen by observing that the first bracketed term of (4.17) gives the idealized result when no losses are present. The second term is a correction term taking into account the losses in the system. Its magnitude relative to the first term is less than the ratio h_ℓ / h_c since

$$\left[\left(\frac{\Delta\theta_o}{\Delta\theta}\right)^{5/4} - 1\right] > \left[\frac{h_{\ell o}}{h_\ell}\,\frac{\Delta\theta_o}{\Delta\theta} - 1\right].$$

This is true because, as previously mentioned, the loss coefficient is fairly constant over the temperature range used so that $h_{\ell o}/h_\ell$ is very close to unity. For the experimental system used in this investigation h_ℓ/h_c has a value of about .10 over the entire temperature range used. Thus, a 10% error made in the overall correction due to losses would cause a uniform error of only about 1% in the values of h_v/h_c as determined by Equation (4.17). Using Equations (4.15) and (4.17), the expression for the vibratory coefficient is now written as

$$h_v = .40 \; \Delta\theta^{\frac{1}{4}} \left\{ \left[\left(\frac{\Delta\theta_o}{\Delta\theta} \right)^{\frac{5}{4}} - 1 \right] + \frac{h_\ell}{h_c} \left[\frac{h_{\ell o}}{h_\ell} \; \frac{\Delta\theta_o}{\Delta\theta} - 1 \right] \right\}. \qquad (4.18)$$

A summary of the heat transfer data as indicated by Equation (4.18) is given in Appendix IVc. This data is plotted as a function of $a_o f$ in Figure 74. The form of the abscissa is arbitrary and no theoretical reason for its use can be given within the limits of the work presented in this report. It was chosen only because the experimental data appear to correlate fairly well with reasonably small scatter when plotted in this way. Since the oscillations discussed in Chapter III increase with both amplitude and frequency, the vibrational heat transfer coefficient, as expected, behaves in a similar manner.

In terms of the symbols used in Chapter III the heated section lies in the region $-.6 < x/c < .6$. Therefore, the maximum amplitude of the potential flow oscillations that affect the heated section occur at the edges of this section where the value is $U_o = \frac{.6}{\sqrt{1-(.6)^2}} = \frac{3}{4} V_o$. For a_o = 1/10 of an inch and f = 50 cycles per second, this gives 23.5 inches per second at the edges of the heated section. On the other hand, the oscillations are smaller at lower values of x/c and are zero at the stagnation point. For purposes of discussion a rough average value over the heated section is taken as 10 inches per second under the vibratory conditions given above. According to Equation (4.2), the maximum free convection velocity at the center of the heated section is about 7.7 inches per second for $\Delta\Theta$ = 100°F. Thus, the average amplitude of the potential flow oscillations and the steady free convection velocities have roughly the same order of magnitude in this case. It is probable then, that the

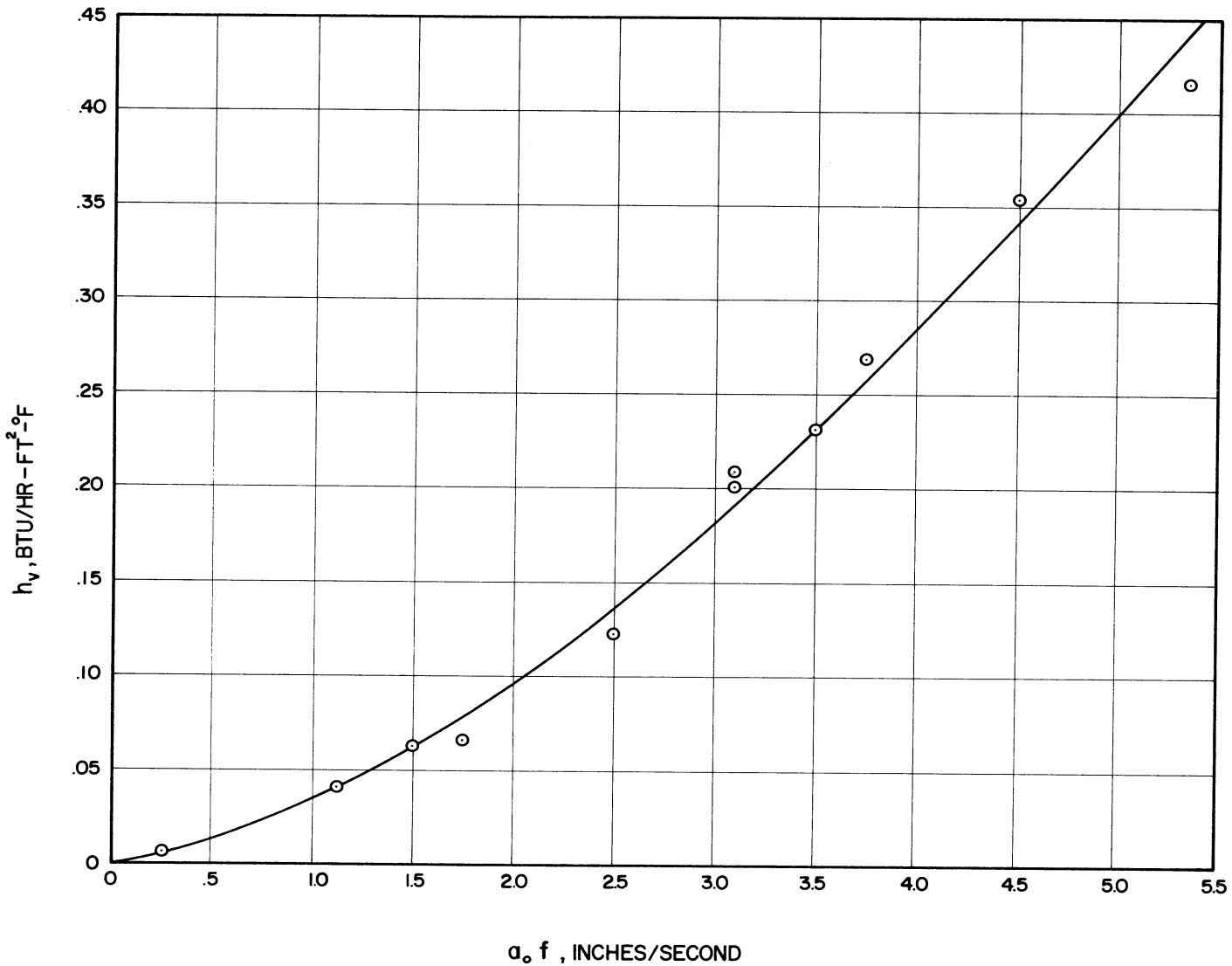

Figure 74. Correlation of Data Showing the Vibratory Effect on the Convection Heat Transfer Coefficient.

amplitude of the oscillating component of heat transfer has about the same order of magnitude as the steady value under these conditions. The change in the time averaged value due to vibration is smaller, however, as indicated by Figures 73 and 74. With $\Delta\theta = 100°F$, the result is $h_v/h_c \approx 32\%$ for a vibration amplitude and frequency of 1/10 of an inch and 50 cycles per second respectively.

It is appropriate to mention here the work of Shine[28] who observed the temperature profiles on a vertical plate vibrating transversely by means of an interferometer. Shine also recorded the temperature differences between the plate and ambient and found results similar to those given in Figure 74. No account was made of the losses so that the correction term of Equation (4.17) cannot be applied. It is probable that the losses in Shine's apparatus are somewhat larger than those involved in the apparatus used for this work. Even when the correction term for losses is ignored, however, Shine's results show values of h_v/h_c approximately twice as large as those given in this report for the same values of amplitude and frequency and with all other conditions being roughly the same. The comparison is made by neglecting the correction term in (4.17) to obtain the approximate form, $h_v/h_c \approx \left[\left(\frac{\Delta\theta_0}{\Delta\theta}\right)^{5/4} - 1\right]$.

The difference between Shine's results and those given in this report is easily explained by the fact that Shine's plate was entirely heated, while the heated portion used in this investigation covered only the 6 inch square central section on a 10 inch square plate. In terms of the analysis of Chapter III, the large oscillations occurring near the edges of the test plate could not affect the heat transfer results in this work, but probably caused large increases in local heat transfer from the plate used by Shine. These large increases near the edges could logically

have very significant effects on the overall mean heat transfer coefficient based on the entire area of the plate. For a more complete description of Shine's work the reader is referred to his original report.[28]

The results of the experimental work done in connection with transverse vibration of a finite plate are summed up by the following. The potential flow and boundary layer velocity oscillations were measured using a hot wire anemometer. These measurements agree fairly well with the analysis given in Chapter III as shown by Figures 51 through 71. These oscillations are large enough to cause significant changes in the heat transfer from a heated plate at nominal ranges of amplitude and frequency available with the vibration equipment used. This data is shown in Figure 74. A qualitative comparison of this data and that given by Shine is made. The reason for the differences is explained based on the analysis of Chapter III.

List of Symbols for Chapter IV

All discussion directly involving the analysis of Chapters II and III is done in terms of symbols used in those chapters. Additional symbols used elsewhere in Chapter IV are given below.

A	The total area of the heated section of the test plate
a_0	The amplitude of plate vibration
C_1, C_2	Constants in Equation (4.7)
D	The diameter of stainless steel rods where they attach to the corners of the heated section. See Figure 72.
f	The frequency of plate vibration
h_c	The free convection heat transfer coefficient under nonvibratory conditions at a particular value of $\Delta\theta$.
h_{co}	The free convection heat transfer coefficient under nonvibratory conditions at a particular energy input to the heated section corresponding to a temperature difference of $\Delta\theta_o$.
h_k	The conduction heat transfer coefficient defined by Equation (4.11)
h_ℓ	The heat transfer coefficient for losses defined by Equation (4.12)
$h_{\ell o}$	The heat transfer coefficient for losses at a particular energy input corresponding to a temperature difference of $\Delta\theta_o$.
h_r	The radiation heat transfer coefficient defined by Equation (4.5)
h_s	The convection heat transfer coefficient for the rods attached to the corners of the heated section. See Figure 72.
h_v	The increase in the convection heat transfer coefficient due to vibration at a particular $\Delta\theta$.
k_r	The thermal conductivity of the rods attached to the corners of the heated section. See Figure 72.
L	The distance between the thermocouples mounted on the rods attached to the corners of the heated section. See Figure 72.
m_r	See Equation (4.6). $m_r = 2\sqrt{\frac{h_s}{Dk_r}}$.
q	The total rate of energy input to the heated section.

q_k Heat transfer loss due to conduction through the rods attached to the corners of the heated section. See Figure 72.

q_ℓ The combined heat transfer lossed due to conduction and radiation. $q_\ell = (q_k + q_r)$.

q_r Heat transfer loss due to radiation

T_p Absolute temperature of the heated section of the test plate

T_a Absolute temperature of the ambient

x_r Distance along the rods attached to the four corners of the heated section. See Figure 72.

Greek Letters

ϵ_m The emissivity of the polished aluminum plates forming the heated section

θ Temperature

θ_o Temperature of the heated section of the test plate

θ_∞ Temperature of the ambient

θ_r Temperature at a point on the rod shown in Figure 72

$\Delta\theta$ Temperature difference between the heated section of the test plate and ambient. $\Delta\theta = (\theta_o - \theta_\infty)$.

$\Delta\theta_o$ Temperature difference $\Delta\theta$ corresponding to steady state under nonvibratory conditions at a particular energy input to the heated section.

$\Delta\theta_r$ Difference between the temperature at a point along the rod shown in Figure 72 and ambient. $\Delta\theta_r = (\theta_r - \theta_\infty)$.

σ_s The Stefan-Boltzman Constant. $\sigma_s = .1713 \times 10^{-8} \dfrac{\text{BTU}}{\text{hr-ft}^2\text{-}(^\circ\text{R})^4}$

CHAPTER V

SUMMARY OF RESULTS

In Chapter II a perturbation technique is used to obtain the velocity and temperature oscillations in a free convection boundary layer on a heated flat plate of infinite extent when the plate is vibrated normal to its own plane. These perturbations are shown to result from an oscillating pressure gradient which arises due to a coupling of the variable density field with the acceleration of the vibratory motion. Solutions are obtained for high and low values of γ, and the entire range of γ is shown to be adequately covered by a comparison of solutions based on the oscillating wall shear stress and temperature gradient. Calculated results are given for Prandtl Numbers of .01, .72, 10, and 1000.

In Chapter III the potential flow and boundary layer response is obtained for the case of a thin plate of finite length vibrating transversely in a fluid otherwise at rest. Due to the linearity of the irrotational flow equations the oscillatory potential flow solution is obtained from the corresponding steady flow problem taken to be the degenerate case of ellipse of zero thickness placed broadside to the stream direction. The potential flow oscillations along the plate are shown to increase from zero at the stagnation point to very high values close to the outer edges of the plate. A method of successive approximations is used to find the boundary layer response corresponding to the pressure gradient obtained from the potential flow solution. The first two approximations are given and it is shown that, within certain limitations, the first approximation alone often gives a fairly accurate result.

In Chapter IV experimental findings are reported. The attempt to measure the velocity perturbations in a free convection boundary layer on a vibrating plate was not successful. However, the small order of magnitude of these perturbations for the available ranges of amplitude and frequency was verified. This was done by observing that no significant change due to vibration occurred in the time averaged heat transfer coefficient. For the case of a finite plate, velocity measurements of the potential flow and boundary layer oscillations were obtained. These show fairly good agreement with the analysis of Chapter III. Measurements of the increase in the time averaged convection heat transfer coefficient for a finite plate are also given. The order of magnitude of these results are discussed in terms of the velocity oscillations predicted by the analysis of Chapter III.

LIST OF REFERENCES

1. Anantanarayanan and Ramachandran, "Effect of Vibration on Heat Transfer from a Wire to Air in Parallel Flow," ASME Paper No. 57-A-100.

2. Andrade, E. N. "On the Circulations Caused by Vibration of Air in a Tube," Proc. Roy. Soc. Lond. A134, 1931, 445-470.

3. Andres, J. M. and Ingard, U. "Acoustic Streaming at High Reynolds Numbers," Journ. Acoust. Soc. Amer., 25,(1953) 928-932.

4. Andres, J. M. and Ingard, U. "Acoustic Streaming at Low Reynolds Numbers," Journ. Acoust. Soc. Amer., 25,(1953) 932-938.

5. Carrier, G. R. and Di Prima, R. C. "On the Torsional Oscillations of a Solid Sphere in a Viscous Fluid," Journ. Applied Mech., 23(1956) 601-605.

6. Eckert, E. R. G. Hartnett, J. P., and Irvine, T. P. "Measurement of Total Emissivity of Porous Materials in Use for Transpiration Cooling," Jet Propulsion, 26 (April, 1956) 280-282.

7. Eckert, E. R. G. and Soehngen, E. E. "Studies on Heat Transfer in Laminar Free Convection with the Zehnder-Mach Interferometer," Tech. Rep. No. 5747, A.T.I. No. 44580, Air Material Command (Dayton, Ohio), December 27, 1948.

8. Fand, R. M. and Kaye, J. "The Effect of High Intensity Stationary and Progressive Sound Fields on Free Convection from a Horizongal Cylinder," WADC Technical Note 59-18, ASTIA Document No. Ad 209532, M.I.T., March, 1959.

9. Gibson, W. E. "Unsteady Laminar Boundary Layers," Ph.D. Thesis, M.I.T., 1957.

10. Glauert, M. B. "The Laminar Boundary Layer on Oscillating Plates and Cylinders," Journal Fluid Mech., 1 (1956) 97-110.

11. Holman, J. P. and Mott-Smith, T.P. "The Effect of High Constant Pressure Sound Fields on Free Convection Heat Transfer from a Horizontal Cylinder," WADC Technical Note 58-352, ASTIA Document No. AD 206906, Aeronautical Research Laboratory, December, 1958.

12. Jackson, T. W., Harrison, W. B. and Boteler, W. C. "Free Convection Forced Convection, and Acoustic Vibrations in a Constant Temperature Vertical Tube," ASME Paper No. 58-HT-6.

13. Kestin, J. and Persen, L.N. "Small Oscillations of Bodies of Revolution in a Viscous Fluid," Brown University Report AF-891/2, 1954.

14. Lamb, Horace, Hydrodynamics, Sixth Edition, Cambridge University Press, (1932) 84-85.

15. Lemlich, R. "Effect of Vibration on Natural Convective Heat Transfer," Industrial and Eng. Chemistry, 47, (1955) 1175-1180.

16. Lighthill, M. J. "The Response of Laminar Skin Friction and Heat Transfer to Fluctuations in the Stream Velocity," Proc. Roy. Soc. Lond. A224, June 9, 1955, 1-23.

17. Lin, C. C. "Motion in the Boundary Layer with a Rapidly Oscillating External Flow," presented at the 9th International Congress of Applied Mechanics, Brussels, Belgium, 1956.

18. Lord Rayleigh, "On the Circulation of Air Observed in Kundt't Tubes, and on Some Allied Acoustical Problems," Phil. Trans. Roy. Soc. Lond. 175, 1884 pp. 1-21.

19. McAdams, W.H. Heat Transmission, Third Edition, McGraw-Hill Book Co. (1954) 173, 177.

20. Medvin, H. and Rudnick, J. "Surface and Volume Sources of Vorticity in Acoustic Fields," Journ. Acoust. Soc. Amer., 25 (1953) 538-540.

21. Nyborg, W. L. "Acoustic Streaming Equations: Laws of Rotational Motion for Fluid Elements," Journ. Acoust. Soc. Amer., 25, (1953) 938-944.

22. Nyborg, W. L. "Acoustic Streaming Due to Attenuated Plane Waves," Journ. Acoust. Soc. Amer., 25 (1953) 68-75.

23. Ostrach, S. "An Analysis of Laminar Free-Convection Flow and Heat Transfer About a Flat Plate Parallel to the Direction of the Generating Body Force," NACA Report 1111, 1953.

24. Rosenblat, S. "Torsional Oscillations of a Plane in a Viscuous Fluid," Journ. Fluid Mech, 6 (1959) 206-220.

25. Rott, N. "Unsteady Viscous Flow in the Vicinity of a Stagnation Point," Quarterly Appl. Math., 13, No. 4, (January 1956) 444-451.

26. Schlichting, H. "Berechnung Ebener Periodischer Grenzschichtstromungen," Phys. Z., 33, (1932) 327-335.

27. Schmidt, R. and Beckmann, W. von. Tech. Mech. u. Thermodynamik, 1 (1930) 341-349, 391-406.

28. Shine, A. J. "The Effect of Transverse Vibrations on the Heat Transfer Rate from a Heated Vertical Plate in Free Convection," Air Force Inst. of Tech., Technical Report 57-13, December, 1957.

29. Snyder, N. W., Gier, J. T. and Dunkle, R. V. "Total Normal Emissivity Measurements on Aircraft Materials Between 100 and 800°F.," Trans. ASME, 77, (1955), 1011-1019.

30. Stuart, J. T. "A Solution of the Navier-Stokes and Energy Equations Illustrating the Response of Skin Friction and Temperature of an Infinite Plate Thermometer to Fluctuations in the Stream Velocity," Proc. Roy. Soc. Lond, A 231, (July 19, 1955), 116-130.

31. Westervelt, P. J. "The Theory of Steady Rotational Flow Generated by a Sound Field," Journ. Acoust. Soc. Amer., 25, (1953) 60-67.

APPENDIX I

TABULATED VALUES FOR CHAPTER II

This section gives the tabulated values of the functions, parameters, and coefficients discussed in Chapter II of this report. Except for Appendix I-a in which Ostrach's results are reproduced, all values have been calculated as a part of this work by means of a desk calculator. The method of calculation has been indicated in connection with each individual tabulation. All integral operations have been carried out numerically using Simpson's one third rule. This rule states that a function f(x) can be numerically integrated by

$$\int_{x_0-h}^{x_0+h} f(x)\,dx \cong \frac{h}{3}\left[f(x_0-h) + 4\,f(x_0) + f(x_0-h)\right]. \qquad \text{(A-1)}$$

In most cases the figures are reported to three digits.

APPENDIX I-a

OSTRACH'S[23] RESULTS

Prandtl number, 0.01

η	F	F'	F''	H	H'	η	F	F'	F''	H	H'
0	0.0000	0.0000	0.9862	1.0000	−0.0812	4.16	1.9319	0.4037	−0.0615	0.6741	−0.0723
.1	.0048	.0936	.8868	.9919	−.0812	4.18	1.9400	.4024	−.0614	.6726	−.0722
.2	.0184	.1774	.7891	.9838	−.0812	4.20	1.9480	.4012	−.0612	.6712	−.0721
.3	.0399	.2516	.6942	.9756	−.0812	4.24	1.9640	.3988	−.0609	.6683	−.0720
.4	.0684	.3164	.6030	.9675	−.0811	4.28	1.9799	.3964	−.0605	.6654	−.0718
.5	.1029	.3723	.5163	.9594	−.0811	4.32	1.9957	.3939	−.0602	.6626	−.0716
.6	.1426	.4198	.4349	.9513	−.0811	4.36	2.0114	.3915	−.0599	.6597	−.0714
.7	.1866	.4595	.3595	.9432	−.0811	4.40	2.0270	.3891	−.0595	.6568	−.0713
.8	.2342	.4919	.2906	.9351	−.0810	4.50	2.0657	.3832	−.0587	.6497	−.0708
.9	.2848	.5178	.2285	.9270	−.0809	4.60	2.1037	.3774	−.0579	.6427	−.0704
1.0	.3376	.5379	.1734	.9189	−.0809	4.70	2.1411	.3716	−.0572	.6357	−.0699
1.1	.3922	.5527	.1253	.9108	−.0808	4.80	2.1780	.3660	−.0564	.6287	−.0695
1.2	.4480	.5631	.0839	.9028	−.0807	4.90	2.2143	.3604	−.0556	.6218	−.0690
1.3	.5047	.5697	.0489	.8947	−.0806	5.00	2.2501	.3548	−.0549	.6149	−.0686
1.4	.5618	.5731	.0198	.8866	−.0804	5.10	2.2853	.3494	−.0541	.6081	−.0681
1.5	.6192	.5739	−.0039	.8786	−.0803	5.20	2.3200	.3440	−.0534	.6013	−.0676
1.6	.6765	.5725	−.0229	.8706	−.0801	5.40	2.3877	.3335	−.0520	.5878	−.0667
1.7	.7336	.5694	−.0379	.8626	−.0800	5.60	2.4534	.3232	−.0506	.5746	−.0657
1.8	.7904	.5650	−.0493	.8546	−.0798	5.80	2.5170	.3132	−.0493	.5615	−.0648
1.9	.8466	.5596	−.0579	.8466	−.0796	6.00	2.5787	.3035	−.0479	.5487	−.0638
2.0	.9023	.5535	−.0641	.8387	−.0794	6.20	2.6384	.2940	−.0467	.5360	−.0628
2.1	.9573	.5469	−.0685	.8307	−.0792	6.40	2.6963	.2849	−.0454	.5236	−.0618
2.2	1.0117	.5399	−.0714	.8228	−.0789	6.60	2.7524	.2759	−.0442	.5113	−.0608
2.3	1.0653	.5326	−.0732	.8150	−.0787	6.80	2.8067	.2671	−.0430	.4993	−.0598
2.4	1.1182	.5253	−.0742	.8071	−.0784	7.00	2.8593	.2586	−.0419	.4874	−.0588
2.5	1.1703	.5178	−.0746	.7993	−.0782	7.40	2.9594	.2423	−.0397	.4643	−.0568
2.6	1.2217	.5104	−.0745	.7915	−.0779	7.80	3.0532	.2269	−.0376	.4420	−.0547
2.7	1.2724	.5029	−.0741	.7837	−.0776	8.20	3.1411	.2123	−.0356	.4205	−.0527
2.8	1.3223	.4956	−.0735	.7760	−.0773	8.60	3.2232	.1984	−.0337	.3998	−.0508
2.9	1.3715	.4882	−.0728	.7682	−.0770	9.00	3.2999	.1853	−.0319	.3799	−.0489
3.0	1.4200	.4810	−.0719	.7606	−.0766	9.40	3.3715	.1729	−.0302	.3607	−.0470
3.1	1.4677	.4739	−.0711	.7529	−.0763	9.80	3.4383	.1612	−.0285	.3423	−.0451
3.2	1.5148	.4668	−.0701	.7453	−.0760	10.20	3.5005	.1501	−.0270	.3246	−.0432
3.3	1.5611	.4598	−.0692	.7377	−.0756	10.60	3.5584	.1396	−.0254	.3069	−.0413
3.4	1.6067	.4530	−.0683	.7302	−.0753	11.00	3.6123	.1297	−.0241	.2915	−.0397
3.45	1.6293	.4496	−.0678	.7264	−.0751	11.40	3.6622	.1203	−.0228	.2759	−.0380
3.5	1.6517	.4462	−.0674	.7227	−.0749	11.80	3.7086	.1114	−.0215	.2610	−.0364
3.55	1.6739	.4428	−.0669	.7189	−.0747	12.20	3.7514	.1031	−.0203	.2468	−.0348
3.6	1.6960	.4395	−.0664	.7152	−.0745	12.60	3.7911	.0952	−.0192	.2332	−.0332
3.65	1.7179	.4362	−.0660	.7115	−.0743	13.00	3.8276	.0877	−.0181	.2202	−.0317
3.7	1.7396	.4329	−.0655	.7078	−.0741	13.60	3.8771	.0773	−.0165	.2018	−.0296
3.75	1.7611	.4296	−.0651	.7041	−.0739	14.20	3.9206	.0679	−.0151	.1847	−.0276
3.8	1.7825	.4264	−.0646	.7004	−.0738	14.80	3.9587	.0592	−.0138	.1687	−.0257
4.85	1.8308	.4232	−.0642	.6967	−.0736	15.40	3.9918	.0513	−.0126	.1538	−.0239
3.9	1.8249	.4200	−.0638	.6930	−.0734	16.00	4.0204	.0441	−.0114	.1399	−.0223
3.95	1.8458	.4168	−.0633	.6893	−.0732	17.00	4.0591	.0335	−.0097	.1189	−.0197
4.00	1.8665	.4136	−.0629	.6857	−.0729	18.00	4.0880	.0246	−.0082	.1003	−.0175
4.05	1.8871	.4105	−.0625	.6821	−.0727	19.00	4.1088	.0171	−.0069	.0839	−.0154
4.10	1.9076	.4074	−.0620	.6784	−.0725	20.00	4.1226	.0108	−.0057	.0694	−.0137
4.12	1.9157	.4061	−.0619	.6770	−.0725	21.00	4.1308	.0057	−.0046	.0565	−.0121
4.14	1.9238	.4049	−.0617	.6755	−.0724	22.00	4.1343	.0015	−.0037	.0452	−.0107

Prandtl number, 0.72

η	F	F'	F''	H	H'
0	0.0000	0.0000	0.6760	1.0000	−0.5046
.1	.0032	.0627	.5785	.9495	−.5045
.2	.0122	.1159	.4866	.8991	−.5037
.3	.0261	.1602	.4007	.8488	−.5016
.4	.0440	.1962	.3210	.7989	−.4979
.5	.0651	.2246	.2479	.7493	−.4921
.6	.0887	.2460	.1817	.7005	−.4840
.7	.1141	.2612	.1224	.6526	−.4735
.8	.1407	.2708	.0700	.6059	−.4607
.9	.1681	.2754	.0246	.5606	−.4456
1.0	.1957	.2759	−.0143	.5168	−.4284
1.1	.2231	.2728	−.0468	.4749	−.4095
1.2	.2501	.2667	−.0734	.4350	−.3891
1.3	.2764	.2583	−.0945	.3972	−.3676
1.4	.3017	.2480	−.1106	.3615	−.3453
1.5	.3260	.2363	−.1224	.3281	−.3227
1.6	.3490	.2236	−.1302	.2970	−.3000
1.7	.3707	.2104	−.1347	.2681	−.2775
1.8	.3910	.1968	−.1363	.2415	−.2556
1.9	.4100	.1832	−.1356	.2170	−.2344
2.0	.4277	.1697	−.1331	.1945	−.2141
2.1	.4440	.1566	−.1290	.1741	−.1949
2.2	.4590	.1440	−.1238	.1555	−.1768
2.3	.4728	.1319	−.1178	.1387	−.1598
2.4	.4854	.1204	−.1113	.1235	−.1441
2.5	.4969	.1097	−.1044	.1098	−.1296
2.6	.5074	.0996	−.0973	.0976	−.1163
2.7	.5168	.0902	−.0903	.0865	−.1041
2.8	.5254	.0815	−.0834	.0767	−.0930
2.9	.5332	.0735	−.0767	.0679	−.0830
3.0	.5401	.0661	−.0703	.0601	−.0739
3.1	.5464	.0594	−.0642	.0531	−.0657
3.2	.5520	.0533	−.0585	.0469	−.0584
3.3	.5571	.0477	−.0531	.0414	−.0518
3.4	.5616	.0427	−.0481	.0365	−.0459
3.6	.5692	.0339	−.0392	.0284	−.0359
3.8	.5735	.0269	−.0317	.0220	−.0281
4.0	.5801	.0212	−.0255	.0170	−.0219
4.2	.5838	.0166	−.0204	.0132	−.0170
4.4	.5868	.0130	−.0162	.0102	−.0132
4.6	.5891	.0101	−.0128	.0078	−.0102
4.8	.5908	.0078	−.0102	.0060	−.0080
5.0	.5922	.0060	−.0079	.0046	−.0061
5.2	.5933	.0046	−.0063	.0035	−.0048
5.4	.5941	.0034	−.0048	.0027	−.0037
5.8	.5951	.0019	−.0029	.0015	−.0022
6.2	.5957	.0010	−.0018	.0009	−.0013
6.8	.5960	.0003	−.0008	.0003	−.0006
7.3	.5961	.0000	−.0004	.0001	−.0003

Prandtl number, 0.733

η	F	F'	F''	H	H'
0	0.0000	0.0000	0.6741	1.0000	−0.5080
.1	.0032	.0625	.5767	.9492	−.5079
.2	.0122	.1155	.4849	.8984	−.5071
.3	.0260	.1597	.3990	.8478	−.5050
.4	.0438	.1955	.3194	.7975	−.5012
.5	.0649	.2238	.2465	.7477	−.4953
.6	.0884	.2451	.1804	.6985	−.4870
.7	.1137	.2601	.1212	.6503	−.4763
.8	.1402	.2695	.0691	.6033	−.4632
.9	.1674	.2741	.0237	.5578	−.4478
1.0	.1949	.2745	−.0149	.5139	−.4303
1.1	.2222	.2713	−.0473	.4718	−.4110
1.2	.2490	.2652	−.0737	.4317	−.3902
1.3	.2752	.2568	−.0946	.3938	−.3684
1.4	.3003	.2465	−.1106	.3581	−.3458
1.5	.3244	.2348	−.1222	.3246	−.3228
1.6	.3473	.2222	−.1299	.2935	−.2998
1.7	.3688	.2090	−.1342	.2647	−.2771
1.8	.3891	.1954	−.1358	.2381	−.2549
1.9	.4079	.1819	−.1350	.2136	−.2335
2.0	.4254	.1685	−.1324	.1913	−.2130
2.1	.4416	.1554	−.1283	.1710	−.1937
2.2	.4565	.1429	−.1230	.1526	−.1754
2.3	.4702	.1309	−.1170	.1359	−.1584
2.4	.4827	.1195	−.1104	.1208	−.1427
2.5	.4941	.1088	−.1035	.1073	−.1281
2.6	.5045	.0988	−.0965	.0952	−.1148
2.7	.5139	.0895	−.0895	.0843	−.1026
2.8	.5224	.0809	−.0826	.0746	−.0916
2.9	.5301	.0729	−.0759	.0660	−.0816
3.0	.5370	.0657	−.0695	.0583	−.0725
3.1	.5433	.0590	−.0635	.0514	−.0644
3.2	.5489	.0530	−.0578	.0454	−.0571
3.3	.5539	.0475	−.0524	.0400	−.0506
3.4	.5584	.0425	−.0474	.0352	−.0448
3.6	.5660	.0339	−.0386	.0273	−.0350
3.8	.5720	.0269	−.0312	.0211	−.0272
4.0	.5769	.0213	−.0250	.0163	−.0211
4.2	.5807	.0169	−.0200	.0126	−.0164
4.4	.5837	.0133	−.0159	.0097	−.0127
4.6	.5860	.0105	−.0125	.0074	−.0098
4.8	.5879	.0082	−.0099	.0057	−.0076
5.0	.5893	.0065	−.0077	.0044	−.0058
5.2	.5905	.0051	−.0061	.0033	−.0045
5.4	.5914	.0040	−.0047	.0025	−.0035
5.6	.5921	.0032	−.0036	.0019	−.0027
5.8	.5927	.0025	−.0028	.0015	−.0021
6.0	.5932	.0021	−.0022	.0011	−.0016
6.4	.5938	.0014	−.0013	.0006	−.0009
6.8	.5943	.0010	−.0008	.0003	−.0006
7.2	.5946	.0007	−.0004	.0001	−.0003
7.6	.5949	.0006	−.0002	.0000	−.0002
8.0	.5951	.0005	−.0001	.0000	−.0001

Prandtl number, 1

η	F	F'	F''	H	H'
0	0.0000	0.0000	0.6421	1.0000	−0.5671
.1	.0030	.0593	.5450	.9433	−.5669
.2	.0115	.1092	.4540	.8867	−.5657
.3	.0246	.1503	.3694	.8302	−.5627
.4	.0413	.1833	.2916	.7742	−.5572
.5	.0610	.2089	.2208	.7189	−.5488
.6	.0829	.2277	.1572	.6645	−.5371
.7	.1064	.2406	.1008	.6116	−.5221
.8	.1308	.2481	.0516	.5602	−.5038
.9	.1558	.2511	.0093	.5109	−.4826
1.0	.1809	.2502	−.0263	.4638	−.4589
1.1	.2058	.2461	−.0557	.4192	−.4330
1.2	.2300	.2393	−.0793	.3772	−.4056
1.3	.2535	.2304	−.0975	.3381	−.3772
1.4	.2761	.2199	−.1110	.3018	−.3484
1.5	.2975	.2083	−.1203	.2684	−.3197
1.6	.3177	.1960	−.1260	.2379	−.2915
1.7	.3367	.1832	−.1287	.2101	−.2642
1.8	.3543	.1708	−.1288	.1850	−.2382
1.9	.3707	.1575	−.1268	.1624	−.2136
2.0	.3859	.1450	−.1233	.1422	−.1907
2.1	.3997	.1239	−.1185	.1242	−.1695
2.2	.4125	.1213	−.1127	.1082	−.1501
2.3	.4240	.1104	−.1064	.0941	−.1324
2.4	.4346	.1001	−.0997	.0817	−.1164
2.5	.4441	.0904	−.0928	.0708	−.1020
2.6	.4527	.0815	−.0859	.0613	−.0892
2.7	.4604	.0733	−.0791	.0529	−.0777
2.8	.4673	.0657	−.0725	.0457	−.0676
2.9	.4736	.0588	−.0662	.0392	−.0587
3.0	.4791	.0524	−.0602	.0339	−.0509
3.1	.4841	.0467	−.0546	.0291	−.0441
3.2	.4885	.0415	−.0493	.0250	−.0381
3.3	.4924	.0368	−.0444	.0215	−.0329
3.4	.4959	.0326	−.0399	.0185	−.0283
3.6	.5016	.0254	−.0321	.0136	−.0210
3.8	.5061	.0197	−.0255	.0009	−.0155
4.0	.5096	.0151	−.0202	.0072	−.0115
4.2	.5122	.0116	−.0158	.0053	−.0084
4.4	.5143	.0087	−.0124	.0038	−.0062
4.6	.5158	.0066	−.0096	.0027	−.0045
4.8	.5169	.0049	−.0075	.0020	−.0034
5.0	.5177	.0035	−.0057	.0014	−.0024
5.2	.5183	.0025	−.0044	.0010	−.0018
5.5	.5189	.0014	−.0029	.0006	−.0011
6.0	.5194	.0004	−.0014	.0002	−.0005
6.25	.5194	.0000	−.0010	.0000	−.0004

Prandtl number, 2

η	F	F'	F''	H	H'
0	0.0000	0.0000	0.5713	1.0000	−0.7165
.1	.0027	.0523	.4749	.9284	−.7161
.2	.0101	.0952	.3861	.8569	−.7135
.3	.0215	.1297	.3049	.7858	−.7069
.4	.0358	.1565	.2318	.7157	−.6949
.5	.0525	.1763	.1666	.6470	−.6768
.6	.0709	.1901	.1095	.5805	−.6523
.7	.0904	.1985	.0602	.5168	−.6215
.8	.1104	.2024	.0185	.4564	−.5852
.9	.1307	.2024	−.0161	.3999	−.5443
1.0	.1508	.1994	−.0440	.3476	−.5002
1.1	.1705	.1938	−*0659	.2999	−.4543
1.2	.1895	.1864	−.0824	.2568	−.4077
1.3	.2077	.1775	−.0942	.2183	−.3619
1.4	.2250	.1677	−.1020	.1844	−.3178
1.5	.2412	.1572	−.1063	.1547	−.2763
1.6	.2564	.1465	−.1078	.1290	−.2380
1.7	.2706	.1357	−.1071	.1069	−.2032
1.8	.2836	.1252	−.1046	.0882	−.1721
1.9	.2956	.1149	−.1008	.0724	−.1446
2.0	.3066	.1050	−.0960	.0592	−.1207
2.1	.3166	.0957	−.0906	.0482	−.1001
2.2	.3257	.0869	−.0849	.0391	−.0826
2.3	.3340	.0787	−.0789	.0316	−.0677
2.4	.3415	.0711	−.0729	.0254	−.0553
2.5	.3483	.0641	−.0671	.0204	−.0450
2.6	.3543	.0577	−.0614	.0164	−.0364
2.7	.3598	.0518	−.0560	.0131	−.0294
2.8	.3647	.0465	−.0509	.0105	−.0237
2.9	.3691	.0417	−.0461	.0083	−.0190
3.0	.3731	.0373	−.0416	.0066	−.0152
3.1	.3766	.0333	−.0375	.0053	−.0121
3.2	.3798	.0298	−.0338	.0042	−.0097
3.3	.3826	.0266	−.0303	.0033	−.0077
3.4	.3851	.0237	−.0272	.0026	−.0061
3.6	.3893	.0188	−.0218	.0017	−.0038
3.8	.3927	.0149	−.0174	.0010	−.0024
4.0	.3953	.0018	−.0138	.0007	−.0015
4.2	.3974	.0094	−.0109	.0004	−.0009
4.4	.3991	.0074	−.0086	.0003	−.0006
4.6	.4004	.0059	−.0068	.0002	−.0004
4.8	.4015	.0047	−.0054	.0001	−.0002
5.0	.4023	.0037	−.0042	.0001	−.0001
5.4	.4035	.0024	−.0026	.0001	−.0001
5.8	.4043	.0015	−.0016	.0000	.0000
6.4	.4049	.0008	−.0008	.0000	.0000
7.0	.4053	.0005	−.0004	.0000	.0000
8.0	.4056	.0002	−.0001	.0000	.0000
9.0	.4058	.0001	.0000	.0000	.0000
10.0	.4059	.0001	.0000	.0000	.0000
11.0	.4059	..0001	.0000	.0000	.0000

Prandtl number, 10

η	F	F'	F''	H	H'
0	0.0000	0.0000	0.4192	1.0000	−1.1694
.1	.0019	.0371	.3251	.8832	−1.1671
.2	.0071	.0654	.2428	.7670	−1.1521
.3	.0147	.0861	.1723	.6534	−1.1155
.4	.0241	.1003	.1134	.5448	−1.0526
.5	.0346	.1091	.0655	.4437	−.9640
.6	.0458	.1137	.0279	.3527	−.8545
.7	.0573	.1150	−.0011	.2733	−.7322
.8	.0687	.1137	−.0221	.2064	−.6061
.9	.0800	.1107	−.0367	.1519	−.4849
1.0	.0908	.1066	−.0462	.1090	−.3753
1.1	.1012	.1016	−.0518	.0763	−.2813
1.2	.1111	.0963	−.0545	.0522	−.2045
1.3	.1205	.0908	−.0552	.0349	−.1445
1.4	.1293	.0853	−.0544	.0228	−.0993
1.5	.1376	.0799	−.0527	.0146	−.0665
1.6	.1453	.0748	−.0505	.0092	−.0435
1.7	.1525	.0699	−.0480	.0056	−.0278
1.8	.1593	.0652	−.0453	.0034	−.0174
1.9	.1656	.0608	−.0427	.0020	−.0107
2.0	.1714	.0567	−.0400	.0012	−.0065
2.1	.1769	.0528	−.0375	.0007	−.0038
2.2	.1820	.0491	−.0351	.0004	−.0022
2.3	.1868	.0458	−.0328	.0002	−.0013
2.4	.1912	.0426	−.0306	.0001	−.0007
2.5	.1953	.0396	−.0286	.0001	−.0004
2.6	.1991	.0369	−.0267	.0000	−.0002
2.7	.2027	.0343	−.0249	.0000	−.0001
2.8	.2060	.0319	−.0232	.0000	−.0001
2.9	.2090	.0297	−.0216	.0000	.0000
3.0	.2119	.0276	−.0201	.0000	.0000
3.1	.2146	.0256	−.0187	.0000	.0000
3.2	.2170	.0238	−.0174	.0000	.0000
3.3	.2193	.0221	−.0162	.0000	.0000
3.4	.2215	.0206	−.0151	.0000	.0000
3.6	.2253	.0178	−.0131	.0000	.0000
3.8	.2286	.0153	−.0113	.0000	.0000
4.0	.2314	.0132	−.0098	.0000	.0000
4.2	.2339	.0114	−.0084	.0000	.0000
4.4	.2360	.0098	−.0073	.0000	.0000
4.6	.2379	.0085	−.0063	.0000	.0000
4.8	.2394	.0073	−.0054	.0000	.0000
5.0	.2408	.0063	−.0047	.0000	.0000
5.4	.2430	.0047	−.0035	.0000	.0000
5.8	.2446	.0035	−.0026	.0000	.0000
6.2	.2458	.0026	−.0019	.0000	.0000
7.0	.2474	.0014	−.0011	.0000	.0000
8.0	.2484	.0007	−.0005	.0000	.0000
9.0	.2489	.0003	−.0002	.0000	.0000
10.0	.2491	.0002	−.0001	.0000	.0000

Prandtl number, 100

η	F	F'	F''	H	H'
0.000	0.0000	0.0000	0.2517	1.0000	−2.191
.025	.0001	.0060	.2274	.9452	−2.191
.050	.0003	.0114	.2044	.8905	−2.188
.075	.0006	.0162	.1828	.8359	−2.180
.100	.0011	.0205	.1626	.7815	−2.166
.125	.0017	.0244	.1438	.7276	−2.144
.150	.0023	.0277	.1263	.6744	−2.113
.175	.0031	.0307	.1101	.6221	−2.071
.200	.0039	.0332	.0952	.5709	−2.018
.225	.0047	.0355	.0816	.5213	−1.954
.250	.0056	.0373	.0692	.4733	−1.880
.275	.0066	.0389	.0580	.4273	−1.786
.300	.0076	.0402	.0479	.3836	−1.704
.325	.0086	.0413	.0389	.3422	−1.604
.350	.0096	.0422	.0309	.3034	−1.498
.375	.0107	.0429	.0238	.2674	−1.388
.400	.0118	.0434	.0176	.2341	−1.276
.425	.0129	.0438	.0126	.2036	−1.163
.450	.0140	.0440	.0076	.1759	−1.052
.475	.0151	.0442	.0036	.1510	−.9430
.500	.0162	.0442	.0002	.1287	−.8393
.525	.0173	.0442	−.0026	.1089	−.7404
.550	.0184	.0441	−.0050	.0916	−.6478
.575	.0195	.0439	−.0070	.0765	−.5621
.600	.0206	.0437	−.0087	.0634	−.4837
.65	.0227	.0432	−.0111	.0427	−.3496
.70	.0249	.0426	−.0126	.0280	−.2440
.75	.0270	.0420	−.0135	.0178	−.1657
.80	.0291	.0413	−.0140	.0111	−.1088
.85	.0311	.0406	−.0142	.0067	−.0693
.90	.0331	.0399	−.0142	.0039	−.0428
.95	.0351	.0392	−.0141	.0022	−.0256
1.00	.0371	.0385	−.0140	.0012	−.0149
1.10	.0408	.0371	−.0136	.0004	−.0046
1.20	.0445	.0357	−.0132	.0001	−.0013
1.30	.0480	.0344	−.0128	.0000	−.0003
1.40	.0514	.0332	−.0124	.0000	−.0001
1.50	.0546	.0320	−.0119	.0000	.0000
1.60	.0578	.0308	−.0116	.0000	.0000
1.70	.0608	.0297	−.0112	.0000	.0000
1.80	.0637	.0286	−.0108	.0000	.0000
1.90	.0665	.0275	−.0104	.0000	.0000
2.0	.0692	.0265	−.0101	.0000	.0000
2.1	.0718	.0255	−.0097	.0000	.0000
2.2	.0743	.0245	−.0094	.0000	.0000
2.3	.0767	.0236	−.0091	.0000	.0000
2.4	.0790	.0227	−.0088	.0000	.0000
2.6	.0834	.0210	−.0082	.0000	.0000
2.8	.0874	.0195	−.0076	.0000	.0000
3.0	.0912	.0180	−.0071	.0000	.0000

Prandtl number, 100—Concluded

η	F	F'	F''	H	H'
3.2	0.0917	0.0166	−0.0066	0.0000	0.0000
3.4	.0979	.0154	−.0061	.0000	.0000
3.6	.1008	.0142	−.0056	.0000	.0000
3.8	.1035	.0131	−.0052	.0000	.0000
4.0	.1061	.0121	−.0049	.0000	.0000
4.4	.1105	.0103	−.0042	.0000	.0000
4.8	.1143	.0088	−.0036	.0000	.0000
5.2	.1176	.0074	−.0031	.0000	.0000
5.6	.1203	.0063	−.0026	.0000	.0000
6.0	.1226	.0053	−.0022	.0000	.0000
6.6	.1254	.0041	−.0018	.0000	.0000
7.2	.1276	.0032	−.0014	.0000	.0000
8.0	.1297	.0022	−.0010	.0000	.0000
9.0	.1315	.0014	−.0007	.0000	.0000
10.0	.1326	.0008	−.0005	.0000	.0000
11.0	.1332	.0004	−.0003	.0000	.0000
12.0	.1335	.0002	−.0002	.0000	.0000
13.0	.1336	.0000	−.0001	.0000	.0000

Prandtl number, 1000

η	F	F'	F''	H	H'
0.	0.0000	0.0000	0.1450	1.0000	−3.966
.025	.0000	.0033	.1212	.9009	−3.962
.050	.0002	.0061	.0999	.8021	−3.933
.075	.0003	.0083	.0811	.7046	−3.861
.100	.0006	.0102	.0647	.6096	−3.731
.125	.0008	.0116	.0506	.5186	−3.538
.150	.0012	.0127	.0387	.4332	−3.283
.175	.0015	.0135	.0289	.3549	−2.975
.200	.0018	.0142	.0209	.2847	−2.628
.225	.0022	.0146	.0146	.2236	−2.261
.250	.0026	.0149	.0096	.1717	−1.893
.275	.0029	.0151	.0059	.1288	−1.541
.300	.0033	.0152	.0032	.0944	−1.220
.325	.0037	.0153	.0012	.0675	−.9381
.350	.0041	.0153	−.0003	.0471	−.7012
.375	.0045	.0152	−.0012	.0321	−.5093
.400	.0048	.0152	−.0019	.0213	−.3596
.425	.0052	.0152	−.0023	.0138	−.2467
.450	.0056	.0151	−.0026	.0087	−.1645
.475	.0060	.0150	−.0027	.0053	−.1066
.500	.0063	.0150	−.0028	.0032	−.0672
.525	.0067	.0149	−.0029	.0019	−.0412
.550	.0071	.0148	−.0029	.0011	−.0245
.575	.0075	.0147	−.0029	.0006	−.0142
.600	.0078	.0147	−.0029	.0003	−.0080
.625	.0082	.0146	−.0029	.0002	−.0044
.800	.0107	.0141	−.0028	.0000	.0000
1.000	.0135	.0136	−.0027	.0000	.0000
1.40	.0187	.0125	−.0025	.0000	.0000
1.80	.0235	.0115	−.0023	.0000	.0000
2.20	.0279	.0106	−.0022	.0000	.0000
2.60	.0320	.0098	−.0020	.0000	.0000
3.0	.0358	.0090	−.0019	.0000	.0000
3.6	.0409	.0080	−.0017	.0000	.0000
4.2	.0454	.0070	−.0015	.0000	.0000
5.0	.0505	.0060	−.0012	.0000	.0000
5.8	.0549	.0050	−.0011	.0000	.0000
7.0	.0603	.0039	−.0008	.0000	.0000
8.0	.0638	.0032	−.0007	.0000	.0000
10.0	.0691	.0022	−.0004	.0000	.0000
12.0	.0727	.0015	−.0003	.0000	.0000
14.0	.0752	.0011	−.0002	.0000	.0000
16.0	.0771	.0008	−.0001	.0000	.0000
18.0	.0786	.0007	.0000	.0000	.0000
20.0	.0798	.0006	.0000	.0000	.0000
22.0	.0809	.0005	.0000	.0000	.0000
23.6	.0816	.0005	.0000	.0000	.0000

APPENDIX I-b

THE FORCING FUNCTION $\zeta(\eta)$

The forcing function is defined as

$$\zeta(\eta) = \int_{\infty}^{\eta} \eta\, H'(\eta)\, d\eta . \tag{A-2}$$

Considering that

$$\frac{d}{d\eta}(\eta H) = \eta H'(\eta) + H(\eta), \tag{A-3}$$

then

$$\zeta(\eta) = \int_{\infty}^{\eta} \eta\, H'(\eta)\, d\eta = \int_{\infty}^{\eta} d\left[\eta H(\eta)\right] + \int_{\eta}^{\infty} H(\eta)\, d\eta , \tag{A-4}$$

and

$$\zeta(\eta) = \int_{0}^{\infty} H(\eta)\, d\eta + \eta H(\eta) - \int_{0}^{\eta} H(\eta)\, d\eta . \tag{A-5}$$

Thus, in order to determine $\zeta(\eta)$ it is necessary to compute the product $\eta H(\eta)$ and to integrate the steady temperature profile $H(\eta)$. The function $\int_0^{\eta} \zeta(\eta) d\eta$ is determined by integration of the forcing function according to the definition.

Prandtl Number = .01

η	$\zeta(\eta)$	$\int_0^\eta \zeta(\eta)d\eta$	η	$\zeta(\eta)$	$\int_0^\eta \zeta(\eta)d\eta$
.0	8.25	0	4.2	7.57	33.68
.2	8.25	1.65	4.4	7.51	35.18
.4	8.24	3.30	4.6	7.45	36.68
.6	8.23	4.95	4.8	7.38	38.16
.8	8.22	6.59	5.0	7.31	39.63
1.0	8.21	8.24	5.8	7.03	45.37
1.2	8.19	9.88	6.6	6.71	50.87
1.4	8.17	11.51	7.4	6.39	56.11
1.6	8.15	13.14	8.2	6.04	61.08
1.8	8.12	14.77	9.0	5.70	65.77
2.0	8.09	16.39	9.8	5.34	70.19
2.2	8.06	18.00	10.6	4.98	74.32
2.4	8.02	19.61	11.4	4.64	78.17
2.6	7.98	21.21	12.2	4.30	81.74
2.8	7.94	22.80	13.0	3.96	85.04
3.0	7.89	24.39	14.2	3.48	89.51
3.2	7.85	25.96	15.4	3.02	93.40
3.4	7.80	27.53	16.0	2.80	95.15
3.6	7.74	29.08	18.0	2.13	100.1
3.8	7.69	30.62	20.0	1.55	103.7
4.0	7.63	32.15	22.0	1.03	100.3
			24.0		107.5

Prandtl Number = .72

η	$\zeta(\eta)$	$\int_0^\eta \zeta(\eta)d\eta$	η	$\zeta(\eta)$	$\int_0^\eta \zeta(\eta)d\eta$
.0	1.252	0	2.4	.396	2.144
.1	1.250	.125	2.5	.363	2.181
.2	1.242	.250	2.6	.332	2.216
.3	1.230	.373	2.7	.302	2.248
.4	1.212	.496	2.8	.275	2.277
.5	1.190	.616	2.9	.250	2.303
.6	1.163	.733	3.0	.227	2.327
.7	1.132	.858	3.1	.206	2.349
.8	1.097	.960	3.2	.187	2.368
.9	1.059	1.067	3.3	.167	2.386
1.0	1.017	1.171	3.4	.152	2.402
1.1	.973	1.271	3.6	.124	2.430

Prandtl Number = .72 (Cont'd)

η	$\zeta(\eta)$	$\int_0^\eta \zeta(\eta)d\eta$	η	$\zeta(\eta)$	$\int_0^\eta \zeta(\eta)d\eta$
1.2	.927	1.366	3.8	.100	2.452
1.3	.880	1.456	4.0	.081	2.470
1.4	.832	1.542	4.2	.065	2.484
1.5	.783	1.622	4.4	.052	2.496
1.6	.735	1.698	4.6	.042	2.505
1.7	.687	1.769	4.8	.033	2.513
1.8	.641	1.836	5.0	.026	2.519
1.9	.596	1.898	5.2	.021	2.523
2.0	.552	1.955	5.4	.016	2.527
2.1	.510	2.008	5.8	.010	2.532
2.2	.470	2.057	6.2	.006	2.535
2.3	.432	2.102	6.8	.002	2.538
			7.3	.001	2.538

Prandtl Number = 10

η	$\zeta(\eta)$	$\int_0^\eta \zeta(\eta)d\eta$	η	$\zeta(\eta)$	$\int_0^\eta \zeta(\eta)d\eta$
.0	.510	0	1.2	.075	.378
.1	.504	.051	1.3	.053	.384
.2	.487	.100	1.4	.037	.388
.3	.458	.148	1.5	.025	.391
.4	.420	.192	1.6	.017	.394
.5	.375	.232	1.7	.011	.395
.6	.325	.267	1.8	.007	.396
.7	.273	.296	1.9	.004	.396
.8	.223	.321	2.0	.003	.397
.9	.177	.341	2.1	.002	.397
1.0	.137	.357	2.2	.001	.397
1.1	.102	.369			

Prandtl Number = 1000

η	$\zeta(\eta)$	$\int_0^\eta \zeta(\eta)d\eta$
0	.148	0
.025	.147	.0037
.050	.143	.0073
.075	.137	.0108
.100	.129	.0141
.125	.118	.0172
.150	.107	.0201
.175	.094	.0226
.200	.081	.0247
.225	.068	.0266
.250	.056	.0281
.275	.044	.0294
.300	.034	.0304
.325	.026	.0311
.350	.019	.0317
.375	.014	.0321
.400	.010	.0324
.425	.007	.0326
.450	.004	.0327
.475	.003	.0328
.500	.002	.0329
.525	.001	.0329

APPENDIX I-c

THE TEMPERATURE FUNCTION $\eta H'(\eta)$

Prandtl Number = .01

η	$-\eta H'(\eta)$	η	$-\eta H'(\eta)$	η	$-\eta H'(\eta)$
0	0	2.8	.216	7.4	.420
.2	.016	3.0	.230	8.2	.432
.4	.032	3.2	.243	9.0	.440
.6	.049	3.4	.256	9.8	.442
.8	.065	3.6	.268	10.6	.438
1.0	.081	3.8	.280	11.4	.433
1.2	.097	4.0	.292	12.2	.425
1.4	.113	4.2	.303	13.0	.412
1.6	.128	4.4	.314	14.2	.392
1.8	.144	4.6	.324	15.4	.368
2.0	.159	4.8	.334	16.0	.357
2.2	.174	5.0	.343	18.0	.315
2.4	.188	5.8	.376	20.0	.274
2.6	.203	6.6	.401	22.0	.235

Prandtl Number = .72

η	$-\eta H'(\eta)$	η	$-\eta H'(\eta)$	η	$-\eta H'(\eta)$
0	0	1.7	.472	3.3	.171
.1	.050	1.8	.460	3.4	.156
.2	.101	1.9	.445	3.6	.129
.3	.150	2.0	.428	3.8	.107
.4	.199	2.1	.409	4.0	.088
.5	.246	2.2	.389	4.2	.071
.6	.290	2.3	.368	4.4	.058
.7	.331	2.4	.346	4.6	.050
.8	.369	2.5	.324	4.8	.038
.9	.401	2.6	.302	5.0	.031
1.0	.428	2.7	.281	5.2	.025
1.1	.450	2.8	.260	5.4	.020
1.2	.467	2.9	.241	5.8	.013
1.3	.478	3.0	.222	6.2	.008
1.4	.483	3.1	.204	6.8	.004
1.5	.484	3.2	.187	7.3	.002
1.6	.480				

Prandtl Number = 10

η	$-\eta H'(\eta)$	η	$-\eta H'(\eta)$	η	$-\eta H'(\eta)$
0	0	.9	.436	1.8	.031
.1	.117	1.0	.375	1.9	.020
.2	.230	1.1	.309	2.0	.013
.3	.335	1.2	.245	2.1	.008
.4	.421	1.3	.188	2.2	.005
.5	.482	1.4	.139	2.3	.003
.6	.513	1.5	.100	2.4	.002
.7	.513	1.6	.070	2.5	.001
.8	.485	1.7	.047		

Prandtl Number = 1000

η	$-\eta H'(\eta)$	η	$-\eta H'(\eta)$	η	$-\eta H'(\eta)$
0	0	.225	.509	.450	.074
.025	.099	.250	.473	.475	.051
.050	.197	.275	.424	.500	.034
.075	.290	.300	.366	.525	.022
.100	.373	.325	.305	.550	.014
.125	.442	.350	.245	.575	.008
.150	.493	.375	.191	.600	.005
.175	.521	.400	.144	.625	.003
.200	.526	.425	.105		

APPENDIX I-d

VALUES OF THE PARAMETERS DEFINED BY EQUATIONS (2.66)

Equations (2.66) are repeated here for convenience.

$$P_0 = \int_0^\infty \zeta(\eta)\, d\eta \tag{A-6a}$$

$$P_1 = F''(0) \tag{A-6b}$$

$$P_2 = \int_0^\infty [F'(\eta)]^2 d\eta \tag{A-6c}$$

$$P_3 = F(\infty) \tag{A-6d}$$

$$P_4 = -2\int_0^\infty \eta\, H'(\eta)\, F'(\eta)\, d\eta \tag{A-6e}$$

$$P_5 = -H'(0)/3\sigma\,. \tag{A-6f}$$

P_1, P_3, and P_5 are obtained directly from Ostrach's results as given in Appendix I-a. P_0 is obtained from the integration of $\zeta(\eta)$ given in Appendix I-c and P_4 is obtained by integration according to its definition.

P_2 can be found without the need for integration by the following reasoning. First, Equation (2.18a) is rewritten as

$$\frac{d}{d\eta} F''(\eta) + 3\frac{d}{d\eta}\left[F(\eta)F'(\eta)\right] - 5\left[F'(\eta)\right]^2 + H(\eta) = 0\,. \tag{A-7}$$

Integrating from the wall to infinity gives

$$F''(\eta)\Big|_0^\infty + 3F(\eta)F'(\eta)\Big|_0^\infty - 5\int_0^\infty \left[F'(\eta)\right]^2 d\eta + \int_0^\infty H(\eta)\, d\eta = 0\,, \tag{A-8}$$

or,

$$\int_0^\infty H(\eta)\, d\eta = F''(0) + 5\int_0^\infty \left[F'(\eta)\right]^2 d\eta\,. \tag{A-9}$$

From Appendix I-b, $\int_0^\infty H(\eta)d\eta = \zeta(0)$, so that now

$$\int_0^\infty [F'(\eta)]^2 d\eta = \frac{1}{5}\left[\zeta(0) - F''(0)\right], \tag{A-10}$$

or,

$$P_2 = \frac{1}{5}\left[\zeta(0) - P_1\right]. \tag{A-11}$$

The integrals $\int_0^\infty \eta H'(\eta)d\eta$ and $\int_0^\infty H(\eta)F'(\eta)d\eta$ in Equations (2.65) are not explicitly defined here because they can be given in terms of those parameters which are already defined. Thus,

$$-\int_0^\infty \eta\, H'(\eta)\, d\eta = \zeta(0) = P_1 + 5\, P_2 . \tag{A-12}$$

Also, since

$$\frac{d}{d\eta}\left[H(\eta)\, F(\eta)\right] = H(\eta)\, F'(\eta) + F(\eta)\, H'(\eta), \tag{A-13}$$

then

$$\int_0^\infty H(\eta)\, F'(\eta)\, d\eta = H(\eta)\, F(\eta)\Big|_0^\infty - \int_0^\infty F(\eta)\, H'(\eta)\, d\eta = -\int_0^\infty F(\eta)\, H'(\eta)\, d\eta. \tag{A-14}$$

But from Equation (2.18b), $F(\eta)H'(\eta) = -H''(0)/3\sigma$ so that

$$-\int_0^\infty F(\eta)\, H'(\eta)\, d\eta = \int_0^\infty \frac{H''(\eta)}{3\sigma}\, d\eta = \frac{H'(\eta)}{3\sigma}\Big|_0^\infty = -H'(0)/3\sigma . \tag{A-15}$$

Therefore,

$$\int_0^\infty H(\eta)\, F'(\eta)\, d\eta = P_5 . \tag{A-16}$$

Tabulated values of the parameters discussed in this section are given below.

Prandtl Number	.01	.72	10	1000
P_0	108	2.54	.397	.0329
P_1	.986	.676	.419	.145
P_2	1.45	.115	.018	.00060
P_3	4.13	.596	.249	.0816
P_4	2.39	.419	.102	.00391
P_5	2.71	.234	.039	.00132

APPENDIX I-e

VALUES OF THE PARAMETERS DEFINED BY EQUATIONS (2.72)

Using the values in Appendix I-d the parameters defined by Equations (2.72) are calculated according to the following relations.

$$Q_0 = \frac{3 P_0 P_5}{4 P_2 P_4} \tag{A-17a}$$

$$Q_1 = \frac{P_0 (P_1 + 5 P_2)}{4 P_2 P_4} \tag{A-17b}$$

$$Q_2 = \frac{P_3 (P_1 + 5 P_2)}{4 P_2 P_4} \tag{A-17c}$$

$$Q_3 = \frac{P_3 P_4 + 4 P_2 (P_1 + 5 P_2)}{4 P_2 P_4} \tag{A-17d}$$

$$Q_4 = \frac{3 P_3 P_5 + P_1 (P_1 + 5 P_2)}{4 P_2 P_4} \tag{A-17e}$$

$$Q_5 = \frac{P_1 P_4 + 12 P_2 P_5 + 2 P_5 (P_1 + 5 P_2)}{4 P_2 P_4} \tag{A-17f}$$

$$Q_6 = \frac{3 P_5 (P_1 + 4 P_2)}{4 P_2 P_4} \tag{A-18g}$$

The values are tabulated below:

Prandtl Number	.01	.72	10	1000
Q_0	62.9	9.21	6.30	13.9
Q_1	63.9	16.5	27.5	519
Q_2	2.46	3.86	17.2	1290
Q_3	4.18	4.28	8.45	71.8
Q_4	3.00	6.55	33.0	2320
Q_5	6.79	6.17	12.3	103
Q_6	3.98	4.13	7.81	62.3

APPENDIX I-f

VALUES OF THE COEFFICIENTS R_n

The coefficients R_n are calculated from Equation (2.73) which gives the recursion formula

$$R_n = \frac{\delta_{n0} Q_0 + i\,\delta_{n1} Q_1 + Q_2 R_{n-2} - i\,(Q_3 n + Q_4) R_{n-1}}{n^2 + (Q_5 + 1) n + Q_6} \qquad \text{(A-18)}$$

Values of Q are given in Appendix I-e. Calculated values of R_n are given below.

Values of R_n when n is even

n	Prandtl Number			
	.01	.72	10	1000
0	15.8	2.23	.808	.223
2	- .232	-3.85×10^{-2}	1.22×10^{-2}	.211
4	-7.46×10^{-2}	-2.66×10^{-2}	-7.89×10^{-2}	-8.43
6	4.47×10^{-3}	2.09×10^{-3}	1.83×10^{-2}	114
8	-1.61×10^{-4}	-7.14×10^{-5}	-1.74×10^{-3}	-844
10	4.81×10^{-6}	1.45×10^{-6}	6.76×10^{-5}	3960
12	-1.25×10^{-7}	-2.01×10^{-8}	1.03×10^{-6}	
14	2.80×10^{-9}	2.09×10^{-10}		

Values of $-R_n/i$ when n is odd

n	Prandtl Number			
	.01	.72	10	1000
1	3.90	.628	.270	$.932 \times 10^{-1}$
3	.164	4.85×10^{-2}	9.43×10^{-2}	1.70
5	-2.03×10^{-2}	-8.56×10^{-3}	-4.33×10^{-2}	-33.8
7	8.77×10^{-4}	4.17×10^{-4}	6.21×10^{-3}	330
9	-2.83×10^{-5}	-1.08×10^{-5}	-3.94×10^{-4}	-1930
11	7.87×10^{-7}	1.78×10^{-7}	6.29×10^{-6}	7400
13	-1.90×10^{-9}	-2.11×10^{-9}		
15		1.97×10^{-11}		

APPENDIX I-g

VALUES OF THE COEFFICIENTS S_n

The coefficients S_n are calculated from Equation (2.70a) which gives the relation

$$S_n = \frac{S_{no} P_o - \left[(P_1 + 4P_2 + 4P_2 n) R_n + i P_3 R_{n-1} \right]}{P_1 + 5P_2} \qquad \text{(A-19)}$$

Values of P are given in Appendix I-d and values of R_n are given in Appendix I-f. Calculated values of S_n are given below

Values of $-S_n$ when n is even

n	Prandtl Number			
	.01	.72	10	1000
0	0	0	0	0
2	1.44	.236	.147	.268
4	- .189	-4.03×10^{-2}	-7.48×10^{-2}	-8.00
6	1.24×10^{-2}	2.43×10^{-3}	1.20×10^{-2}	106
8	-6.01×10^{-4}	-7.68×10^{-5}	-6.11×10^{-4}	-768
10	2.36×10^{-5}	1.54×10^{-6}	-3.11×10^{-5}	3520
12	-7.61×10^{-7}	-2.23×10^{-8}	5.82×10^{-6}	
14	2.04×10^{-8}			

Values of $-S_n/i$ when n is odd

n	Prandtl Number			
	.01	.72	10	1000
1	1.97	.261	$.964 \times 10^{-1}$	2.88×10^{-2}
3	- .599	-.116	-.125	- 1.66
5	5.09×10^{-2}	1.17×10^{-2}	3.39×10^{-2}	31.8
7	-2.81×10^{-3}	-4.61×10^{-4}	-3.24×10^{-3}	-304
9	1.22×10^{-4}	1.14×10^{-5}	3.40×10^{-5}	1730
11	-4.34×10^{-6}	-1.92×10^{-7}	1.72×10^{-5}	-6510
13	1.27×10^{-7}	2.46×10^{-9}		

APPENDIX II

EXPRESSIONS FOR THE MAGNITUDE AND PHASE OF THE TEMPERATURE OSCILLATIONS FOR LARGE VALUES OF $\omega\sqrt{4x}$ (CHAPTER II)

Away from the wall, the magnitude and phase of the temperature oscillations are obtained from Equation (2.38) as

$$|N| = \left[\frac{-H'(0)\,S(0)}{(4x)^{3/4}\,\gamma^2}\right] \times \tag{A-20a}$$

$$\sqrt{\left\{2\int_0^\eta S(\eta)/S(0)\,d\eta - \frac{3}{\sqrt{2\gamma}}\left[1 - e^{-\sqrt{\gamma/2}\,\eta}\left(\cos\sqrt{\gamma/2}\,\eta - \sin\sqrt{\gamma/2}\,\eta\right)\right] + \eta\, e^{-\sqrt{\gamma/2}\,\eta}\cos\sqrt{\gamma/2}\,\eta\right\}^2 + \left\{\frac{3}{\sqrt{2\gamma}}\left[1 - e^{-\sqrt{\gamma/2}\,\eta}\left(\cos\sqrt{\gamma/2}\,\eta + \sin\sqrt{\gamma/2}\,\eta\right)\right] - \eta\, e^{-\sqrt{\gamma/2}\,\eta}\sin\sqrt{\gamma/2}\,\eta\right\}^2}$$

and

$$\alpha = \mathrm{Arctan}\left\{\frac{\frac{3}{\sqrt{2\gamma}}\left[1 - e^{-\sqrt{\gamma/2}\,\eta}\left(\cos\sqrt{\gamma/2}\,\eta + \sin\sqrt{\gamma/2}\,\eta\right)\right] - \eta\, e^{-\sqrt{\gamma/2}\,\eta}\sin\sqrt{\gamma/2}\,\eta}{2\int_0^\eta \frac{S(\eta)}{S(0)}\,d\eta - \frac{3}{\sqrt{2\gamma}}\left[1 - e^{-\sqrt{\gamma/2}\,\eta}\left(\cos\sqrt{\gamma/2}\,\eta - \sin\sqrt{\gamma/2}\,\eta\right)\right] + \eta\, e^{-\sqrt{\gamma/2}\,\eta}\cos\sqrt{\gamma/2}\,\eta}\right\} - \pi\,. \tag{A-20b}$$

Close to the wall, the magnitude and phase of the temperature oscillations are obtained from Equations (2.44) as

$$|N| = \left[\frac{-H'(0)\,S(0)}{\gamma^2\,(4x)^{3/4}}\right] \times$$

$$\sqrt{\left\{2\eta - \frac{3}{\sqrt{2\gamma}}\left[1 - e^{-\sqrt{\gamma/2}\,\eta}\left(\cos\sqrt{\gamma/2}\,\eta - \sin\sqrt{\gamma/2}\,\eta\right)\right] + \frac{1}{4}\,e^{-\sqrt{\gamma/2}\,\eta}\left[7\eta\cos\sqrt{\frac{\gamma}{2}}\,\eta + \sqrt{\frac{\gamma}{2}}\,\eta^2\left(\cos\sqrt{\frac{\gamma}{2}}\,\eta + \sin\sqrt{\frac{\gamma}{2}}\,\eta\right)\right]\right\}^2 + \left\{\frac{3}{\sqrt{2\gamma}}\left[1 - e^{-\sqrt{\frac{\gamma}{2}}\,\eta}\left(\cos\sqrt{\frac{\gamma}{2}}\,\eta + \sin\sqrt{\frac{\gamma}{2}}\,\eta\right)\right] - \frac{1}{4}\,e^{-\sqrt{\gamma/2}\,\eta}\left[7\eta\sin\sqrt{\frac{\gamma}{2}}\,\eta - \sqrt{\frac{\gamma}{2}}\,\eta^2\left(\cos\sqrt{\frac{\gamma}{2}}\,\eta - \sin\sqrt{\frac{\gamma}{2}}\,\eta\right)\right]\right\}^2}\,, \tag{A-21a}$$

and

$$\alpha = \text{Arc tan}\left\{\frac{\frac{3}{\sqrt{2\gamma}}\left[1 - e^{-\sqrt{\frac{\gamma}{2}}\,\eta}\left(\cos\sqrt{\gamma/2}\,\eta + \sin\sqrt{\gamma/2}\,\eta\right)\right] - \frac{1}{4}\,e^{-\sqrt{\frac{\gamma}{2}}\,\eta}\left[7\eta\sin\sqrt{\frac{\gamma}{2}}\,\eta - \sqrt{\frac{\gamma}{2}}\,\eta^2\left(\cos\sqrt{\frac{\gamma}{2}}\,\eta - \sin\sqrt{\frac{\gamma}{2}}\,\eta\right)\right]}{2\eta - \frac{3}{\sqrt{2\gamma}}\left[1 - e^{-\sqrt{\gamma/2}\,\eta}\left(\cos\sqrt{\frac{\gamma}{2}}\,\eta - \sin\sqrt{\frac{\gamma}{2}}\,\eta\right)\right] + \frac{1}{4}\,e^{-\sqrt{\gamma/2}\,\eta}\left[7\eta\cos\sqrt{\frac{\gamma}{2}}\,\eta + \sqrt{\frac{\gamma}{2}}\,\eta^2\left(\cos\sqrt{\frac{\gamma}{2}}\,\eta + \sin\sqrt{\frac{\gamma}{2}}\,\eta\right)\right]}\right\} - \pi \tag{A-21b}$$

if $\sigma = 1$, while

$$|N| = \left[\frac{-H'(0)\ S(0)}{\gamma^2\ (4x)^{3/4}}\right] \times$$

$$\sqrt{\left\{2\eta - \frac{3}{\sqrt{2\gamma}}\left[1 - e^{-\sqrt{\frac{\gamma\sigma}{2}}\eta}\left(\cos\sqrt{\frac{\gamma\sigma}{2}}\eta - \sin\sqrt{\frac{\gamma\sigma}{2}}\eta\right) + \frac{\sigma(5-3\sigma)}{(1-\sigma)^2\sqrt{2\gamma}} \times \left[e^{-\sqrt{\frac{\gamma\sigma}{2}}\eta}\left(\cos\sqrt{\frac{\gamma\sigma}{2}}\eta - \sin\sqrt{\frac{\gamma\sigma}{2}}\eta\right) - e^{-\sqrt{\frac{\gamma}{2}}\eta}\left(\cos\sqrt{\frac{\gamma}{2}}\eta - \sin\sqrt{\frac{\gamma}{2}}\eta\right)\right]\right.\right.$$
$$\left.\left. - \frac{\sigma}{1-\sigma}\eta\, e^{-\sqrt{\frac{\gamma}{2}}\eta}\cos\sqrt{\frac{\gamma}{2}}\eta\right\}^2 + \left\{\frac{3}{\sqrt{2\gamma}}\left[1 - e^{-\sqrt{\frac{\gamma\sigma}{2}}\eta}\left(\cos\sqrt{\frac{\gamma\sigma}{2}}\eta + \sin\sqrt{\frac{\gamma\sigma}{2}}\eta\right)\right] - \frac{\sigma(5-3\sigma)}{(1-\sigma)^2\sqrt{2\gamma}}\left[e^{-\sqrt{\frac{\gamma\sigma}{2}}}\left(\cos\sqrt{\frac{\gamma\sigma}{2}}\eta\right.\right.\right.$$
$$\left.\left.\left. + \sin\sqrt{\frac{\gamma\sigma}{2}}\eta\right) - e^{-\sqrt{\frac{\gamma\sigma}{2}}\eta}\left(\cos\sqrt{\frac{\gamma}{2}}\eta + \sin\sqrt{\frac{\gamma}{2}}\eta\right) + \frac{\sigma}{1-\sigma}\eta\, e^{-\sqrt{\frac{\gamma}{2}}\eta}\ \sin\sqrt{\frac{\gamma}{2}}\eta\right\}^2\right.} \tag{A-22a}$$

and

$$\alpha = \text{Arc}\tan$$

$$\left\{\frac{\frac{3}{\sqrt{2\gamma}}\left[1 - e^{-\sqrt{\frac{\gamma\sigma}{2}}\eta}\left(\cos\sqrt{\frac{\gamma\sigma}{2}}\eta + \sin\sqrt{\frac{\gamma\sigma}{2}}\eta\right)\right] - \frac{\sigma(5-3\sigma)}{(1-\sigma)^2\sqrt{2\gamma}}\left[e^{-\sqrt{\frac{\gamma\sigma}{2}}\eta}\left(\cos\sqrt{\frac{\gamma\sigma}{2}}\eta + \sin\sqrt{\frac{\gamma\sigma}{2}}\eta\right) - e^{-\sqrt{\frac{\gamma}{2}}\eta}\left(\cos\sqrt{\frac{\gamma}{2}}\eta + \sin\sqrt{\frac{\gamma}{2}}\eta\right)\right] + \frac{\sigma}{1-\sigma}\eta\, e^{-\sqrt{\frac{\gamma}{2}}\eta}}{2\eta - \frac{3}{\sqrt{2\gamma}}\left[1 - e^{-\sqrt{\frac{\gamma\sigma}{2}}\eta}\left(\cos\sqrt{\frac{\gamma\sigma}{2}}\eta - \sin\sqrt{\frac{\gamma\sigma}{2}}\eta\right)\right] + \frac{\sigma(5-3\sigma)}{(1-\sigma)^2\sqrt{2\gamma}}\left[e^{-\sqrt{\frac{\gamma\sigma}{2}}\eta}\left(\cos\sqrt{\frac{\gamma\sigma}{2}}\eta - \sin\sqrt{\frac{\gamma\sigma}{2}}\eta\right) - e^{-\sqrt{\frac{\gamma}{2}}\eta}\left(\cos\sqrt{\frac{\gamma}{2}}\eta - \sin\sqrt{\frac{\gamma}{2}}\eta\right)\right] - \frac{\sigma}{(1-\sigma)}\eta\, e^{-\sqrt{\frac{\gamma}{2}}\eta}\cos\sqrt{\frac{\gamma}{2}}\eta}\right\} \tag{A-22b}$$

$-\pi$

if $\sigma \neq 1$.

APPENDIX III

AN ALTERNATE METHOD OF OBTAINING SOLUTIONS FOR LOW VALUES OF $\omega\sqrt{4x}$ (CHAPTER II)

An integral method has been used in this work to obtain solutions for the velocity and temperature perturbations for low values of $\gamma = \omega\sqrt{4x}$. An alternate procedure for obtaining the corresponding exact solutions will be developed here.

For this case a pair of solutions corresponding to Equations (2.64) are written as

$$M = \sum_{n=0}^{\infty} \left[E_n(\eta) + i\gamma I_n(\eta) \right] \gamma^{2n} \tag{A-23a}$$

$$N = (4x)^{-3/4} \sum_{n=0}^{\infty} \left[J_n(\eta) + i\gamma L_n(\eta) \right] \gamma^{2n} \tag{A.23b}$$

These quantities along with $\psi_o = (4x)^{3/4} F(\eta)$ and $T_o = H(\eta)$ are now entered into Equations (2.21) and all derivative operations are carried out yielding

$$(4x)^{-3/4} \sum_{n=0}^{\infty} \Big\{ \Big[E_n'''(\eta) + 3F(\eta) E_n''(\eta) - (4n+1) F'(\eta) E_n'(\eta) + 4n F''(\eta) E_n(\eta) \tag{A-24a}$$

$$+ J_n(\eta) + I_{n-1}'(\eta) \Big] \gamma^{2n} + i \Big[I_n'''(\eta) + 3F(\eta) I_n''(\eta) - (4n+3) F'(\eta) I_n(\eta)$$

$$+ (4n+2) F''(\eta) I_n(\eta) + L_n(\eta) - E_n'(\eta) \Big] \gamma^{2n+1} \Big\} + (4x)^{-3/4} \zeta(\eta) = 0 \ ,$$

and

$$(4x)^{-5/4} \sum_{n=0}^{\infty} \Big\{ \Big[\frac{1}{\sigma} J_n''(\eta) + 3F(\eta) J_n'(\eta) - (4n-3) F'(\eta) J_n(\eta) \tag{A-24b}$$

$$+ 4n H'(\eta) E_n(\eta) + L_{n-1}(\eta) \Big] \gamma^{2n} + i \Big[\frac{1}{\sigma} L_n''(\eta) + 3F(\eta) L_n'(\eta)$$

$$- (4n-1) F'(\eta) L_n(\eta) + (4n+2) H'(\eta) I_n(\eta) - J_n(\eta) \Big] \gamma^{2n+1} \Big\} = 0 \ .$$

x cancels in both equations leaving only powers of γ with functions of η as coefficients. Both real and imaginary parts of each equation must be zero, and therefore the coefficients of all powers of γ must vanish. Thus,

$$E'''(\eta) + 3F(\eta)\,E''(\eta) - (4n+1)\,F'(\eta)\,E'(\eta) + 4n\,F''(\eta)\,E_n(\eta) + J_n(\eta) + I'_{n-1}(\eta) + \delta_{no}\,S(\eta) = 0 \tag{A-25a}$$

$$\frac{1}{\sigma}\,J''_n(\eta) + 3F(\eta)\,J'_n(\eta) - (4n-3)\,F'(\eta)\,J_n(\eta) + 4n\,H'(\eta)\,E_n(\eta) + L_{n-1}(\eta) = 0\,, \tag{A-25b}$$

and

$$I'''_n(\eta) + 3F(\eta)\,I''_n(\eta) - (4n+3)\,F'(\eta)\,I'_n(\eta) + (4n+2)\,F''(\eta)\,I_n(\eta) + L_n(\eta) - E'_n(\eta) = 0 \tag{A-26a}$$

$$\frac{1}{\sigma}\,L''_n(\eta) + 3F(\eta)\,L'_n(\eta) - (4n-1)\,F'(\eta)\,L_n(\eta) + (4n+2)\,H'(\eta)\,I_n(\eta) - J_n(\eta) = 0\,, \tag{A-26b}$$

where n = 0, 1, 2, 3, 4, ...

The boundary conditions for the first pair of Equations (A-25) are

$$E_n(0) = E'_n(0) = E'_n(\infty) = J_n(0) = J_n(\infty) = 0.$$

The boundary conditions for the second pair (A-26) are

$$I_n(0) = I'_n(0) = I'_n(\infty) = L_n(0) = L_n(\infty) = 0.$$

The problem is now reduced to two pairs of simultaneous differential equations whose solutions for successive values of n become corresponding successive approximations to the oscillating stream function M and the oscillating temperature profile N. The real parts are obtained from the first pair (A-25) and the imaginary parts from the second pair (A-26).

The procedure is to solve (A-25) for n = 0 giving E_o and J_o, then to enter these functions into (A-26) for n = 0 which are then solved

for I_o and L_o. These are then put back into (A-25) which are solved for $n = 1$ giving E_1 and J_1. This procedure is repeated as many times as is desired to order to obtain a sufficiently large number of successive approximations to produce results which are accurate within a given required range of γ. If this required range is large, then a large number of approximations may be necessary. A good idea of the number of terms required for a given value of γ can be obtained by studying the results of the integral method used in this work, for example, by referring to Appendices I-f and I-g where the tabulated coefficients of the series $\sum_{n=0}^{\infty} R_n \gamma^n$ and $\sum_{n=0}^{\infty} S_n \gamma^n$ are given. Since integral techniques are known to give approximately the same results as exact methods, the series of functions being dealt with here may be expected to converge at about the same rate as the series used in connection with the integral methed. Once these functions are available the magnitudes and phase angles of the velocity are temperature perturbations can be obtained from

$$\left|\frac{\partial M}{\partial \eta}\right| = \sqrt{\left[\sum_{n=0}^{\infty} \gamma^{2n} E_n'(\eta)\right]^2 + \left[\sum_{n=0}^{\infty} \gamma^{2n+1} I_n'(\eta)\right]^2} \quad , \tag{A-27a}$$

$$\phi = \operatorname{Arc\,tan}\left\{\frac{\sum_{n=0}^{\infty} \gamma^{2n+1} I_n'(\eta)}{\sum_{n=0}^{\infty} \gamma^{2n} E_n'(\eta)}\right\}, \tag{A-27b}$$

$$\left|N\right| = (4x)^{-3/4}\sqrt{\left[\sum_{n=0}^{\infty} \gamma^{2n} J_n(\eta)\right]^2 + \left[\sum_{n=0}^{\infty} \gamma^{2n+1} L_n(\eta)\right]^2} \quad , \tag{A-28a}$$

and

$$\alpha = \operatorname{Arc\,tan}\left\{\frac{\sum_{n=0}^{\infty} \gamma^{2n+1} L_n(\eta)}{\sum_{n=0}^{\infty} \gamma^{2n} J_n(\eta)}\right\} \tag{A-28b}$$

It can be seen that the pairs of Equations (A-25) and (A-26) have variable coefficients formed from $F(\eta)$, $H(\eta)$, and their derivatives. The equations are linear, however, but the fact that only three of the five boundary conditions are known at the wall would tend to make their solution difficult. The other two boundary conditions are given at infinity. It appears that a fair amount of labor would be involved in solving these equations, and one possible approach is the use of a high speed digital computer.

Some results can be obtained analytically for $n = 0$ since Equation (A-25b) is independent of (A-25a) in this case. Thus,

$$\frac{1}{\sigma} J_0''(\eta) + 3F(\eta)\, J_0'(\eta) + 3F'(\eta)\, J_0(\eta) = 0 \,, \tag{A-29}$$

or,

$$\frac{1}{\sigma} \frac{d}{d\eta} J_0'(\eta) + 3 \frac{d}{d\eta}\left[F(\eta)\, J_0(\eta)\right] = 0 \,. \tag{A-30}$$

Integrating from infinity to η gives

$$\frac{1}{\sigma} J_0'(\eta)\Big|_{\infty}^{\eta} + 3\, F(\eta)\, J_0(\eta)\Big|_{\infty}^{\eta} = 0 \,, \tag{A-31}$$

and

$$J_0'(\eta) + 3\sigma F(\eta)\, J_0(\eta) = 0. \tag{A-32}$$

An integrating factor is $e^{3\sigma \int_0^{\eta} F(\eta)\, d\eta}$ so that

$$\frac{d}{d\eta}\left[e^{3\sigma \int_0^{\eta} F(\eta) d\eta}\, J_0(\eta)\right] = 0 \,, \tag{A-33}$$

and

$$e^{3\sigma \int_0^{\eta} F(\eta) d\eta}\, J_0(\eta) = \text{CONSTANT} \,. \tag{A-34}$$

But $J_0(0) = J_0(\infty) = 0$ while $e^{3\sigma \int_0^{\eta} F(\eta) d\eta}$ has nonzero values both at the

wall and at infinity. Therefore, the constant must be zero and $J_o(\eta) = 0$. This agrees with the result given by Equation (2.59b) that the temperature perturbations are zero in the steady or quasi-steady case. The corresponding velocity perturbations are to be obtained from

$$E'''(\eta) + 3F(\eta)\, E_o''(\eta) - F'(\eta)\, E_o'(\eta) + S(\eta) = 0 \;, \tag{A-35}$$

and are written as $M = E_o(\eta)$. This shows the same result as indicated by Equation (2.59a) that the velocity perturbations occur along lines of constant η in the quasi-steady case. Since $T_o = H(\eta)$, these paths are lines of constant steady temperature so that the temperature perturbations are zero. The corresponding phase angles of the velocity and temperature perturbations are given by

$$\phi = \lim_{\gamma \to 0} \operatorname{Arc\,tan}\left\{\frac{\sum_{n=0}^{\infty} \gamma^{2n+1} I_n'(\eta)}{\sum_{n=0}^{\infty} \gamma^{2n} E_n'(\eta)}\right\} = \lim_{\gamma \to 0} \operatorname{Arc\,tan}\left\{\frac{\gamma I_0'(\eta) + \gamma^3 I_1'(\eta) + \cdots}{E_0'(\eta) + \gamma^2 E_1'(\eta) + \cdots}\right\} \tag{A-36}$$

$$= \operatorname{Arc\,tan}\left(\frac{0}{E_0'(\eta)}\right) = 0 \;,$$

and

$$\alpha = \lim_{\gamma \to 0} \operatorname{Arc\,tan}\left\{\frac{\sum_{n=0}^{\infty} \gamma^{2n+1} L_n(\eta)}{\sum_{n=0}^{\infty} \gamma^{2n} J_n(\eta)}\right\} = \lim_{\gamma \to 0} \operatorname{Arc\,tan} \tag{A-37}$$

$$\left\{\frac{\gamma L_0(\eta) + \gamma^3 L_1(\eta) + \cdots}{J_0(\eta) + \gamma^2 J_1(\eta) + \gamma^4 J_2(\eta) + \cdots}\right\} = \lim_{\gamma \to 0} \operatorname{Arc\,tan}\left[\frac{L_0(\eta)}{\gamma J_1(\eta)}\right] = 90^\circ .$$

These results are in agreement with the phase relationships shown in Figures 18 and 19 for $\gamma \to 0$. The 90° phase angle for the temperature perturbations as $\gamma \to 0$ is in agreement with previous discussion in Chapter II. There it was pointed out that only the lagging components of velocity have an effect on the temperature perturbations at very small values of γ since the in phase components lie along constant η trajectories.

APPENDIX IV

SUMMARY OF EXPERIMENTAL DATA

APPENDIX IV-a

Summary of Data from Potential Flow

Measurements Along the Wall of a Vibrating Plate

Values of $\frac{U_o}{V_o}$ Measured at y = 1/10 of an Inch

f(Cycles/Sec.)		15			20			25		
a_o (Inches)		.050	.075	.100	.050	.075	.100	.050	.075	.100
V_o(Inches/Sec.)		4.70	7.05	9.40	6.30	9.45	12.6	7.85	11.75	15.7
x/c where c = 5"	0	0	0	0	0	0	0	0	0	0
	.10	-	-	-	-	.05	.06	.09	.09	.10
	.15	-	.13	.14	.14	.14	.14	.19	.17	.17
	.20	.12	.13	.19	.14	.17	.21	.21	.27	.29
	.25	.28	.23	.26	.28	.23	.25	.27	.29	.28
	.30	.23	.35	.37	.29	.36	.37	.45	.44	.47
	.35	.38	.38	.38	.38	.39	.40	.40	.35	.39
	.40	.35	.50	.56	.55	.52	.52	.60	.56	.61
	.45	.53	.52	.53	.52	.49	.55	.49	.53	.51
	.50	.59	.65	.67	.66	.59	.64	.72	.67	.69
	.55	.69	.78	.70	.65	.73	.72	.74	.68	.67
	.60	.91	.90	.98	.96	.88	.89	.86	.87	.89
	.65	.88	1.01	.96	1.06	.86	.94	.84	.78	.96
	.70	1.17	1.07	1.15	1.00	1.08	.92	1.00	.94	1.04
	.75	1.24	1.18	1.21	1.11	1.20	1.20	1.00	1.19	1.18
	.80	1.41	1.34	1.41	1.17	1.25	1.19	1.19	1.22	1.21
	.85	1.46	1.60	1.53	1.67	1.60	1.47	1.43	1.33	1.36

Values of $\frac{U_o}{V_o}$ (Cont'd)

30			35			40		
.050	.075	.100	.050	.075	.100	.050	.075	.100
9.40	14.1	18.8	11.0	16.5	22.0	12.6	18.9	25.2
0	0	0	0	0	0	0	0	0
.06	.06	.06	.06	.05	.07	.05	.04	.05
.14	.13	.13	.14	.13	.14	.12	.10	.11
.12	.13	.18	.13	.19	.29	.11	.16	.17
.22	.22	.20	.20	.21	.23	.18	.18	.19
.28	.30	.33	.30	.32	.32	.25	.27	.30
.33	.33	.33	.30	.32	.30	.26	.28	.27
.41	.41	.43	.39	.40	.43	.37	.38	.41
.43	.47	.47	.37	.44	.43	.38	.36	.36
.56	.53	.56	.53	.53	.54	.47	.51	.51
.61	.59	.60	.53	.52	.49	.49	.44	.54
.63	.65	.67	.69	.66	.66	.62	.63	.64
.72	.73	.77	.64	.65	.71	.62	.67	.69
.81	.84	.82	.83	.85	.76	.76	.68	.68
.88	1.07	.93	.83	.92	.89	.78	.83	.83
1.07	1.05	.99	.88	.96	.98	1.07	.93	.80
1.33	1.27	1.18	1.20	1.23	1.07	1.37	1.25	.93

APPENDIX IV-b

SUMMARY OF DATA FROM VELOCITY MEASUREMENTS MADE IN THE BOUNDARY LAYER ON A VIBRATING PLATE

$f = 20$ cycles/sec.

$x/c = .55$

$c = 5$ inches

For air at 80°F, $\nu = 1.7 \times 10^{-4}$ ft^2/sec.

$\eta/\sqrt{2} = y\sqrt{\frac{\pi f}{\nu}} = 50.7y$ where y is in inches

Values of $\frac{|u|}{U_o}$

$\eta/\sqrt{2}$	$a_o = .050"$	$a_o = .075"$	$a_o = .100"$
.26	---	.20	.25
.51	.51	.50	.46
.76	.61	.59	.62
1.01	.77	.74	.78
1.52	.93	.95	1.00
1.78	1.00	1.03	1.05
2.03	1.06	1.08	1.09
2.54	1.09	1.08	1.09
3.04	1.06	1.03	1.05
3.55	1.03	1.03	1.03
4.05	1.03	1.03	1.0
5.07	1.00	1.00	1.00

APPENDIX IV-c

SUMMARY OF HEAT TRANSFER MEASUREMENTS MADE UNDER VIBRATORY CONDITIONS
(10 Inch Square Plate with a 6 Inch Square Heated Section)

a_o (inches)	f (cycles/sec)	$a_o f$ (inches/sec)	$\Delta\theta_o$ (°F)	$\Delta\theta$ (°F)	h_v/h_c Eqn (4-17)	$h_c = .40\Delta\theta^{1/4}$ (Btu/hr-ft^2-F°)	h_v (Btu/hr-ft^2-F°)
0.075	15	1.125	102.2	99.7	0.0315	1.26	0.040
0.100	15	1.50	102.2	98.5	0.0493	1.26	0.062
0.125	25	3.125	102.2	91.4	0.163	1.24	0.202
0.150	25	3.75	102.2	88.4	0.219	1.23	0.269
0.005	50	0.25	33.5	33.3	0.006	0.965	0.006
0.035	50	1.75	33.5	31.9	0.068	0.95	0.065
0.050	50	2.50	33.5	30.7	0.128	0.94	0.120
0.062	50	3.10	33.5	28.8	0.222	0.93	0.207
0.070	50	3.50	33.5	28.3	0.250	0.920	0.230
0.090	50	4.50	33.5	26.2	0.390	0.905	0.353
0.107	50	5.35	33.5	25.0	0.465	0.892	0.415

UNIVERSITY OF MICHIGAN
3 9015 03525 1860